UNIVERSITÀ DI PARMA

UNIVERSITA' DEGLI STUDI DI PARMA

DOTTORATO DI RICERCA IN
FISICA

CICLO XXXIII

ADVANCED MULTI-ANALYTICAL METHODS FOR THE STUDY OF MICROSCOPIC LAYERED STRUCTURES: THE CASE OF MUSICAL INSTRUMENTS

Coordinatore:
Chiar.mo Prof. Stefano Carretta

Tutore:
Chiar.mo Prof. Danilo Bersani

Co-tutore:
Chiar.mo Prof. Marco Malagodi

Dottorando: Claudia Invernizzi

Anni Accademici 2017/2018 – 2019/2020

Rights of use

The content of this PhD Thesis, partially based on unpublished research and involving images and data which property is shared among different institutions, can be consulted and quoted in the appropriate forms, but images and whole texts cannot be used if not under the author's permission, after a proper request (at: claudia.invernizzi@hotmail.it).

To the consciousness

Abstract

The stratigraphy of historical bowed string musical instruments is a complex and heterogeneous system composed of multiple varnish layers coated on previously treated wood. The entire coating system, collectively called *wood finish*, is representative of the instrument makers' working techniques. However, the extended use of the instruments by the musicians as well as the restoration interventions over the centuries could have altered it in terms of layer thickness and composition. Moreover, sampling is rarely feasible because of the need to preserve the value and the integrity of these precious artefacts.

In this thesis, we first evaluated potential and limits of a suite of non-invasive spectroscopic and optical imaging techniques in the study of *wood finish* systems of laboratory mock-ups. Reflection FTIR spectroscopy, XRF, Raman spectroscopy and OCT were applied to the mock-ups by means of portable instrumentation. This non-invasive methodology was supported by SEM-EDX and ATR micro-FTIR analyses. Moreover, the effects of the progressive artificial solar exposure were non-invasively assessed from chemical and chromatic points of view. Then, we explored novel multi-analytical approaches on historical musical instruments by combining the most efficient techniques considered in the experimental study with other advanced non-invasive instrumentation, both non-destructive (NMR-MOUSE, synchrotron radiation micro-CT) and micro-destructive (LIBS), for the characterization of their stratigraphy. Finally, the availability of micrometric samples collected on esteemed instruments represented an extraordinary opportunity to perform analyses by the use of advanced invasive techniques such as the synchrotron radiation FTIR microspectroscopy in reflection geometry.

This study involved multiple complementary techniques to obtain high-level information from microscopic layered structures with the final aim of disclosing materials and technologies employed by old violin makers, as well as by restorers and experts in later interventions. Its importance is also related to the preventive conservation of objects that, being played over time and often still nowadays, have undergone different kinds of degradation and wear.

Table of contents

Introduction

1. Analytical results on laboratory mock-ups by non-invasive portable instrumentation

2. Innovative applications of advanced non-invasive techniques

3. Innovative applications of advanced invasive techniques

Appendices

Acknowledgements

Introduction

0.1 Organization of the dissertation

This dissertation is organized as follows.

Introduction firstly describes the flourishing of the Italian lutherie in the 16th century, its great development under the leadership of few influential Cremonese families and then its decline towards the late 18th century. Subsequently, a background on the materials and procedures employed to treat and finish the wood of musical instruments is provided, followed by the analytical techniques used so far for their study. The context of the research problem and the objectives of the thesis are finally reported.

Chapter 1 is dedicated to the experimental study of laboratory mock-ups by a non-invasive multi-analytical approach, with the aim of evaluating potential and limits of different techniques in the investigation of coating systems organized as those encountered on bowed string musical instruments. The study is supported by invasive analyses on the cross-sectioned samples.

Chapter 2 contains results obtained on inestimable historical instruments through different novel combinations of non-invasive and contactless advanced instrumentation, whose access was granted thanks to the collaboration with national and international research infrastructures. Except for LIBS, which is micro-destructive, all the analytical techniques employed totally preserve the integrity of the objects. In some cases, the methodological approach is previously tested on laboratory mock-ups.

Chapter 3 reports results achieved on cross-sections of ancient valuable instruments by the application of advanced invasive techniques, and discussed using both univariate and multivariate approaches. The study is supported by non-invasive data acquired on the instruments under investigation.

Appendices I and II report detailed information, respectively, on the analytical instrumentation used to study the mock-ups and the real case studies, and on the musical instruments investigated. Appendices III and IV include analytical insights related to Chapter 3.

0.2 State of the art on historical bowed string musical instruments

0.2.1 The golden age of the Italian violin making

The most esteemed violins, violas and cellos were produced over a period of time from approximately 1550 to around 1750, which is known as the golden age of the Italian lutherie [Cacciatori, 2014; Cacciatori, 2018]. These instruments have always aroused curiosity and fascination because of their remarkable value and their colourful histories strictly intertwined with those of celebrated owners and musicians.

In the course of the 16th century, two cities had become renowned as centres of production of violins and the other instruments in the family of the modern string quartet: Brescia and Cremona [Chiesa, 2017]. In Brescia musical instrument making, especially the building of viols, had its origin in the 15th century, and the names of some of those actual craftsmen are known, even though none of their instruments appear to have survived to our own times [Beare, 1987]. In the early 17th century, however, there had been no generational turnover in the principal Brescia workshops for different reasons, also of a historical and contingent nature. The Cremona luthiers thus consolidated an unchallenged leadership in a market sector that saw an unrelenting, fast growth.

Cremonese lutherie was not a mass industry: the market, in fact, was controlled by few families whose genealogy, in the heyday of the Cremonese violin making, is displayed in Fig. 0.1 [Cacciatori, 2018].

The Amati dynasty of violin makers was one of the most long lasting and successful [Chiesa, 2006]. They were active in Cremona for almost two centuries during the time of greatest achievement in Cremonese making, prospering in the good times and facing difficulties in the period of decline. Although living over such a long period of time, they comprised only five craftsmen, spread over four long-lived generations. The first violin maker of the family and founder of the workshop was Andrea Amati (ca 1505-1577). He was the first great Cremonese violin maker and he seems to have been active in the city by about 1540-1550, ten years or so after the first paintings and drawings that depict true violins, as opposed to their precursors represented by the viols and liras. To the best of our knowledge, there may have been some early Cremonese craftsmen from whom Andrea was able to learn his art, or perhaps he may have apprenticed in Brescia. Whatever the answer, it was he who brought the shape of the violin to perfection, establishing the size and proportions of the instrument as it still exists nowadays. He crafted extraordinary instruments, among which violins, violas and cellos for the Spanish Court of Philip II and for the French king Charles IX’s orchestra, and his name is recognized internationally as the key figure in the production of the new family of bowed string instruments. In those decades Cremona, ruled by the Spanish, was a place of innovation, art and music: *Cremonensis* scientists, artists, musicians and violinists were invited to the major courts of Europe to show off their skills. When Andrea died, his sons Antonio (ca 1540-1607) and Girolamo (ca. 1548-1630) took over a fully flourishing workshop, labelling their instruments with both their names even long after the death of Antonio. The Girolamo's son, Nicolò (1596-1684), started to assist the workshop of the father early on in his career and, when the plague epidemic struck down Girolamo in 1630, he run the workshop single-handedly. The rise of Nicolò's workshop was extraordinary and he soon required the assistance of young apprentices, including Andrea Guarneri (1623-1698) and Giacomo Gennaro (ca. 1624-1701), in order to fulfil the increasing commissions. In 1649 his son Girolamo II (1649-1740) was born and everything seemed to point to the family's continued dominance [Cacciatori, 2014; Cacciatori, 2018].

The course of history, however, radically changed in the final decades of the 17th century with the appearance of young first-generation craftsmen either with connections to the workshop of Nicolò Amati or influenced by his construction technique and style. First of all, the *familio* Andrea Guarneri who was active until the end of the century, then leaving - on his death - the difficult task of continuing the business to his son Giuseppe (1666-ca. 1740); his older son Pietro (1655-1720), a violin maker and musician, moved to Mantova some time previously. A new family of luthiers emerged, then, in this scenario: Francesco Rugeri (ca. 1620-1698) and his four sons, who later continued their father's business. No evidence of Francesco Rugeri completing an apprenticeship in the Amati workshop is recorded, but his instruments witness a strong connection between the two. Finally, the arrival of Antonio Stradivari (ca. 1644-1737): in his early years of business, he produced instruments that show the Nicolò's stylistic influence, although there is no record that he spent time in the Amati workshop [Cacciatori, 2014; Cacciatori, 2018]. Over these years, he created extraordinary plucked instruments and inlaid violins, the *Sunrise* 1677 and the *Hellier* 1679, and after he had been entrusted with important commissions like the one from Ferdinando de' Medici in 1690, he acquired an unmatched reputation in town [Villa et al., 2011].

In 1698 Andrea Guarneri and Francesco Rugeri died, and the same year the son of Giuseppe Guarneri, Bartolomeo Giuseppe known universally as Guarneri "del Gesù" (1698-1744), was born. Guarneri "del Gesù", however, was troubled with financial difficulties all his life and he was recognized renowned only during the following century, when his name became associated with that of Nicolò Paganini. The continued success of the Guarneri workshop was ensured by Giuseppe, and his son Bartolomeo Giuseppe after him, while the Rugeri's business was continued in the eighteen century thanks to the efforts of the Francesco's sons. Girolamo II Amati, the last heir of the family business, ended up fleeing his debts and Cremona in search of fortune, after the ruin of his family's business - the craft of making instruments in which the Amatis had excelled for over a century [Cacciatori, 2014; Cacciatori, 2018].

The beginning of the 18th century was certainly dominated by Antonio Stradivari, who had reached his golden period by that time, establishing himself as the leading violin maker in the town. Assisted in the work by his sons Francesco (1671-1743) and Omobono (1679-1742), he produced a succession of inestimable instruments as a result of intense and ongoing research and innovation, with attention to the changes in the violin repertoire occurring at the time. Meanwhile, the difficulties faced by Girolamo II Amati, by the Rugeri family and by the Guarneris in the early eighteenth century were the harbinger of what would occur in the second half of the century. In those years, Carlo Bergonzi (1683-1747) arrived on the Cremonese scene, the last violin maker to have worked in Stradivari's workshop and the last to have used the moulds and models he had received from Antonio's heirs [Cacciatori, 2014; Cacciatori, 2018].

The years from 1737 to 1747 represent a terrible period for Cremonese violinmaking, seeing the death of Antonio Stradivari and his sons, Guarneri "del Gesù" and his father Giuseppe, Girolamo II Amati and Carlo Bergonzi.

After having dominated European lutherie for two centuries, the tradition of Cremona was on the wane: in the late 18th century and early 19th century, Cremonese violin makers such as the Bergonzis, Lorenzo Storioni, Giovanni Rota, the Cerutis and Gaetano Antoniazzi played a minor role compared to that of their predecessors, experiencing the slow and gradual decline of the town. In these years, competition from violinmakers elsewhere in Italy and Europe was felt ever more keenly, with the quality produced in other cities presenting a valid alternative to the Cremonese instruments. Luthiers working in places like Venice, Naples and Turin had access to many more opportunities than the small Cremona, which was unable to find a way to return to its prestigious past. In that period, the economic and cultural development the town had reached in the sixteen century was long-lost [Cacciatori, 2014; Cacciatori, 2018].

After centuries of greatness, Cremona was short on both talent and music, and in the early twentieth century the previous trajectory continued, with the end of family traditions and the closing of historical workshops. Only in the last decades of the 20th century, Cremonese violin making regained its European and international role thanks to its International Violin Making School and to the increasing workshops where luthiers continue to produce instruments for musicians all over the world [Cacciatori, 2014; Cacciatori, 2018].

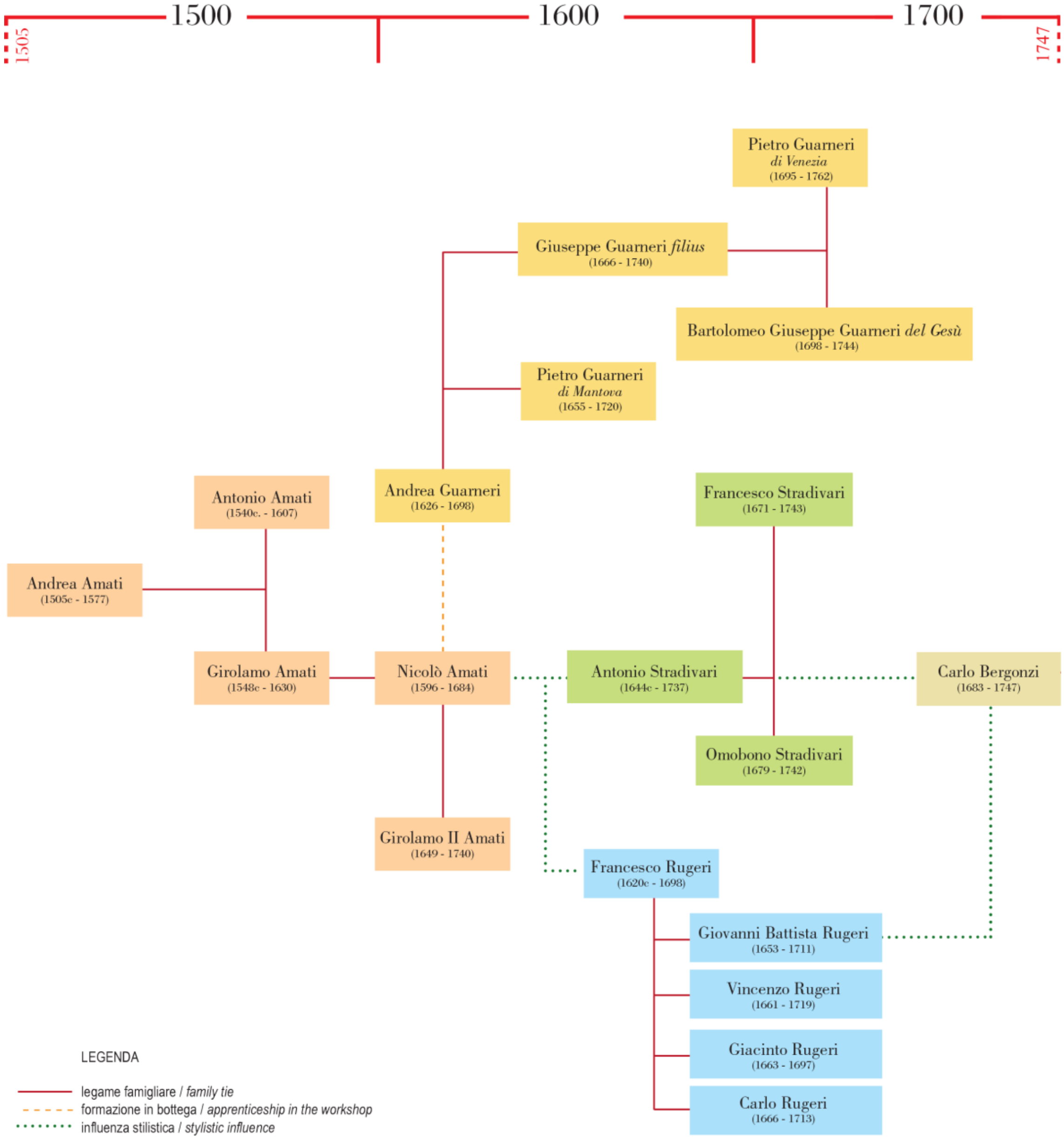

Figure 0.1 *Genealogy of the Cremonese families in the golden age of the Italian violin making [Cacciatori et al., 2018].*

0.2.2 Materials and stratigraphic structure

Historically, wood of artworks such as polychrome sculptures, paintings, furniture or musical instruments has undergone a large variability of treatments according to the artefact and its main function (e.g., aesthetical, acoustic, etc.). A schematic representation of a typical stratigraphy of bowed string musical instruments is displayed in Fig. 0.2.

Wood for violins and the other instruments in the family of the modern string quartet is usually cut during the cold dormant months, when the amount of sap in it is at a minimum, and seasoned for years before being shaped and treated. The front plate is made of a softwood, typically spruce, while maple is normally used for the back plate, the ribs, the neck and the head [Hsieh, 2004].

First of all, wood can be pre-treated by different chemical and physical processes depending on the results to be achieved, for example modifying its natural colour, making it antiqued or more permeable to subsequent filler treatments. However, no certain information about pre-treatments of the wood employed for ancient bowed string musical instruments has been obtained from scientific analyses so far [Bohlen et al., 2007]. Drawing from sources and documents in the wider field of arts and crafts, physical pre-treatments consisted in the exposure of the wood to solar radiation or to high temperature for long time [Cennini, 2003; Obataya, 2017]. Moreover, Nagyvary documented ancient aqueous treatments consisting in boiling the wood for violin for a short time or soaking it in seawater [Nagyvary, 1988]. According to the author, the boiled or fermented wood is more permeable than that dried aseptically: air moves freely through the open holes from cell to cell, consequently removing internal pressures and tensions. Chemical pre-treatments, instead, could be alkaline or acid. While not much is known about the acid pre-treatments [Lemery, 1685], the use of alkaline ammonia- and lye-based ones has been more documented in the history of art [Ruscelli, 1557; Lemery 1763; Brugnatelli, 1790; Bersch, 1890; Nagyvary, 1988; Aquinas, 1996] and their effects studied by scientific community [Yamashiki et al., 1990; Nakano et al., 2000; Colombini et al., 2009; Weigl et al., 2009; Čermák and Dejmal, 2013; Tamburini et al., 2015]. The alkaline solutions modify the structure of the wood fibres, hydrolysing the hemicellulose and the crystalline cellulose as well as promoting the bleaching and the detergency of the wood.

Subsequently, wood is isolated to prevent that the ground coat applied afterwards penetrates much and heterogeneously inside it. As documented in historical treatises on wooden artefacts, this size treatment was mostly realized using organic materials, such as animal or casein glues [Fioravanti, 1592; Norgate, 1997; Cennini 2003; Brandmair and Greiner, 2010] and oils [De Mayerne, 1620-1646; Michelman, 1946; Beal, 1984], which partially or totally fill up the voids in the wood acting as impregnating agents. The impregnation should also have considerable preservative value, thus protecting the inside wood of the instruments [Michelman, 1946]. The study performed by the authors of [Barlow et al., 1988], moreover, highlighted the presence of inorganic particles containing Si, S, Cl, K and Ca in the wood interior of a rib fragment from a Stradivari cello 1711. Mineral deposits, including clay and calcium carbonate, and high concentration of salt were also found by Nagyvary analysing different spruce specimens from instruments made by Stradivari, Guarneri, Giovanni Battista Guadagnini and Francesco Rugeri [Nagyvary, 1988]; almost twenty years later, the same author hypothesized a Cremona “salt of gems” for hardening the wood, which could have contained crushed crystals of gypsum, quartz, calcite, fluorite, and barite, in addition to some water-soluble salts like borax and the sulphates of Fe, Cu, Zn and Cr [Nagyvary et al., 2009].

A transparent ground is then applied on the wood to fill up its surface pores and create a film-forming layer. This coat is composed of organic materials, alone or with the addition of inorganic phases therein. Proteins or siccative oils were mainly detected on musical instruments [Echard et al., 2008a; Echard et al., 2010; Bertrand et al., 2011; Malagodi et al., 2013; Echard et al., 2015; Invernizzi et al., 2016; Fiocco et al., 2017; Invernizzi et al., 2017; Invernizzi et al., 2018; Rovetta et al., 2019; Invernizzi et al., 2020], although it was generally believed that also other substances like gum, wax or resin could be employed for the ground [Tai, 2007]. As concerns the proteinaceous substances, animal or casein glues could be used but there is no evidence of the specific proteins, except few results obtained on a Stradivari micro-sample by advanced analyses such as the Enzyme-Linked Immunosorbent Assay (ELISA) technique [Brandmair and Greiner, 2010]; in particular, in the activated form of casein, it is not historically known which cations (Ca, K, NH_3, etc.) form bonds with the caseinate anions, or again, if the casein was applied directly as milk. Inorganic particles, when present, act as pigments or colourless fillers: the first class of compounds modifies the colour of the wood surface, while the second one increases the viscosity of the medium and reduces its penetration in wood pores [Echard et al., 2008]. Silicates and aluminosilicates, amorphous and crystalline silica, sulphates, carbonates, iron and manganese oxides were identified at this stratigraphic level in ancient bowed musical instruments [Barlow et al., 1988; Fulton and Schmidt, 1988; Barlow and Woodhouse, 1989; Echard et al., 2008a; Fiocco et al., 2017; Invernizzi et al., 2018; Invernizzi et al., 2020; Rovetta et al., 2017; Rovetta et al., 2019].

Finally, the varnish enhances the visual appearance of wooden instruments as well as protecting them from moisture, dust, mechanical damage or biological growth [Invernizzi et al., 2018]. It is made of one or several layers of organic film-making substances coated onto the surface, sometimes containing mineral particles. Three families of varnishes are usually distinguished by instrument makers: spirit varnishes (resins dissolved in alcohol), oil varnishes (resins mixed with siccative oils) and essential oil varnishes (resins dissolved in volatile oils) [Echard and Lavédrine, 2008b]. Scientific analyses performed on varnishes of bowed string instruments built in the 16th to 18th centuries revealed the use of vegetal resins, mainly exuded from trees of the *Pinaceae* family (e.g., pine rosin or Venetian turpentine), mixed with siccative oils, mostly linseed or walnut oils [White, 1984; Echard et al., 2007; Caruso et al., 2007; Echard et al., 2009; Echard and Bertrand, 2010; Bertrand et al., 2010; Brandmair and Greiner, 2010; Bonizzoni et al., 2014; Caruso et al., 2014; Echard et al., 2015; Fiocco et al., 2017; Invernizzi et al., 2016; Invernizzi et al., 2017; Rovetta et al., 2019]. In some varnishes, inorganic particles have been added as pigments (e.g., orpiment, zinc white, lead tin yellow, white lead, red lead, earths such as ochre, umber or Sienna), fillers (e.g., sulphates, carbonates, silica and silicates), siccative (e.g., litharge and other Pb compounds) or substrates for lakes (e.g., alumina) [Michelman, 1955; Tove et al., 1980; Fulton and Schmidt, 1988; Nagyvary, 1988; Nagyvary and Ehrman, 1988; Bohlen and Meyer, 1997; Echard, 2004; Echard et al., 2009; Echard and Bertrand, 2010; Caruso et al., 2012; Caruso et al., 2014; Invernizzi et al. 2016; Fiocco et al., 2017; Invernizzi et al., 2018; Invernizzi et al., 2020; Rovetta et al., 2019].

The finding of materials like shellac, benzoin, paraffin or calcium-based substances on the exterior surfaces have been attributed to polishers, commonly used by restorers and instrument makers in undocumented routine operations of maintenance to give gloss effect to the musical instrument [Caruso et al., 2014; Invernizzi et al., 2017; Invernizzi et al., 2020].

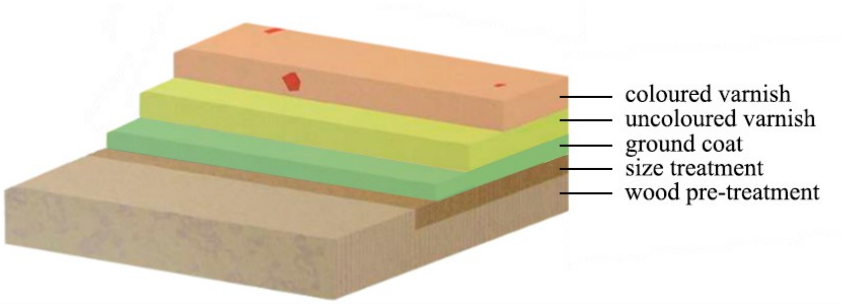

Figure 0.2 *Schematic representation of a typical stratigraphy of bowed stringed musical instruments. Figure modified from [Brandmair and Greiner, 2010].*

0.2.3 Analytical techniques

In the field of cultural heritage materials, analyses can be invasive or non-invasive. Invasive techniques require the removal of small fragments from the object, while the non-invasive instrumentation allows one to gather information directly on artworks without the need for sampling, in a contact or contactless way. Both these categories of techniques can be then classified into destructive and non-destructive according to whether or not the integrity of the sample is preserved.

Over the years, the stratigraphy of ancient bowed musical instruments as well as the complex and heterogeneous nature of its materials have been studied both visually with microscopic techniques and instrumentally by a suite of analytical techniques [Echard and Lavédrine, 2008b]. Researchers are currently engaged in improving analytical procedures intended to maximize the information that can be retrieved from esteemed masterpieces, with the aim of disclosing how the finishing treatments were realized and if they are preserved over time. In recent years, in particular, increasing efforts have been addressing towards the use of a non-invasive and non-destructive approach.

The composition of varnishes was mostly investigated through infrared and Raman spectroscopies [Echard et al., 2008a; Bertrand et al., 2010; Daher et al., 2014; Invernizzi et al., 2016; Invernizzi et al., 2017; Invernizzi et al., 2018], and micro-chemical chromatographic techniques [Echard et al., 2009; Caruso et al., 2014; Lattuati-Derieux et al., 2014; Tirat et al., 2016; Rovetta et al., 2019], while their morphology and distribution on the surface were analysed by OCT [Latour et al., 2009] and by UV-light fluorescence [Dondi et al., 2015; Echard et al., 2015; Dondi et al., 2016; Dondi et al., 2017].

As regards the pigments and fillers dispersed in organic layers, information about their nature was gathered using XRF, PIXE, SR-XRD and SEM-EDX/WDX techniques [Fulton and Schmidt, 1988; Nagyvary, 1988; Barlow and Woodhouse; 1989; Bohlen and Meyer, 1997; Echard, 2004; Bohlen et al., 2007; Echard et al., 2008a; Echard et al., 2009; Caruso et al., 2011; Malagodi et al., 2013; Bonizzoni et al., 2014; Caruso et al., 2014; Invernizzi et al., 2016; Fiocco et al., 2017; Rovetta et al., 2017; Rovetta et al., 2019].

Multiphoton microscopy (MPM), or nonlinear optical microscopy, also provided highly contrasted 3D images of multi-layered coatings at micrometre scale, with information on both particles and binders by specific signals collected as a function of the chemical nature of the studied materials [Latour et al., 2012].

0.3 Context of the research problem and aims

When approaching the stratigraphic study of historical bowed string musical instruments, it is necessary to consider their peculiarity in the field of cultural heritage.

First of all, musical instruments are produced to be played. Their main function is therefore acoustic, unlike the purely aesthetic one of most of artworks. Nowadays, ancient instruments of cultural relevance are hosted in museums whilst others, equally important, are still played by talented musicians around the world.

Primary consequence of their extensive handling, due to hours long practice and performance over the years, was the *soft* wear of the varnishes: these coats were gradually thinned, or even removed from the surface, in the areas where the instrument came in direct contact with the musician's body, mostly visible on the front plate where the chin rested, on the back plate where the instrument rested on the shoulder and on the neck area of the ribs, as well as with its case (Fig. 0.3a). In those areas in contact with the player, in particular, the varnish was softened by exposure to body heat and the hand sweat caused further decomposition. *Abrupt* wear of varnishes, instead, was generally produced by accidents, such as shock (Fig.0.3b) or abrasion (Fig.0.3c) by contact with hard objects and surfaces [Brandmair and Greiner, 2010]. Thousands of concerts, in fact, represent just a part of their long lives: plagues, travels, robberies, revolutions and wars are in the background of a large number of ownership changes. Some instruments were destroyed, others lost, and still others survived properly thanks to their acoustic functionality.

Figure 0.3 *Stereomicroscopy images under VIS-light illumination of soft (a) and abrupt (b,c) wear of varnish on the Bracco small violin 1793 by Lorenzo Storioni. Examples of abrupt wear due to shock (b) and abrasion (c) are shown.*

New materials, then, could have been added by restorers during later interventions, especially where the varnish was partially or totally worn off and in correspondence of wood cracks. Furthermore, the use of polishers before and after the exhibition is a common practice used by musicians and experts to confer gloss effect to the musical instrument.

The extensive playing, as well as the undocumented ordinary and extraordinary procedures of maintenance and restoration, inevitably caused alterations in the original coating thickness and composition. The centuries-long history of a violin, or of another family instrument, has therefore left evident traces on the stratigraphy, making its study even more challenging for today's researchers.

Beyond the effects of the time, the original coating system of these objects is itself complex to be analysed, and the main factors are reported as follows: (i) presence of numerous and heterogeneous materials in just few tens of microns of thickness, (ii) extremely high brittleness of the matter, due to its mostly organic nature, and (iii) very low concentration of inorganic particles dispersed in the binders. As for the small quantity of pigments, fillers or substrates for lakes, in particular, it is motivated by the necessity of the visible light to pass through the layers and arrive to the wood, in this way enhancing the pattern produced by its fibres. This point represents a substantial difference from the polychrome artworks, where the material (e.g., canvas, wood, etc.) hosting the coating system merely acts as support and, for this reason, it is obscured by the overlying ground and paint layers. Unlike polychrome artworks, furthermore, the varnish of musical instruments is considered an original part not to be removed or changed over time.

A further significant factor to be considered is that sampling is mostly denied on musical instruments of such cultural and commercial relevance as Guarneri and Stradivari violins and, when permitted, it is usually strictly limited as to the size, location and number of fragments collected. If, on one hand, the most reliable and informative method to characterize the stratigraphy is the cross-sectional study, on the other it is evident how this invasive approach is rarely feasible with these examples of high artistic craftsmanship.

In this thesis, several non-invasive and contactless techniques were differently combined - for the first time - to investigate the stratigraphy of renowned ancient bowed string instruments, after the development of an analytical experimental study conducted on laboratory mock-ups. The availability of some micrometric fragments collected on esteemed instruments, likewise, represented an extraordinary opportunity to perform analyses by the use of advanced invasive techniques. Novel multi-analytical approaches were explored in order to comprehend the potential of complementary techniques in gathering high-level information from the stratigraphies. Given the state of art presented in 0.2.2, with the main results obtained on the musical instrument stratigraphies by scientific analyses together with the information collected from the historical treatises, our final aim was to further increase knowledge on the materials and technologies employed by the old masters in their workshops, as well as by restorers and experts in later interventions. Its importance is also related to the preventive conservation of objects that, being played over the centuries and often still nowadays, have undergone different kinds of degradation and wear.

0.4 References

Aquinas T. (ps.), Tractatus in arte alchemiae, P. Cortesi, Roma, 1996.

Barlow C.Y., Edwards P.P., Millward G.R., Raphael R.A., Rubio D.J., Wood treatment used in Cremonese instruments, *Nature*. 332 (1988) 313–313. doi:10.1038/332313a0.

Barlow C.Y., Woodhouse J., Of old wood and varnish: peering into the can of worms, *Catgut Acoustical Society*, 1.4 (1989) 2–9.

Beal M., A study of Richard Symonds: his Italian notebooks and their relevance to seventeenth century-painting techniques, Garland, New York & London, 1984.

Beare C., Capolavori di Antonio Stradivari, Arnoldo Mondadori Editore, Cremona, 1987.

Bersch J., Lexikon der Farben-Technik, Vienna, 1890.

Bertrand L., Robinet L., Cohen S.X., Sandt C., Hô A.-S.L., Soulier B., et al., Identification of the finishing technique of an early eighteenth century musical instrument using FTIR spectromicroscopy, *Analytical and Bioanalytical Chemistry*. 399 (2010) 3025–3032. doi:10.1007/s00216-010-4288-1.

Bohlen A.V., Meyer F., Microanalysis of old violin varnishes by total-reflection X-ray fluorescence, *Spectrochimica Acta Part B: Atomic Spectroscopy*. 52 (1997) 1053–1056. doi:10.1016/s0584-8547(96)01596-0.

Bohlen A.V., Röhrs S., Salomon J., Spatially resolved element analysis of historical violin varnishes by use of μPIXE, *Analytical and Bioanalytical Chemistry*. 387 (2007) 781–790. doi:10.1007/s00216-006-0777-7.

Bonizzoni L., Canevari C., Galli A., Gargano M., Ludwig N., Malagodi M., et al., A multidisciplinary materials characterization of a Joannes Marcus viol (16th century), *Heritage Science*. 2 (2014) 15. doi:10.1186/2050-7445-2-15.

Brandmair B., Greiner S.-P., Stradivari Varnish, Eigenverlag, London and Munich, 2010.

Brugratelli L.V., Annali di chimica, 1790.

Cacciatori F., Liuteria cremonese un'antica tradizione, in: Cacciatori F. (ed.), Lo scrigno dei tesori, Fondazione Museo del Violino Antonio Stradivari Cremona, Cremona, 2014, 16–19.

Cacciatori F., Liuteria cremonese: cinque secoli di saper fare, in: La materia e il Suono, Bracco e Cremona per la Liuteria tra musica e scienza, Fondazione Museo del Violino Antonio Stradivari Cremona, Cremona, 2018, 47–71.

Caruso F., Orecchio S., Cicero M.G., Stefano C.D., Gas chromatography–mass spectrometry characterization of the varnish and glue of an ancient 18th century double bass, *Journal of Chromatography A*. 1147 (2007) 206–212. doi:10.1016/j.chroma.2007.02.048.

Caruso F., Saverwyns S., Bos M., Chillura Martino D.F., Ceulemans A.-E., Valck J., et al., Micro-X-Ray Fluorescence and the Old Masters, *Applied Physics A*. 107 (2011) 197–202. doi:10.1007/s00339-011-6729-x.

Caruso F., Martino D.F.C., Saverwyns S., Bos M.V., Burgio L., Stefano C.D., et al., Micro-analytical identification of the components of varnishes from South Italian historical musical instruments by PLM, ESEM–EDX, microFTIR, GC–MS, and Py–GC–MS, *Microchemical Journal*. 116 (2014) 31–40. doi:10.1016/j.microc.2014.04.002

Cennini C., Come si dee incominciare a lavorare in tavola, o vero in ancone., in: Frezzato F. (ed.), Il libro dell'arte, Neri Pozza Editore, Vicenza, 2003, 142–143.

Čermák P., Dejmal A., The effect of heat and ammonia treatment on colour response of oak wood (Quercus robur) and comparison of some physical and mechanical properties, Maderas. *Ciencia y Tecnología*. (2013). doi:10.4067/s0718-221x2013005000029.

Chiesa C., Una breve storia della famiglia Amati, in: Cacciatori F., Carlson B. and Chiesa C. (Eds.), Il DNA degli Amati, una dinastia di liutai a Cremona, Consorzio Liutai Antonio Stradivari Cremona, Cremona, 2006, 20–30.

Chiesa C., Antonio Stradivari and his "rivals" in the late seventeenth-century Cremana, in: Zanrè A. (ed.), The 1690 "Tuscan" Stradivari violin in the Accademia di Santa Cecilia, Scrollavezza & Zanrè, Parma, 2017, 37–40.

Colombini M.P., Lucejko J.J., Modugno F., Orlandi M., Tolppa E.-L., Zoia L., A multi-analytical study of degradation of lignin in archaeological waterlogged wood, *Talanta*. 80 (2009) 61–70. doi:10.1016/j.talanta.2009.06.024.

Daher C., Pimenta V., Bellot-Gurlet L., Towards a non-invasive quantitative analysis of the organic components in museum objects varnishes by vibrational spectroscopies: Methodological approach, *Talanta*. 129 (2014) 336–345. doi:10.1016/j.talanta.2014.05.059.

De Mayerne, Pictoria, Sculptoria et quae subalternarum artium, Ms. Sloane 2052, Londra British Library, 1620-1646.

Dondi P., Lombardi L., Malagodi M., Licchelli M., Cacciatori F., Color-based automatic detection of worn out varnishes on Stradivari's "Scotland University" violin back plate, *Color Research & Application*. 41 (2015) 313–316. doi:10.1002/col.22012.

Dondi P., Lombardi L., Malagodi M., Licchelli M., Automatic identification of varnish wear on historical instruments: The case of Antonio Stradivari violins, *Journal of Cultural Heritage*. 22 (2016) 968–973. doi:10.1016/j.culher.2016.05.010.

Dondi P., Lombardi L., Invernizzi C., Rovetta T., Malagodi M., Licchelli M., Automatic Analysis of UV-Induced Fluorescence Imagery of Historical Violins, *Journal on Computing and Cultural Heritage*. 10 (2017) 1–13. doi:10.1145/3051472.

Echard J.-P., In situ multi-element analyses by energy-dispersive X-ray fluorescence on varnishes of historical violins*, Spectrochimica Acta Part B: Atomic Spectroscopy*. 59 (2004) 1663–1667. doi:10.1016/j.sab.2004.05.026.

Echard J.-P., Benoit C., Peris-Vicente J., Malecki V., Gimeno-Adelantado J., Vaiedelich S., Gas chromatography/mass spectrometry characterization of historical varnishes of ancient Italian lutes and violin, *Analytica Chimica Acta*. 584 (2007) 172–180. doi:10.1016/j.aca.2006.10.048.

Echard J.-P., Cotte M., Dooryhee E., Bertrand L., Insights into the varnishes of historical musical instruments using synchrotron micro-analytical methods, *Applied Physics A*. 92 (2008a) 77–81. doi:10.1007/s00339-008-4449-7.

Echard J.-P., Lavédrine B., Review on the characterisation of ancient stringed musical instruments varnishes and implementation of an analytical strategy, *Journal of Cultural Heritage*. 9 (2008b) 420–429. doi:10.1016/j.culher.2008.03.005.

Echard J.-P., Bertrand L., Von Bohlen A., Le Hô A.-S., Paris C., Bellot-Gurlet L., et al., The Nature of the Extraordinary Finish of Stradivari's Instruments, *Angewandte Chemie International Edition*. 49 (2009) 197–201. doi:10.1002/anie.200905131.

Echard J.-P., Bertrand L., Complementary spectroscopic analyses of varnishes of historical musical instruments, *SpectroscopyEurope*, 22.2 (2010), 12–13.

Echard J.-P., Thoury M., Berrie B.H., Séverin-Fabiani T., Vichi A., Didier M., et al., Synchrotron DUV luminescence micro-imaging to identify and map historical organic coatings on wood, *The Analyst*. 140 (2015) 5344–5353. doi:10.1039/c5an00483g.

Fiocco G., Rovetta T., Gulmini M., Piccirillo A., Licchelli M., Malagodi M., Spectroscopic Analysis to Characterize Finishing Treatments of Ancient Bowed String Instruments, *Applied Spectroscopy*. 71 (2017) 2477–2487. doi:10.1177/0003702817715622.

Fioravanti L., Compendio de i secreti rationali, di m. Leonardo Fiorauanti bolognese, medico, & cirurgico. Diuiso in cinque libri.Opera non meno diletteuole, che utile, alla medicina, & cirurgia, ad alchimisti, a quelle donne, che si dilettano di belletti, & a molte altre arti, & essercitij. Con la tauola de tutti i capitoli., Torino, 1592.

Fulton W., Schmidt S., Violin varnish now and then. *Journal of the Violin Society of America*, 9 (1988), 48–70.

Hsieh A., Cremona revisited: The science of violin making, *Engineering and Science*. 67 (2004) 28–35.

Invernizzi C., Daveri A., Rovetta T., Vagnini M., Licchelli M., Cacciatori F., et al., A multi-analytical non-invasive approach to violin materials: The case of Antonio Stradivari "Hellier" (1679), *Microchemical Journal*. 124 (2016) 743–750. doi:10.1016/j.microc.2015.10.016.

Invernizzi C., Daveri A., Vagnini M., Malagodi M., Non-invasive identification of organic materials in historical stringed musical instruments by reflection infrared spectroscopy: a methodological approach, *Analytical and Bioanalytical Chemistry*. 409 (2017) 3281–3288. doi:10.1007/s00216-017-0296-8.

Invernizzi C., Fichera G.V., Licchelli M., Malagodi M., A non-invasive stratigraphic study by reflection FT-IR spectroscopy and UV-induced fluorescence technique: The case of historical violins, *Microchemical Journal*. 138 (2018) 273–281. doi:10.1016/j.microc.2018.01.021.

Invernizzi C., Fiocco G., Iwanicka M., Kowalska M., Targowski P., Blümich B., et al., Non-invasive mobile technology to study the stratigraphy of ancient Cremonese violins: OCT, NMR-MOUSE, XRF and reflection FT-IR spectroscopy, *Microchemical Journal*. 155 (2020) 104754. doi:10.1016/j.microc.2020.104754.

Latour G., Echard J.-P., Soulier B., Emond I., Vaiedelich S., Elias M., Structural and optical properties of wood and wood finishes studied using optical coherence tomography: application to an 18th century Italian violin, *Applied Optics*. 48 (2009) 6485. doi:10.1364/ao.48.006485.

Latour G., Echard J.-P., Didier M., Schanne-Klein M.C., In situ 3D characterization of historical coatings and wood using multimodal nonlinear optical microscopy, *Optics Express*. 20 (2012) 24623-24635. doi:10.1364/OE.20.024623

Lattuati-Derieux A., Gomes S., Tirat S., Thao-heu S., Echard J.-P., New insights into molecular evolution of oil/colophony varnishes: towards pyrolysis–gas chromatography/mass spectrometry-based quantitation, *E-Preservation Science*. 11 (2014) 76–85.

Lemery N., Nouveau recueil de curiositez, rares & nouvelles des plus admirables effets de la nature & de l'art, Chez Pierre vander Aa, Leide, 1685.

Lemery N., Pharmacopée universelle contenant toutes les compositions de pharmacie qui sont en usage dans la médicine, tant en France que par toute l'Europe; leurs vertus, leurs dose, les maniéres d'opérer les plus simples & les meilleures: Avec un lexicon pharmaceutique, plusieurs remarques, et des raisonnémens sur chaque opération, Chez De Saint &amp, Saillant, 1763.

Malagodi M., Canevari C., Bonizzoni L., Galli A., Maspero F., Martini M., A multi-technique chemical characterization of a Stradivari decorated violin top plate, *Applied Physics A*. 112 (2013) 225–234. doi:10.1007/s00339-013-7792-2.

Michelman J., Preliminary treatment of the wood, in: Michelman J. (ed.), Violin varnish A plausible re-creation of the varnish used by the Italian violin makers between the years 1550 and 1750, A. D., Joseph Michelman, Cincinnati, Ohio, 1946.

Michelman J., Lost art of Strad varnish, *The Scientific Monthly*. 81.5 (1955) 221–223.

Nagyvary J., The Chemistry of a Stradivarius, Chemical & *Engineering News*. 66 (1988) 24–31. doi:10.1021/cen-v066n021.p024.

Nagyvary J., Ehrman J.M., The composite nature of the antique Italian varnish, *Naturwissenschaften*. 75 (1988) 513–515. doi:10.1007/bf00361287.

Nagyvary J., Guillemette R.N., Spiegelman C.H., Mineral Preservatives in the Wood of Stradivari and Guarneri, *PLoS ONE*. 4 (2009). doi:10.1371/journal.pone.0004245.

Nakano T., Sugiyama J., Norimoto M., Contractive force and transformation of microfibril with aqueous sodium hydroxide solution for wood, *Holzforschung*. 54 (2000) 315–320. doi:10.1515/hf.2000.053.

Norgate E., Miniatura or the art of limning, Yale University Press, New Haven and London, 1997.

Obataya E., Effects of natural and artificial ageing on the physical and acoustic properties of wood in musical instruments, *Journal of Cultural Heritage*. 27 (2017). doi:10.1016/j.culher.2016.02.011.

Rovetta T., Invernizzi C., Licchelli M., Cacciatori F., Malagodi M., The elemental composition of Stradivari's musical instruments: new results through non-invasive EDXRF analysis, *X-Ray Spectrometry*. 47 (2017) 159–170. doi:10.1002/xrs.2825.

Rovetta T., Invernizzi C., Fiocco G., Albano M., Licchelli M., Gulmini M., et al., The case of Antonio Stradivari 1718 ex-San Lorenzo violin: History, restorations and conservation perspectives, *Journal of Archaeological Science: Reports*. 23 (2019) 443–450. doi:10.1016/j.jasrep.2018.11.010.

Ruscelli G., Secreti di don Alessio piemontese nuouamente stampati. Con una bellissima aggiunta de' Secreti hauti da un religioso pratichissimo et eccellente et esperimentati, Lucca, 1557.

Tai B.H., Stradivari's varnish a review of scientific findings - part I, *Journal of the Violin Society of America: VSA papers*. XXI (2007) 119–144.

Tamburini D., Łucejko J.-J., Ribechini E., Colombini M.-P., Snapshots of lignin oxidation and depolymerization in archaeological wood: an EGA-MS study, *Journal of Mass Spectrometry*. 50 (2015) 1103–1113. doi:10.1002/jms.3495.

Tirat S., Degano I., Echard J.-P., Lattuati-Derieux A., Lluveras-Tenorio A., Marie A., et al., Historical linseed oil/colophony varnishes formulations: Study of their molecular composition with micro-chemical chromatographic techniques, *Microchemical Journal*. 126 (2016) 200–213. doi:10.1016/j.microc.2015.11.045.

Tove P.A., Sigurd D., Petersson S., Ion Backscattering And X-Ray Investigations Of Violin Varnish And Wood, *Ion Beam Analysis*. (1980) 441–446. doi:10.1016/b978-1-4832-2889-1.50072-4.

Villa V., Cacciatori F., Sturm G., Whiteley J., Bordas Ibanez C., Heyligers M.A., et al., Antonio Stradivari, L'estetica sublime, Consorzio Liutai Antonio Stradivari Cremona, Cremona, 2011.

Weigl M., Pöckl J., Grabner M., Selected properties of gas phase ammonia treated wood, *European Journal of Wood and Wood Products*. 67 (2009) 103–109. doi:10.1007/s00107-008-0301-1.

White R., Varnish, 18th-century instruments examined, *Strad.* 95 (1984), 258–259.

Yamashiki T., Matsui T., Saitoh M., Okajima K., Kamide K., Sawada T., Characterisation of cellulose treated by the steam explosion method. Part 1: Influence of cellulose resources on changes in morphology, degree of polymerisation, solubility and solid structure, *British Polymer Journal*. 22 (1990) 73–83. doi:10.1002/pi.4980220111.

Chapter 1

Analytical results on laboratory mock-ups by non-invasive portable instrumentation

1.1 Aims and methods

This experimental study was conducted thanks to the collaboration with the University of Pavia through the Arvedi Laboratory of Non-Invasive Diagnostics, the Nicolaus Copernicus University within the MOLAB Transnational Access-EU H2020 Project IPERION CH (Grant Agreement No. 654028, project proposal "Non-invasive Examination of Stratigraphic System in violins", acronym: thickNESS), the Associazione Laboratorio di Diagnostica per i Beni Culturali, the Fondazione Arvedi Buschini, the Civica Scuola di Liuteria di Milano, and the Cultural District of Violin Making. The results have been published in the journal Coatings [Invernizzi et al., 2021].

The present research project was aimed at evaluating potentialities and limits of a non-invasive multi-technique approach in the study of the coating system of laboratory mock-ups. The mock-ups under investigation were prepared by varying and stressing different parameters in the stratigraphy, this representing a preliminary step before the study of musical instrument coating systems. Additionally, the mock-ups were progressively aged with artificial solar radiation in order to determine to what extent the chemical and chromatic changes of the stratigraphic layers could be monitored by the techniques considered in this work. A detailed description of the mock-up preparation and ageing is reported in 1.2.

The non-invasive study included optical imaging and spectroscopic techniques applied - without a preferential order - by means of portable instrumentation: OCT, FTIR spectroscopy in reflection mode, Raman spectroscopy and XRF spectroscopy. These methods were selected because of their ability to provide in situ microstructural, molecular and elemental information in a non-destructive way. Preliminary observations of the coating systems at different magnifications were made by UVIFL and VIS photography. In the light of the results obtained on dried mock-ups by the techniques above-mentioned, we decided to use reflection FTIR spectroscopy, together with colorimetry, to non-invasively monitor the effects induced by the progressive artificial exposure.

The non-invasive investigation was supported by observations of the cross-sectional samples under VIS and UV optical microscopy and scanning electron microscopy, as well as by EDX microanalysis in the electron microscope and ATR micro-FTIR spectroscopic analysis. The possibility of removing small fragments from the mock-ups, in fact, allowed us to investigate the stratigraphies using invasive methods which provide highly spatially-resolved information in terms of morphology and distribution of materials.

Detailed information about the analytical instrumentation and the acquisition parameters used in this study is reported in appendix I.

Univariate and multivariate data analysis approaches were combined to extract relevant information from XRF and FTIR data. With the goal of exploring the results with a multivariate perspective, principal component analysis was considered.

1.2 Experimental

1.2.1 Preparation of the mock-ups

A total of eight mock-ups (m.A-m.H) were prepared by the master Claudio Canevari (Civica Scuola di Liuteria, Milano, Italy) by varying the following parameters at different stratigraphic levels: (i) concentration of the filler in the ground coat, (ii) concentration of the pigment in the coloured varnish, (iii) thickness of the uncoloured varnish, and (iv) order of application of the coloured and uncoloured varnishes. The stratigraphies were properly realized to test the efficiency of the techniques under investigation. The selection of the materials was based both on the historical documentation - albeit fragmented - and on the scientific results conducted in the last decades on historical musical instruments (see 0.2.2); the methods employed to apply the layers fulfilled the need for thicknesses as uniform and controlled as possible. A schematic representation of the mock-ups, with their multi-layered coating systems, is reported in Fig. 1.1.

Wood boards of maple (*Acer pseudoplatanus*) were obtained by cutting the log along the radial-longitudinal direction. The sizes of the maple boards are 15 cm (longitudinal direction) x 5 cm (radial direction) x 0.3 cm (tangential direction) each and, to prevent warping, a 0.9-cm-thick piece of multi-layered birch plywood was glued on one radial longitudinally cut face of the boards. The opposite radial longitudinally cut face was smoothed with Abranet sandpapers (P400, P1000) and its residual powder removed by brush and akapad gum before being treated. A potassium-caseinate-based size treatment (S) was applied by brush, completely penetrating the wood. After the smoothing with Abranet P1000 sandpaper, the surface of each sized board was subdivided into three areas and coated, by brush, with a ground coat (G) composed of a dispersion of mineral talc in K-caseinate in different concentrations (respectively 1%, 5% and 10% w/w). Considering the premises described in 0.2.2, the choice of K as cation to form bonds with the caseinate anions was deliberated done to study the variations of K-signals by XRF. The surface was smoothed again with Abranet P1000 sandpaper and then covered with multiple layers of varnish using a bar film applicator (K Hand Coatermodel, Erichsen GmbH). In detail, a first layer of uncoloured linseed oil-colophony varnish (Uv) was laid on the mock-ups from m.B to m.F, while a first layer of linseed oil-colophony varnish containing Fe_2O_3 pigment in concentrations of 5 and 10% w/w was respectively laid on the mock-ups m.G and m.H. In the four mock-ups m.C-m.F, the second layer is made of linseed oil-colophony varnish containing Fe_2O_3 pigment in concentrations of 1%, 2%, 5% and 10% w/w respectively, whilst in the mock-ups m.B, m.G and m.H it is composed of uncoloured linseed oil-colophony varnish. Just in m.B, m.G and m.H, a third layer of uncoloured linseed oil-colophony varnish was added to the stratigraphy. After every varnish application, the mock-ups were dried in a hand-made box under UV lamps (Philips TL60 W/10-R 1SL/25 Attiniche UVA/10) for 18h (t_0). The application of each subsequent layer was made shortly after that the UV exposition was completed. The mock-up named m.A, instead, was not varnished.

The solution of potassium caseinate was obtained by adding casein powder to distilled water (10% w/w), subsequently dissolved in KOH solution 0.5 M. According to an ancient recipe [Baraldi, XV century; Frezzato and Seccaroni, 2010], the procedure used to prepare the linseed oil-colophony varnish (ratio 2:1 w/w) is described as follows: linseed oil was first heated up to 250°C and it was maintained at this temperature for 30 min, then milled colophony was added under magnetic stirring up to complete dissolution and the resulting mixture was maintained at 250°C for 30 min.

The compounds under study were acquired from Kremer Pigmente GmbH & Co., Aichstetten, Germany (casein cat. no. 63200, iron oxide Fe_2O_3 120M cat. no. 48120, linseed oil cat. no. 73054, talc cat. no. 58420) and Cremona Tools SAS, Cremona, Italy (colophony cat. no. 504434). For this study, it is important to report the elemental qualitative composition of the mineral talc, as obtained by the XRF analysis: Mg, Al, Si, S, Ca, Fe and Zn.

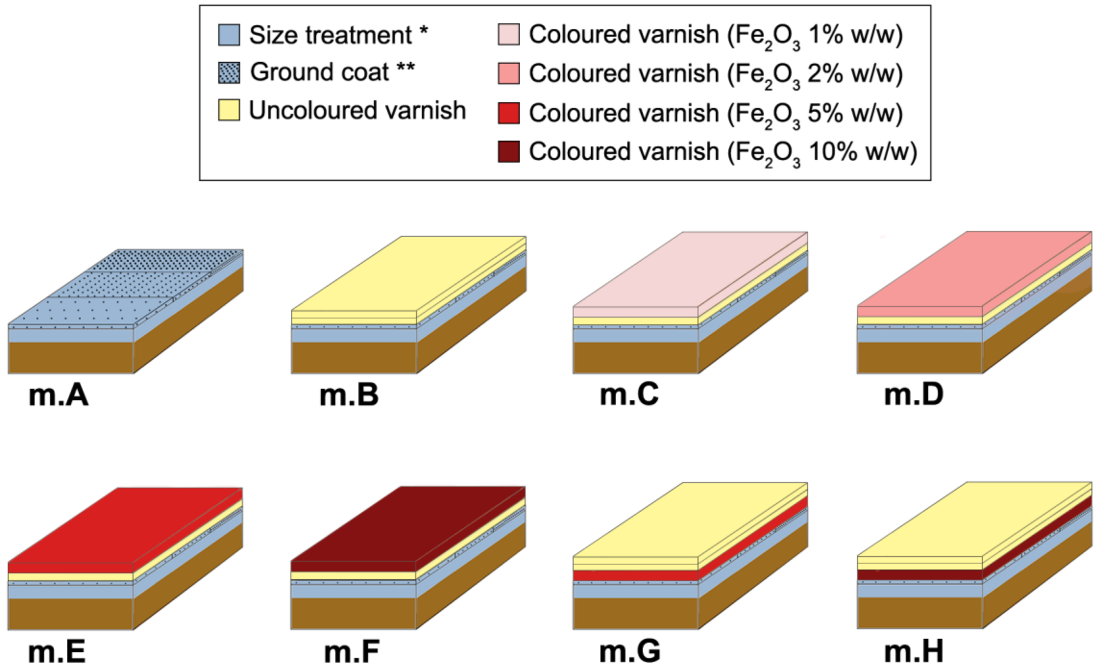

Figure 1.1 *Schematic representation of the mock-ups, with their multi-layered coating systems.*
** Size treatment: completely penetrated the wood; ** Ground coat: different black point abundances indicate different concentrations of talc in K-caseinate (respectively 1%, 5%, 10% w/w). Figure modified from [Invernizzi et al., 2021].*

1.2.2 Exposure to artificial solar ageing

Dried mock-ups (t_0 = 18h under UV lamps after varnishing) were symmetrically halved along the longitudinal direction (dimensions 15 cm x 2.5 cm x 0.3 cm each). The portion - of one half of each mock-up - characterized by a ground coat with 1% w/w of talc concentration in K-caseinate was exposed to artificial daylight in the ageing chamber Heraeus Suntest CPS (Hanau, Germany) equipped with a filtered Xenon lamp (non-ageing coated quartz glass simulating a 3 mm thick window glass, cutting wavelengths <300 nm). The average irradiation was 750 W/m^2 and the air-venting system of the chamber kept the internal temperature at about 50°C. Humidity was not controlled. The mock-ups were aged in two steps (t_1 = 25h and t_2 = 425h under simulated solar irradiation) in order to evaluate the response of the coating systems over time. The portion of each mock-up which underwent artificial solar ageing is highlighted in Fig. 1.2.

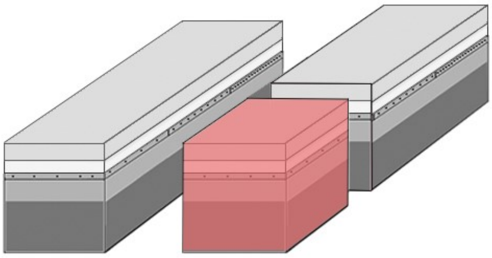

Figure 1.2 *Representative mock-up with the portion exposed to artificial solar ageing highlighted in red colour. This portion is characterized by 1% w/w of talc concentration in K-caseinate at the ground level. Figure published in [Invernizzi et al., 2021].*

1.2.3 Analytical strategy

Preliminary observations by UVIFL photography showed that a heterogeneous accumulation of the varnish film occurred, after its application, along the external longitudinal edges of the mock-ups. In Fig. 1.3, red dotted rectangles highlight these areas on the UVIFL photo of a representative mock-up (m.B) after it was symmetrically cut along the longitudinal direction. From this evidence, we decided to focus the analyses on the areas where the varnish was more uniformly laid, as displayed in Fig. 1.4.

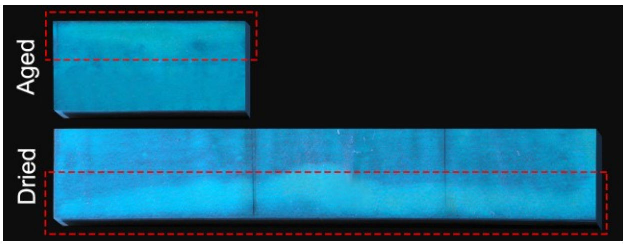

Figure 1.3 *UVIFL photo of a representative mock-up (m.B) with the heterogeneous varnish accumulation highlighted with red dotted rectangles. Dried (t_0) and aged (t_2) stages of the mock-up, after the halving, are shown.*

Three analytical spots were selected for each portion of the mock-ups characterized by different concentration of talc in K-caseinate at the ground level. In total, nine spots for each dried mock-up (t_0) were analysed by reflection FTIR spectroscopy, Raman spectroscopy, XRF and colorimetry (Fig. 1.4a). For each of these techniques, therefore, the whole set is composed of 9 x 8 = 72 data referred to dried mock-ups (t_0). Moreover, three spots for each aged mock-up (t_1, t_2) were analysed by reflection FTIR spectroscopy and colorimetry (Fig. 1.4a) in correspondence of the portion with 1% of talc in K-caseinate. Hence, 3 x 8 = 24 data referred to aged mock-ups (t_1) and 3 x 8 = 24 data referred to aged mock-ups (t_2) were further collected by these two techniques. As for OCT, instead, its application was limited to six dried mock-ups (i.e., m.A-m.D, m.F, m.H) by selecting a unique spot for each portion above mentioned (Fig. 1.4b). The OCT data set is thus composed of tomograms acquired on 3 x 6 = 18 areas of dried mock-ups (t_0) and 6 areas of aged mock-ups (t_1, t_2).

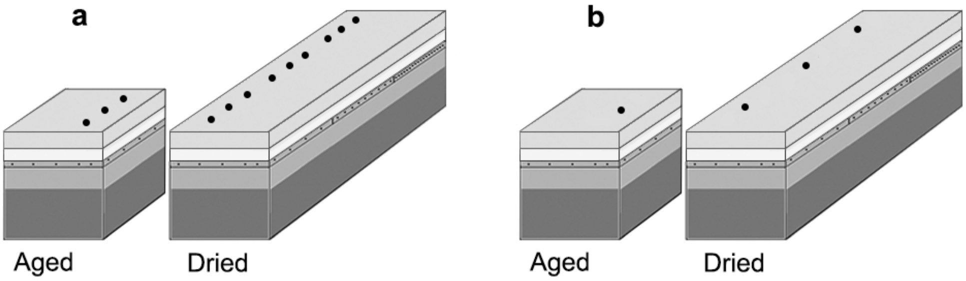

Figure 1.4 *Representative dried (t_0) and aged (t_1,t_2) mock-ups with the spots analysed by reflection FTIR spectroscopy, Raman spectroscopy, XRF and colorimetry (a) and by OCT (b). In (a), aged mock-ups were analysed only by reflection FTIR spectroscopy and colorimetry.*

In order to support the non-invasive analyses, micrometric fragments were detached from selected mock-ups (i.e., m.A, m.B, m.D, m.F, m.H), embedded into epoxy resin (Epofix Struers and Epofix Hardener with ratio 15:2) and cut to obtain cross-sections (Fig. 1.5). The surface was then dry-polished with silicon carbide fine sandpapers (1200-8000 mesh) and observed by optical microscopy under VIS and UV lights. Subsequently, microchemical analyses through ATR micro-FTIR spectroscopy and EDX probe were conducted on the cross-sectional samples. The morphological investigation of the coating systems was performed by SEM using both low and high vacuum conditions. Working in low vacuum mode did not require any sample preparation, while the high vacuum mode needed the metallisation of the sample by coating a graphite film with the Cressington 208HR sputter coater.

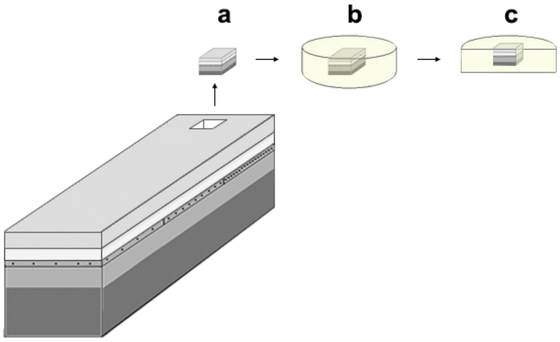

Figure 1.5 *Schematic representation of the following phases: micro-sampling (a), embedding of the fragment into epoxy resin (b) and cutting of the capsule to obtain cross-section (c).*

1.2.4 Multivariate statistical data analysis

IR and XRF data were explored from a multivariate point of view by chemometric tools. In particular, PCA was applied to the spectra collected on dried mock-ups (t_0) in order to extract the dominant patterns in the data matrix in terms of a complementary set of score and loading plots. In a typical *m* x *n* matrix, the rows (*m*) are filled with the objects and the columns (*n*) with the variables. The score plot involves the projection of the objects onto the principal components, which represent the directions of maximum variation of the original data, and the loading plot identifies which original variables have the largest effect on each principal component and how they correlate with one another.

As for the IR data set, we considered a matrix composed of as many rows as the number of spectra at t_0 (72) and as many columns as the number of wavenumbers (490). For this multivariate study, reflectance spectra are considered in the restricted interval 1400-400 cm^{-1} in order to investigate the impact of the varnish layers on the diagnostic bands produced by the mineral talc. First derivative (Savitzky-Golay) and mean centring spectral pre-treatments were applied.

As for the XRF data, we considered a matrix composed of as many rows as the number of spectra (72) and as many columns as the number of chemical elements selected as diagnostic for the stratigraphic study (i.e., Si, S, K, Fe) (4). The value of the XRF variables corresponds to the net area counts of the peak (Kα) of each element normalized to the average of net area counts of the coherent scattering Rh-Kα peak of the entire data set. Mean centring and scaling pre-treatments were combined.

The optimal number of PCs to be retained was selected by evaluating the scree plot [Bro et al., 2014]. PCA data analysis was performed using the Nonlinear Iterative Partial Least Squares (NIPALS) algorithm with the R-based software CAT (Chemometric Agile Tool), freely available on the site of the Italian Group of Chemometrics [CAT].

1.3 Results and discussion

1.3.1 Optical coherence tomography

OCT examinations allowed us to non-invasively measure the thickness of the coats lying above the wood support in the stratigraphies. Although no layer of K-caseinate - used to size the wood - was detected, it is probable that the sizing had enhanced the translucency of the wooden support since the near IR radiation penetrated the wood down to a depth of ca. 100 µm, which would not be the case for untreated wood. The OCT thickness measurements of surface coatings, supported by the observations of cross-sectional samples under OM, are reported in Table 1.1.

Table 1.1 *Thickness measurements (µm) of the different stratigraphic levels of the mock-ups (n.d. not detected). Estimated thickness measurement uncertainty is 3 µm (see appendix I). Table published in [Invernizzi et al. 2021].*

Stratigraphic level	**Mock-up**							
	m.A	**m.B**	**m.C**	**m.D**	**m.E**	**m.F**	**m.G**	**m.H**
Size treatment (S)*	n.d.	n.d.	n.d.	n.d.	n.d.	n.d.	n.d.	n.d.
Ground coat (G)	5	5	5	5	5	5	5	5
Uncoloured varnish (Uv)	-	20**	10	10	10	10	20**	20**
Coloured varnish (Cv)	-	-	20	20	20	20	20	20
Total thickness	5	25	35	35	35	35	45	45

** Size treatment: completely penetrated the wood. ** The thickness of 20 µm is the result of two varnish applications (10 µm thick each).*

Interestingly, it was possible to identify three cases - in the mock-up series - where the technique was not able to discriminate adjacent layers, and consequently measure their thicknesses accurately: (i) comparable intensity of light scattering at particles dispersed in different layers, as for instance observed for the ground (talc) and coloured varnish (hematite) in m.H (Fig. 1.6a), (ii) close in time applications of transparent layers characterized by the same refractive index, as occurred for the two uncoloured linseed oil-colophony varnish layers of m.H (Fig. 1.6a), and (iii) layer with very high concentration of particles concealing visibility of a thin transparent undercoat, as the case of m.F where the varnish film containing hematite in concentration of 10% is laid over ca. 10 µm of uncoloured varnish (Fig. 1.6b). In the last case, the high scattering and absorbing of near IR radiation in the pigmented layer totally obscured the underlying thin transparent film and the interface between them, which was not the case with pigment concentrations of 1% and 2% .

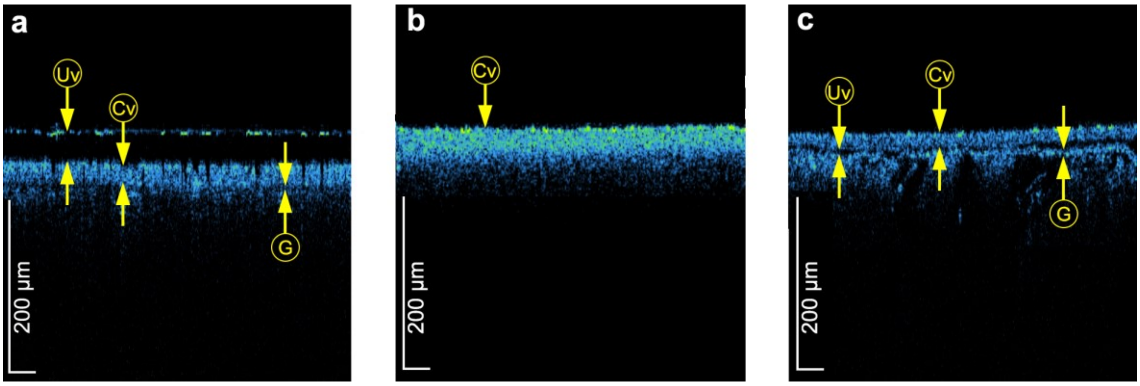

Figure 1.6 *OCT analysis of the mock-ups: m.H (a) and m.F (b) in correspondence of the areas with talc concentration of 1%, and m.D (c) in correspondence of the area with talc concentration of 10%. Arrows indicate the stratigraphic layers (Uv: uncoloured varnish, Cv: coloured varnish, G: ground coat). In (b) the layers G and Uv, as well as the lower boundary of Cv, are not defined for the reasons explained in the text. Figure modified from [Invernizzi et al., 2021].*

In case of semi-scattering and scattering layers, OCT was able to detect the presence of particles and their distribution in the stratigraphies. However, the “grains” in the structures visible in OCT tomograms should not be always interpreted as realistic imaging of the particles. For instance, in the mock-up series, the ground and the coloured varnish appeared as grainy structures which could be discriminated from each other only due to the presence of an interlayer of transparent varnish lying between them. Within each layer, however, the individual scattering centres could not be distinguished from each other (Fig. 1.6c). This evidence was found for both hematite and talc, acting as pigment and filler respectively, and it can be likely ascribed to jointly contributing factors related to the particles: (i) size and average distance among the particles (also at a minimum concentration of 1%) lower than the lateral resolution of the instrument, and (ii) uniformity of dispersion. It is important to point out, moreover, that every layer scattering light weakly or moderately is seen in OCT imaging as composed of small dots (speckles) whose size depends on coherence properties of probing light and instrument’s optics rather than the actual size of scattering centres. To investigate the real size and distribution of both hematite and talc grains, SEM observations on the cross-section of a representative mock-up stratigraphy were performed (Fig. 1.7).

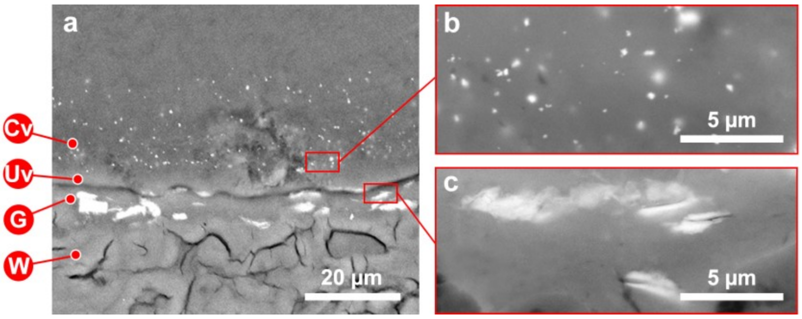

Figure 1.7 *BSE-SEM images of the mock-up m.D (a), with hematite (b) and talc (c) particles at higher magnifications highlighted in red rectangles. Letters refer to the stratigraphic layers (Cv: coloured varnish, Uv: uncoloured varnish, G: ground coat, W: wood).*

Another consideration concerned the OCT sensitivity in discriminating different concentrations of filler or pigment. As the particle concentration increases, the tomograms generally show a slight increment in the scattering intensity - with the colour varying from blue to green - as well as in the local concentration of dots, and vice versa. In particular, these variations resulted more evident for the coloured varnish (Fig. 1.8a-c) than for the ground coat (Fig. 1.8d-f), this last being laid in direct contact with the wood support.

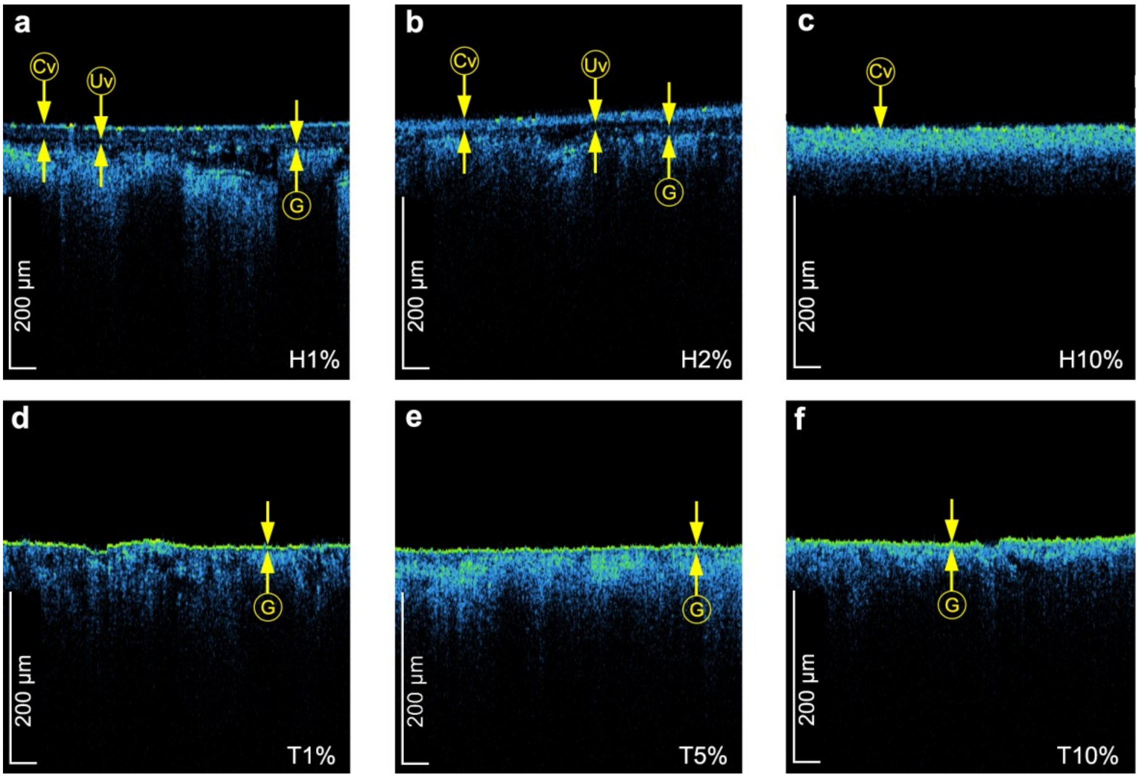

Figure 1.8 *OCT analysis of the mock-ups: m.C (a), m.D (b) and m.F (c), with the coloured varnish characterized by increasing concentrations of hematite (respectively, H1%, H2%, H10%, where the letter H stands for hematite), and of the mock-up m.A (d-f), with the ground coat characterized by increasing concentrations of talc (respectively, T1%, T5%, T10%, where the letter T stands for talc). Arrows indicate the stratigraphic layers (Uv: uncoloured varnish, Cv: coloured varnish, G: ground coat). In (c) the layers G and Uv, as well as the lower boundary of Cv, are not defined for the reasons explained in the text. Figure modified from [Invernizzi et al., 2021].*

Finally, an interesting phenomenon strictly involved the coloured varnish of some stratigraphies under investigation. The pigmented oil-colophony varnish in m.H (Fig. 1.6a), in fact, appeared to be more transparent to the near IR radiation - or less scattering - than that of the mock-up m.F (Fig. 1.6b). It must be underlined that the hematite concentration, as well as the thickness of the coloured layer, are identical in both the mock-ups. The observed difference in light scattering intensity can be likely ascribed to the transparent uncoloured varnish which, covering the pigmented one in m.H, caused a change in its refractive index. On the contrary, the uncoloured varnish in m.F is positioned underneath the coloured one.

1.3.2 Reflection FTIR spectroscopy

By the FTIR study, we wanted to assess to what extent the different varnish films affect the detection of spectral bands produced by the organic and inorganic components of the underlying ground coat, respectively K-caseinate and talc. This technique, in fact, provides information about the chemical composition of the most surface layers of the stratigraphy, with a depth penetration depending on the characteristics of the materials under investigation (e.g., absorption index, thickness, etc.). Working in reflection mode, the integrity of the object is fully granted. However, the main difficulty consists in the interpretation of the reflection spectra, since they are affected by distortions of band shape, intensity and absorption frequency compared with the transmission spectra. These anomalies depend on different factors like the refraction (*n*) and absorption (*k*) indices as well as the surface roughness, which contribute to the extension of the specular (or surface) and diffuse (or volume) reflection components. Specifically, the Fresnel's law rules the specular contribution producing derivative-like bands with materials characterized by $k < 1$ and *Reststrahlen* (or inverted) bands when $k >> 1$, whereas the spectral signals originated from the diffuse contribution are comparable to those acquired in transmission mode with the exception of changes in the relative intensity of bands [Fabbri et al., 2001; Miliani et al., 2011]. The application of specific data-processing algorithms, such as the Kramers-Kronig Transformations (KKT), produces absorbance spectra whose accuracy and reliability depend on the fact that specific required conditions are fulfilled [Griffiths and De Haseth, 2007]. In previous studies, in particular, we proved that KKT work correctly with spectra collected on optically flat, smooth organic layers as the varnish ones [Invernizzi et al., 2016; Invernizzi et al., 2017; Invernizzi et al., 2018]. In other conditions, the reflection spectra need to be studied without corrections.

From the mock-up analysis, the diagnostic bands of K-caseinate (νN-H at 3300 cm^{-1}, νC=O or amide I at 1650 cm^{-1}, combination of νC-N and δN-H or amide II at 1540 cm^{-1}) [Invernizzi et al., 2018; Stuart, 2004] were merely identified in the KKT spectra acquired on the mock-up m.A, where the ground surface is directly exposed. Therefore, any overlying varnish coat here considered - included the ca. 20 μm of uncoloured varnish in m.B - made the proteinaceous bands undetectable (Fig. 1.9a).

As for the talc, the picture appeared rather more complicated from a spectral point of view because its bands behaved differently from each other. Three groups of *Reststrahlen* bands were firstly identified as diagnostic of the talc in the reflectance spectra of these stratigraphies, namely (i) ν_{as}Si-O (ν_3) at 1015 cm^{-1}, (ii) ν+δSi-O (ν_4) at 670 cm^{-1} and the third one (iii) comprising in-plane δMg-O (ν_7) at 465 and 450 cm^{-1}, δSi-O (ν_5) at 425 cm^{-1} and δSi-O at 395 and 385 cm^{-1} [Farmer, 1958; Salisbury et al., 1987; Miliani et al., 2011] (Fig. 1.9b, spectrum of m.A). A general trend was then recognized by observing the spectra collected on the mock-up areas characterized by the same talc concentration in the ground (Fig. 1.9b): the intensity of the talc marker bands diminished with the increase in the varnish coating thickness and in the hematite concentration. Interestingly, the signals at 670 and around 400-300 cm^{-1} - albeit reduced in intensity - are always detectable in the mock-ups differently from the signal at 1015 cm^{-1} (Fig. 1.9b), whose intensity dramatically decreased up to completely disappearing. This suggests that, in presence of multi-layered structures, the silicate mineral can be identified merely by its lower-wavenumber bands.

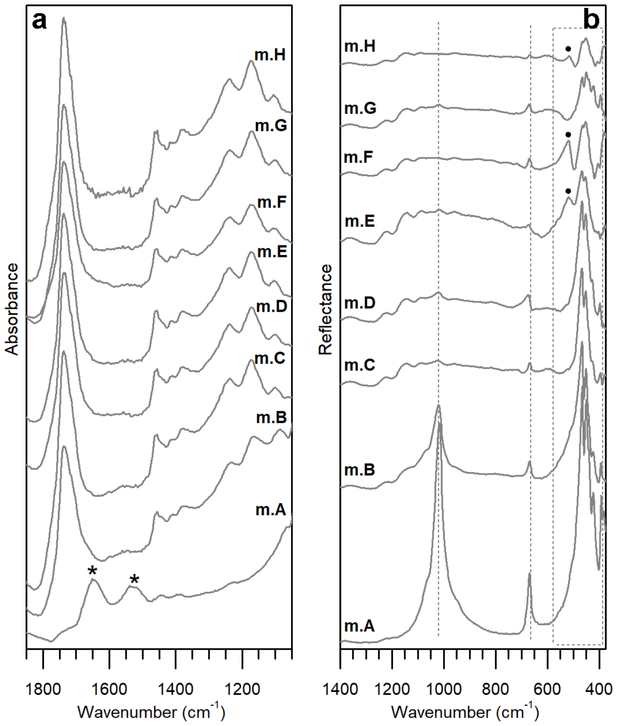

Figure 1.9 *Representative reflection FTIR spectra collected on the mock-ups in correspondence of the areas characterized by talc concentration of 1%. The spectra after (a) and before (b) KK transformations are displayed for the study of organic and inorganic compounds, respectively. Marker bands of K-caseinate (asterisk symbol), talc (dotted line and rectangle) and hematite (round) are highlighted. Figure published in [Invernizzi et al., 2021].*

The intensity variation was confirmed by the PCA analysis of the dataset in the restricted range 1400-400 cm^{-1}. The PC1 vs PC2 scatter score plot (accounting for 81.4% of the total variance) shows a clear separation between the spectra acquired on m.A and m.B, with negative PC1 score values, and the spectra from all the other mock-ups, with positive - or null - PC1 scores (Fig. 1.10, left graph). As visible in Fig. 1.9b, the band intensities of talc in m.A and m.B spectra are in fact the most pronounced of the entire dataset.

From the spectra, moreover, it is evident how the presence of varnish layers led to a marked change in the relative intensities of the three groups of talc marker bands (Fig. 1.9b).

As concerns the hematite pigment, the presence of its derivative marker band at around 530 cm^{-1} (maximum point) was detected in the spectra collected on m.E, m.F and, more weakly, on m.H [Bikiaris et al., 1999] (Fig. 1.9b). The other characteristic band of Fe_2O_3 - falling at about 480 cm^{-1} - was not considered because of its overlapping with the third group of talc signals above identified as (iii). When the pigmented layer is exposed (m.E, m.F), hence, the iron oxide can be revealed if its concentration is at least of 5%; when it is covered by ca. 20 μm of uncoloured varnish (m.H), instead, the minimum concentration to be detected is 10%. Interestingly, spectra of these mock-ups group in the area of the PC1 vs PC2 score plot mostly characterized by positive PC1 and negative PC2 score values (Fig. 1.10, right graph).

While the PC1 direction mainly described the intensity variation of the bands, the second PC seemed to be affected by the variation in their shape. As shown in the loading plot of PC1 and PC2 (Fig. 1.11), the highest variations - for both the PCs - occurred in the lowest-wavenumber region (i.e., original variables between 400 and 500).

Finally, it is worth reporting that the reflection FTIR spectroscopy was not able to discriminate different concentrations of talc in the ground layer: band intensities related to that mineral, in fact, did not significantly change in the three areas of each mock-up corresponding to concentrations of 1%, 5% and 10%.

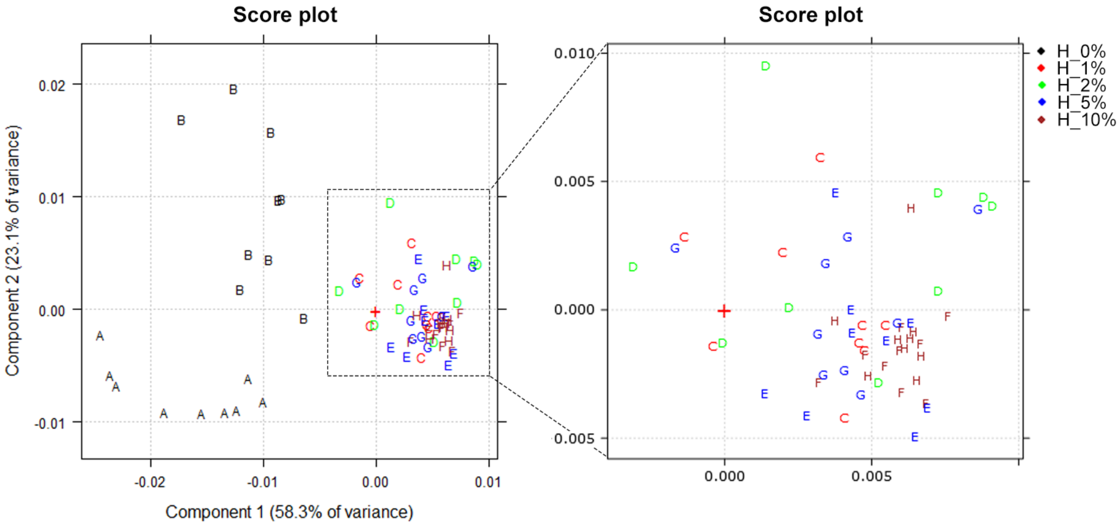

Figure 1.10 *Results of the PCA performed on the reflection FTIR spectral dataset in the range 1400-400 cm^{-1}: PC1 vs PC2 scatter score plot (left) and its magnification in correspondence of the region enclosed in the dotted rectangle (right). Letters indicate the mock-ups under investigation; colours highlight different hematite concentrations in the coloured varnish as reported in the legend (i.e., H_0%, H_1%, H_2%, H_5% and H_10%, where the letter H stands for hematite). Figure published in [Invernizzi et al., 2021].*

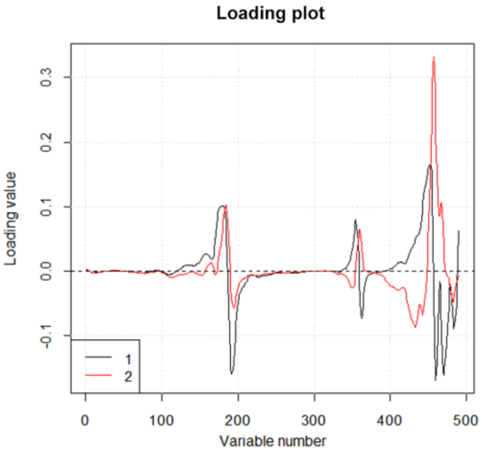

Figure 1.11 *Results of the PCA performed on the reflection FTIR spectral dataset in the range 1400-400 cm^{-1}: loading plot of PC1 and PC2. Figure published in [Invernizzi et al., 2021].*

The non-invasive approach was supported by the application of micro-FTIR spectroscopy to the cross-sectional samples, which allowed us to gather spatially-resolved chemical information on the stratigraphies, with a clear distribution of their different components. Chemical maps were acquired in ATR imaging mode and a representative result, related to m.H (aged t$_2$), is reported in Fig. 1.12. It is worth reporting that the spatial resolution achievable by micro ATR-FTIR imaging with Ge crystal is ca. 10 µm (up to 3-4 µm in specific conditions [Chan and Kazarian, 2003]), compared to the 5 millimetres of the portable, non-contact FTIR spectrometer working in reflection mode (see appendix I).

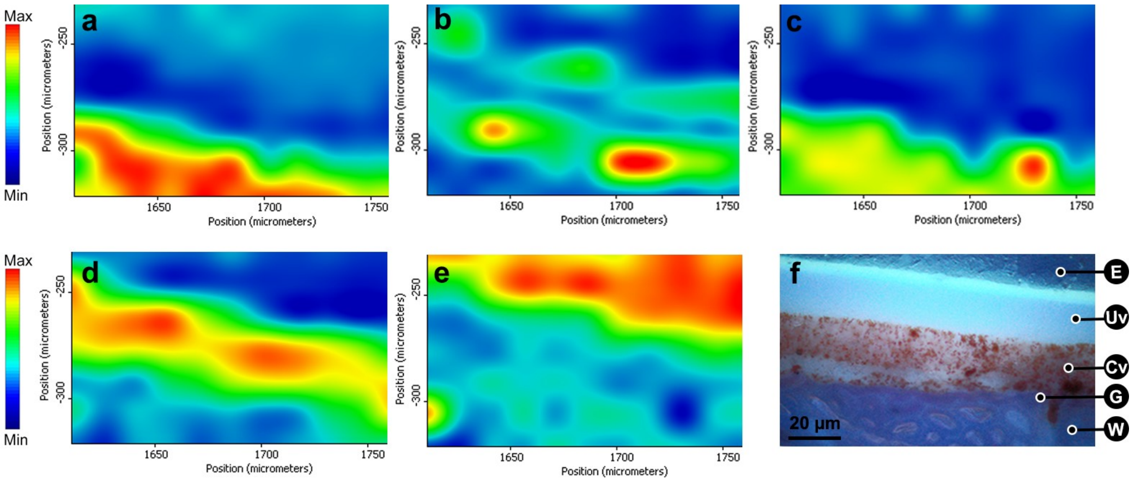

Figure 1.12 *FTIR-ATR chemical maps (a-e) and UV-light optical microscopy image (f) of the cross-sectional mock-up m.H (aged t$_2$). The colour scale in each map refers to the intensity of the marker bands at the wavenumber value selected as diagnostic of wood (a), K-caseinate (b), talc (c), oil-colophony varnish (d) and epoxy resin (e). Letters in (f) indicate the stratigraphic layers (E: epoxy resin, Uv: uncoloured varnish, Cv: coloured varnish, G: ground coat, W: wood).*

In Fig. 1.12, the maps were obtained by selecting the diagnostic bands of the different materials involved in the stratigraphy of mock-up m.H (aged t$_2$), as reported in Table 1.2.

These bands are highlighted in Fig. 1.13, where the spectra acquired in correspondence of each stratigraphic layer are displayed.

Table 1.2 *Wavenumber values, and their assignment, of the ATR-FTIR bands selected for each material of the mock-up m.H (aged t_2) to obtain chemical maps.*

Material	Wavenumber (cm^{-1})	Assignment	Chemical map
Maple wood	1040	v_{as}C-O	Fig. 1.12a
K-caseinate	1650	vC=O	Fig. 1.12b
Talc	1015	v_{as}Si-O	Fig. 1.12c
Linseed oil-colophony varnish	1725	cC=O	Fig. 1.12d
Epoxy resin	1240	vC-O-C (oxirane group)	Fig. 1.12e

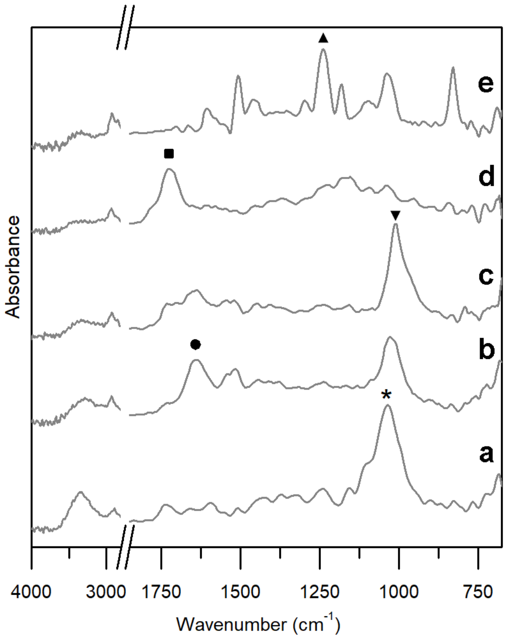

Figure 1.13 *FTIR-ATR spectra of the materials composing the coating system of the cross-sectional mock-up m.H (aged t_2): wood (a), K-caseinate (b), talc (c), oil-colophony varnish (d) and epoxy resin (e). Symbols highlight the wavenumber values of the bands selected as diagnostic for the creation of the maps displayed in figure. 1.12: * (V_{as}C-O of wood at 1040 cm^{-1}), ● (vC=O of K-caseinate at 1650 cm^{-1}), ▼ (v_{as}Si-O of talc at 1015 cm^{-1}), ■ (vC=O of oil-colophony varnish at 1725 cm^{-1}) and ▲ (vC-O-C of epoxy resin at 1240 cm^{-1}).*

By comparing the UV-light optical microscopy (Fig. 1.12f) and FTIR (Fig. 1.12a-e) images, it is evident how the chemical maps were able to discriminate all the different layers of the coating system, except for those composed of the same varnish but differentiating in the presence of the colouring agent (Fig. 1.12d). In fact, the lower wavenumber limit of the spectral range (equal to 675 cm^{-1}) hindered the detection of the hematite marker bands falling at around 570 and 480 cm^{-1} (Fig. 1.14). Moreover, at the wavenumber selected as diagnostic of the talc (i.e., 1015 cm^{-1}), also the wood absorbs at medium-high intensity: as a result, the map displayed in Fig. 1.12c clearly shows a round mineral grain, highlighted in red colour due to its high absorption intensity, and the underneath region - related to the wood - is mostly coloured in yellow. On the other hand, the wavenumber value selected as diagnostic of the wood (i.e., 1040 cm^{-1}) turned out to weakly interfere with the band of the talc, and the map of Fig. 1.12a better discriminates the wood from the upper ground layer.

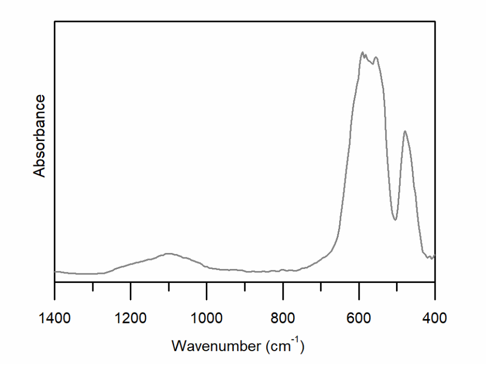

Figure 1.14 *FTIR spectrum of the hematite powder acquired in transmission mode at room temperature.*

1.3.3 Raman spectroscopy

In the range from 3200 to 300 cm^{-1}, Raman spectra collected on the mock-ups are all characterized by the predominant profile of the wood. Signals produced by linseed oil-colophony mixture and K-caseinate were not revealed in any of the stratigraphies, suggesting that the thicknesses of ground and varnish layers are too low to be investigated by this portable spectrometer. As evident by this result, the incident lasers directly arrived at the wooden support without being scattered by the organic components of the overlying coating system. Also the bands of the mineral talc were never detected, not even in m.A where the ground is exposed.

The hematite bands occurring in the investigated spectral region are positioned at 608, 495 and 408 cm^{-1}. These signals, assigned to the Fe-O stretching vibrations [Košařová et al., 2013], are well visible in the spectra of m.E, m.F and m.H, with their characteristic relative Raman intensities (Fig. 1.15). However, since the weaker and broader band centred at 495 cm^{-1} overlaps with a wood signal at the same frequency, we could not consider this band as diagnostic of the pigment in these stratigraphies and, consequently, it was not highlighted in Fig. 1.15. By the analysis of the spectra collected on the mock-ups with the coloured varnish exposed, the intensity of the marker band at 408 cm^{-1} was found to gradually increase from m.C to m.D, m.E and m.F, according to the increment in the hematite concentration (Fig. 1.15). With the intensity increase, also the shape of this band becomes better resolved and sharper. In the mock-up series above mentioned, the signal at 608 cm^{-1} is instead evident only with varnish layers characterized by Fe_2O_3 concentrations of 5% (m.E) and 10% (m.F).

Interestingly, the presence of the uncoloured varnish at the top of the stratigraphy turned out to affect the intensity of the hematite bands. In particular, the spectrum acquired on m.G merely shows the band at 408 cm^{-1}, with a far lower intensity compared to the mock-up with the same pigment concentration of 5% (m.E). Furthermore, a broad band centred at 620 cm^{-1} was detected in this spectrum, but both the shape and the wavenumber shift allowed us to attribute it to the wood. As for the spectrum from m.H, the diagnostic bands of the hematite are well visible, but appearing less intense than those of the corresponding - in terms of Fe_2O_3 concentration - mock-up m.F.

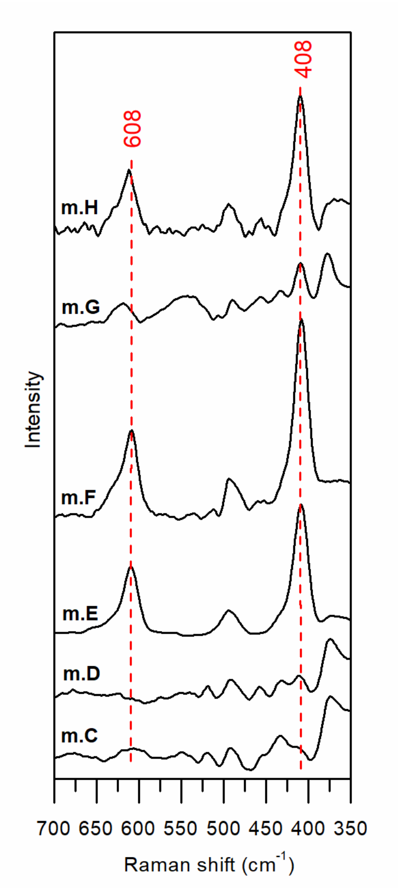

Figure 1.15 *Representative Raman spectra collected on the mock-ups in correspondence of the areas characterized by talc concentration of 1%. Marker bands of hematite (red dotted line) are highlighted. Figure published in [Invernizzi et al., 2021].*

1.3.4 X-ray fluorescence spectroscopy

XRF investigation was aimed at observing the influence of the differently overlapped layers on the net area counts related to four chemical elements, namely Si (Kα = 1.740 keV), S (Kα = 2.309 keV), K (Kα = 3.314 keV), and Fe (Kα = 6.405 keV). These elements were selected because representative of the materials composing the mock-up stratigraphies (i.e., Si: talc; S: potassium caseinate and, as impurity, talc; K: potassium caseinate; Fe: hematite and, as impurity, talc). It is worth remembering that the elemental qualitative composition of the mineral talc is reported in 1.2.1. The normalized values of the net area counts are reported in Table 1.3.

As regards Si (Fig. 1.16a), XRF results highlighted a significant variation in the area counts within the mock-up set. In particular, high counts of Si were detected in m.A -

where the ground is directly exposed - while its values significantly decreased nearly to the detection limit in m.B, m.C, m.D, m.E, and m.G, as a twofold consequence of the layer application on the ground and of the low atomic weight of silicon [Fiocco et al., 2018]. The 10% of Fe_2O_3 concentration in the coloured varnish (m.F), together with the superimposition of additional uncoloured varnish layers (m.H), then brought the counts of Si and S up to zero in the two mock-ups in exam (Fig. 1.16a,b). Observing the elemental trends in relation to the talc concentration in the K-caseinate binder for each mock-up, moreover, it was found a general increase in the Si-Kα line intensity (Fig. 1.16a) and, complementarily, a decrease in the counts of S and K, both mainly ascribed to the K-caseinate (Fig. 1.16b,c): this behaviour can be justified by the decrease in the amount of binder as the filler concentration increases in the mixture, and vice versa.

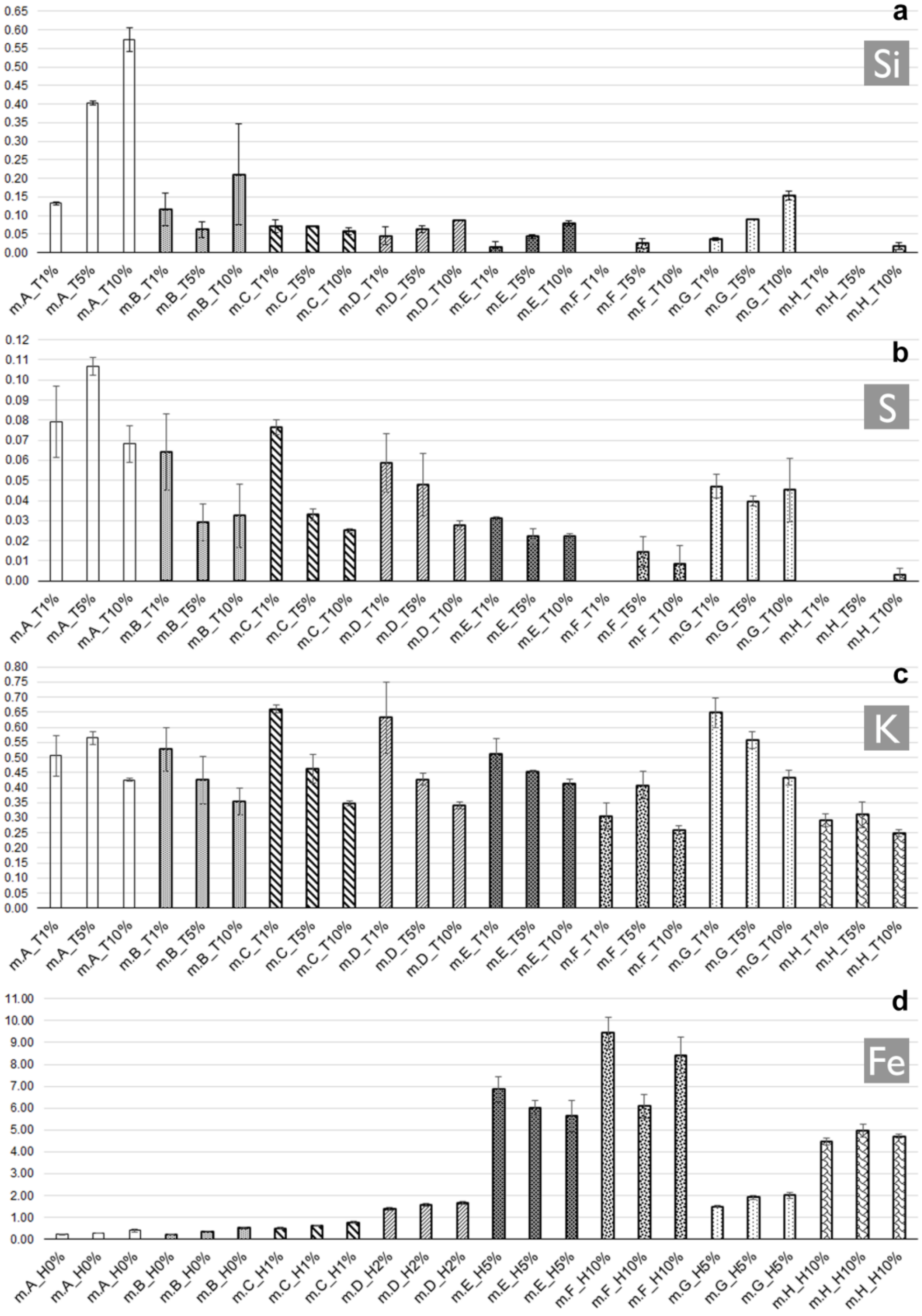

Figure 1.16 *Net area count estimation of the peak Kα of Si (a), S (b), K (c) and Fe (d) detected by XRF, with the related Standard Deviation of Mean (SDOM). Each bar corresponds to the average of three measurements, normalized to the mean value - calculated on the whole data set - of the net area counts of the coherent scattering peak (Kα) of Rh. For all the elements investigated, the three bars per mock-up correspond to the areas with different talc concentrations (i.e., T1%, T5%, T10%, where the letter T stands for talc), as highlighted in the X-axis labels of graphs a-c. In the graph d, the x-axis labels highlight the different hematite concentrations (i.e., H0%, H1%, H2%, H5%, H10%, where the letter H stands for hematite). Numerical values are reported in Table 1.3.*
Figure published in [Invernizzi et al., 2021].

Table 1.3 *Net area count estimation of the peak Kα of the elements detected by XRF on the different stratigraphic systems of the mock-ups, with the related Standard Deviation of Mean (SDOM). Each value corresponds to the average of three measurements, normalized to the mean value - calculated on the whole data set - of the net area counts of the coherent scattering peak (Kα) of Rh. The second and third columns indicate the percentages of talc in K-caseinate (T1%, T5%, T10%) and of hematite in varnish (H0%, H1%, H2%, H5%, H10%), respectively. Table published in [Invernizzi et al., 2021].*

Name	Talc %	Fe_2O_3 %	Si	SDOM (Si)	S	SDOM (S)	Fe	SDOM (Fe)	K	SDOM (K)
m.A	T1%	H0%	0.133	0.004	0.079	0.018	0.222	0.015	0.506	0.066
	T5%		0.404	0.006	0.107	0.005	0.278	0.011	0.565	0.021
	T10%		0.574	0.031	0.068	0.009	0.402	0.060	0.425	0.005
m.B	T1%	H0%	0.116	0.044	0.064	0.019	0.239	0.023	0.527	0.073
	T5%		0.063	0.021	0.029	0.009	0.358	0.001	0.425	0.078
	T10%		0.211	0.137	0.033	0.016	0.520	0.039	0.356	0.044
m.C	T1%	H1%	0.072	0.017	0.076	0.004	0.512	0.039	0.661	0.013
	T5%		0.070	0.001	0.033	0.003	0.608	0.017	0.463	0.047
	T10%		0.058	0.009	0.025	0.001	0.775	0.038	0.347	0.008
m.D	T1%	H2%	0.045	0.025	0.059	0.014	1.396	0.059	0.632	0.119
	T5%		0.063	0.009	0.048	0.015	1.578	0.073	0.428	0.020
	T10%		0.086	0.001	0.028	0.002	1.669	0.073	0.341	0.013
m.E	T1%	H5%	0.014	0.014	0.031	0.001	6.849	0.585	0.513	0.050
	T5%		0.043	0.006	0.023	0.003	6.022	0.343	0.454	0.002
	T10%		0.079	0.006	0.022	0.001	5.625	0.703	0.413	0.014
m.F	T1%	H10%	-	-	-	-	9.441	0.729	0.305	0.043
	T5%		0.025	0.012	0.014	0.008	6.082	0.541	0.408	0.045
	T10%		-	-	0.009	0.009	8.407	0.818	0.258	0.014
m.G	T1%	H5%	0.036	0.004	0.047	0.006	1.503	0.042	0.649	0.048
	T5%		0.090	0.002	0.040	0.002	1.915	0.082	0.558	0.029
	T10%		0.154	0.012	0.045	0.016	2.010	0.150	0.434	0.025
m.H	T1%	H10%	-	-	-	-	4.476	0.154	0.292	0.021
	T5%		-	-	-	-	4.969	0.286	0.310	0.042
	T10%		0.018	0.009	0.003	0.003	4.713	0.083	0.249	0.012

A more accurate picture was obtained by combining XRF spectral results with the PCA analysis performed on the entire XRF dataset. The PC2 vs PC4 scatter score plot (accounting for 23.1% of total variance) (Fig. 1.17a) was chosen for representation because it clearly reveals a separation of the objects on the basis of different talc concentrations in the K-caseinate binder. Positive PC2 score values are related to spectra collected on the areas with 10% of talc (Fig. 1.17a, green objects) and, consequently, characterized by higher Si counts. Negative PC2 values are instead referred to spectra with increasing values of K, collected on the areas with 5% (Fig. 1.17a, red objects) and 1% (Fig. 1.17a, black objects) of talc in K-caseinate. As visible from the biplot in Fig. 1.17b, objects with high Si counts are mainly scattered in the first quadrant, and those with progressively higher values of K are grouped in second and third quadrants.

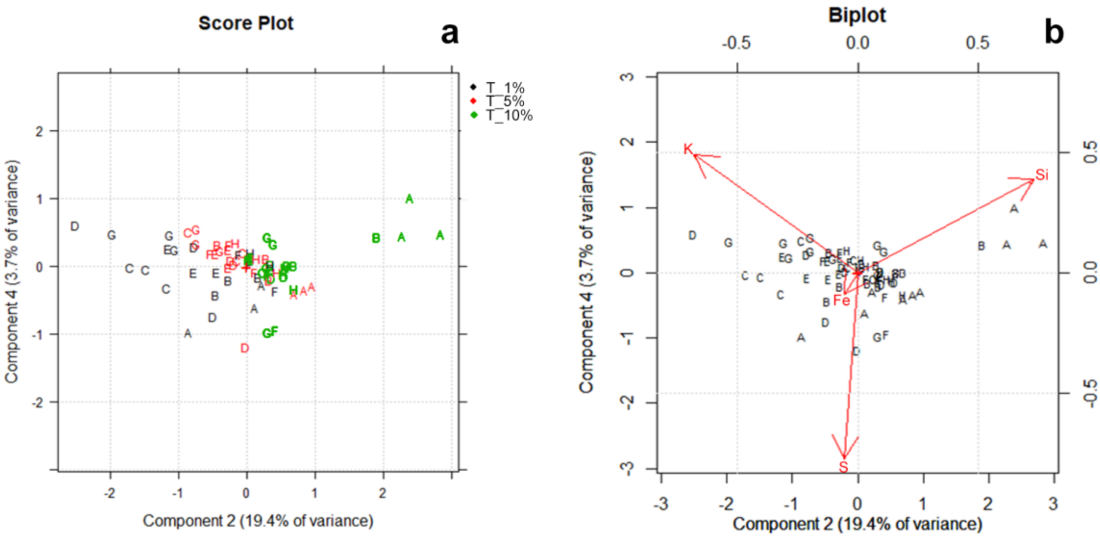

Figure 1.17 *Results of the PCA performed on the XRF spectral dataset: PC2 vs PC4 scatter score plot (a) and the related biplot (b). Letters in (a) and (b) indicate the mock-ups under investigation; colours in (a) highlight different talc concentrations in the ground as reported in the legend (i.e., T_1%, T_5% and T_10%, where the letter T stands for talc). Figure published in [Invernizzi et al., 2021].*

XRF results related to Fe (Fig. 1.16d) appeared to be strongly affected by the hematite concentration and by the presence of uncoloured varnish at the top of the stratigraphy. In fact, the Fe-Kα line intensity progressively increased from m.C and m.D, respectively with 1% and 2% of hematite in the coloured film, up to m.E and m.F, where the concentration reaches respectively 5% and 10%. On the other hand, the presence of ca. 20 µm of uncoloured varnish dramatically affected the net area counts of the element: spectra recorded on m.G and m.H show Fe counts almost halved if compared to those collected respectively on the mock-ups m.E and m.F.

Exploring the PC1 vs PC3 scatter score plot (Fig. 1.18a), which accounts 76.8% of the total variance, objects with negative PC1 and positive PC3 score values are well grouped in the second quadrant. These objects are characterized by higher Fe counts, as visible in the biplot of Fig. 1.18b, and are related to m.E and m.F. As for the m.G group, the presence of uncoloured varnish over the coloured one likely affected the PC score values: in this case, objects are grouped around the origin of axes, similarly to m.D. As visible in Fig. 1.16d, the net area counts of Fe in m.G and m.D are in fact comparable although the concentration of Fe_2O_3 in m.G is much higher than that of m.D. Also for the mock-up m.H, the external uncoloured varnish brought these objects at a certain distance from the group of m.E and m.F, falling in the third quadrant.

A final consideration concerns the mock-up m.C, characterized by 1% of hematite concentration: the XRF investigation was not able to clearly discriminate it from the non-pigmented mock-ups.

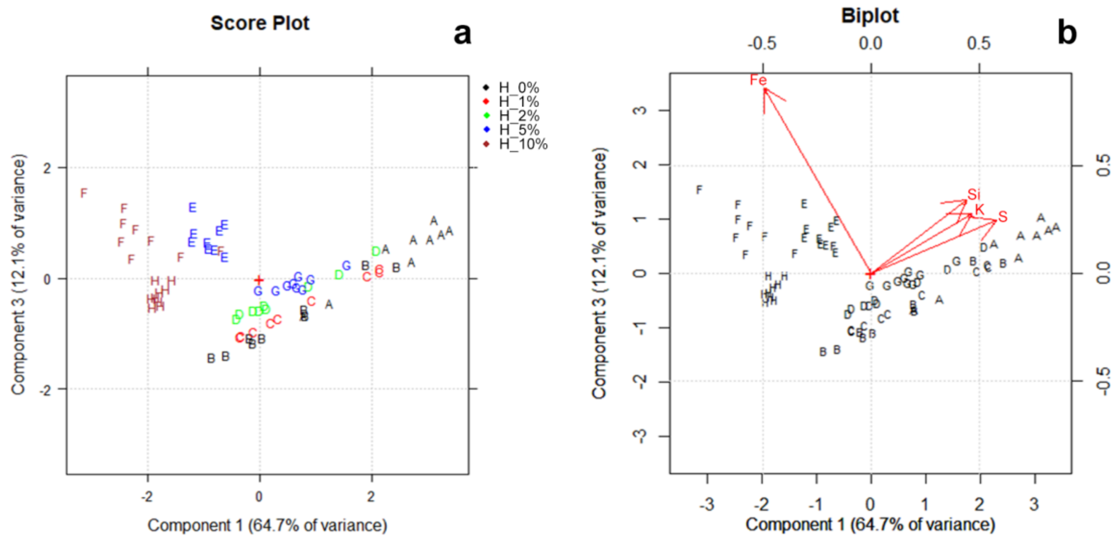

Figure 1.18 *Results of the PCA performed on the XRF spectral dataset: PC1 vs PC3 scatter score plot (a) and the related biplot (b). Letters in (a) and (b) indicate the mock-ups under investigation; colours in (a) highlight different hematite concentrations in the coloured varnish as reported in the legend (i.e., H_0%, H_1%, H_2%, H_5%, H_10%, where the letter H stands for hematite). Figure published in [Invernizzi et al. 2021].*

1.3.5 Artificial ageing

Figure 1.19 shows the time evolution of L*, a*, b* coordinates and the total colour variation ΔE* as a function of the ageing time of the layered mock-ups.

The mock-ups generally underwent the twofold effect of darkening and yellowing as a result of the decrease in L* and increase in b*, respectively. This effect was expected by the ageing of oil-colophony varnishes [Ciofini et al., 2016], representing one of the main conservation problems in paintings [Colombini et al., 2000]. Interestingly, the behaviour above described was also observed - in a marked way - in m.A, where neither uncoloured nor coloured varnishes are present: the wooden support was mostly responsible for the great variation recorded in m.A. In the light of this, we can suppose that the variations observed in the mock-ups with transparent or semi-transparent layers (i.e., m.B, m.C and mD) partially derive from the underneath wood. Within the series characterized by negative ΔL^* and positive Δb^* variations, some mock-ups (namely m.A, m.B, m.C and m.G) showed an increase in the a* values: these changes indicate a shift towards a brown-orange hue [Ciofini et al., 2016].

An opposite trend, instead, was found for those mock-ups (m.E and m.F) where the pigmented varnish is directly exposed and its Fe_2O_3 concentration is high (5% and 10%, respectively): in these conditions, the simultaneous increase in L* and decrease in b* occurred.

Particular cases are finally represented by the mock-up m.D, which showed a discolouration behaviour towards the yellow-green direction (increase in b* and decrease in a*), and by the mock-up m.H, where a* values increased and b* values decreased over time.

After 25h of exposure $\Delta E^*_{t1\text{-}t0}$ varied between 2.3 and 5.3, with the minimum and maximum variations observed in m.H and m.B, respectively. The total colorimetric variation in m.B can be mainly ascribed to the b* increase, and after additional 400h of ageing the further significant increment in b* and decrease in L* determined a value of $\Delta E^*_{t2\text{-}t1} = 13.1$ for this mock-up, with a total $\Delta E^*_{t2\text{-}t0} = 16.6$. The greatest total colour variation between t_1 and t_2 ageing stages, however, was observed in m.A ($\Delta E^*_{t2\text{-}t1} = 19.7$), with L* values varying from 77.2 to 66.9 and b* values from 19.0 to 34.7. As aforementioned, this important variation was attributed to the wood used as support of the stratigraphy. On the other hand, the mock-up m.D - which is the only one of the series that underwent a discolouration towards the yellow-green hue - was characterized by the minimum total colour variation ($\Delta E^*_{t2\text{-}t0} = 4.4$), followed by m.G ($\Delta E^*_{t2\text{-}t0} = 7.3$) and m.H ($\Delta E^*_{t2\text{-}t0} = 9.4$). For the other mock-ups, the total variation of colour is comprised between ca. 14 and 18.

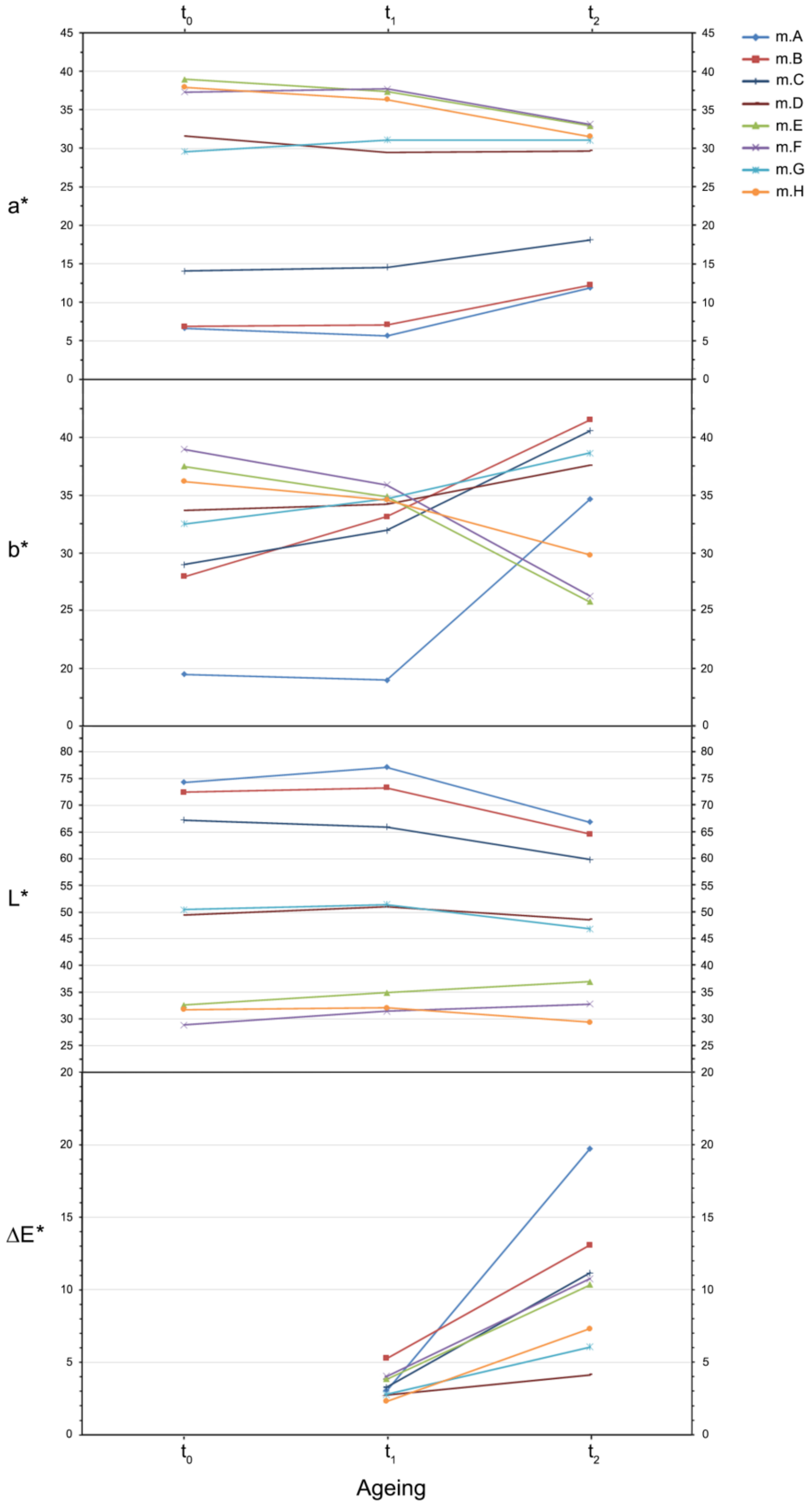

Figure 1.19 *L^*, a^*, b^* coordinates of the mock-ups as a function of the ageing time. The calculated values $\Delta E^*_{t1\text{-}t0}$ and $\Delta E^*_{t2\text{-}t1}$ are reported in correspondence with the x-axis labels t_1 and t_2, respectively. Figure published in [Invernizzi et al. 2021].*

The light-induced effects on the mock-up surface layers were evaluated during ageing by the reflection FTIR spectroscopy. It is worth reporting that, for the first time, this technique was employed to monitor the chemical changes over time of an oil-colophony mixture applied to bulk material. When approaching the study of complex mixtures as varnishes, in fact, the transmission or ATR modes are certainly to be preferred because more suitable to investigate band variations in both qualitative and quantitative terms. However, if the integrity of the object needs to be totally preserved, the use of non-invasive reflection techniques is mandatory, with all the drawbacks deriving from its application such as distortions of band, distortions of baseline, or impossibility of using conventional databases for substance identification [Invernizzi et al., 2018].

Spectra collected on m.B (Fig. 1.20a) and m.F (Fig. 1.20b) were selected because representative of two different types of layer at the top of their stratigraphy: the pure linseed oil-colophony varnish, on one hand, and the same mixture with hematite pigment dispersed therein, on the other. The frequency shifts over time of the varnish bands, and their assignment, are listed in Table 1.4.

The infrared reflection study of the mock-ups was conducted on the spectra after the application of KKT. Although necessary for the analysis of organic bands, these transformations created artefacts between 4000 and 3000 cm^{-1} and around 1000 cm^{-1}, making undetectable the evolution of the varnish spectral behaviour in those regions (respectively related to the νO-H band and to the νC-O and δC-H bands, produced by colophony). In particular, the *Reststrahlen* band of talc at around 1000 cm^{-1} - giving rise to the artefact when KKT is applied - is pronounced only in m.B (Fig. 1.20a); as shown in Fig. 1.9, in fact, this signal turned out to be absent - or almost - in all the other mock-ups. From Fig. 1.20, we can see that after 25h of exposure the spectral profiles did not undergo any variation compared to those acquired on dried mock-ups. This evidence is true for all the mock-ups, whether the uncoloured or coloured varnish is directly exposed to the air. After additional 400h of ageing, significant qualitative variations were clearly revealed in all the mock-ups: the intensity of C-H bands at around 2900-2800 cm^{-1} and 1460 cm^{-1} displayed a remarkable decrease, whereas the νC=O band increased in intensity and slightly broadened in shape. The intensity increase of νC=O band, in particular, appeared more pronounced in pure linseed oil-colophony mixture than in the pigmented varnish. Moreover, the bands in the νC-O-O region underwent a broadening effect and, just for the pure mixture, a slight increment in intensity. The spectral changes observed at t_2 witness the photo-induced oxidation effects of oil-based varnishes, as described in [Ciofini et al., 2016].

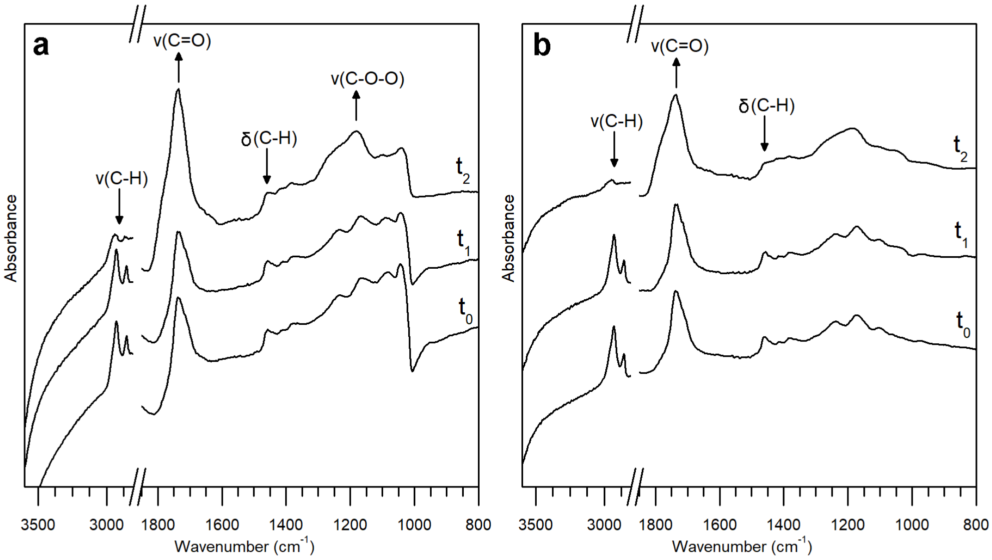

Figure 1.20 *Representative reflection FTIR spectra, after KK transformations, collected on the mock-ups m.B (a) and m.F (b) at different ageing times:* t_0 *(dried),* t_1 *(25h),* t_2 *(425h). Arrows indicate the main change observed and discussed in the text. Figure published in [Invernizzi et al. 2021].*

Table 1.4 *Assignment of the KKT bands of the linseed-oil colophony varnish [Ciofini et al., 2016] at different ageing times:* t_0 *(dried),* t_1 *(25h),* t_2 *(425h). The spectral study was limited to the region not interested by artefacts, and the precise wavenumber values of the KKT band maxima derived from the second-derivative analysis. Abbreviation (sh) corresponds to shoulder bands. Table published in [Invernizzi et al. 2021].*

Linseed oil-colophony varnish				
Assignment	**Contribution**	**t_0**	**t_1**	**t_2**
$\nu_{as}(CH_3)$	oil, resin	2960 (sh)	2960 (sh)	2960 (sh)
$\nu_{as}(CH_2)$	oil, resin	2927	2927	2935
$\nu_s(CH_3)$	oil, resin	2870 (sh)	2870 (sh)	2865
$\nu_s(CH_2)$	oil, resin	2853	2853	2850 (sh)
$\nu(C=O)$	oil	1741	1741	1735
$\nu(C=O)$	resin	1705-10 (sh)	1705-10 (sh)	1720 (sh)
$\delta(CH_3/CH_2)$	oil, resin	1460	1460	1460
$\delta_s(CH_2)$–CH_2-CO-O-	oil	1412	1412	1420
$\delta_s(CH_3)$	oil, resin	1382	1382	1382
$\nu(C-O)$	oil, resin	1240	1240	1240 (sh)
$\nu_{as}(C-O)$ $\delta(CH)$, $\nu(C-O)$	oil resin	1175	1175	1175
$\nu_{as}(O-CH_2-C)$ $\delta(CH)$, $\nu(C-O)$	oil resin	1100	1100	1100

1.4 Conclusions

In the developed research project, we assessed strengths and limits of different non-invasive techniques in the study of mock-ups properly prepared by varying certain parameters in their stratigraphy. The gathered data were analysed through both the univariate and multivariate approaches and the results for each technique are summarized in Table 1.5. The non-invasive approach was supported by the use of invasive techniques on the cross-sections obtained from the mock-ups.

Subsequently, the effects of the progressive artificial solar exposure were non-invasively evaluated from chemical and chromatic points of view. After 425h of ageing, reflection FTIR spectroscopy revealed spectral changes in band intensity and shape related to specific functional groups composing the surface layers, witnessing the photo-induced oxidation effects of oil-based varnishes. Meanwhile, colorimetry recorded yellowing and darkening effects of the wood support and varnishes, except for those mock-ups with the highest hematite concentrations at the top layer. Other chromatic effects were also singled out in some mock-ups.

This multi-technique study would represent a significant, first step towards the use of a totally non-invasive approach applied to the stratigraphy of peculiar artworks such as musical instruments, paintings on panel, sculptures, and furniture. When approaching a wood artefact stratigraphy, information on number and thickness of the layers above support can be straightforwardly gathered, except in specific cases, by OCT. If tomographic techniques are not available, some indirect hypotheses could be drawn through the reflection FT-IR analysis of areas of the artwork at different states of preservation, that is to say, exposing different coats to air. The presence of inorganic fillers and pigments dispersed in the coating system can be visually detected in the OCT tomograms, with limitations mainly related to the instrumental properties, while the chemical identification of their nature is provided by FT-IR, Raman, and XRF spectroscopies according to the respective conditions reported in Table 1.5. Moreover, it is possible to obtain approximative information about the particle concentration by the OCT and XRF data. As for the organic binders, reflection FT-IR turned out to be the most suitable method for their investigation; Raman spectroscopy, in fact, was not able to reveal proteinaceous and oil-based layers with thicknesses of few tens of microns (explored up to about 50 µm). Finally, an indirect assumption on the presence of a size treatment can be made from the transparency of wood to the near-IR light by OCT, and, if the procedure involved the use of marker compounds, XRF allows one to advance further hypotheses.

Table 1.5 *Summary of the potential and limits of different non-invasive techniques applied to the study of the laboratory mock-ups investigated in this chapter. Table published in [Invernizzi et al. 2021].*

Analytical technique	Potential	Limits
OCT	✓ Discrimination of layers above the wood in terms of number and thickness	✗ Non-discrimination of adjacent layers above the wood in the specific cases below reported: 1. comparable intensity of light scattering at particles dispersed in the layers 2. close in time applications of transparent layers characterized by the same refractive index 3. layer with very high concentration of particles concealing visibility of a thin transparent undercoat
	✓ Indirect assumption about the presence of size layer from the wood transparency to the near-IR light	✗ Non-discrimination of size layer into the wood
	✓ Detection of particles	✗ Non-discrimination of individual particles in semi-scattering and scattering layers in the specific cases below reported: 1. size and average distance among particles lower than the lateral resolution of the instrument (ca. 15 µm) 2. uniformity of dispersion ✗ Size of dots (speckles) depending on coherence properties of probing light and instrument's optics rather than the actual size of particles in case of layers scattering light weakly or moderately
	✓ Discrimination of different particle concentrations	✗ Apparent scattering properties of given strata may depend on scattering properties of upper layers
Reflection FTIR spectroscopy	✓ Identification of proteinaceous components in the ground in case of its direct exposition to air	✗ Non-identification of proteinaceous components in the ground in presence of overlying layers with minimum thickness of 20 µm (minimum value for uncoloured oil-colophony varnish)
	✓ Identification of hematite pigment in case of its high concentration in oil-colophony varnish (at least 5% w/w when coloured varnish is exposed to air; at least 10% w/w when coloured varnish is covered by 20 µm of uncoloured oil-colophony varnish)	✗ Non-identification of hematite pigment in case of its low concentration in oil-colophony varnish (below 5% w/w when coloured varnish is exposed to air; below 10% w/w when coloured varnish is covered by 20 µm of uncoloured oil-colophony varnish)
		✗ Non-discrimination of different concentrations of silicate mineral
	✓ Identification of silicate mineral in the ground in the specific cases below reported:	✗ Non-detection of v_{as} band of silicate mineral in the ground in presence of overlying multi-layered varnish coating

	1. direct exposition of the ground to the air 2. presence of thin overlying uncoloured varnish layer (verified up to 20 µm of thickness) ✓ Hypothesis about the presence of silicate mineral in the ground by the detection of its lower-wavenumber bands when overlying multi-layered varnish coating is present	
	✓ Indirect hypothesis about the thickness of varnish coating on the basis of the band intensity variation of the silicate mineral in the ground	
Raman spectroscopy	✓ Identification of hematite pigment in case of its high concentration in oil-colophony varnish (at least 5% w/w when coloured varnish is exposed to air; at least 10% w/w when coloured varnish is covered by 20 µm of uncoloured oil-colophony varnish)	✗ Non-detection of the higher-wavenumber marker band of hematite pigment in case of its low concentration in oil-colophony varnish (below 5% w/w when coloured varnish is exposed to air; below 10% w/w when coloured varnish is covered by 20 µm of uncoloured oil-colophony varnish)
		✗ Scattering intensity attenuation of hematite bands when coloured varnish is covered by 20 µm of uncoloured oil-colophony varnish
		✗ Non-detection of organic components in layers with thicknesses up to ca 50 µm (not explored beyond this value)
		✗ Non-detection of silicate mineral in the ground
XRF spectroscopy	✓ Discrimination of different concentrations of silicate mineral and hematite pigment (concerning hematite, the minimum concentration value to distinguish coloured layers from uncoloured ones is 2% w/w)	✗ Non-detection of silicate mineral in presence of overlying varnish layers containing hematite pigment in concentrations equal to or higher than 10% w/w ✗ Scattering intensity attenuation of Fe signal when coloured varnish is covered by 20 µm of uncoloured oil-colophony varnish
	✓ Indirect discrimination of different amounts of proteinaceous binder in the ground (inversely proportional to the filler concentration)	
	✓ Indirect hypothesis about the thickness and the pigment concentration of the varnish coating on the basis of the intensity variation of Si signal related to the silicate mineral in the ground	

1.5 References

Baraldi P., Manoscritto Bolognese 2861 XV sec., Biblioteca Universitaria di Bologna.

Bikiaris D., Daniilia S., Sotiropoulou S., Katsimbiri O., Pavlidou E., Moutsatsou A., et al., Ochre-differentiation through micro-Raman and micro-FTIR spectroscopies: application on wall paintings at Meteora and Mount Athos, Greece, *Spectrochimica Acta Part A: Molecular and Biomolecular Spectroscopy*. 56 (2000) 3–18. doi:10.1016/s1386-1425(99)00134-1.

Bro R., Smilde A.K., Principal component analysis, *Analytical Methods*. 6 (2014) 2812–2831. doi:10.1039/c3ay41907j.

Chan K.L.A., Kazarian S.G., New Opportunities in Micro- and Macro-Attenuated Total Reflection Infrared Spectroscopic Imaging: Spatial Resolution and Sampling Versatility, *Applied Spectroscopy*. 57 (2003) 381–389.

Ciofini D., Striova J., Camaiti M., Siano S., Photo-oxidative kinetics of solvent and oil-based terpenoid varnishes, *Polymer Degradation and Stability*. 123 (2016) 47–61. doi:10.1016/j.polymdegradstab.2015.11.002.

Colombini M., Modugno F., Giannarelli S., Fuoco R., Matteini M., GC-MS characterization of paint varnishes, *Microchemical Journal*. 67 (2000) 385–396. doi:10.1016/s0026-265x(00)00098-9.

Fabbri M., Picollo M., Porcinai S., Bacci M., Mid-Infrared Fiber-Optics Reflectance Spectroscopy: A Noninvasive Technique for Remote Analysis of Painted Layers. Part II: Statistical Analysis of Spectra, *Applied Spectroscopy*. 55 (2001) 428–433. doi:10.1366/0003702011952181.

Farmer V.C., The infra-red spectra of talc, saponite, and hectorite, *Mineralogical Magazine and Journal of the Mineralogical Society*. 31 (1958) 829–845. doi:10.1180/minmag.1958.031.241.03.

Fiocco G., Rovetta T., Gulmini M., Piccirillo A., Canevari C., Licchelli M., et al., Approaches for Detecting Madder Lake in Multi-Layered Coating Systems of Historical Bowed String Instruments, *Coatings*. 8 (2018) 171. doi:10.3390/coatings8050171.

Frezzato F., Seccaroni C., Segreti di arti diverse nel Regno di Napoli - Manuscript It. III 10 of the Biblioteca Marciana di Venezia, Il Prato, Saonara (PD), 2010.

Griffiths P.R., De Haseth J.A., Fourier Transform Infrared Spectrometry, JohnWiley & Hoboken, New Jersey, 2007.

Invernizzi C., Daveri A., Rovetta T., Vagnini M., Licchelli M., Cacciatori F., et al., A multi-analytical non-invasive approach to violin materials: The case of Antonio Stradivari "Hellier" (1679), *Microchemical Journal*. 124 (2016) 743–750. doi:10.1016/j.microc.2015.10.016.

Invernizzi C., Daveri A., Vagnini M., Malagodi M., Non-invasive identification of organic materials in historical stringed musical instruments by reflection infrared spectroscopy: a methodological approach, *Analytical and Bioanalytical Chemistry*. 409 (2017) 3281–3288. doi:10.1007/s00216-017-0296-8.

Invernizzi C., Rovetta T., Licchelli M., Malagodi M., Mid and Near-Infrared Reflection Spectral Database of Natural Organic Materials in the Cultural Heritage Field, *International Journal of Analytical Chemistry*. 2018 (2018) 1–16. doi:10.1155/2018/7823248.

Invernizzi C., Fiocco G., Iwanicka M., Targowski P., Piccirillo A., Vagnini M., et al., Surface and interface treatments on wooden artefacts: potentialities and limits of a non-invasive multi-technique study, *Coatings*. 11 (2021) 29. doi:10.3390/coatings11010029.

Košařová V., Hradil D., Němec I., Bezdička P., Kanický V., Microanalysis of clay-based pigments in painted artworks by the means of Raman spectroscopy, *Journal of Raman Spectroscopy*. 44 (2013) 1570–1577. doi:10.1002/jrs.4381.

Miliani C., Rosi F., Daveri A., Brunetti B.G., Reflection infrared spectroscopy for the non-invasive in situ study of artists' pigments, *Applied Physics A*. 106 (2011) 295–307. doi:10.1007/s00339-011-6708-2.

Salisbury J.W., Walter L.S., Vergo N., Mid-infrared (2.1-25 um) spectra of minerals, 1st ed., Open-File Report 87-263, U.S. Geological Survey, Greenbelt, MD, 1987.

Stuart B.H., Infrared Spectroscopy: Fundamentals and Applications, Analytical Techniques in the Sciences, 2004.

[Web]

http://gruppochemiometria.it/index.php/software. CAT (Chemometric Agile Tool)

Chapter 2

Innovative applications of advanced non-invasive techniques

Preface

In this chapter different advanced non-invasive techniques, non- and micro-destructive, have been differently combined to study the stratigraphy of historical bowed string musical instruments. The objects under investigation present themselves in their complete integrity or in form of large fragments removed during past functional restorations, in which damaged parts of original instruments were replaced.

In order to better comprehend the content of each subchapter and the interactions among them, on page 56 we provide a scheme that allows for a direct visualization of the investigated musical instruments and the main techniques involved. In this way, we would like the attained results to be more clearly singled out throughout the chapter. Other techniques - not reported in the scheme - were also employed in the three studies described in the chapter, with the aim of supporting the research as well as integrating the results.

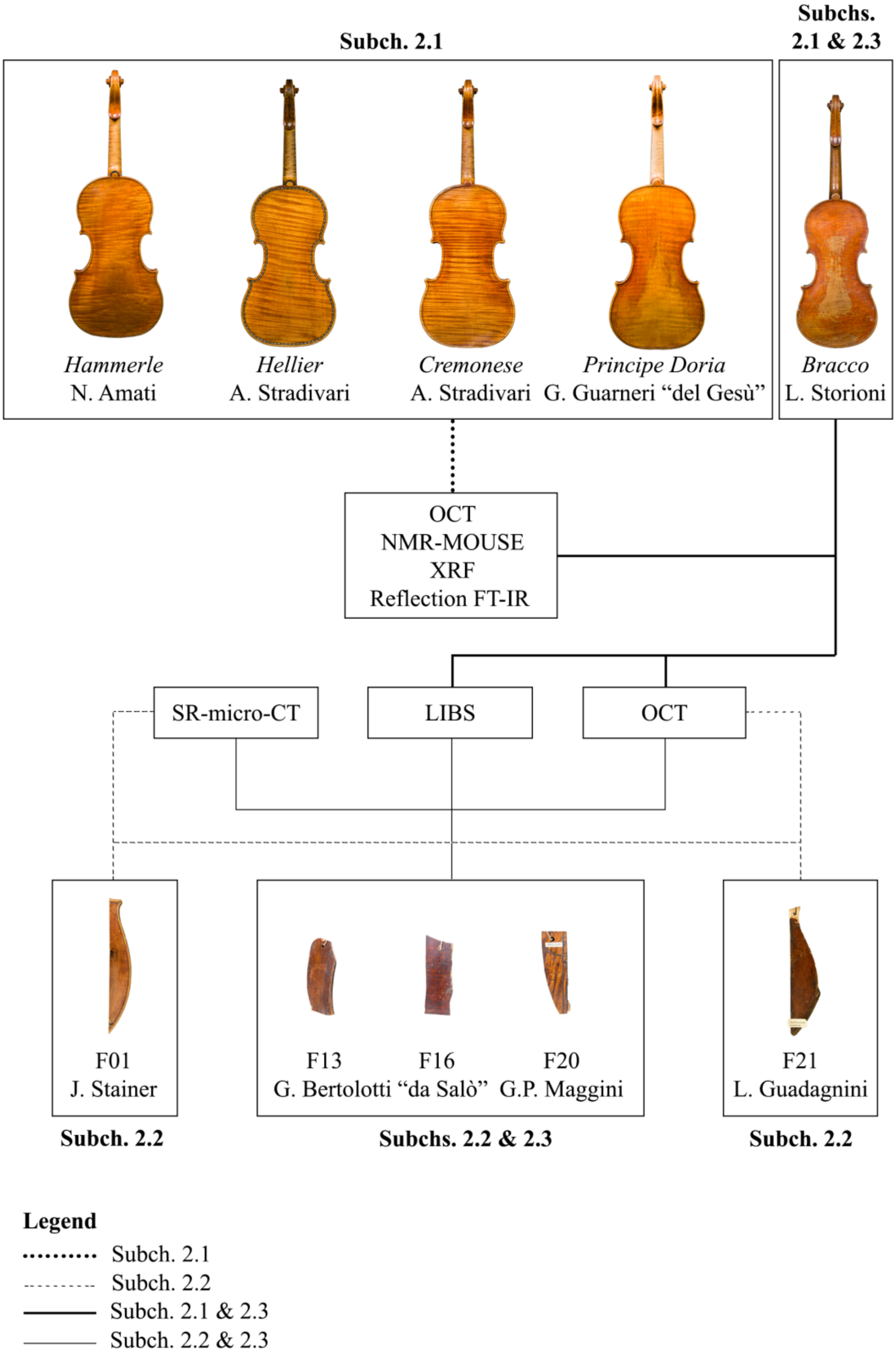
Subch. 2.1
Subchs. 2.1 & 2.3
Hammerle
N. Amati
Hellier
A. Stradivari
Cremonese
A. Stradivari
Principe Doria
G. Guarneri "del Gesù"
Bracco
L. Storioni
OCT
NMR-MOUSE
XRF
Reflection FT-IR
SR-micro-CT
LIBS
OCT
F01
J. Stainer
F13
F16
G. Bertolotti "da Salò"
F20
G.P. Maggini
F21
L. Guadagnini
Subch. 2.2
Subchs. 2.2 & 2.3
Subch. 2.2
Legend
Subch. 2.1
Subch. 2.2
Subch. 2.1 & 2.3
Subch. 2.2 & 2.3

2.1 Non-invasive and non-destructive mobile technology to study the stratigraphy of ancient Cremonese violins: OCT, NMR-MOUSE, XRF and reflection FTIR spectroscopy

2.1.1 Introduction

This multi-analytical study was made possible thanks to the collaboration with the University of Pavia through the Arvedi Laboratory of Non-Invasive Diagnostics, the Nicolaus Copernicus University and the RWTH Aachen University within the Access to Research Infrastructures activity in the H2020 Programme of the EU (IPERION-CH), the Fondazione Museo del Violino Antonio Stradivari Cremona, the Associazione Friends of Stradivari, the Fondazione Arvedi Buschini, the Fondazione Bracco, the Civica Scuola di Liuteria di Milano, and the Cultural District of Violin Making. The results have been published in Microchemical Journal [Invernizzi et al., 2020].

In the previous research described in [Invernizzi et al., 2018a], we developed a preliminary non-invasive method aimed at hypothesizing the physic-chemical structure and the varnish thickness on Stradivari and Guarneri violins. On the basis of the reflection FTIR spectra, in particular, hypothetical value ranges of varnish thickness were ascribed to differently UV coloured areas of the ancient instruments. However, this method proved its high potential in the unique case of a remarkably well-preserved violin. In the case of violins that suffered from maintenance and restoration work, instead, the methodology revealed its major limitations: the presence of over-polish or protective coatings as well as the heterogeneous dispersion of inorganic materials in the layers, in fact, did not allow us to correctly understand the stratigraphy of these violins.

From the limits described above, we have had the necessity to improve the FTIR/UVIFL methodology in order to obtain more accurate and complete answers to the following issues: the real thickness of coats, the occurrence of fillers and pigments - and their precise location - in the stratigraphy, and the effects on the wood of possible treatments not only on the outside of the instrument plate but also on the inside of it. For this purpose, we replied to the call for proposals launched by the Integrated Platform for the European Research Infrastructure ON Culture Heritage (IPERION-CH) within the Access to Research Infrastructures activity in the H2020 Programme of the EU. The project proposal, entitled “Non-invasive Examination of Stratigraphic System in violins” (acronym: thickNESS), was addressed to the advanced MOLAB (MObile LAboratory) transnational platform in order to request access to OCT and NMR-MOUSE instrumentation. The acceptance of the proposal (Grant Agreement No. 654028) allowed researchers from the Nicolaus Copernicus University (Toruń, Poland) and the RWTH

Aachen University (Aachen, Germany) to respectively perform OCT and NMR-MOUSE analyses on historical violins preserved at the Museo del Violino (Cremona, Italy) (Fig. 2.1). The two analytical campaigns were conducted in 2018 at the Arvedi laboratory, with the access to the instruments that was granted by the Conservator of the Museo del Violino collection. OCT and NMR-MOUSE measurements were part of a wider-ranging analytical campaign aimed at studying the musical instrument stratigraphy and its conservation state by a non-invasive and non-destructive approach. In this perspective, we performed analyses on the same violins by reflection FTIR and XRF spectroscopies. Detailed information about the analytical instrumentation and the acquisition parameters used in this study is reported in appendix I.

OCT provides high resolution cross-sectional views of surface structures of semi-transparent objects in a non-contact and non-invasive way. It originates from medicine diagnostics [Drexler and Fujimoto, 2015] and its use in the conservation science field is attested since 2004 [Targowski et al., 2011; Targowski et al., 2020; http://www.oct4art.eu/]. However, few studies record its application to the musical instruments [Latour et al., 2009; Fiocco et al., 2019; Poggialini et al., 2020]. The high transparency of the varnish and ground layers in violins to short IR radiation makes this technique well suited for their investigation, providing information about the number and thickness of layers, as well as detecting particles embedded therein.

NMR-MOUSE [Eidmann et al., 1996; Casanova et al., 2010] provides depth profiles across layered structures following the principles of Magnetic Resonance Imaging (MRI) [Blümich, 2004; Callaghan, 2011]. Applications of this technique to non-destructive material testing have concerned, among others, the analysis of biological materials, polymer products, porous media and food stuffs [Blümich et al., 2008; Casanova et al., 2010; Blümich et al, 2014; Blümich, 2019]. Only recently, this methodology has found increasing interest in the characterization of cultural heritage objects like easel paintings, wall polychromies and paper [Blümich et al., 2010; Capitani et al., 2012; Baias and Blümich, 2017]. Some results from NMR studies of historical violins and bows are already reported in [Blümich et al., 2014; Rehorn and Blümich, 2018]. By the investigation of the density and elasticity of the wood composing the ancient violins, NMR-MOUSE can reveal information about pre-treatments and treatments of the wood on the outer and inner surfaces of the plates, as well as their preservation state.

XRF and reflection FTIR techniques are commonly used for the material characterization in artworks [Miliani et al., 2011; Ridolfi, 2012; Alberti et al., 2017]. XRF identifies the elemental composition of a volume of material that, in the case of string musical instruments, is mostly represented by the wood plate in its entire thickness (few millimetres). It provides information about pigments and fillers in the finishing layers and hypotheses about possible pre-treatments can also be drawn [Echard, 2004; Caruso et al., 2011; Rovetta et al., 2017; Fiocco et al., 2018a]. Reflection FTIR spectroscopy identifies the molecular composition of the external layers, with a light penetration depth which chiefly depends on the thickness, the optical properties and the roughness of the material. As for the string musical instruments, information about the composition of the underlying ground can be achieved whereas varnish is partially or totally worn off and hypotheses on the varnish thicknesses have been made following the methodology above described [Invernizzi et al., 2016; Invernizzi et al., 2018a].

For the first time, we combined OCT, NMR-MOUSE, reflection FTIR spectroscopy and XRF for the study of five valuable historical Cremonese violins preserved in the Museo del Violino in Cremona (Italy) by means of portable and non-contact instrumentation. These masterpieces notably marked the Italian Baroque period from the 1650s to the 1790s. Final aim of this multi-analytical study was the stratigraphy characterization of historical violins from the outermost varnish layers to the innermost wood treatments. Reflection FTIR spectroscopy provides information on the most surface layers (up to few µm in depth); OCT is able to investigate the coating system, penetrating the wood down to a depth of ca. 100 µm; X-ray beam passes through the entire thickness of the plate (few millimetres), bringing information on the elements contained in the layers and in the wood; and NMR-MOUSE mainly focuses on the wood plate in its whole thickness.

In order to support the data interpretation of real case studies, an experimental study was carried out on a mock-up reproducing violin stratigraphies. This mock-up was specifically created with different characteristics, in the layer thickness and composition, compared to the series studied in chapter 1 (for details, see 2.1.2.1).

This study would provide a deeper insight into the antique manufacturing procedures employed in the Cremonese violin making workshops and subsequent restoration efforts.

Figure 2.1 *Laboratory-built high-resolution portable spectral domain OCT instrument (left) and Kea spectrometer and Profile NMR-MOUSE instrument (right) during the analysis of historical violins at the Arvedi Laboratory of Non-Invasive Diagnostics (Cremona, Italy).*

2.1.2 Materials

2.1.2.1 Mock-up

A laboratory mock-up reproducing the violin stratigraphy was prepared by the master Claudio Canevari (Civica Scuola di Liuteria, Milano, Italy). The selection of the materials was based both on the historical documentation - albeit fragmented - and on the scientific evidence gained by previous research (see 0.2.2); the methods employed to apply the layers fulfilled the need for thicknesses as uniform and controlled as possible. A wood board of maple *(Acer pseudoplatanus)* - dimensions of 15 cm (longitudinal direction) x 2.5 cm (radial direction) x 0.3 cm (tangential direction) - was realized by cutting the log along the radial-longitudinal direction. The board was then glued on a 9-mm-thick piece of multi-layered birch plywood in order to prevent warping. As for the treatments, the longitudinally cut smoothed face of the maple board was firstly ground coated by brush with a dispersion of mineral talc in ammonium caseinate (10% w/w), thus filling up the exposed wood pores and creating a film-forming layer. The surface was then smoothed with silicon carbide paper (3000 mesh) and its residual powder removed by brush and akapad gum. Secondly, a linseed oil-colophony varnish was applied by bar film applicator (K Hand Coater model, Erichsen GmbH), obtaining two different thicknesses in consecutive areas of the mock-up. After each varnish application, the mock-up was dried under UV lamps (Philips TL 60W/10-R 1SL/25 Attiniche UVA/10) for 24h. As a result, three main stratigraphic systems - each one occupying one-third of the surface - compose the sample: S1 (ground coat only), S3 (ground coat and one varnish layer) and S4 (ground coat and two varnish layers). In correspondence of the shrinking of the varnish in S3, the additional - albeit narrow - S2 stratigraphy was further considered hence widening the number of varnish thickness ranges to four. The mock-up and its stratigraphic systems are displayed in Fig. 2.2. In real case studies, a varnish thickness comprised between the values of S1 and S2 (i.e., between 0 and 20 μm, see OCT results in 2.1.3.1) - and named as S5 - was hypothesized when the IR proteinaceous signals simultaneously occurred with those of an oil-resin mixture. In this way, the gap existing between S1 and S2 is filled.

As for the sourcing of the materials used to finish the mock-up, they were purchased from Kremer Pigmente GmbH & Co., Aichstetten, Germany (talc cat. No. 58420, casein cat. No. 63200, linseed oil cat. No. 73054), Cremona Tools SAS, Cremona, Italy (colophony cat. No. 504434) and Carlo Erba Reagents S.r.l., Cornaredo (Milano), Italy (ammonia solution 30% cat. No. 419941).

The solution of ammonium caseinate was realized by adding casein powder to distilled water (15% w/w), then dissolved in aqueous ammonia solution 30 wt% (0.5% w/w). The linseed oil-colophony varnish (ratio 1:1 w/w) was prepared according to an ancient recipe [Baraldi, XV century; Frezzato and Seccaroni, 2010]: linseed oil was heated up to 270°C and it was maintained at this temperature for 3h; after that, the cooked linseed oil was cooled to 200°C and milled colophony was added under magnetic agitation till complete dissolution; the resulting mixture was maintained again at 200°C for other 30 min.

To better interpret the effects of the stratigraphic layers on the mock-up, an untreated maple wood was additionally analysed by NMR-MOUSE.

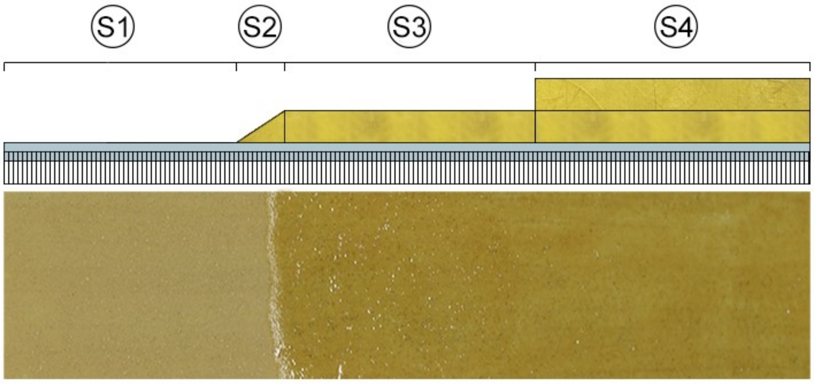

Figure 2.2 *The mock-up (bottom) and the schematic representation of its stratigraphic systems (top): ground coat only (S1), ground coat and varnish shrinking (S2), ground coat and one varnish layer (S3), ground coat and two varnish layers (S4). Figure published in [Invernizzi et al., 2020].*

2.1.2.2 Historical violins

The real case studies are five renowned violins preserved in the Museo del Violino (Cremona, Italy) and manufactured over the thriving period from the mid-17th century to the end of the 18th century. In chronological order, the investigated violins are the *Hämmerle* 1658 by Nicolò Amati, the *Hellier* 1679 and the *Cremonese* 1715 by Antonio Stradivari, the *Principe Doria* 1734 by Giuseppe Guarneri "del Gesù" and the *Bracco* 1793 small violin by Lorenzo Storioni. The instruments are described and shown in appendix II.

On the basis of preliminary examinations under UV and VIS lights, we selected differently preserved regions on the back plate of the violins for the multi-technique investigation. Numerous and variously-distributed areas - also depending on the specific technique requirements - were analysed by each analytical instrument and, subsequently, those overlapped ones representing the two stratigraphic extremes in terms of varnish thickness were chosen for this study and referred to as LT (Lowest Thickness) and HT (Highest Thickness), as highlighted in Figs. 2.3 and 2.4. It is worth reporting that the varnish thickness could involve original and restored layers.

Figure 2.3 *UVIFL photos of the back plate of the violins with the two representative Lowest Thickness (LT) and Highest Thickness (HT) areas highlighted. Figure published in [Invernizzi et al., 2020].*

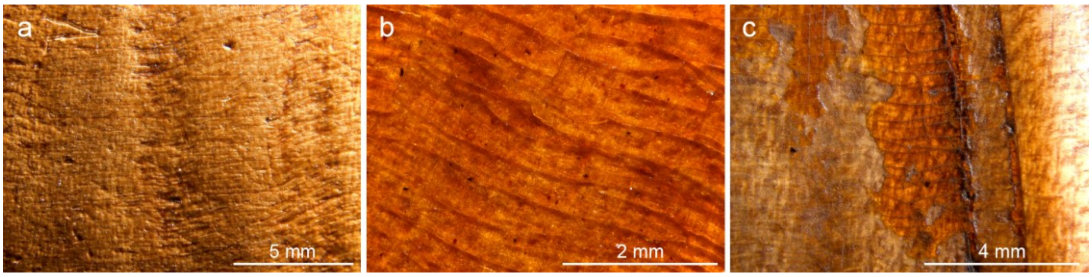

Figure 2.4 *Stereomicroscopy images under VIS-light illumination of Lowest Thickness (LT) area (a), Highest Thickness (HT) area (b) and interface between the two types of areas (c) on the back plate of the Bracco 1793.*

2.1.3 Results

In this section, the results from the mock-up - first - and those ones from the violins - then - are presented technique by technique. The cross-interpretation of the whole data set is subsequently discussed in 2.1.4.

2.1.3.1 Optical coherence tomography

OCT analysis of the mock-up allowed us to the identify the varnish thickness range in each stratigraphic system: 0 µm (S1), 20-30 µm (S2), 30-50 µm (S3) and 100-120 µm (S4). The boundary between the two varnish applications was not discriminated in the OCT tomograms of S4. Concerning the ground coat, its thickness measures ca. 20-30 µm and diffusely dispersed fine particles are clearly visible within it. It is important to highlight that variations in thickness were expected for coatings as those ones applied, and this is the reason why we considered ranges of values instead of precise measurements. The OCT tomograms showing the different stratigraphic systems of the mock-up, as well as the thickness values of their layers, are displayed in Fig. 2.5.

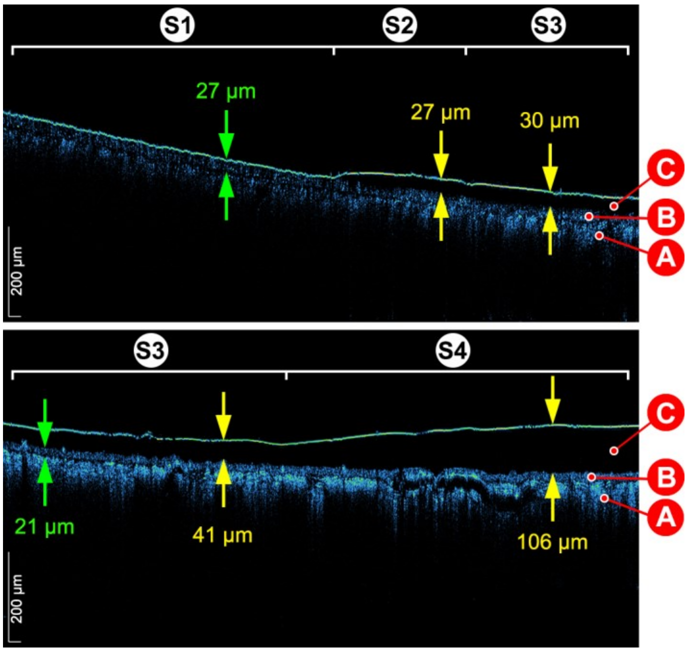

Figure 2.5 *OCT analysis of the mock-up showing the different stratigraphic systems: ground coat only (S1), ground coat and varnish shrinking (S2), ground coat and one varnish layer (S3), ground coat and two varnish layers (S4). Arrows indicate varnish (yellow) and ground (green) layers. Letters refer to wood substrate (A), ground (B) and varnish (C) layers. The images are corrected for refraction with* $n_R = 1.5$. *Figure published in [Invernizzi et al., 2020].*

Thickness measurements of the ground and varnish layers composing the five historical violins derive from a large-scale analysis of the tomograms collected on each area. This information is summarized in Table 2.1 and the most representative tomograms of the LT and HT areas of the violins are displayed in Fig. 2.6. Moreover, a wide analytical session exclusively dedicated to the *Bracco* small violin allowed the researchers of the Nicolaus Copernicus University to reconstruct the 2D and 3D OCT layer thickness maps of most of the back plate, as shown in Fig. 2.7. The procedure adopted to create these maps is reported in appendix I.

Considering the LT areas, the varnish is almost absent - approximating the stratigraphy S1 of the mock-up - on the *Hämmerle* and *Bracco* violins while, in the other violins, a varnish layer between 10 and 25 µm was measured and a reasonable comparison with the hypothesized S5 can be made. As regards the HT areas, the largest value was observed on the *Bracco* small violin with a thickness falling in the range from 50 to 120 µm. High values were also registered on the *Principe Doria* violin where the stratigraphy is composed of two varnish layers respectively measuring 25-65 µm (bottom) and 10-15 µm (top), with a total range of 35-80 µm which roughly falls in S3 of the mock-up; this result is discussed in detail in 2.1.4. In the HT areas of the other investigated violins, a lower thickness range between 20 and 40 µm - approaching that of S2 - was recorded. Some fine particles were possibly detected in the varnish coat of the *Hämmerle* and *Bracco* violins.

Focusing on the ground coat, a thickness value of about 10 µm was measured on the whole set of violins. Except for the *Hämmerle*, embedded particles were identified in the ground layer of the violins.

Table 2.1 *OCT thickness measurements of the varnish and ground layers in correspondence of the Highest Thickness (HT) and Lowest Thickness (LT) areas of the five violins. The value ranges here reported derived from a large-scale analysis of the tomograms, not limited to the figures shown in this study. Estimated thickness measurement uncertainty is 3 µm (see appendix I). Table modified from [Invernizzi et al., 2020].*

Layer		**Violin**				
		Hämmerle 1658	*Hellier* 1679	*Cremonese* 1715	*P. Doria* 1734	*Bracco* 1793
Varnish	**HT**	20-25 µm*	20-40 µm	20-35 µm	35-80 µm	50-120 µm*
	LT	0 µm	10-25 µm	10-25 µm	10-15 µm	0-10 µm
Ground		5-10 µm	5-10 µm**	10-15 µm**	5-15 µm**	5-10 µm**

** Possible particles detected; ** Particles detected.*

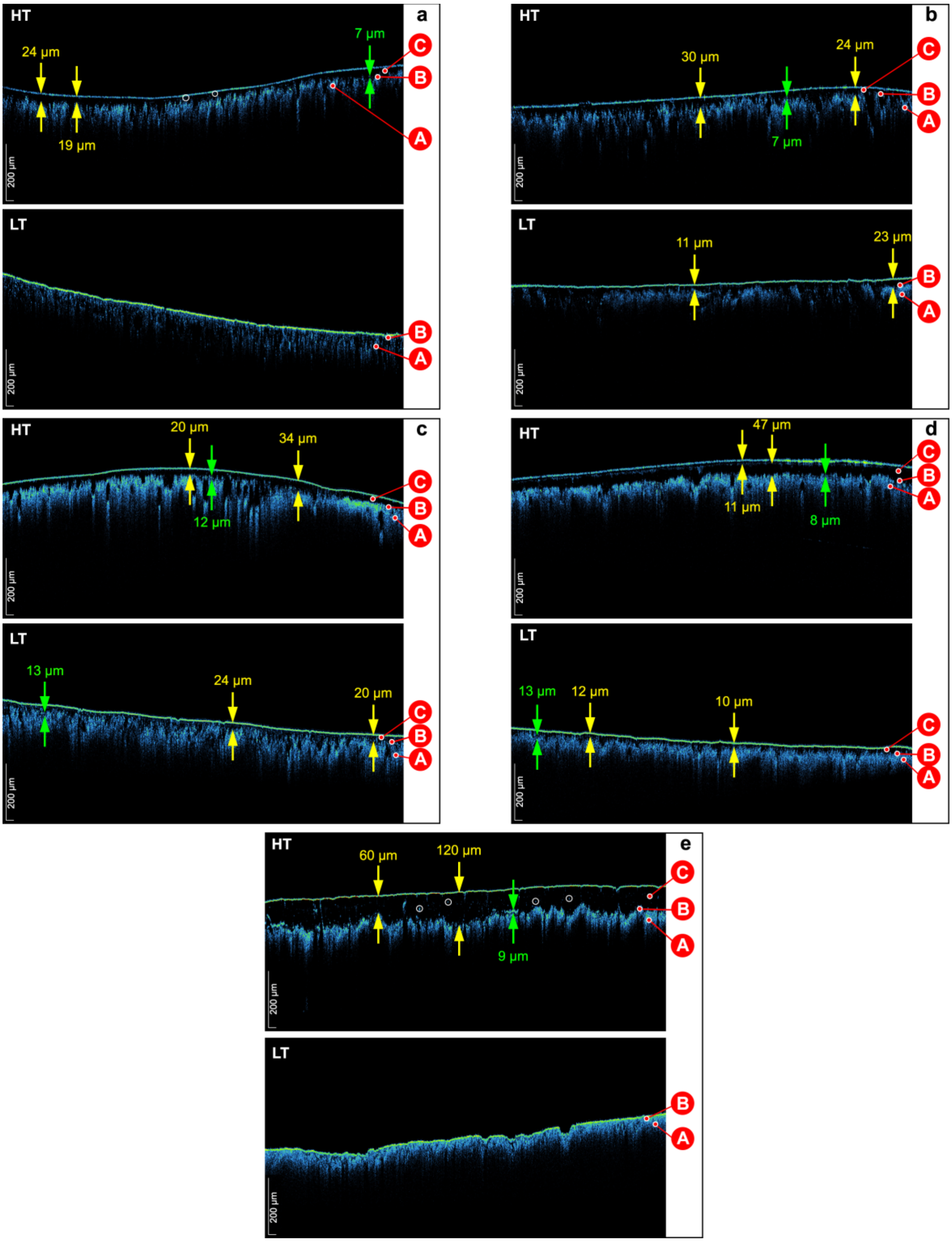

Figure 2.6 *OCT analysis of the Hämmerle (a), Hellier (b) and Cremonese (c), Principe Doria (d) and Bracco (e) violins in correspondence of the Highest Thickness (HT) and Lowest Thickness (LT) areas. Arrows measure varnish (yellow) and ground (green) layers. Letters refer to wood substrate (A), ground (B) and varnish (C) layers. Some of the possible particles embedded in the varnish layer of the Hämmerle and Bracco are indicated with white circles. The images are corrected for refraction with* $n_R = 1.5$*. Figure modified from [Invernizzi et al., 2020].*

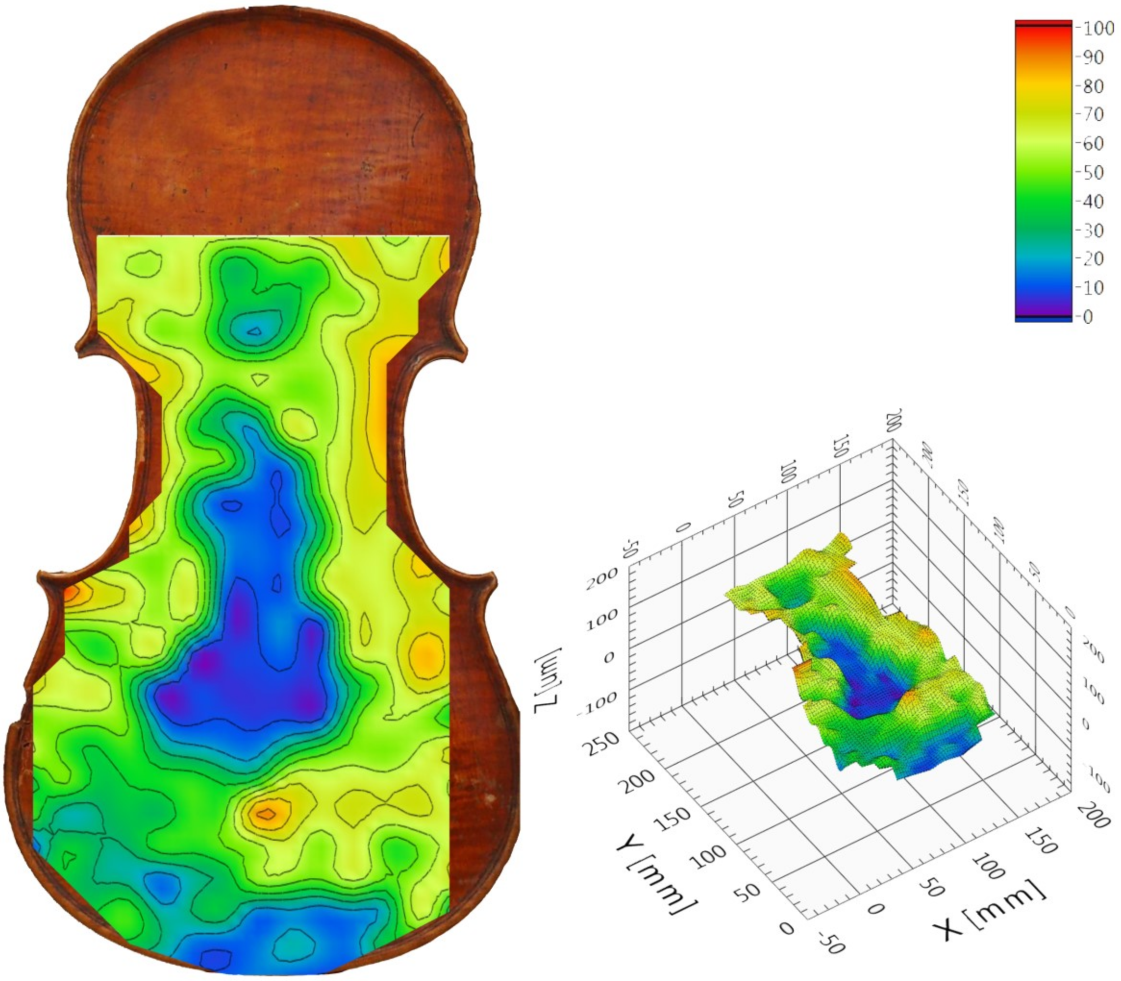

Figure 2.7 *2D (left) and 3D (right) OCT layer thickness maps of the Bracco small violin. Measurement unit of the coloured scale bar: µm.*

2.1.3.2 Reflection FTIR spectroscopy

The reflection FTIR analysis of the mock-up enabled us to study the spectral behaviour of the materials composing the stratigraphy in relation to the varnish thickness increase. As shown in Fig. 2.8a, the *Reststrahlen* bands of the mineral talc (see 1.3.2 for wavenumber values and assignments) remarkably decreased in intensity from S1 to S4. In S4, in particular, the weak bending bands at lower frequencies are the only vibrations of the mineral detected in the spectrum. With regard to the diagnostic bands of the linseed oil-colophony varnish (vCH$_3$/CH$_2$ in the region 2900-2800 cm^{-1}, vC=O from 1740 to 1700 cm^{-1}, δCH$_3$/CH$_2$ at ca. 1460 cm^{-1}, δ$_s$CH$_3$ at 1380 cm^{-1}, v$_{ar}$C-O at 1240 cm^{-1} and vC-O at 1170 and 1100 cm^{-1}) [Stuart, 2004; Invernizzi et al., 2017; Invernizzi et al., 2018b], they did not show any significant variation in intensity while, on the other hand, the proteinaceous bands from the ground coat (vN-H at 3300 cm^{-1}, vC=O or amide I at 1655 cm^{-1}, combination of vC-N and δN-H or amide II at 1540 cm^{-1}) [Stuart, 2004; Invernizzi et al., 2017; Invernizzi et al., 2018b] were never recorded in presence of any overlying varnish layer here considered (Fig. 2.8b). The bands of proteins, in fact, were uniquely detected in the stratigraphic system S1.

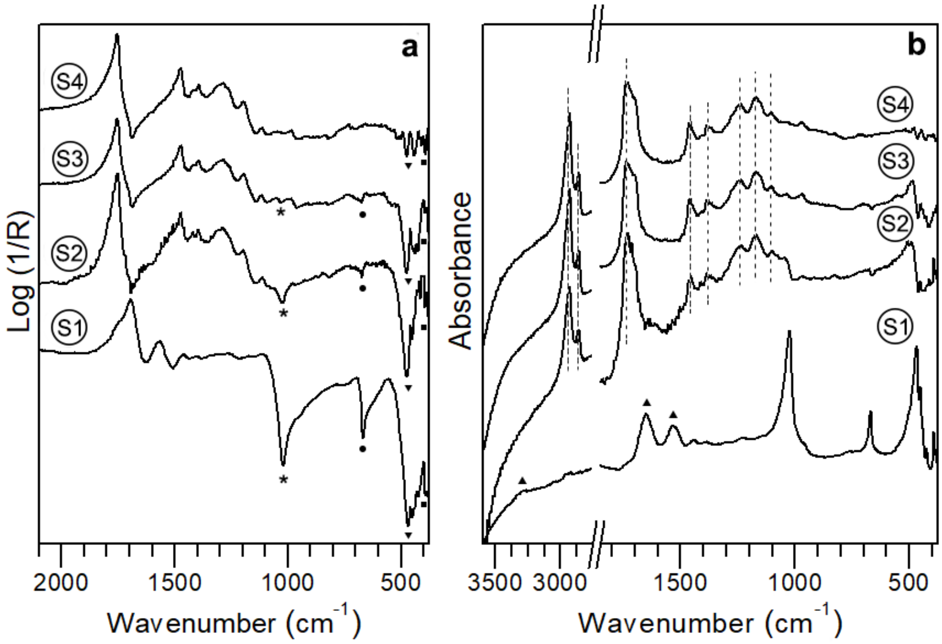

Figure 2.8 *Reflection FTIR spectra before (a) and after (b) KK transformations from the different stratigraphic systems of the mock-up; marker bands of the mineral talc (* v_{as}Si-O (v3); ● v+δSi-O (v4); ▼ δMg-O (v7) and δSi-O (v5); ■ δSi-O), linseed oil-colophony varnish (dotted line) and caseinate (▲) are highlighted. Figure published in [Invernizzi et al., 2020].*

From the IR analysis performed on the LT areas of the ancient violins, the presence of proteinaceous and silicate-based materials in all five instruments was ascribed to the composition of the ground coat (Fig. 2.9). The frequencies of the silicate bands seemed to match well with those of the mineral talc. Minerals of the sulphate group (likely gypsum: vO-H at 3400 cm^{-1}, inverted $v_{as}SO_4$ (*v3*) at 1150 and 1110 cm^{-1}, inverted $\delta_{as}SO_4$ (*v4*) at 670 and 600 cm^{-1} [Invernizzi et al., 2018a]) are also visible in the LT area of the *Bracco* small violin (Fig. 2.9e). Together with sulphates, bands of silica compounds (likely quartz: inverted v_{as}Si-O at 1080 cm^{-1}, v_sSi-O at 800 and 780 cm^{-1}, inverted δSi-O at 455 cm^{-1} [Invernizzi et al., 2018a]) were found in some spectra (shown in [Invernizzi et al., 2018a]) of the *Principe Doria* violin. However, these inorganic phases were identified in areas of the back plate at different varnish thicknesses - as highlighted in [Invernizzi et al., 2018a] - and thus it is difficult to understand their location in the stratigraphy, since no OCT analysis was performed in the study above reported.

As concerns the composition of the varnish film in the HT areas, oil-terpenic resinous mixtures were detected in almost all spectra of the whole set of instruments (Fig. 2.9). Following the spectral evidence obtained by the IR study on the mock-up, we can estimate the varnish thickness ranges on real case studies. The oil-resinous varnish is absent (S1) - or almost absent - in the LT areas of the *Hämmerle* (Fig. 2.9a) and *Bracco* (Fig. 2.9e) violins. In these areas, the sharp and often intense CH_2 signals can be ascribed to long chain aliphatic hydrocarbons such as paraffin [Rosi et al., 2016]. Thicknesses comprised between 0 and 20 μm (S5) were hypothesized in the LT areas of the other violins (Fig. 2.9b-d). With regard to the HT areas, instead, a varnish thickness range of 20-30 μm (S2) was estimated on the *Hämmerle* (Fig. 2.9a), *Hellier* (Fig. 2.9b) and *Cremonese* (Fig. 2.9c) violins and that of 30-50 μm (S3) on the *Principe Doria* (Fig. 2.9d). The *Bracco* small violin represents a doubtful case: if, on one hand, the combined presence of proteins and oil-resin bands in the HT areas would make it hypothesize varnish thicknesses between 0 and 20 μm (S5) (Fig. 2.9e), on the other the high opacity under UV light - preventing the wood fibres from being visible [Invernizzi et al., 2018a] - would suggest that thick varnish coats can be still preserved. However, we cannot rule out that the UV imaging was affected by the conservation conditions of the instrument. In addition to the oil-terpenic resin signals, benzoin and shellac resins were detected on the *Hämmerle* (Fig. 2.9a), *Cremonese* (Fig. 2.9c) and *Bracco* (Fig. 2.9e) violins. The characteristic bands of these resins, with their assignments, are reported in Table 2.2.

Table 2.2 *Wavenumber values, with their assignment, of the FTIR reflection bands of the benzoin and shellac resins identified on the Hämmerle, Cremonese and Bracco violins.*

Resin	Wavenumber (cm^{-1})	Assignment
Benzoin [Chen et al., 2016]	2900, 2850	vC-H
	1705	vC=O (conjugate ketone)
	1630	$\delta_{in\ plane}$O-H (adsorbed water)
	1630,1615,1600,1515	Aromatic skeletal
	1462,1450	Aromatic skeletal + δC-H
	1380	δC-H
	1270,1170,1120,1035	vC-O
	835,770	Undefined
Shellac [Invernizzi et al., 2017; Invernizzi et al., 2018b]	2930,2855	vC-H
	1715	vC=O
	1460	δCH_2
	1370	δCH_3
	1250	vC-O
	940,925	$\delta H_2C=C$
	720	δCH_2

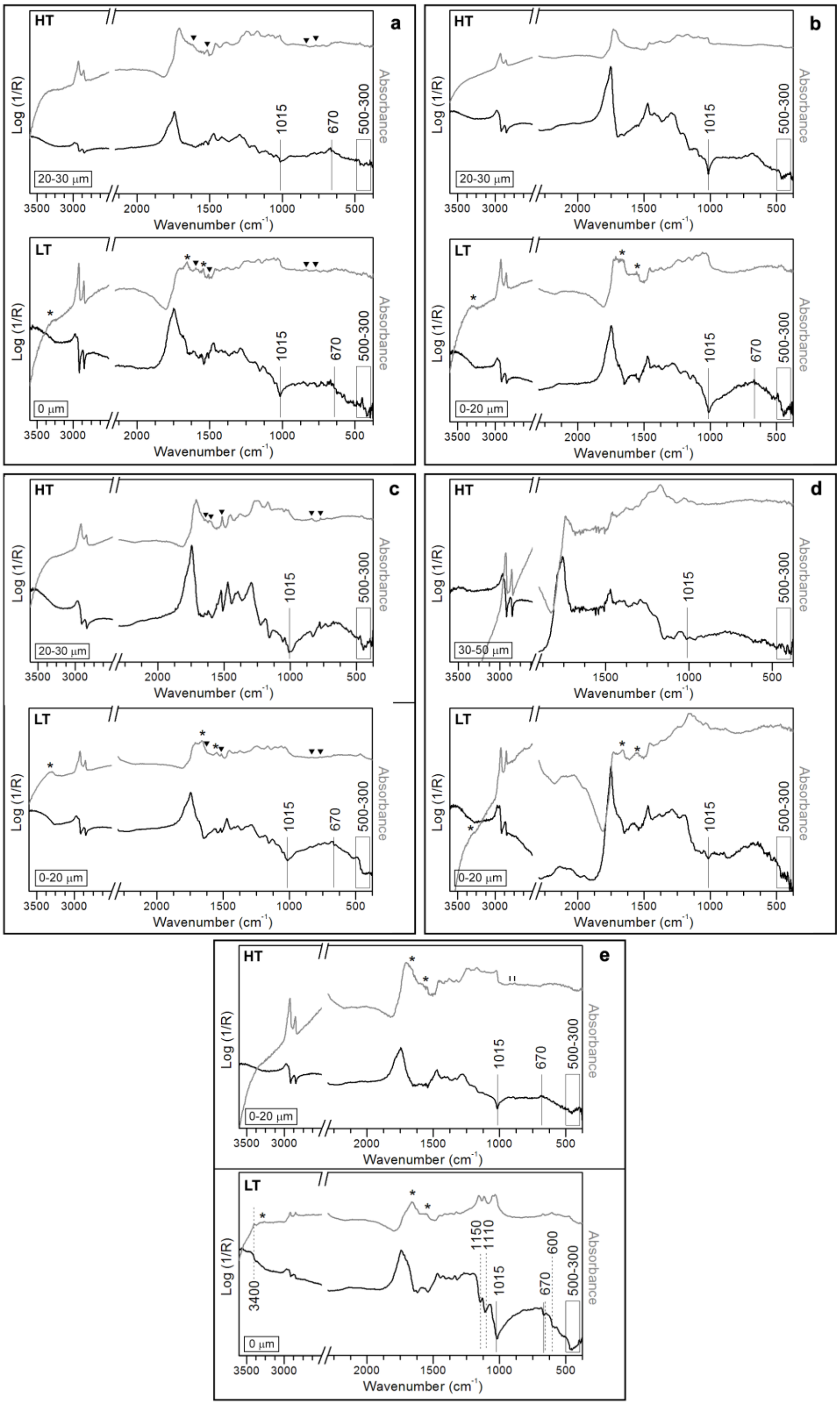

Figure 2.9 *Reflection FTIR spectra before (black) and after (grey) KK transformations from the Highest Thickness (HT) and Lowest Thickness (LT) areas of the Hämmerle (a), Hellier (b), Cremonese (c), Principe Doria (d) and Bracco (e) violins. Marker bands of proteins (*), benzoin resin (▼), shellac resin (I), silicates (solid line) and sulphates (dotted line) are highlighted. Varnish thickness range hypothesized by the experimental study is reported at the bottom left. Figure modified from [Invernizzi et al., 2020].*

2.3.3.3 X-ray fluorescence spectroscopy

For the XRF investigation, we focused on the elements of the mineral talc distributed in the ground (i.e., Si; and S, Ca, Fe as impurities). Mg and Al were not considered because their secondary radiations have a low penetrating power and are severely attenuated by the air and by organic matrices as those ones within which the mineral is dispersed [Rovetta et al., 2017]. It is worth remembering that the elemental qualitative composition of the mineral talc is reported in 1.2.1. In the mock-up stratigraphies, XRF counts from S2 cannot be considered consistent due to the irregular shape of the area in exam, as visible in Fig. 2.10. Additionally, in all stratigraphic systems the number of counts of K, deriving from the wood, is too low - in relation to error - to enable a real trend evaluation. None of the collected signals is associated, instead, to the varnish. As displayed in Fig. 2.10, the counts of Si and S (this last partially deriving also from the caseinate) underwent a considerable break down till almost zeroing in S3 and S4. We considered the value of 0.05 as limit below which the counts approach to zero. As for Ca, instead, a gradual downward trend was registered from S1 to S4. Finally, the intensity of Fe-Kα line appeared not to be affected by any significant variation at all, differently from what observed in chapter 1 in relation to varnish layers pigmented with hematite and covered by coats of uncoloured varnish.

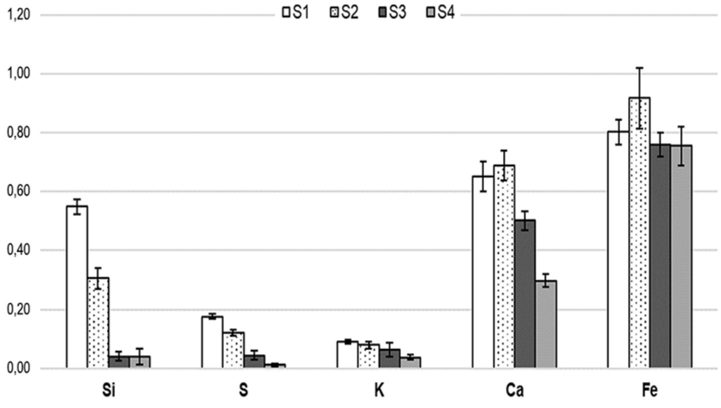

S1	0.55 ± 0.03	0.18 ± 0.01	0.09 ± 0.01	0.65 ± 0.05	0.80 ± 0.04
S2	0.31 ± 0.04	0.12 ± 0.01	0.08 ± 0.01	0.69 ± 0.05	0.92 ± 0.1
S3	0.04 ± 0.02	0.04 ± 0.02	0.06 ± 0.02	0.50 ± 0.03	0.76 ± 0.04
S4	0.04 ± 0.03	0.01 ± 0.01	0.04 ± 0.01	0.30 ± 0.02	0.76 ± 0.07

Figure 2.10 *Estimate of elements detected by XRF on the stratigraphic systems of the mock-up; the displayed values correspond to the net area counts of the peak (Kα) normalized to time and to net area counts of the coherent scattering peak of Rhodium (Kα), with their Standard Deviation of Mean (SDOM). Figure published in [Invernizzi et al., 2020].*

XRF counts collected on the five violins showed a non-negligible variation between the LT and HT areas, as reported in Table 2.3. Despite its low number of counts, Si was always detected in the LT areas of the entire set of violins, except for the *Hämmerle*. From this result, we can draw an analogy between this type of area and S1 of the mock-up. In all HT areas, instead, the number of counts of Si approaches almost zero, as also experimentally observed in S3 and S4 of the mock-up. Concerning S and Ca, we found a heterogeneous condition in the violins: the counts, in fact, significantly decrease from LT to HT in the *Hämmerle, Hellier* and *Bracco* while an opposite upward trend is shown in the *Cremonese* and *Principe Doria*. The K-Kα line intensity increases in the LT areas. Although this trend was not highlighted in the mock-up, it is in line with our expectation: the more exposed the wood, the higher the counts of K. It is worth mentioning that much higher counts of this element were revealed in the LT areas of the *Hämmerle* and *Cremonese*, if compared to those of the other three violins under study. The Fe-Kα line intensity is characterized by non-significant variations between the LT and HT areas, except for the *Hellier* and *Cremonese*. An opposite trend, in fact, was observed for the two Stradivari violins: the number of Fe counts almost tripled in the LT area of the *Hellier*, while it doubled in the HT area of the *Cremonese*.

Table 2.3 *Estimate of elements detected by XRF analysis in correspondence of the Lowest Thickness (LT) and Highest Thickness (HT) areas of the five violins. The displayed value corresponds to the net area counts of the peak (Kα) normalized to time and net area counts of the coherent scattering peak of Rh-Kα. Table modified from [Invernizzi et al., 2020].*

Element		**Violin**				
		Hämmerle 1658	*Hellier* 1679	*Cremonese* 1715	*P. Doria* 1734	*Bracco* 1793
Si	**LT**	0.04	0.11	0.11	0.09	0.23
	HT	0.03	-	0.05	0.02	0.03
S	**LT**	0.60	0.86	0.40	0.23	0.67
	HT	0.28	0.25	0.75	0.31	0.25
K	**LT**	5.23	3.01	3.91	1.80	2.68
	HT	2.16	1.39	1.66	1.38	1.40
Ca	**LT**	4.21	4.94	1.45	1.45	4.51
	HT	2.43	0.87	2.63	2.18	3.12
Fe	**LT**	0.91	1.68	0.68	0.60	1.28
	HT	0.67	0.62	1.22	0.92	1.10

2.3.3.4 Nuclear Magnetic Resonance - Mobile Universal Surface Explorer

NMR depth profiles collected on the mock-up and the untreated maple wood are reported in Fig. 2.11. The untreated wood displayed a step-like hydrogen density profile (Fig. 2.11a1); a spatial resolution of about 200 μm can be estimated from the width of the slope of the step. The hydrogen density is provided by the integral of the relaxation-time distribution. As shown in Fig. 2.11a2, the relaxation-time distribution is constant within the precision of the measurements. Two peaks characterize this distribution, as well as those from the mock-up: the strong peak at short T_2 (near 0.09 ms), which gives rise to the bottom trace, corresponds to the protons of wood matrix (i.e., amorphous cellulose and lignin), while the weak peak at long T_2 (near 1 ms), which produces the top trace, corresponds to the protons of bound water[1]. The peak of free water, at higher relaxation times, was never detected in this study. In the untreated wood, both the traces extend equally from the surface into the wood (Fig. 2.11a2). The variations in the NMR stiffness or relaxation contrast - obtained by the ratio of peak integrals from short and long relaxation times - can be ascribed to the wood structure (Fig. 2.11a3). In general, the relaxation contrast is strongly affected by the molecular mobility and provides information about the stiffness of the material, with high values registered whenever the peak of bound water is low or the peak of wood matrix is high. The effect of the ground application was the shift of the initial portion of the bound water trace a bit (< 200 µm) away from the surface into the wood, as visible in Fig. 2.11b2. On the other hand, the hydrogen density (Fig. 2.11b1) and the NMR relaxation contrast (Fig. 2.11b3) profiles seemed not to be affected by the ground layer. In particular, comparing the graphs a3 and b3 of the figure, the relaxation contrast variations are of the same size but at different locations, which can be attributed to local variations of the wood itself. Significant changes in the relaxation contrast profile were detected, instead, with the application of the varnish layer. Specifically, the profile exhibited in Fig. 2.11c3 suggests that the wood stiffness incremented in less than 200 µm of depth. This behaviour is confirmed by the depth-resolved relaxation-time distribution of Fig. 2.11c2: if, on one hand, the weak water bound signal at long T_2 remains suppressed, on the other the strong wood matrix signal at short T_2 is shifted to shorter relaxation times near the surface at less than 200 µm of depth.

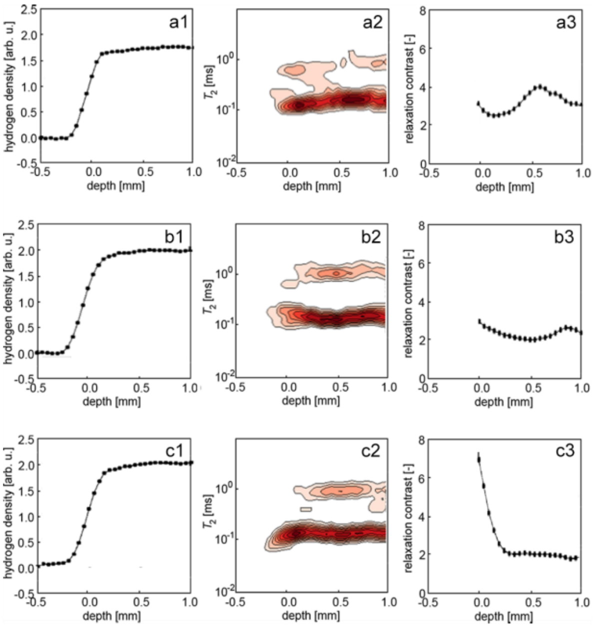

Figure 2.11 *NMR depth profiles: hydrogen density of untreated wood (a1), S1 of the mock-up (b1) and S4 of the mock-up (c1); depth-resolved relaxation-time distribution of untreated wood (a2), S1 of the mock-up (b2) and S4 of the mock-up (c2); relaxation contrast of untreated wood (a3), S1 of the mock-up (b3) and S4 of the mock-up (c3). Figure published in [Invernizzi et al., 2020].*

---

[1] The water that accumulates to various degrees among the chains of D-glucose units of cellulose by forming hydrogen bonds is called bound water. It is considered immobile in the scope of most NMR experiments. The water filling in the cellular lumen is called free water. These molecules are mobile and only rarely collide with surfaces in the cellulose structure, giving rise to long relaxation times in the range of tens to hundreds of milliseconds [Rehorn, 2019].

NMR depth profiles acquired on the historical violins are shown in Fig. 2.12. The hydrogen density profiles are mostly uniform within the violin backs (Fig. 2.12 columns 1,3): they report the density of the wood, apart from the protons in the ground and the varnish. The small variations observed in the density profiles may be ascribed to the wood texture, resulting from the signal loss by fast relaxation of the rigid components like the crystalline cellulose within the 40 μs deadtime of the instrument. The NMR relaxation contrast profiles, instead, show much larger variation (Fig. 2.12 column 5). Peaks in this graph could result from surface treatments and striking examples of this behaviour were detected in the *Cremonese* (Fig. 2.12c5) and *Bracco* (Fig. 2.12e5) violins: the presence of peaks is here documented not only on the outside surface near 0 to 1 mm but also on the inside surface near 2 to 3 mm. The relaxation-time distributions of the entire set of violins show signals at long relaxation time $T_2 \approx 1$ ms and at short relaxation time $T_2 \approx 0.09$ ms, resulting respectively from bound water and wood matrix (Fig. 2.12 columns 2,4). Considering the relaxation-time distributions of the HT (Fig. 2.12 column 2) and LT (Fig. 2.12 column 4) areas for the five violins, we can note that the depth profiles from the LT areas generally contain more variations than those from the HT areas, except for the *Cremonese*. For the *Cremonese* violin, instead, the relaxation-time depth profiles are similarly complicated in correspondence of its LT and HT areas (Fig. 2.12c2,c4). The HT area of the *Hellier* shows little to no variation of the T_2 distribution (Fig. 2.12b2), similarly to what encountered in the untreated and regular maple wood of Fig. 2.11a1. In particular, the signal of bound water is absent only at the inner and outer surfaces, suggesting a surface treatment, while the wood trace is approximately constant across the depth of the violin back plate. Non-degraded wood was also recorded in the *Principe Doria* at both areas of analysis (Fig. 2.12d2,d4). Besides the *Hellier*, also the *Principe Doria* and *Bracco* violins show a suppression of the bound water signal, respectively for about 1 mm and 0.5 mm, in the outer and inner HT surfaces (Fig. 2.12d2,e2). Observing the wood signal in the T_2 distributions, the LT area of the *Hellier* shows some variations (Fig. 2.12b4) whilst strong variations were found in the *Cremonese* and the *Hämmerle* violins, and somewhat less in the *Bracco*. For the *Hämmerle* and *Bracco*, these are more marked in their LT areas (Fig. 2.12a4,e4) compared to the HT ones. At some depths, in particular, the wood relaxation peak shifts to higher values than those of normal wood: this is the case found in the middle part of both types of area of the *Cremonese* (Fig. 2.12c2,c4) as well as in the LT area of the *Hämmerle* (the outer first millimeter) and, even if less pronounced, of the *Bracco* (Fig. 2.12a4,e4). A relative reduction in the short T_2 component could indicate a degradation of the wood at these points.

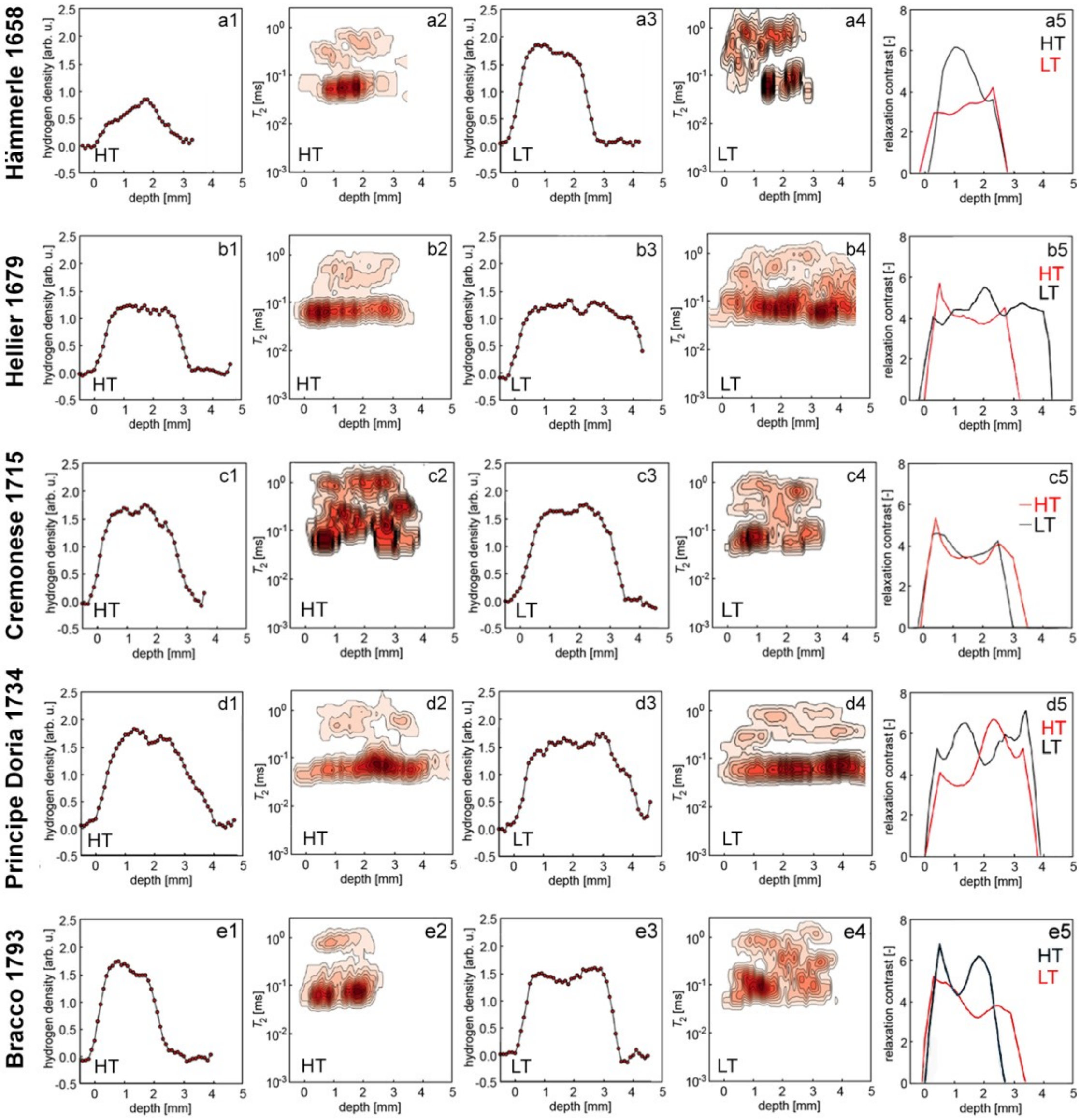

Figure 2.12 *NMR depth profiles from the Highest Thickness (HT) and Lowest Thickness (LT) areas of the violins: depth-resolved relaxation-time distribution (a-e1, a-e3), hydrogen density (a-e2, a-e4), relaxation contrast (a-e5). Each letter refers to the violin considered: Hämmerle (a), Hellier (b), Cremonese (c), Principe Doria (d) and Bracco (e). Figure modified from [Invernizzi et al., 2020].*

2.1.4 Discussion

Thanks to the experimental study on the mock-up, we were able to comprehend strengths and limits of the combined non-invasive techniques in the stratigraphic analysis of bowed string musical instruments. By OCT, we measured the thickness of finishing layers. As already highlighted in chapter 1, however, this technique was not able to discriminate consecutively applied multiple layers with similar refractive indices, and this was observed in the tomogram collected on S4. Concerning the ground, we could identify it mainly by the detection of the inorganic particles highly dispersed therein. By reflection

FTIR spectroscopy, we characterized the molecular composition of the finishing layers as well as studying the spectral behaviour of diagnostic bands at the different varnish thickness ranges provided by OCT. Specifically, the band intensity of the inorganic filler in the ground - which varies with different varnish thicknesses - and of its binder was considered diagnostic for this study. The association between spectral profile and varnish thickness, made in this experimental section, was then used to draw indirect thickness hypotheses on the varnish layers of ancient violins on the basis of the IR results, and it could be exploited when the OCT technique is not included in an analytical campaign. By XRF, we could investigate the effect of uncoloured varnish coats on the detection of the chemical elements composing the substances of the ground. Silicon and sulphur were no more detected with a varnish thickness from 30-50 μm (S3) on; the low-energy secondary radiation produced by light elements of the ground was dramatically attenuated, in fact, by the air and the matrix effect of the overlying layers. The intensity of Ca-Kα line gradually declined with the varnish thickness increase, never approaching to zero. On the other hand, the Fe-Kα line intensity was not affected by the varnish layer. By NMR-MOUSE, we studied the effects of the ground and varnish applications on the depth profiles. The ground appeared to expel the bound water in a depth of wood <200 μm from the surface - as the suppressed signal in the T_2 distribution would witness - but its stiffness and density were not affected.

The varnish, instead, would likely have increased the wood stiffness in a depth <200 μm, as corroborated by the simultaneous suppression of the water bound signal and the shift of the wood matrix signal towards shorter relaxation times. Whereas the stiffness increment affects higher depths of wood, this may be associated to other treatments. These results are summarized in Table 2.4.

Table 2.4 *Summary of the information provided by each analytical technique on the laboratory mock-up investigated in this chapter.*

Analytical technique	Information
OCT	• Thickness measurement of ground and varnish* layers • Detection of particles in ground layer
Reflection FTIR spectroscopy	• Molecular characterization of ground and varnish layers • Indirect hypothesis about the varnish thickness on the basis of the band intensity variation of silicate and caseinate related to the ground
XRF spectroscopy	• Investigation of effects produced by uncoloured varnish layers on the detection of elements related to the ground: - Si, S: detected up to 30 μm of varnish thickness - Ca: gradual downward trend (never approaching to zero) - Fe: no variation
NMR-MOUSE	• Effects of ground layer on depth profiles: - no variation in wood density - suppression of bound water T_2 signal in a depth of wood <200 μm from the surface - no variation in wood stiffness • Effects of varnish layer on depth profiles:

	- no variation in wood density - suppression of bound water T_2 signal & shift of wood matrix T_2 signal towards shorter relaxation times in a depth of wood <200 μm from the surface - wood stiffness increase in a depth of wood <200 μm from the surface

** OCT technique was not able to discriminate consecutively applied multiple layers with similar refractive indices.*

Crossing the data acquired through the different analytical techniques on the historical violins enabled us to figure out their stratigraphy from the innermost wood treatments to the outermost varnish layers.

The maple wood of the entire set of violins is largely uniform in terms of density across the back plate, as shown by the NMR depth profiles. The wood seemed degraded in the centre of the *Bracco* and *Cremonese* plates, this indicating a likely pre-treatment which had affected the whole depth of wood. In particular, the high concentration of K in the LT areas of the *Cremonese* could be related to the possible use of a lye-based pre-treatment [Etiégni and Campbell, 1991; De Mayerne and Rinaldi, 1995], which largely contributes to the degradation of the cellulose and hemicellulose [Rovetta et al., 2017] - while other possible chemical or physical pre-treatments [Nagyvary et al., 2006; Nagyvary et al., 2009] could have been used for the *Bracco*. Also the *Hämmerle* could have undergone a pre-treatment based on a high-alkaline solution as the lye, in this case affecting only the outer first millimetre of the back plate. A subsequent size treatment was hypothesized for the *Cremonese* and *Bracco* violins, causing an increase in the NMR stiffness of the wood to a depth of about 1 mm from the surface on both the outside and inside of the plate. The size treatment has the function of isolating the wood, preventing a heterogeneous and substantial penetration of the ground applied afterwards inside it [Stols-Witlox, 2017]. Stradivari would have adopted this treatment even thirty-six years before, in 1679, on both sides of the *Hellier* back plate, affecting the same depth as that detected in the *Cremonese*, with the difference that the non-degraded wood in this case would allow us to exclude the use of a pre-treatment. Similar condition to the *Hellier* was detected in the *Principe Doria*, although the inside of its plate appeared more affected by the size treatment.

A large consistency in the materials and methods adopted by the old violin makers to finish their instruments was found. This assumption was suggested by the identification of proteinaceous grounds, with silicate-based compounds embedded therein, and oil varnishes in the entire set of violins.

The roles of the ground coat are to fill up the surface wood pores and to provide optical and aesthetic characteristics to the wood. Together with silicates, identified on all violins by FTIR spectroscopy, sulphate-base compounds (possibly gypsum) were also detected on the *Bracco*. The presence of these inorganic phases - possibly acting as fillers - at the ground level can be confirmed by the finding of silicon in the LT areas of almost all violins (except the *Hämmerle*) and of calcium and sulphur in this type of area of the *Bracco*. Furthermore, the integration of OCT and XRF data acquired on the HT areas of the violins allows us to claim that, even with a varnish thickness of ca. 20 µm, silicon was almost no longer revealed. As concerns the *Principe Doria*, we cannot rule out that sulphate compounds (possibly gypsum) are distributed at some levels within the varnish: on one hand, in fact, IR bands of sulphates were found in several heterogeneous UVIFL areas [Invernizzi et al., 2018a] and, on the other hand, the calcium and sulphur Kα line intensities resulted higher in the HT areas than the LT ones. In those cases where the IR bands of sulphate were not revealed, instead, we cannot attribute Ca and S to specific compounds and just speculation can be drawn about their nature (e.g., sulphur likely originating from dirt or environmental pollution). The *Hellier*, *Principe Doria* and *Bracco* violins represent significant examples of the effect produced by the ground on the wood, with the suppression of a fraction of the bound water trace in the T_2 distribution. The *Hämmerle* is the only example where the presence of silicate-based compounds in the ground is very doubtful since neither OCT revealed particles in this layer nor XRF detected Si in the LT areas.

As concerns the varnish coats, the ranges of thickness indirectly hypothesized by FTIR spectroscopy could be all confirmed by the OCT measurements, except for the HT area of the *Bracco*. In this peculiar case, in fact, a thickness range of 0-20 µm (S5) was supposed against a real - much higher - thickness varying from 50 to 120 µm. The incorrect attribution of range can arise from the presence of proteins in the varnish layer, as highlighted in chapter 3 by the IR maps acquired on one cross-section using Synchrotron radiation FTIR microspectroscopy; moreover, we cannot rule out that the particles detected in the varnish by OCT are proper silicate-based compounds. For this reason, the general assumption made on the region S5 - as reported in 2.1.2.1 - cannot be considered valid for this area of the *Bracco*. If we focus on the varnish thickness values, it is worth highlighting that the absence of varnish in the LT areas of the *Hämmerle* and *Bracco* witnesses that these specific areas have undergone high levels of wear consequently to extensive handling over time, whilst residual varnish thicknesses of 10-20 µm are still present in this type of area of the other violins. Interestingly, the highest thickness value - among all HT areas - was recorded on the *Bracco* itself: this evidence proves the outstanding state of preservation of the coating system in correspondence of this type of area, which also characterizes most of its back plate (except for the central and bottom portions, where the varnish is not present at all). Much lower varnish thicknesses - around 20-40 µm - characterize the back of the *Hämmerle*, *Hellier* and *Cremonese* violins in their best-preserved areas. Fe can be attributed to iron earth pigments [Bevilacqua et al., 2010]; since these pigments can contain accessory minerals as silicates, carbonates and sulphates [Eastaugh et al., 2008], it is possible that Fe is sometimes attributed to the inorganic minerals found by FTIR spectroscopy. If these Fe-based pigments can be distributed in the ground of the *Hämmerle*, *Principe Doria* and *Bracco* violins, the higher intensity of Fe-Kα line in the HT area of the *Cremonese* - if compared to the LT one - allowed us to hypothesize the embedding of the Fe-based pigments in its varnish coat. Probable pigment particles were detected by OCT in the HT varnish layers of the *Hämmerle* and *Bracco* violins.

The last considerations deal with issues related to restoration and maintenance procedures. The *Principe Doria* is characterized, for instance, by a distinctive finish in its HT area: the detection of a double varnish coating by OCT would indicate that the two varnishes belong to different chronological phases [Targowski et al., 2010]. In particular, the bright reddish-orange UV colour of this area suggests that the application of the top varnish layer - at least that one - occurred during restoration interventions. Another example is the finding of compounds commonly used as surface polish (i.e., benzoin and shellac resins) [Rivers and Umney, 2013] in the stratigraphy of the *Cremonese*, *Hämmerle* and *Bracco* violins. The very thin over-polishing films likely formed by these substances were not revealed by OCT - due to resolution limits - and, partially covering the IR signals of the underlying varnish, make the spectral interpretation difficult. In addition, aliphatic hydrocarbons like paraffin seemed to be identified in the least preserved areas of the *Hämmerle* and *Bracco*; their use can be related to undocumented routine operations of maintenance to provide a glossy appearance to the musical instrument.

On the basis of the results obtained by combining the different techniques, in Table 2.5 we propose a summary of the stratigraphic systems hypothesized for the five violins.

2.1.5 Conclusions

In this project, the stratigraphy of ancient Cremonese violins was non-invasively studied with portable instrumentation by combining, for the first time, OCT, reflection FTIR spectroscopy, XRF and NMR-MOUSE. Firstly, we identified strengths and limitations of this approach by conducting a focussed experimental study on a mock-up where stratigraphic systems at different varnish thickness were reproduced on a piece of maple wood. The different thicknesses of varnish on the mock-up originate from the necessity of taking into consideration the consumption to which some areas of musical instruments have been subjected. After the investigation of the mock-up, we applied the multi-technique approach to areas characterized by different degrees of preservation (i.e., most and least preserved in terms of varnish thickness) of five ancient violins held in the Museo del Violino in Cremona. By integrating the results from this wide-ranging campaign, we were able to propose hypotheses on the stratigraphy of these masterpieces. In this way, we added a further contribution to the knowledge of the processes adopted by the old masters, from the wood treatments to the finishing layers, as well as those employed by restorers and conservators over the years.

Table 2.5 *Stratigraphic systems hypothesized for the five violins on the basis of the analytical evidence. Parallel lines indicate the wood support, circles and triangles indicate the inorganic phases acting as fillers/pigments. Table published in [Invernizzi et al., 2020].*

Violin	Stratigraphy
Hämmerle 1658	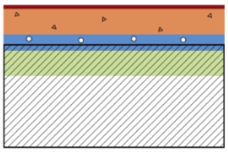 🟥 **Polish**: benzoin and shellac resins; aliphatic hydrocarbons 🟧 **Varnish**: oil-resinous mixture with possible pigments 🟦 **Ground**: proteins with possibile silicate- and Fe-based fillers/pigments 🟩 **Pre-treatment**: possibly with lye solution
Hellier 1679	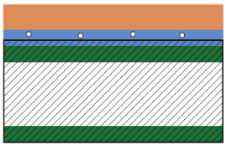 🟧 **Varnish**: oil-resinous mixture 🟦 **Ground**: proteins with silicate- and Fe-based fillers/pigments 🟩 **Size treatment**
Cremonese 1715	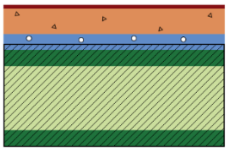 🟥 **Polish**: benzoin resin 🟧 **Varnish**: oil-resinous mixture with possible Fe-based pigments 🟦 **Ground**: proteins with silicate-based fillers 🟩 **Size treatment** 🟩 **Pre-treatment**: possibly with lye solution
Principe Doria 1734	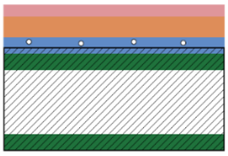 🟥 **Restoration varnish**: oil-resinous mixture (sulphates?) 🟧 **Varnish**: possibly oil-resinous mixture (sulphates?) 🟦 **Ground**: proteins with silicate- and Fe-based fillers/pigments 🟩 **Size treatment**
Bracco 1793	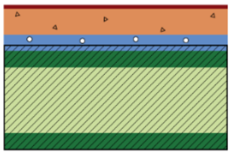 🟥 **Polish**: shellac resin; aliphatic hydrocarbons 🟧 **Varnish**: oil-resinous mixture with possible pigments 🟦 **Ground**: proteins with silicate- and Fe-based fillers/pigments and sulphate-based fillers 🟩 **Size treatment** 🟩 **Pre-treatment**

2.2 A non-invasive and non-destructive micro-tomographic insight into the coating systems of fragments from historical bowed string musical instruments: synchrotron radiation micro-CT and OCT

2.2.1 Introduction

This micro-tomographic study was conducted thanks to the collaboration with the University of Pavia through the Arvedi Laboratory of Non-Invasive Diagnostics, the Nicolaus Copernicus University within the Access to Research Infrastructures activity in the H2020 Programme of the EU (IPERION-CH), the SYRMEP beamline of the Elettra synchrotron laboratory, the University of Turin, the International Violin Making School of Cremona, and the Cultural District of Violin Making. The results have been published in the journal Coatings [Fiocco et al., 2019].

The objects under investigation are five fragments of historical bowed string musical instruments belonging to the “Collezione Sgarabotto”, whose history is reported in appendix II. The selected fragments - as part of a larger set - have been provided for research purposes by the International Violin Making School of Cremona (Italy), where they were exposed for about thirty years during the last century [Spotti, 1991]. In this work, we studied the micro-morphology of their complex coating systems by two micro-tomographic techniques: OCT and X-ray SR-micro-CT (Fig. 2.13). Although the micro-tomographic systems play a prominent role among the most promising non-invasive techniques in the Cultural Heritage field [Morigi et al., 2010], their application to the investigation of the finishing layers of musical instruments is presently quite rare [Latour et al., 2009; Gilani et al., 2016; Lämmlein et al., 2017; Fiocco et al., 2018b].

OCT analyses were performed in 2018 at the Arvedi laboratory by the researchers of the Nicolaus Copernicus University (Toruń, Poland) within the MOLAB Transnational Access-EU H2020 Project IPERION CH (Grant Agreement No. 654028). The project proposal “Non-invasive Examination of Stratigraphic System in violins” (acronym: thickNESS) was primarily addressed to the study of ancient violins preserved at the Museo del Violino (Cremona, Italy), whose results are reported in 2.1. However, during the five-day-long analytical session, we managed to collect OCT measurements also on several historical fragments of the “Collezione Sgarabotto” and mock-ups (the results of these last ones are described in chapter 1). In the field of Cultural Heritage, this technique provides information on the microscopic layered structures in terms of thicknesses, particulate, cracks and other optical destructive. A brief scientific background of this technique has been already given in the introduction of 2.1.

The SR-micro-CT study was carried out in 2017 at the SYRMEP beamline of the Elettra synchrotron laboratory (Trieste, Italy) by the researchers of the Arvedi laboratory within the Elettra project proposal entitled “Rediscovering the Cremonese finishing treatments for bowed string instruments by combining micro-invasive in-the-lab analyses with non-invasive synchrotron X-ray micro-CT” (Proposal No. 20170163). The project is part of a broader investigation campaign focused on a large group of fragments, these representing a valuable set of samples because suitable for obtaining an in-depth overview of the materials and techniques of the violin making masters over the 16th to 18th centuries. The specific project at the SYRMEP beamline of Elettra aimed at linking the new X-ray micro-CT images to the results that previously had emerged on these fragments by non-invasive and micro-invasive approaches using portable and bench-top instruments, and reported in [Fiocco et al., 2017; Fichera et al., 2018]. Final goal was to robustly highlight - through a non-invasive micro-CT investigation - some specific target features that can be possibly related to a specific violin making workshop. Computed tomography exploits X-rays to achieve morphological and physical information on the inner structures and it has been frequently applied to Cultural Heritage diagnostics [Borman and Stoel, 2009; Morigi et al., 2010; Re et al., 2014; Re et al., 2015; Re et al., 2016]. The high-flux polychromatic beam used in SR-micro-CT allows for measurements at high spatial resolution. The bowed string musical instruments were investigated by this technique, for the first time, in 2012. The experiment was conducted at the Elettra synchrotron laboratory using spatial resolutions between 9 and 50 μm, and the aim was to acquire morphological information on the violin as a whole [Sodini et al., 2012; Sodini et al., 2017]. After some years, a micro-tomographic investigation was performed in the same facility using a spatial resolution of 1 μm [Fiocco et al., 2018b]; in this case, the authors set up a procedure specifically dedicated to the examination of the coating system of these particular objects.

Detailed information about the analytical instrumentation and the acquisition parameters used in this study is reported in appendix I.

In this research project, for the first time, we combined the SR-micro-CT and OCT techniques to investigate the complex coating system of five fragments from historical cellos and double basses. The capability of the two tomographic techniques to discriminate multiple layers, as well as to measure their thicknesses, was assessed. In particular, we focused our attention at the interface between wood and finishing layers, since no alteration caused by sampling occurred. Likewise, the work aimed at understanding the effectiveness of the techniques in detecting (i) the presence of particles, (ii) their concentration and (iii) some of their morphological characteristics, like mean grain-size and tendency to create aggregates. The results previously gathered, and reported in [Fiocco et al., 2017; Fichera et al., 2018], have been accurately examined in order to combine them with the new morphological information.

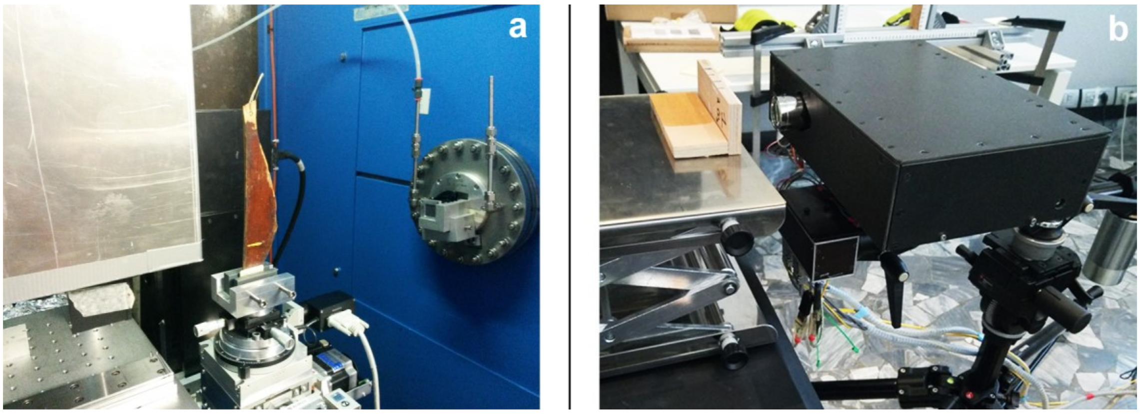

Figure 2.13 *Tomographic setups: high-resolution SR-micro-CT in phase-contrast mode, at the SYRMEP beamline of the Elettra Synchrotron laboratory (Trieste, Italy) (a); prototype high-resolution portable SdOCT instrument built at N. Copernicus University for FP 7 CHARISMA project, at the Arvedi Laboratory of Non-Invasive Diagnostics (Cremona, Italy) (b). The object under investigation in (b) is not among those ones investigated in this study. Figure published in [Fiocco et al., 2019].*

2.2.2 Materials

The five investigated fragments of historical bowed string musical instruments, coming from the "Collezione Sgarabotto", are listed and described in Table 2.6. Their history and photos are shown in appendix II.

Table 2.6 *List of the investigated fragments with inventory number, name, life period and geographical area of provenance of the violin maker, and identification of the original instrument from which the relics were removed.*

Inv. N°	Violin Maker	Period	Area	Instrument
F01	Jacobus Stainer	?1617-1683	Absam, Austria	Cello
F13	Gasparo Bertolotti "da Salò"	1540-1609	Brescia, Italy	Cello
F16	Gasparo Bertolotti "da Salò"	1540-1609	Brescia, Italy	Cello
F20	Giovanni Paolo Maggini	1580-1631	Brescia, Italy	Double bass
F21	Lorenzo Guadagnini	1685-1746	Piacenza, Italy	Double bass

2.2.3 Results and discussion

In this section, we discuss the micro-tomographic results of each fragment within the frame of the chemical and physical characterization previously carried out on these objects by non-invasive (i.e., visible and UV photography, stereoscopic microscopy, radiography and XRF) and micro-invasive (i.e., optical microscopy and SEM-EDX on cross-sections, and micro-FTIR spectroscopy on micro-samples of varnish) approaches

[Fiocco et al., 2017; Fichera et al., 2018]. A summary of the new results from SR-micro-CT and OCT scans, as well as of those previously obtained, is displayed in Table 2.8 at the end of 2.2.3, thus allowing for a direct comparison of the different analytical approaches. In Fig. 2.14 we show the planes considered for the virtual slicing of SR-micro-CT volume renderings, in order to better understand how the 2D images of the radial, tangential, and transverse sections of the fragments are produced. In the slices obtained from the SR-micro-CT volume, the discrimination of layers is based on the grayscale variations between adjacent layers and on the identification of different types of particles in the coating system.

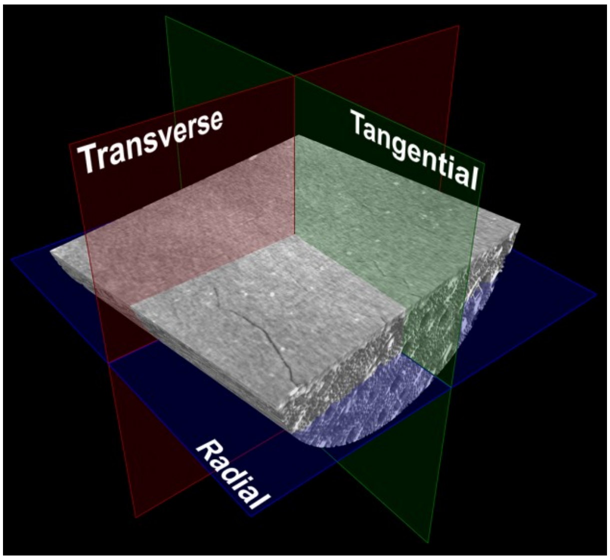

Figure 2.14 *Planes considered for the virtual slicing of SR-micro-CT volume renderings (fragment F01 is shown here as an example). These planes produce 2D images of radial, tangential, and transverse sections of the wood. Figure published in [Fiocco et al., 2019].*

2.2.3.1 F01 – Jacobus Stainer

Previous analyses performed on a micro sample detached from the fragment F01 revealed a stratigraphy mainly composed of two superimposed layers [Fiocco et al., 2017]. The proteinaceous ground, with some carbonate particles detected therein, was found to be characterized by a light blue UV-induced fluorescence and a thickness of about 15 μm. The upper oil-resinous varnish, likely containing iron-based pigments, has a yellowish UV-induced fluorescence and a thickness of about 30 μm. In Fig. 2.15, we report the UV-light optical microscopy image acquired on the cross-section of the micro sample collected on the fragment F01 and published in [Fiocco et al., 2017].

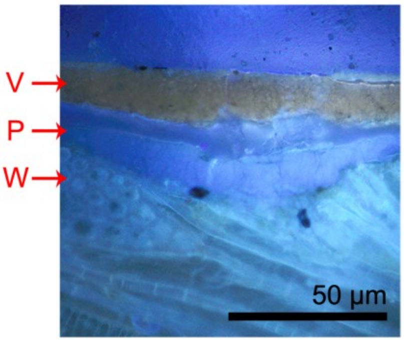

Figure 2.15 *UV-light optical microscopy image of the cross-section from the fragment F01 with two overlying layers (P refers to preparation, V refers to varnish) applied on the maple wood (W). Figure published in [Fiocco et al., 2017].*

The 2D transverse slice obtained from the SR-micro-CT volume of the fragment (Fig. 2.16a) confirmed the stratigraphic structure identified in [Fiocco et al., 2017]: above the maple wood (indicated as A in Fig. 2.16a), the superimposed layers B and C are visible. By the SR-micro-CT technique, we can also identify an additional 10-µm-thick external layer (D) which appears brighter than the underneath layer C. Moreover, this investigation highlighted the presence of particles within all the mentioned layers. The radial slices reported in Fig. 2.16b-e show the morphological features of these particles. Besides those ones investigated in the layers B (indicated as P1 in Fig. 2.16a,c, diameter of about 5 µm) and C (indicated as P2 in Fig. 2.16a,d, diameter of 5-10 µm), thinner particles were also identified in the external layer D (indicated as P3 in Fig. 2.16a,e). This last evidence was not found by the previous morphological and chemical analyses. In the 3D virtual reconstruction (Fig. 2.16f), the different inclusions are represented with false colours according to their position in the stratigraphy.

By the OCT examination (Fig. 2.16g), we were able to discriminate two layers over the wood (indicated as A in Fig. 2.16g): the bottom 12-µm-thick layer (B) and the top layer, whose thickness measures from 26 to 33 µm. No trace of a third separated layer (D in Fig. 2.16a,f) was identified by OCT: this can be ascribed to the similar optical properties of the layers C and D, imaging them as one single stratum in the OCT tomogram. If this hypothesis is true, it can be explained why the OCT thickness of the top layer has a similar value to the sum of the thicknesses of the layers C and D measured by the SR-micro-CT (reported in Table 2.8). For this reason, in Fig. 2.16g we labelled the top layer as C+D. Also by the OCT technique, we observed some dispersed particles in the bottom and top layers (indicated as P1 and P2 in Fig. 2.16g, respectively). In particular, lots of those ones revealed in the varnish are visibly sedimented at the bottom of this coat.

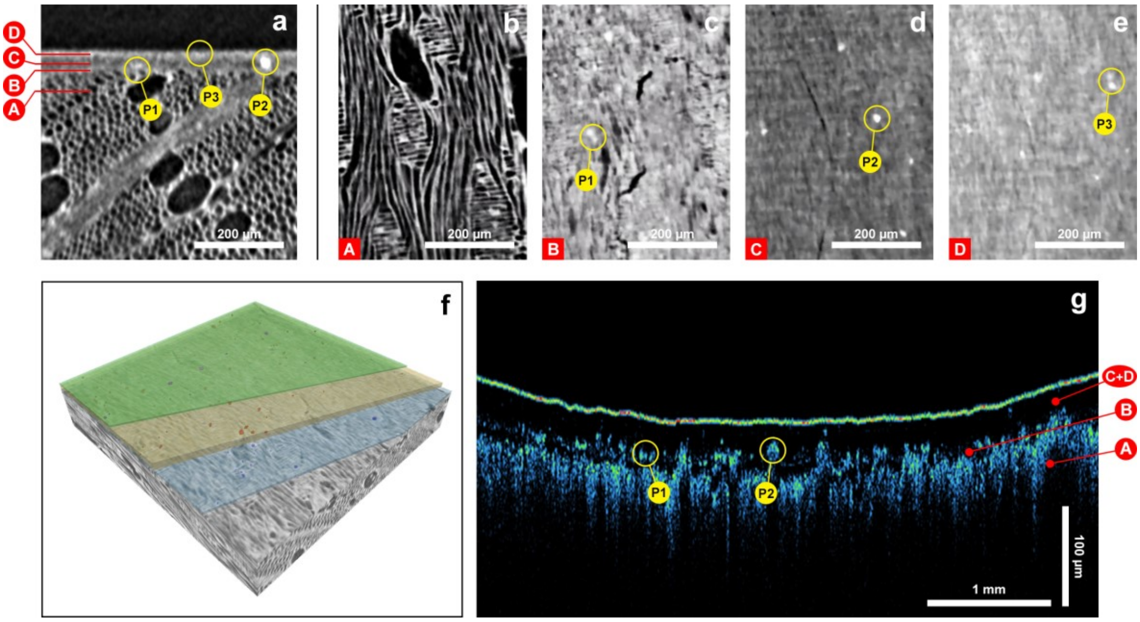

Figure 2.16 *Fragment F01, Jacobus Stainer. Transverse slice (a) from the SR-micro-CT volume: wood substrate is highlighted as A, layers as B, C and D, and particles as P1, P2, and P3. Radial slices (b-e) from the SR-micro-CT volume: the different layers and particles highlighted in (a) are here shown. Virtual reconstruction based on SR-micro-CT volume (f): the layer B is coloured in blue with dark blue particles, the layer C is shown in yellow with particles coloured in red, and the outermost layer D is green with violet particles. OCT tomogram presented in false-colour scale (g): wood substrate A, layer B, and layer C+D are shown. Particles embedded in the bottom and top layers are indicated as P1 and P2, respectively. The OCT image is corrected for refraction with* n_R *= 1.5. Figure published in [Fiocco et al., 2019].*

2.2.3.2 F13 – Gasparo "da Salò"

From the analyses previously carried out on the cross-section of a micro sample detached from the fragment F13, we discriminated at least five layers and numerous particles dispersed therein [Fichera et al., 2018]. In Fig. 2.17, we report the UV-light optical microscopy image of the cross-section as published in [Fichera et al., 2018], in order to better comprehend the description of its complex stratigraphy. The most exposed, very thin coat (L1 in Fig. 2.17) is characterized by a fine dispersion of black and red particles. The underneath varnish layer (L2), uniformly white-pinkish under UV light, is around 10 µm thick and no embedded particles were detected inside it. A further layer (L3) - thinner than 5 µm - showed a UV colour which is very similar to that of L1 and it embeds particles composed of Si, Al, Ca, K, S, Fe and P. The underlying layer (L4) is characterized by a white-pinkish UV fluorescence, similar to that of L2, and a thickness of about 10 µm; this layer was found to contain fine particles of iron-based pigment and larger gains of calcium sulphate (likely gypsum). Finally, a thin ground layer (L5) is laid on the maple wood: it showed a brownish UV colour and a considerable amount of organic thin black particles and Fe-based pigments.

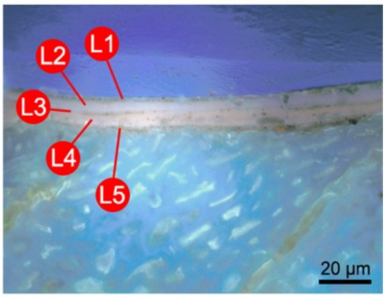

Figure 2.17 *UV-light optical microscopy image of the cross-section from the fragment F13 with five superimposed layers, indicated as L1-L5, applied on the maple wood. Figure published in [Fichera et al., 2018].*

Unlike the very complex stratigraphy highlighted in [Fichera et al., 2018], both the micro-tomographic investigations distinguished just two hypothetical varnish layers (Fig. 2.18).

The 3D virtual reconstruction from the SR-micro-CT scans is displayed in Fig. 2.18f: in this picture, the first layer detected on the wood is shown in blue colour - with the particles P1, diffused in it, which are coloured in green - while the second layer and the particles P2 are coloured in yellow and red, respectively. As concerns the thin ground layer, evidenced in [Fichera et al., 2018] and discriminated by OCT, no trace of it was found in the 2D transverse and tangential SR-micro-CT slices (Fig. 2.18a,b). The two layers C and D (Fig. 2.18a) - with an overall thickness of about 20-30 µm - over the maple wood (indicated as A) were distinguished by the SR-micro-CT technique on the basis of two distinct types of inorganic inclusions (P1 and P2 in Fig. 2.18) found at different depths. The stratigraphic distribution of these particles - appearing bright in the images - is clearly shown by radial slicing (Fig. 2.18d,e).

If we compare the multi-layered stratigraphy in [Fichera et al., 2018] with the simpler 3D reconstruction (Fig. 2.18f), a correspondence between the five layers discriminated under optical microscopy and the two layers detected by SR-micro-CT can be suggested. Considering the thickness of the coats as well as the distribution of the particles, in fact, the layers L3 and L4 (10-15 µm of overall thickness by previous studies) could have been detected as one single coat in the SR-micro-CT images (Fig. 2.18a, layer C; Fig. 2.18 f, blue layer), whereas the outer L1 and L2 (10-15 µm of overall thickness by previous studies) could have virtually merged into one in the SR-micro-CT images (Fig. 2.18a, layer D; Fig. 2.18f, yellow layer).

In the OCT tomogram (Fig. 2.18g), the detection of only some layers is reasonable if we take into consideration the axial resolution of the instrument (see appendix I). As previously investigated, in fact, the thickness of some layers was expected to be equal to or lower than 5 µm. This is the case of the layers L1 and L3 investigated in [Fichera et al., 2018]. In Fig. 2.18g, two light-scattering varnish layers - overall thickness of 15 µm - were detected (layers C+D) over the wood substrate (A). They lay on a low-scattering thin layer - indicated as B in Fig. 2.18g - which may be related to the ground coat named as L5 in [Fichera et al., 2018]. The particles dispersed in the varnish are too fine to be discriminated as separate structures in the OCT tomogram (lower than the instrumental lateral resolution). Nevertheless, their presence is corroborated by the strong light scattering of these layers.

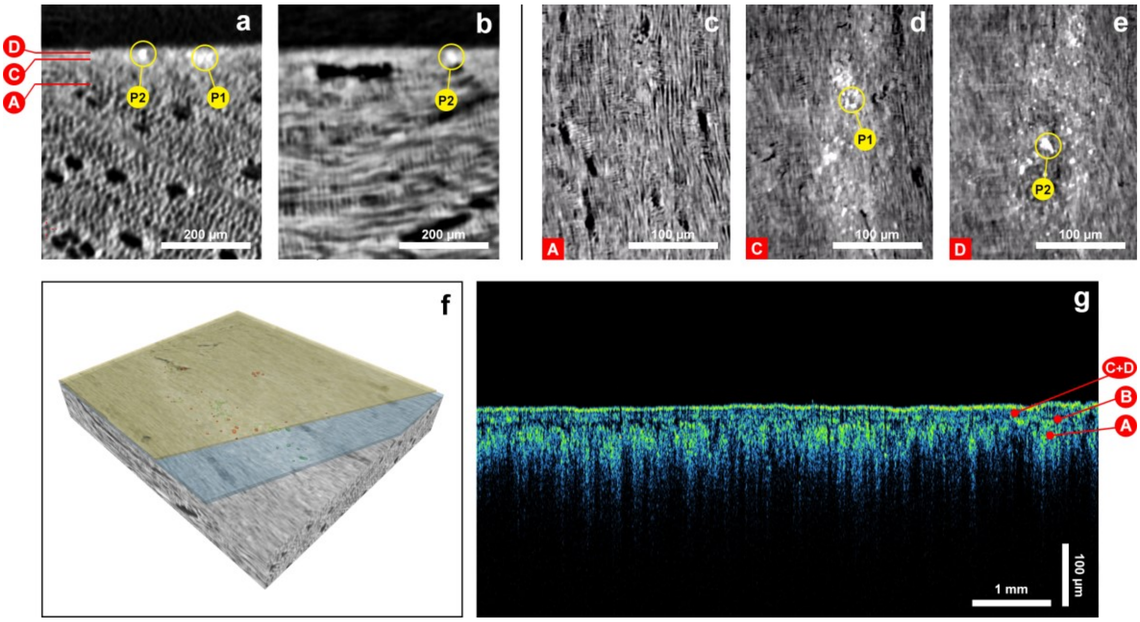

Figure 2.18 *Fragment F13, Gasparo "da Salò". Transverse (a) and tangential (b) slices from the SR-micro-CT volume showing the levels for radial slices reported in (c-e) and the different kinds of particles P1 and P2 embedded in the layers. Radial slices (c-e) from the SR-micro-CT volume: the different layers and particles highlighted in (a) are here shown. Virtual reconstruction based on SR-micro-CT volume (f): the layer C is coloured in blue with green particles and the layer D is shown in yellow with red particles. OCT tomogram presented in false-colour scale (g): wood substrate A, low-scattering layer B, and two light-scattering layers C+D with fine scattering particles are shown. The OCT image is corrected for refraction with $n_R = 1.5$. Figure published in [Fiocco et al., 2019].*

2.2.3.3 F16 – Gasparo "da Salò"

From the previous analyses [Fichera et al., 2018], this second fragment by Gasparo "da Salò" was found to be characterized by a simpler stratigraphy compared to F13. The UV-light optical microscopy image of the cross-section (Fig. 2.19), as published in [Fichera et al., 2018], shows two distinct overlying coats on the treated wood substrate: the layer L2 - ascribed to the varnish - is about 20 µm thick while the upper coat L1 is much thinner, measuring approximately 5 µm. In the varnish layer L2, at least two different types of particles were detected: some large grey particles, characterized by high content of Pb, and some finer red particles (2-3 µm in diameter), attributed to Fe-based pigments (possibly red ochre). Moreover, some grains of gypsum - possibly acting as filler - were found at the interface between layer L2 and wood, and some black organic particles were observed in the external layer L1.

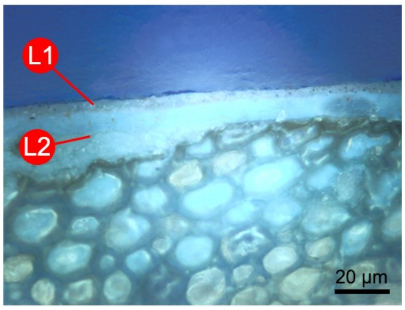

Figure 2.19 *UV-light optical microscopy image of the cross-section from the fragment F16 with two superimposed layers (L1, L2) applied on the maple wood. Figure published in [Fichera et al., 2018].*

The 2D transverse and radial SR-micro-CT slices (Fig. 2.20a-c) highlight the presence of only one single varnish layer (B) over the wood substrate (A). In this layer, displaying cracks (F1 in Fig. 2.20c), we detected several bright-white particles (P1 and P2 in Fig. 2.20a,c). Focusing on the greyscale and the grain size, in particular, we discriminated the finer Fe-based particles (P1 in Fig. 2.20a,c) from the bigger Pb-based ones (P2 in Fig. 2.20a,c). The 3D virtual reconstruction in Fig. 2.20e clearly shows a homogeneous dispersion of these pigments in the varnish and highlights the bimodal distribution of the grain-size. As concerns the external layer (L1) investigated in [Fichera et al., 2018], instead, no evidence of it was found by SR-micro-CT technique. The possible causes are to be found in the very reduced thickness of the layer, the similar chemical composition of the adjoining organic coats, or the lack of layers in some areas of the fragment as a consequence of the heterogeneous distribution of the layering.

On the contrary, OCT was able to distinguish the two organic layers (indicated as B and C in Fig. 2.20f) over the wood (A) and several particles embedded therein (P1-P3). In particular, the particles indicated as P1 and P2 were detected in the layer B, and those labelled as P3 are located in the external layer C. While the thickness of the layer B measures 23 to 26 µm, in consistence with the optical microscopy investigation [Fichera et al., 2018], the layer C is much thicker (10-19 µm) by OCT if compared to the 5 µm recorded using the microscope. Nevertheless, we expected slight thickness variations in different areas for coatings applied by brush.

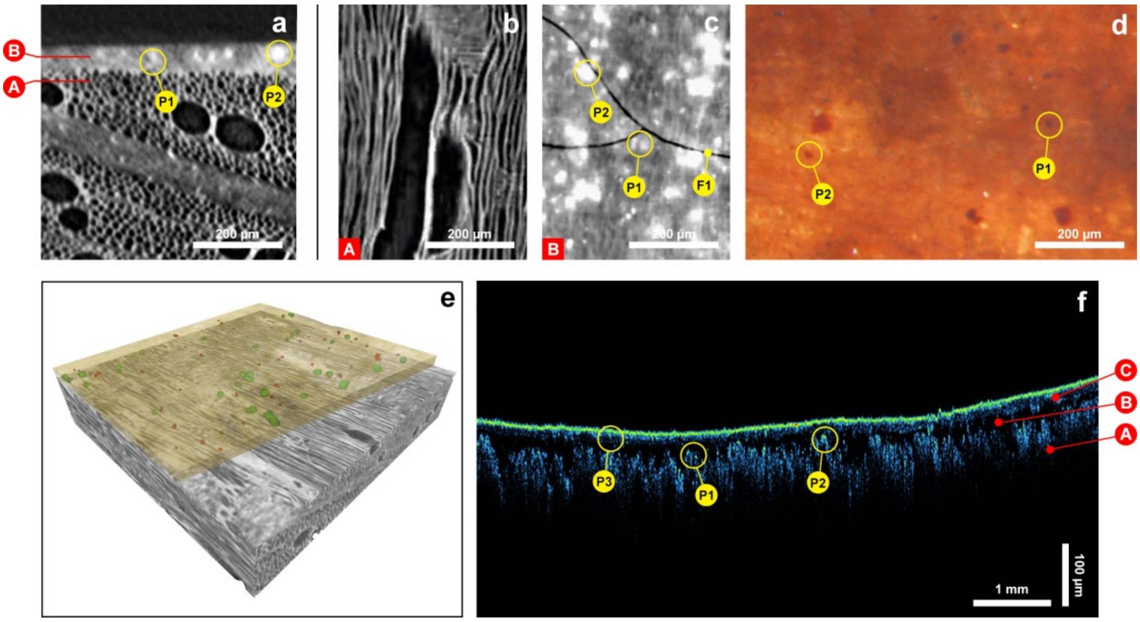

Figure 2.20 *Fragment F16, Gasparo "da Salò". Transverse slice (a) from the SR-micro-CT volume: wood substrate is highlighted as A, layer as B, and particles as P1 and P2. Radial slices (b,c) from the SR-micro-CT volume: the wood substrate, layers and particles highlighted in (a) are here shown. Cracks are indicated as F1. Stereomicroscopic image (d) of the surface showing the different particles P1 and P2 embedded in the finishing layers. Virtual reconstruction based on SR-micro-CT volume (e): layer B is coloured in yellow, with Pb- and Fe-based particles respectively coloured in green and red. OCT tomogram presented in false-colour scale (f): wood substrate (A), layers B and C are shown. Particles embedded in layer B are indicated as P1 and P2, and those embedded in the layer C are indicated as P3. The OCT image is corrected for refraction with $n_R = 1.5$. Figure published in [Fiocco et al., 2019].*

2.2.3.4 F20 – Giovanni Paolo Maggini

From the previous analyses [Fichera et al., 2018], the sample detached from a double bass attributed to Giovanni Paolo Maggini was found to be composed of one single 25- to 30-µm-thick layer, likely varnish, laid on the maple wood substrate. This layer showed a yellow UV-fluorescence and rarely dispersed reddish particles (around 2-3 µm of diameter) of possible iron oxides and aluminosilicates, attributable to ochres. The UV-light optical microscopy image of the cross-section, as published in [Fichera et al., 2018], is reported in Fig. 2.21. In this figure, the identified layer is indicated as L1.

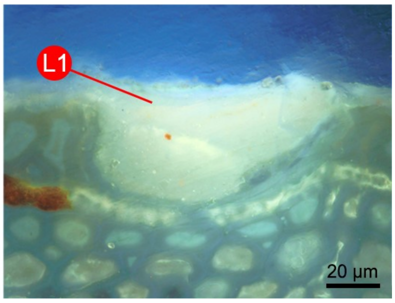

Figure 2.21 *UV-light optical microscopy image of the cross-section from the fragment F20 with single layer (L1) applied on the maple wood. Figure published in [Fichera et al., 2018].*

The 2D slices obtained by SR-micro-CT exhibit the maple wood (indicating its inner portion as A and its outer portion as A’ in Fig. 2.22 a,c,d), within which we identified a woodworm tunnel (about 1 mm of diameter) running some µm under the layer stratigraphy (see the grey rounds partially occupying the slices in Fig. 2.22b,c). The layer indicated as A’ (Fig. 2.22a,d) highlights the cells of wood as partially filled with an organic binder. Over the wood substrate, we discriminated one organic layer (C), which is characterized by an approximate thickness of 30 µm, and some rare particles embedded in it (Fig. 2.22a,e). The distribution as well as the concentration of these particles is clearly displayed in the 3D volume rendering (Fig. 2.22f).

OCT confirmed a thickness ranging from 19 to 36 µm for the layer C, as observed on the cross section by optical microscopy and on the fragment by SR-micro-CT (Fig. 2.22g). However, no particle was discriminated in this layer. Differently from the other techniques, OCT was able to discriminate a further thin layer (9-12 µm of thickness) - indicated as B in Fig. 2.22g - between the layer C and the wood A: the presence of moderate-scattering centres, in fact, allowed us to define the boundary between the layers B and C. This layer possibly acts as ground in the stratigraphy.

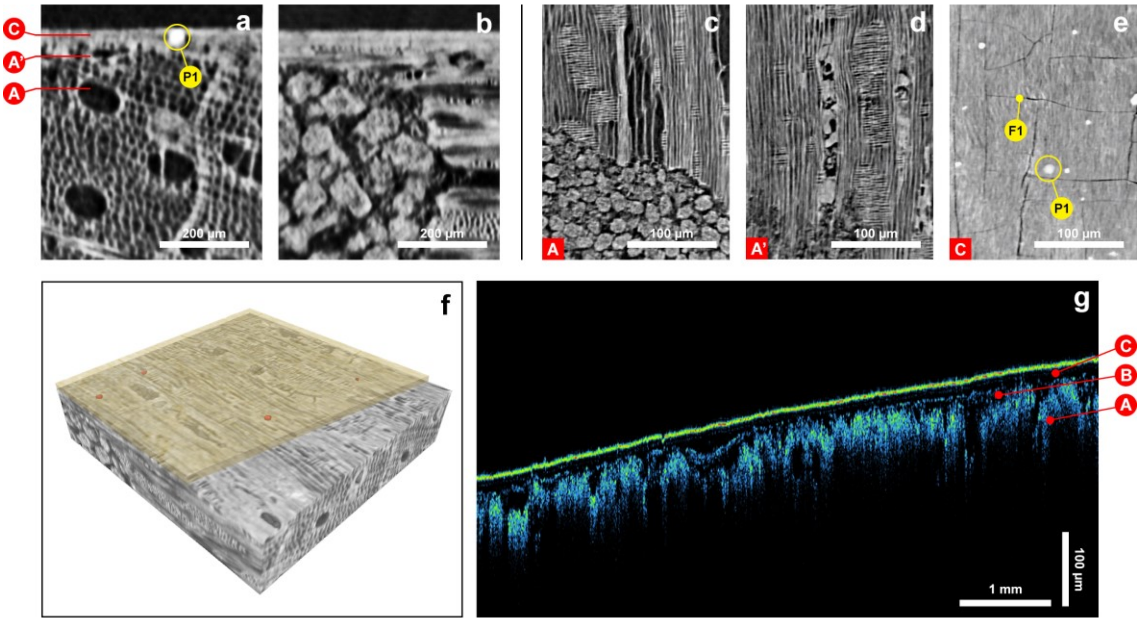

Figure 2.22 *Fragment F20, Giovanni Paolo Maggini. Transverse (a) and tangential (b) slices from the SR-micro-CT volume: inner wood is highlighted as A, outer wood as A’, layer as C, and particles as P1. Signs of previous infestations by woodworms are visible in (b) as close grey rounds. Radial slices (c-e) from the SR-micro-CT volume: the different layers and particles highlighted in (a) are here shown. Cracks are indicated in as F1. Signs of woodworms are visible in (c) as close grey rounds. Virtual reconstruction based on SR-micro-CT volume (f): layer C is coloured in yellow and particles in red. OCT tomogram presented in false-colour scale (g): wood substrate (A), layers B and C are shown. The OCT image is corrected for refraction with* $n_R = 1.5$*. Figure published in [Fiocco et al., 2019].*

2.2.3.5 F21 – Lorenzo Guadagnini

The analyses on the fragment attributed to Lorenzo Guadagnini, reported in [Fiocco et al., 2017], revealed a stratigraphy composed of two superimposed layers applied on the spruce wood. A 10-µm-thick proteinaceous layer - likely acting as ground - shows a brown-reddish UV fluorescence and two different types of particles embedded in it: some grains were identified as gypsum, while some others as aluminosilicates and iron oxides/hydroxides (likely red ochre pigments). The upper varnish layer, composed of natural diterpenic resins, was found to measure about 50 µm of thickness and no particle was detected within it. Furthermore, the study of Fiocco et al. highlighted a deformation of the tracheids in the first micrometres of the spruce wood under the ground layer, which made the authors hypothesize a chemical or mechanical wood treatment before the application of the finishing layers. In Fig. 2.23, we report the UV-light optical microscopy image acquired on the cross-section of a micro sample collected on the fragment F21, as published in [Fiocco et al., 2017].

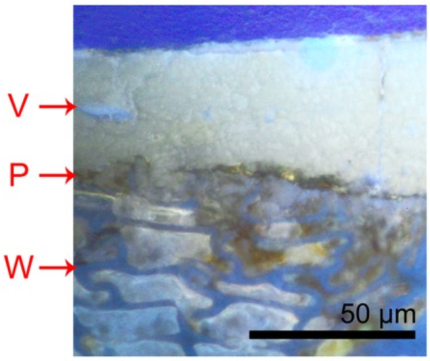

Figure 2.23 *UV-light optical microscopy image of the cross-section from the fragment F21 with two superimposed layers (P refers to preparation, V refers to varnish) applied on the spruce wood (W). Figure published in [Fiocco et al., 2017].*

The 2D SR-micro-CT slices (Fig. 2.24a-c) highlight the spruce wood substrate (indicated as A in Fig. 2.24), whose upper tracheids - as visible in the radial slice of Fig. 2.24c - were found to be partially filled with the overlying ground layer (B). Differently from what observed in Fig. 2.23, the deformation of the tracheids was not corroborated by the transverse slicing of the tomographic volume. In the light of this, we may attribute the wood deformation seen by optical microscopy to the sampling (and to the phases of the cross-section preparation involved) rather than to pre-treatments applied by the violin maker. In the layer B, we detected some fine bright particles which are indicated as P1 in Fig. 2.24a,c. As concerns the varnish layer (C), its thickness confirmed that one measured in the microscopic investigation, but some relevant differences emerged by the SR-micro-CT analysis about the presence of particles inside it. In fact, several grains clearly appeared as bright spots in this layer (P2 in Fig. 2.24 a,d) together with some air bubbles. The particle distribution is well visible also under the VIS-light stereomicroscope (Fig. 2.24e). Furthermore, both radial micro-CT slice and stereomicroscope image show the presence of cracks (F1 in Fig. 2.24d,e). The 3D virtual reconstruction of the volume clearly shows the distribution of the particles in the stratigraphy (Fig. 2.24f).

As concerns the thickness values, OCT results are consistent with those measured by micro-CT and microscopy: 12-15 µm for the low detectable ground layer (B) and a range from 30 to 50 µm for the varnish coat (C) (Fig. 2.24g). As investigated by micro-CT, grains (P2 in Fig. 2.24g) as well as diffuse cracks (F1 in Fig. 2.24g) were well discriminated in the layer C. However, no particle P1 was detected in the layer B despite its inorganic nature.

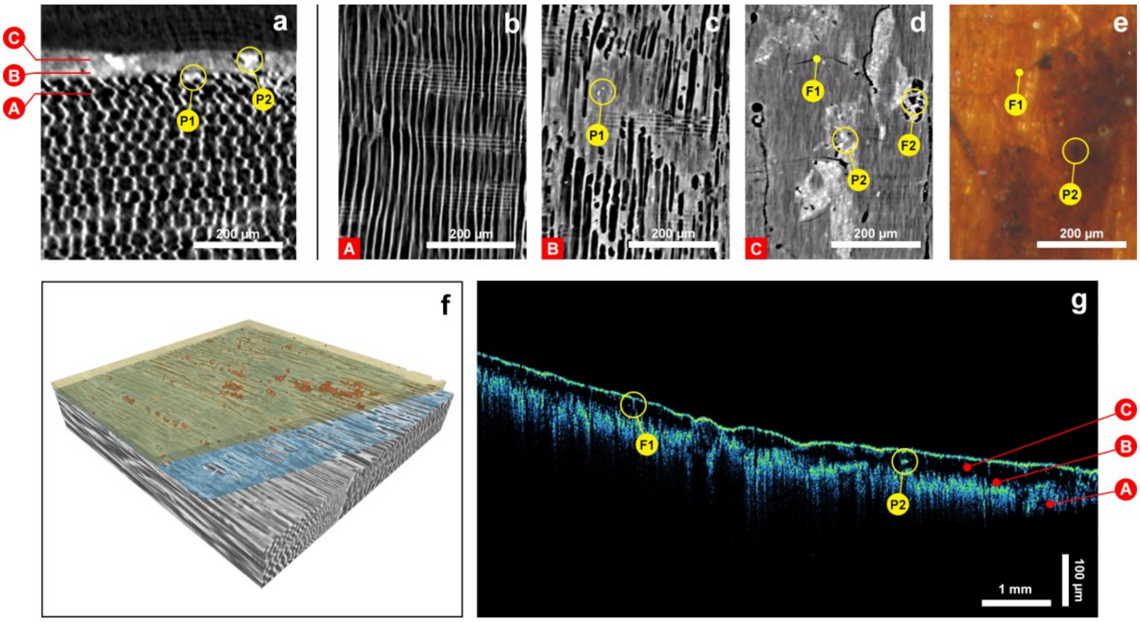

Figure 2.24 *Fragment F21, Lorenzo Guadagnini. Transverse slice (a) from the SR-micro-CT volume: wood substrate is highlighted as A, layers as B and C, and particles as P1 and P2. Radial slices (b-d) from the SR-micro-CT volume: the different layers and particles highlighted in (a) are here shown. Cracks and air bubbles are indicated as F1 and F2, respectively. Stereomicroscopic image of the external surface showing the particles P2 and the cracks F1. Virtual reconstruction based on SR-micro-CT volume (f): layer B is coloured in blue (it was difficult to colour the fine rare particles detected therein) and layer C is shown in yellow with particles coloured in red. OCT tomogram presented in false-colour scale (g): wood substrate (A), layers B and C are shown. Particles and cracks are indicated as P2 and F1, respectively. The OCT image is corrected for refraction with* $n_R = 1.5$*. Figure published in [Fiocco et al., 2019].*

Table 2.8 *List of the fragments from historical musical instruments with a schematic comparison of their layers according to the previous data [Fiocco et al., 2017; Fichera et al., 2018] and to the present results from SR-micro-CT and OCT scans. Capital letters identify the layers described in the text and shown in the figures. Table modified from [Fiocco et al., 2019].*

Fragment	Layer	Microscopic examination & Chemical analyses [11,12]	SR-micro-CT	OCT
J. Stainer F01-Cello	D	Not detected	10-µm-thick layer with particles	26- to 33-µm-thick layer with particles
	C	30-µm-thick oil-resinous varnish with Fe-based pigments	20-µm-thick layer with particles	
	B	15-µm-thick proteinaceous binder with carbonate-based particles	10- to 15-µm-thick layer with particles	12-µm-thick layer with particles
	A	Maple wood	Maple wood	Wood substrate (not recognized)
Gasparo "da Salò" F13-Cello	D	5-µm-thick layer with black and red particles	10- to 15-µm-thick layer with particles	15-µm-thick layer composed of two thin layers with particles
		10-µm-thick layer		
	C	5-µm-thick layer with inorganic particles	10- to 15-µm-thick layer with particles	
		10-µm-thick layer with Fe-based pigments and gypsum grains		
	B	5-µm-thick layer with black particles and Fe-based pigments	Not detected	About 5-µm-thick layer
	A	Maple wood	Maple wood	Wood substrate (not recognized)
Gasparo "da Salò" F16-Cello	C	5-µm-thick layer embedding organic black particles	About 30-µm-thick layer with two types of particles identified through grayscale variations and with cracks	10- to 19-µm-thick layer with particles
	B	20-µm-thick layer with Fe- and Pb-based particles		23- to 26-µm-thick layer with particles
	A	Maple wood	Maple wood	Wood substrate (not recognized)
G.P. Maggini F20-Double Bass	C	25- to 30-µm-thick layer with Fe-based pigments	30-µm-thick layer with particles and cracks	19- to 36-µm-thick layer
	B	Not detected	Not detected	9- to 12-µm-thick layer
	A	Maple wood	Maple wood	Wood substrate (not recognized)
L. Guadagnini F21-Double Bass	C	50-µm-thick varnish layer	50-µm-thick layer with particles, cracks and air bubbles	30- to 50-µm-thick layer with particles and cracks
	B	10-µm-thick proteinaceous binder with Fe-based and gypsum particles	10-µm-thick layer with particles	12- to 15-µm-thick layer
	A	Spruce wood	Spruce wood	Wood substrate (not recognized)

2.2.4 Conclusions

The overall results obtained by this joint study merit some general comments.

Optical microscopy previously carried out on cross-sections resulted the most effective technique to discriminate layers composing the physical structure of historical bowed string instruments. Numerous thin layers were distinguished, in particular, on the basis of their different UV fluorescence under optical microscope, as observed for example in the fragment F13 [Fichera et al., 2018]. However, we must take into consideration that this approach is invasive since it required the sampling of micro-fragments. Moreover, the collected sample could not be representative of the entire object.

If we consider the number of layers identified by optical microscopy as a benchmark, we can claim that both the OCT and SR-micro-CT techniques have mostly reached equal or lower performances. In general, OCT was able to discriminate layers with thickness equal to or higher than 5 μm (see axial resolution in appendix I), while the SR-micro-CT capability of highlighting the number of layers (even with thicknesses lower than 5 μm) was mainly reached by the identification of different types of particles in the stratigraphy and by the variations in the grayscale between coats. Moreover, the two micro-tomographic techniques allowed us to determine the thickness of the identified layers. For these values, we generally expect a large variability because the coat application was made by brush.

As concerns the particles embedded in the layers, the 3D virtual reconstructions obtained from SR-micro-CT volumes and post-processed by an image editing software were important to identify the accurate position of the particles in the stratigraphy as well as the multi- or bi-modal grain size distribution. On the other hand, the representation of the particles in the OCT tomograms was not as detailed as that of SR-micro-CT because of the worse lateral resolution compared to the axial one. In this regard, possible advancements could be investigated in the future (e.g., the development of an appropriate software dedicated to the data treatment). Additionally, the SR-micro-CT examination provided information also on the wood cells, differently from OCT which was able to penetrate it up to few tens of μm.

In conclusion, we can claim that the combined micro-tomographic approach provided complementary information about the coating systems of bowed string instruments: OCT was able to discriminate organic layers even in absence of particulate dispersed therein, while SR-micro-CT allowed us to focus on the inorganic particles more deeply in terms of their location, distribution and morphology as well as on the wood structure. The most advantageous aspect of the tomographic approach applied to the study of such complex multi-layered systems was certainly the possibility of collecting pictures of the undisturbed material. If the microscopic investigation of the cross-sections provides the most complete information about the stratigraphy of the micro samples, however, the original structures could be deformed by the invasive method of sampling and this may lead to incorrect interpretations of the morphology

2.3 Stratigraphic analysis of fragments from historical bowed string instruments and a small violin by combining micro-destructive and non-destructive approaches: LIBS and OCT

2.3.1 Introduction

This combined study was made possible thanks to the collaboration with the University of Pavia through the Arvedi Laboratory of Non-Invasive Diagnostics, the Applied and Laser Spectroscopy Laboratory of CNR and the Nicolaus Copernicus University within the Accesses to Research Infrastructures activity in the H2020 Programme of the EU (IPERION-CH), the Fondazione Museo del Violino Antonio Stradivari Cremona, the International Violin Making School of Cremona, the Civica Scuola di Liuteria di Milano, the Fondazione Arvedi Buschini, the Fondazione Bracco, and the Cultural District of Violin Making. The results have been published in Journal of Cultural Heritage [Poggialini et al., 2020].

Objects of this research are three fragments of historical bowed string musical instruments belonging to the “Collezione Sgarabotto”, already investigated by micro-tomographic techniques in 2.2, and the *Bracco* 1793 small violin made by Lorenzo Storioni, whose non-invasive results are reported in 2.1. The history of these instruments is described in appendix II. For the first time in the musical instrument field, we coupled LIBS and OCT techniques to gather information on the elemental composition of the finishing layers and the subsurface stratigraphy (or internal structure). In 2009, the two techniques were combined to study panel paintings [Kwiatkowska et al., 2009] and coins [Amaral et al., 2009]. In these works, researchers measured the depth of the LIBS crater by OCT and linked the changes of its profile with the number of laser pulses. As a result, the concentration trends of the different elements were scaled in-depth, and the thickness of the layers was defined in the units of length, instead of in the number of LIBS pulses. Four years later, the same group of [Kwiatkowska et al., 2009] further developed the method by applying more accurate techniques for the depth determination of the LIBS crater [Kaszewska et al., 2013].

LIBS analyses were performed in 2018 at the Arvedi laboratory by the researchers of the Applied and Laser Spectroscopy Laboratory of the Research Area of CNR (Pisa, Italy) within the E-RIHS.it (already IPERION CH.it), a project funded by the European commission H2020 under Grant Agreement No. 739503. Our project, entitled “STratigraphic Reconstruction through Advanced Technologies In Valuable Ancient Rare Instruments” (acronym STRATIVARI), is part of a larger-scale investigation campaign on 26 fragments of historical bowed musical instruments realized in the period from the 16th to 19th century. The entire set previously underwent preliminary non-invasive and invasive studies and PCA was applied to classify relics, highlighting the most relevant and particular elements in the dataset as well as the correlations among fragments [Fichera et al., 2018]. However, the stratigraphic structure and the inorganic phases dispersed in the organic binders needed to be deeply studied for a more accurate determination. From this necessity, we have addressed the ST.R.A.T.I.V.A.R.I. project to a limited number of these fragments, selected on the basis of their geographic (i.e., Brescia area) and chronological (i.e., 16-17th centuries) attribution, with the aim of characterizing the materials and the manufacturing techniques developed over the first years of the modern lutherie in this specific area of Italy by the LIBS technique (Fig. 2.25). This analysis provides information on the elemental composition of the coating system of the instruments under study. As presented in the critical review by Botto et al. [Botto et al., 2019], LIBS has been widely applied in cultural heritage and archaeology over the years. The wide use can be surely ascribed to some of the advantages of this method: no specific preparation of the sample is needed for the experiment, the measurement time is short, it is micro-destructive, the total emission spectra of the sample can be usually recorded and analysed within a single measurement. However, LIBS has so far never been applied to investigate the stratigraphy of musical instruments.

Briefly, in the LIBS technique a small quantity of sample is ablated during the laser-induced plasma generation. The ablation creates a micro-crater on the surface of the sample, with a depth of several dozen micrometres, and the spectrum of light emitted from the plasma produced by ablated material is analysed. The further development of the technique into the LIBS stratigraphic method [Anderson et al., 1995; Romero and Laserna, 1997; Vadillo and Laserna, 1997; St-Onge, 2002; Mateo et al., 2003] was reached when a train of pulses of low energy has been delivered to the same analytical spot of the sample. Every pulse ablates a new layer, and the analysis of each layer allows for the identification of the stratigraphic system of the sample. This stratigraphic approach was exploited for the analysis of steel coatings in industrial applications [Nagy et al, 2017; Pacher et al., 2018] and also in cultural heritage, for instance in the study of historical painting model samples [Pospíšilová et al., 2018] and ancient painted artefacts [Nassef et al., 2016]. With regard to this approach, measuring the crater depth and the quantity of ablated mass in relation to the number of consecutive laser shots represents one of the main issue. In general, the quantity of ablated mass and the depth of the crater depend on the laser parameters, like wavelength, pulse energy and duration, dimension of the ablation spot, but also on the composition of the sample matrix. If the sample is homogeneous, mathematical models can be used to calculate approximately the ablation rate as a function of the number of pulses [Nagy et al., 2017; Pacher et al., 2018]. However, in the case of complex and heterogeneous stratigraphies, the mathematical approach is no longer suitable and other techniques, like optical microscopy, can be employed to investigate the morphology of the LIBS crater [Nassef et al., 2016;

Pospíšilová et al., 2018]. For non-homogeneous samples (e.g., those composed of different overlying layers), it is important to stress the fact that ablation does not advance at the same rate throughout the various layers of the material. Consequently, the information about the elemental composition of subsequent layers cannot be fully scaled simply by measuring of the crater depth uniquely at the end of LIBS experiments.

Focus of the current research was also to measure the thickness of the layers composing the physical structure of the object. In the cultural heritage field, OCT has successfully fulfilled this aim since 2004 and a brief scientific background of this technique is reported in the introduction of 2.1. The OCT analyses were carried out in 2018 at the Arvedi laboratory by the researchers of the Nicolaus Copernicus University (Toruń, Poland) within the MOLAB Transnational Access-EU H2020 Project IPERION CH (Grant Agreement No. 654028). As already explained in 2.1 and 2.2, the project "Non-invasive Examination of Stratigraphic System in violins" (acronym: thickNESS) involved the OCT analysis of violins, as primary goal, and then of fragments from instruments belonging to the "Collezione Sgarabotto" and mock-ups. OCT cross-sections were used in this study to examine both the original stratigraphy, gathering information on the thickness of the layers and the presence of particles in the binders, and the LIBS craters in terms of depth, volume, shape and range within the investigated subsurface structures.

Detailed information about the analytical instrumentation and the acquisition parameters is reported in appendix I. This information concerns not only the two leading techniques of this research but also XRF and SEM-EDX, employed to help interpret the LIBS data. The use of these supporting techniques is documented in the introduction paragraph of 2.3.3.

In this study, we combined the LIBS and OCT techniques to study three fragments of ancient Bresciani cellos and double basses belonging to the "Collezione Sgarabotto" and a Cremonese small violin, with the aim of identifying the multiple layers and the materials constituting the instrument stratigraphy. LIBS may perform a stratigraphic study by estimating the elemental composition of the layers, whereas OCT would allow us to characterize shape and dimension of the LIBS craters as well as helping attribute the LIBS data to the layers of the coating system. Before being applied to the real case studies, we have tested this approach on a mock-up. The interpretation of the LIBS results was supported by the analysis with XRF (and SEM-EDX for one fragment). Moreover, when present, we also considered information from previous microscopic examination and chemical analyses [Fichera et al., 2018].

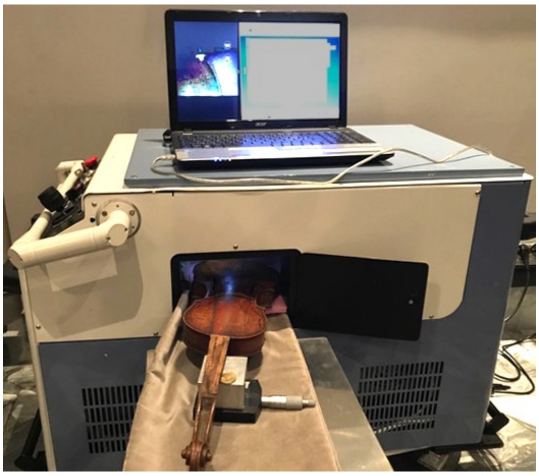

Figure 2.25 *Modì portable LIBS instrument during the analysis of the Bracco 1793 small violin at the Arvedi Laboratory of Non-Invasive Diagnostics (Cremona, Italy).*

2.3.2 Materials

2.3.2.1 Mock-up

A schematic representation of the stratigraphy under study is illustrated Fig. 2.26. The mock-up is part of the experimental series prepared by the master Claudio Canevari (Civica Scuola di Liuteria, Milano, Italy) and investigated in chapter 1 (in detail, mock-up m.C). It consists of a 3-mm-thick maple wood *(Acer pseudoplatanus)* glued on a 9-mm-thick piece of multi-layered birch plywood to prevent warping. The exposed radial longitudinally cut smoothed face was first sized by brush with potassium caseinate to isolate the wood. After the smoothing of the surface with Abranet P1000 sandpaper, it was ground coated by brush with a dispersion of mineral talc in potassium caseinate (10% w/w). The surface was smoothed, again, with Abranet P1000 sandpaper and then coated with a linseed oil-colophony varnish using a bar film applicator (K Hand Coatermodel, Erichsen GmbH). Finally, a layer of linseed oil-colophony varnish containing Fe_2O_3 pigment dispersed therein (1% w/w) was laid on the mock-up through bar film applicator and dried under UV lamps (Philips TL60 W/10-R 1SL/25 Attiniche UVA/10) for 18h. The provenance of the selected products as well as the preparation procedures of ammonium caseinate and linseed oil-colophony varnish are described in 1.2.1. As for the mineral talc, we report the composition as stated by Kremer in the technical specifications: SiO_2 47%, MgO 31%, Al_2O_3 10 %, Fe_2O_3 1.5%, CaO 1%.

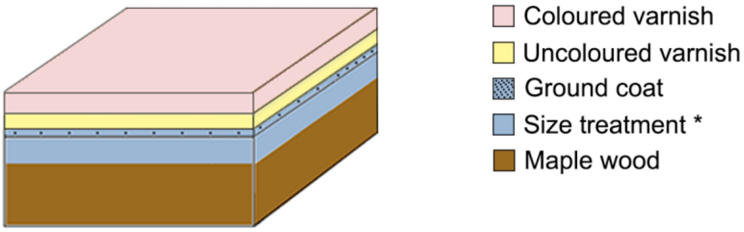

Figure 2.26 S*chematic representation of the mock-up stratigraphy as described in the text. The stratigraphy represents a portion of the mock-up C investigated in chapter 1. * Size treatment: completely penetrated the wood.*

2.3.2.2 Historical musical instruments

The three fragments of historical bowed string musical instruments belonging to the "Collezione Sgarabotto" and the *Bracco* 1793 small violin by Lorenzo Storioni are listed and described in Table 2.7. The photos and the history of the selected case studies are reported in detail in appendix II. The LIBS and OCT examinations were performed on the back plate of the instruments and the analytical areas are displayed in Fig. 2.27.

Additionally, a microsample was collected from the historical fragment F13, embedded in epoxy resin (Epofix Struers and Epofix Hardener with ratio 15:2) and cut as cross-section. The section was then polished with silicon carbide fine sandpapers (500-8000 mesh) and, before the SEM-EDX examination, it was made conductive with a graphite coating obtained by a Cressington Carbon Coater 208C.

Table 2.7 *List of the instruments investigated in this study with inventory number, name, life period and geographical area of provenance of the violin maker, and type of instrument. The last information, for the fragments, refers to the original instrument from which the relic was removed during restoration interventions. Table modified from [Poggialini et al., 2020].*

Inv. N°	Violin Maker	Period	Area	Instrument
F13	Gasparo Bertolotti "da Salò"	1540-1609	Brescia, Italy	Cello
F16	Gasparo Bertolotti "da Salò"	1540-1609	Brescia, Italy	Cello
F20	Giovanni Paolo Maggini	1580-1631	Brescia, Italy	Double bass
SL793	Lorenzo Storioni	1744-1816	Cremona, Italy	Small violin

Figure 2.27 *UVIFL photos of the back plate of the instruments with the analytical areas highlighted.*

2.3.3 Results and discussion

In this section, we present and discuss the results from the experimental part on the mock-up, first, and then those obtained on the real case studies. On the basis of the tests performed on the mock-up, a series of 15 measurement pulses was delivered on the same spot of each historical object. The fragments and the small violin were preliminarily investigated by XRF spectroscopy, in order to identify the elemental markers for the LIBS analysis. The XRF results are displayed in Table 2.9. The fragment F13 by Gasparo "da Salò" was additionally micro sampled and the cross-section analysed by SEM-EDX. The XRF and EDX results helped us attribute the LIBS data to the different layers.

Table 2.9 *Estimation of elements detected through the XRF analysis on the fragments and the Bracco small violin. The displayed values correspond to the net area counts of the peak (Kα) normalized to time and to net area counts of the coherent scattering peak of Rh-Kα. The calculated Standard Deviation of Mean (SDOM) is less than 0.03 for all XRF values. Table modified from [Poggialini et al., 2020].*

Inv. N°	Detected elements						
	Si	S	K	Ca	Mn	Fe	Pb
F13	0.08	0.38	0.73	2.24	0.21	1.95	–
F16	0.11	1.47	1.05	4.34	0.20	6.14	6.87
F20	0.08	–	1.24	3.13	–	0.74	–
SL793	0.05	0.17	0.87	1.22	0.18	0.43	–

2.3.3.1 Mock-up

In order to estimate the rate of ablation by LIBS pulses, we performed five LIBS stratigraphy sequences on the mock-up, each one respectively with a number of laser shots of 1, 2, 5, 10 and 15. After each sequence, thickness measurements were conducted in the ablated area by OCT and an estimation of the depth of the LIBS craters in relation to the number of laser shots is reported in Fig. 2.28. The graph shows that the ablation rate varies through the depth profiling. We can attribute this analytical evidence to the matrix composition, which is different for the layers of the stratigraphy. From the OCT cross-sectional image of Fig. 2.29, in particular, the layers A (ca. 20 μm) and B (ca. 5-10 μm) are composed of varnish for a total thickness of about 25-30 μm, with the external one (A) containing Fe_2O_3 particles dispersed therein. The underlying ground (C) - laid on maple wood (D) - was found to measure ca. 5 μm and includes mineral talc as filler.

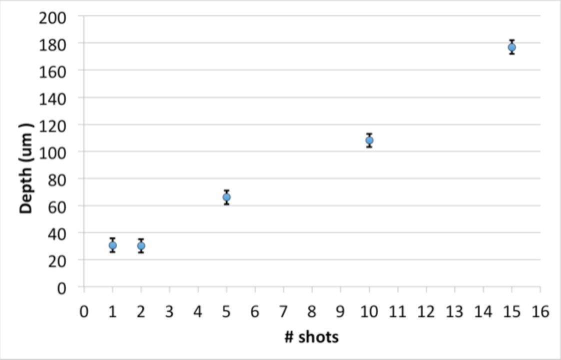

Figure 2.28 *LIBS crater depth estimated with OCT in relation to the number of laser shots. Figure published in [Poggialini et al., 2020].*

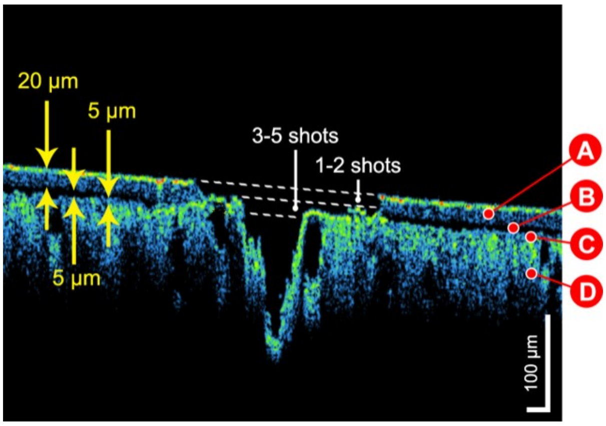

Figure 2.29 *OCT analysis of the mock-up showing the LIBS crater formed by 15 laser shots. Letters refer to coloured oil-colophony varnish (A), uncoloured oil-colophony varnish (B), proteinaceous ground with dispersion of talc (C) and maple wood substrate (D). The image is corrected for refraction with $n_R = 1.5$. Figure published in [Poggialini et al., 2020].*

As displayed in Fig. 2.29, the first 1-2 laser shots directly ablated the two varnish layers forming a quite large but surface crater characterized by not increasing depth of about 25-30 μm. Interestingly, the diameter of the varnish crater was estimated between 700 and 800 μm for all the stratigraphy sequences (i.e., 1, 2, 5, 10 and 15 shots); the large size of this crater can be ascribed to the brittle nature of the varnish coats. Differently from the dimension of a crater formed on more structured layers (diameter of ca. 100-200 µm), a larger amount of material was removed from the varnish layers due to the combined effect of pulse shockwave, laser ablation and plasma plume expansion. From the OCT tomogram, we can see that the ground layer and the first tens of microns of the wood are ablated with the shots from 3 to 5. After the 5th shot, we can estimate a steady ablation rate in the wood of ca. 10 µm per measurement, using a linear fitting.

In the musical instruments, we know that there exists a variability of thicknesses from an area to another of the layers, and that the wood density may not be homogeneous as well. As a consequence, the trends produced by LIBS experiments were expected to be variable.

Firstly, we estimated the relative concentration of Si, Mg, Ca, Al, K and Fe - elements of interest in this study - using the Calibration-Free (CF-LIBS) method [Tognoni et al., 2010]. In Fig. 2.30 we can see the concentration trend of Si - selected as a marker of the ground layer in the mock-up - as a function of the number of laser shots (CF-LIBS). As displayed in the figure, Si reached its maximum abundance at the 3rd laser shot, and the same trend was found for Mg (here not shown). This was likely associated to the ablation of the ground, within which the mineral talc is dispersed. From this estimation, we can assume that the ground was ablated between the 3rd and the 5th laser shot. From the 5th laser shot on, the ablation rate started following an almost linear trend: the wood was completed exposed and its matrix did not vary significantly. An image of the full LIBS crater after 5 laser shots is reported in Fig. 2.31.

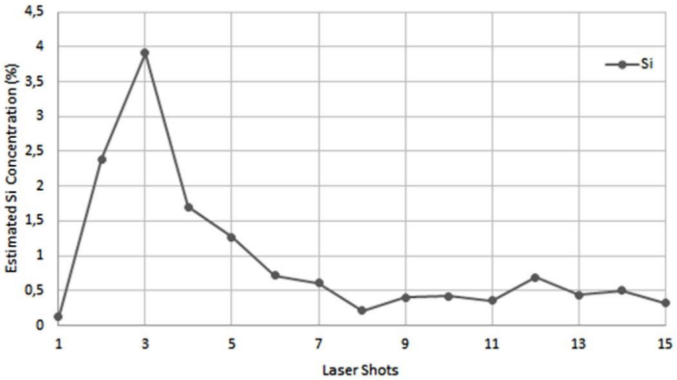

Figure 2.30 *Concentration trend of Si in the mock-up as a function of the number of laser shots (CF-LIBS). Figure published in [Poggialini et al., 2020].*

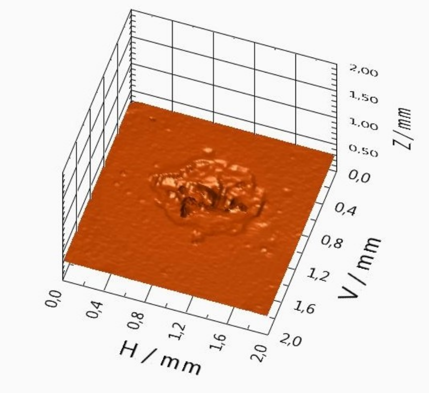

Figure 2.31 *3D view of the crater after 5 shots in the mock-up. Figure published in [Poggialini et al., 2020].*

The finding obtained by CF-LIBS suggested the possibility of using the concentration of talc, provided by Kremer Pigmente (and reported in 2.3.2.1), as a reference to improve the CF-LIBS approach. The method is called One Point Calibration (OPC-LIBS): only one standard of known composition is necessary to empirically identify the essential experimental and spectroscopic parameters, whose knowledge is inaccurate or lacking. The commercial talc was analysed, and its concentration estimated by the CF method: the instrument was then calibrated taking the concentration values provided by Kremer as reference. With this method, the trueness of the LIBS analysis definitely improves compared to the traditional CF approach [Agrosì et al., 2014; Cavalcanti et al., 2013]. Once the 3rd laser shot spectra were assigned to talc, the OPC-LIBS method was developed. The results are displayed in Fig. 2.32. The 1st laser shot can be related to the ablation of the external Fe_2O_3-coloured layer (layer A in Fig. 2.29) since the concentration of Fe was found to have its maximum at this measurement (Fig. 2.32b). Observing the low concentrations at the 2nd laser shot, we can ascribe this measurement to the ablation of the underlying uncoloured varnish (layer B in Fig. 2.29), which has a purely organic nature. As previously reported, we attributed the 3rd laser shot to the ablation of the ground (layer C in Fig. 2.29) because of the high concentration of Si and Mg, but also of Al e Fe, related to the mineral talc. The trend of these elements is well highlighted in Fig. 2.32a,b. The increase in the content of Ca and K (Fig. 2.32b), at the 3rd shot, was attributed to the K-caseinate acting as binder in the layer C as well. From the 3rd shot on, we detected a gradual reduction in the concentrations: this evidence indicates that the external layers have been removed and the wood starts being targeted by laser pulses.

We want to specify that the values reported in the present study refer to the relative concentration of the elements, as a function of the crater depth on the surface, rather than to the absolute abundance of them. In this way, we identified the variations in concentration of the elements which, in turn, can be related to the layers in the stratigraphy. Considered the nature of the musical instruments coating, as well as its heterogeneity, the interest focuses on the variability trend of the elements instead of the accurate estimation of their concentrations. The re-deposition effect might cause a less defined transition from one layer to another; in this case, however, this effect did not compromise a correct estimation of the trends since the composition of the layers is different. The combined use of the CF-LIBS and OPC-LIBS methods has improved the reliability of the results.

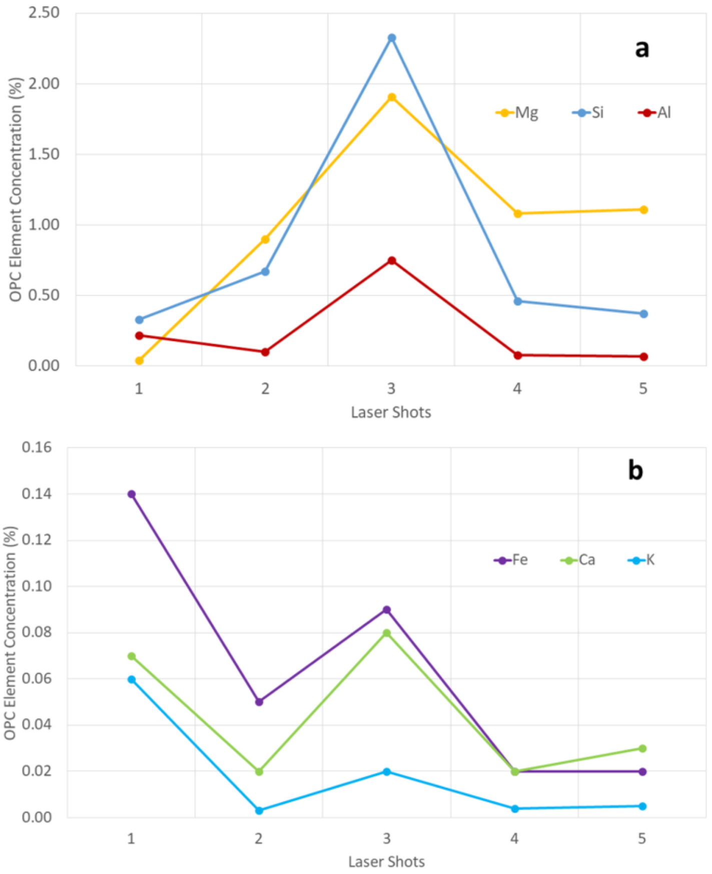

Figure 2.32 *Concentration trend of Mg, Si, Al (a) and Fe, Ca, K (b) in the mock-up as a function of the number of laser shots (OPC-LIBS). A relative error of 10% was estimated for each elemental concentration. Figure published in [Poggialini et al., 2020].*

2.3.3.2 F13 – Gasparo "da Salò"

The SEM-EDX analysis performed on the cross-section of a micro sample detached from the fragment F13 by Gasparo "da Salò" revealed a very complex stratigraphy. The SEM backscattered image and the EDX map related to the most interesting elements are displayed in Figs. 2.33 and 2.34, respectively. As already described in 2.2, the stratigraphy is made of five overlapped layers: the external layer A is very thin (ca. 5 µm) and embeds a fine dispersion of Fe-, Si- and Al-based particles (Fig. 2.34a-c) and possibly Ca-containing grains (Fig. 2.34e); the second layer B is around 10 µm thick and does not contain any particle in the varnish; the third layer C (ca. 5 µm) embeds some Fe- and Si- (Fig. 2.34a,b), with Al- and K-based particles (Fig. 2.34c,d) attributable to aluminosilicates; the varnish layer D (ca. 10 µm) shows a dispersion of Ca-based grains (Fig. 2.34e), likely gypsum, together with few particles composed of Si (Fig. 2.34b); the ground layer E, directly laid on the maple wood substrate F, is finally characterized by a thickness of about 5 µm and by Fe- and Ca-based particles (possibly gypsum, Fig.

2.34a,e) dispersed therein. The SEM-EDX results added some information to the stratigraphy previously analysed through microscopic and chemical examinations [Fichera et al., 2018], as reported in 2.2.

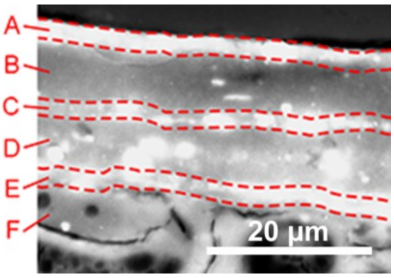

Figure 2.33 *SEM-BSE image of the cross-sectional micro sample of the fragment F13. The highlighted layers are described in the text. Figure published in [Poggialini et al., 2020].*

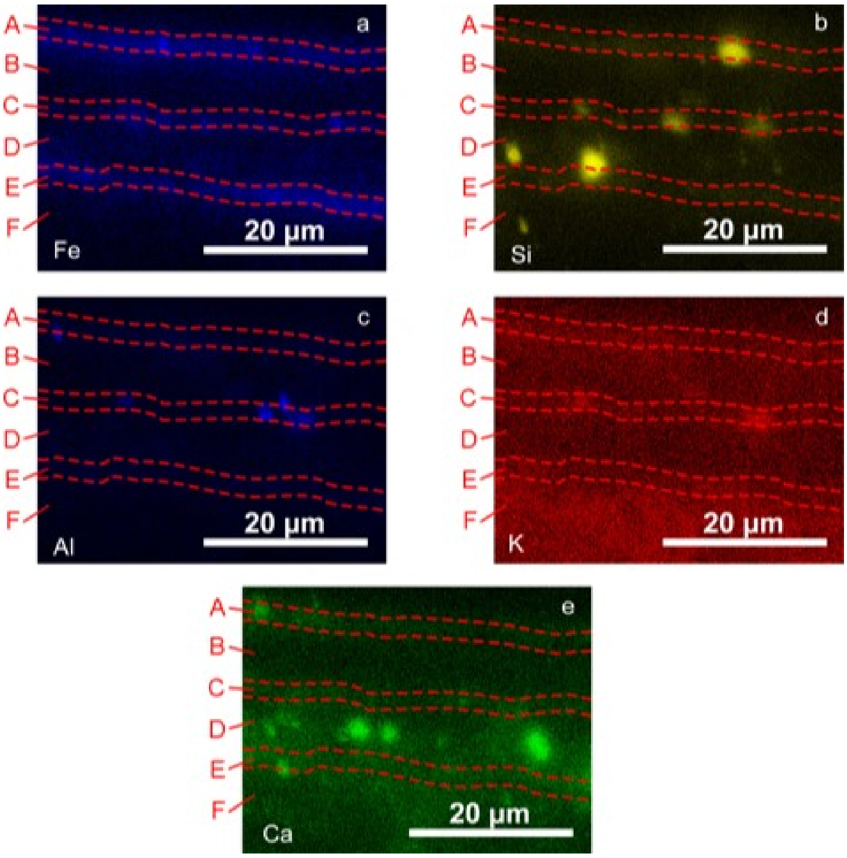

Figure 2.34 *EDX maps of the fragment F13 related to Fe (a), Si (b), Al (c), K (d) and Ca (e) elements.*
Figure published in [Poggialini et al., 2020].

By the OCT analysis, some varnish layers were not discriminated due to the low thicknesses involved (Fig. 2.35). Only two light-scattering varnish layers - overall thickness of ca. 15 µm (indicated as A in Fig. 2.35) - with fine scattering particles dispersed therein, and the ground coat (indicated as B), are visible on the wood substrate C.

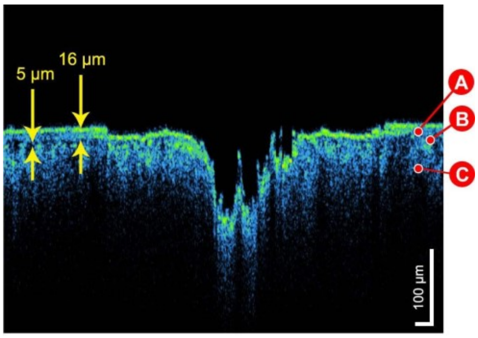

Figure 2.35 *OCT tomogram of the fragment F13, with the LIBS crater formed by 15 laser shots. A possible partial re-deposition of material is visible at the bottom centre of the crater. Letters refer to varnish (A), ground (B) and wood substrate (C). The image is corrected for refraction with n_R = 1.5. Figure published in [Poggialini et al., 2020].*

Preliminary XRF analysis on the fragment revealed high intensity of Fe- and Ca-Kα lines in the coating system, as reported in Table 2.9. Additionally, the presence of Si, S, K and Mn was detected. In particular, the presence of Mn in association with Fe could be ascribed to the earth pigments (e.g., Umber or burnt Umber) [Rovetta et al., 2017].

The OPC-LIBS results, shown in Fig. 2.36, revealed a higher concentration of Fe, Al and Si in the spectra related to the laser shots 2, 5 and 7. In accordance with the EDX results, we can try to associate this concentration increase to the real distribution of these elements in the stratigraphy. The surface layer (indicated as A in Fig. 2.34) may be too thin - or missing - in the area where the LIBS pulses have been delivered, as a possible result of the direct exposition of this layers to the external agents. If this is true, the spectrum of the 1st laser shot may be ascribed to the layer B (as indicated in Fig. 2.34), where no particle has been found therein, while the 2nd shot can be related to the ablation of the layer C (as indicated in Fig. 2.34) containing Fe-, Al-, and Si-based particles. In correspondence of the shots 5 and 7, the concentration of Ca, Fe, Si and Al increased. We can attribute these two shots to the lower part of the layer D (as indicated in Fig. 2.34) and to the whole thickness of the ground layer E (as indicated in Fig. 2.34) up to the wood, validating the presence - revealed by EDX - of Ca-based grains as well as of particles containing Fe and Si. Combining the results, we can speculate that each laser shot has incrementally penetrated ca. 5 µm into the coating system. This value is approximately half of the rate estimated in the coating system of the mock-up, likely due to the higher density of the materials employed to finish the fragment F13.

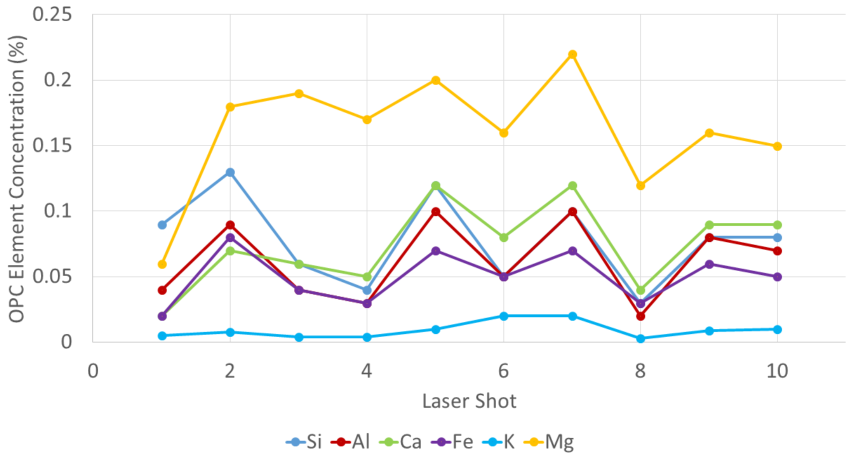

Figure 2.36 *Concentration trend of Si, Al, Ca, Fe, K and Mg in the fragment F13 as a function of the number of laser shots (OPC-LIBS). A relative error of 10% was estimated for each elemental concentration. Figure published in [Poggialini et al., 2020].*

2.3.3.3 F16 – Gasparo "da Salò"

The fragment F16 by Gasparo "da Salò" is composed of two varnish layers laid on maple wood, as visible by the OCT tomogram of Fig. 2.37. The external layer (indicated as A in Fig. 2.37) measures 13 µm of thickness and contains fine particles, while the underlying coat (indicated as B) - spread on the wood C - is 17 µm thick and embeds particles which previous analyses identified as rich in Fe and Pb (see 2.2 and references therein).

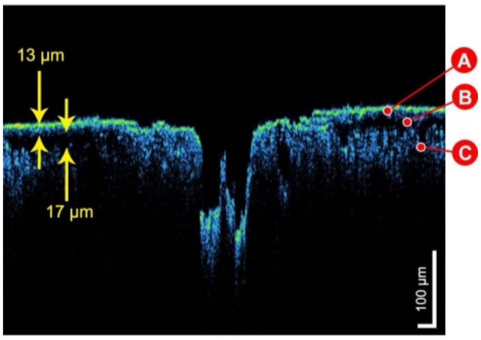

Figure 2.37 *OCT tomogram of the fragment F16, with the LIBS crater formed by 15 laser shots. A possible partial re-deposition of material is visible at the bottom centre of the crater. Letters refer to varnish layers (A, B) and wood substrate (C). The image is corrected for refraction with n_R = 1.5. Figure published in [Poggialini et al., 2020].*

Preliminary XRF analysis highlighted the presence of Si, S, K, Ca, Mn and Fe (Table 2.9). Additionally, high counts of Pb were recorded; this element can be ascribed to lead compounds or pigments possibly acting as driers of oil-based films [Tumosa and Mecklenburg, 2005]. Further information on the microscopic examination and the chemical analysis is reported in [Fichera et al., 2018].

From the OPC-LIBS results, we can see that 7 laser shots were needed to completely ablate the two varnish layers, before starting the interaction with the wood (Fig. 2.38). This information is particularly pointed out if we observe the Pb trend: its concentration reached the maximum value at the 5th shot, returning to the starting value at the 7th shot. From the 8th shot on, the concentration lowered indicating that the plasma intensity was being dampened by the ablation of the organic wood matrix. Also for this fragment, we estimated the ablation rate in approximately 5 µm per shot.

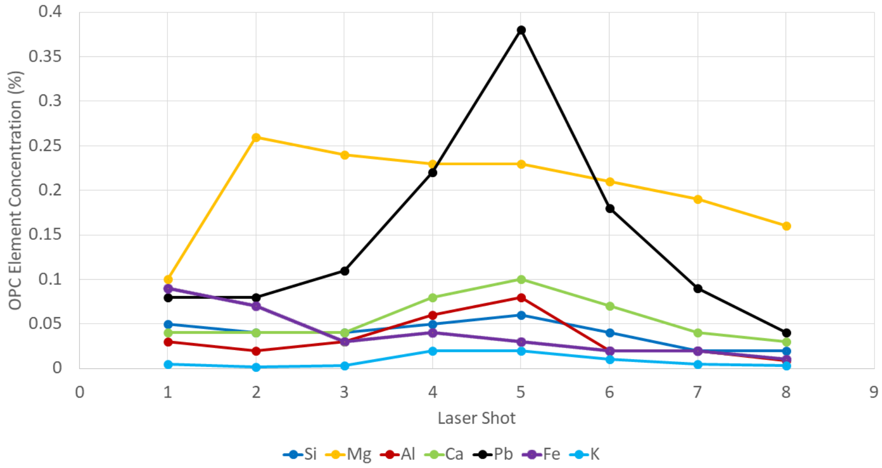

Figure 2.38 *Concentration trend of Si, Mg, Al, Ca, Pb, Fe and K in the fragment F16 as a function of the number of laser shots (OPC-LIBS). A relative error of 10% was estimated for each elemental concentration. Figure published in [Poggialini et al., 2020].*

2.3.3.4 F20 – Giovanni Paolo Maggini

The OCT tomogram of the fragment F20 by Giovanni Paolo Maggini (Fig. 2.39) is characterized by a simple coating system: one single 28-µm-thick varnish layer (indicated as A) is spread on the maple wood B. From previous analyses reported in 2.2 (and references therein), this layer was found to contain possible iron oxides and aluminosilicates, attributable to ochres. In the OCT analysis on the same fragment reported in 2.2, then, a further thin layer was discriminated between the varnish and the wood, likely acting as a ground.

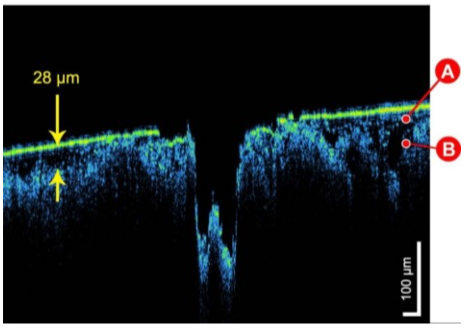

Figure 2.39 *OCT tomogram of the fragment F20, with the LIBS crater formed by 15 laser shots. A possible partial re-deposition of material is visible at the bottom centre of the crater. Letters refer to varnish (A) and wood substrate (B). The image is corrected for refraction with n_R = 1.5. Figure published in [Poggialini et al., 2020].*

From the XRF analysis, Fe was detected together with Si, K and Ca (Table 2.9). Additional information from the microscopic examination and the chemical analysis is reported in [Fichera et al., 2018].

Most of the elements investigated through the OPC-LIBS analysis are related to the materials dispersed in the varnish (Fig. 2.40). In particular, we want to focus the attention on the trend of Fe since we know its certain attribution to the particles dispersed in the layer A: the concentration decrease of this element suggests that the 1st and 2nd laser shots ablated the varnish layer and, from the 3rd shot on, the laser interacted with the wood. If we consider Ca, K and Mg characteristic of the wood, the increase in their concentration after the third shot could support these hypotheses. We can estimate an ablation rate of the coating system in about 15 μm per shot.

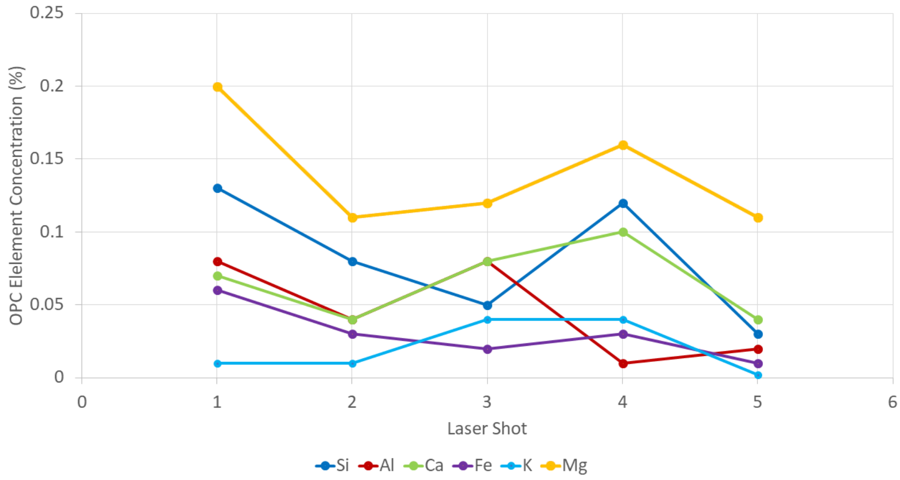

Figure 2.40 *Concentration trend of Si, Al, Ca, Fe, K and Mg in the fragment F20 as a function of the number of laser shots (OPC-LIBS. A relative error of 10% was estimated for each elemental concentration. Figure published in [Poggialini et al., 2020].*

2.3.3.5 *Bracco* 1793 small violin – Lorenzo Storioni

The OCT tomogram of Fig. 2.41 shows the stratigraphy of the *Bracco* back plate composed of three overlapping layers spread on maple wood. An external 13-μm-thick layer (indicated as A in Fig. 2.41) is laid on the varnish film B, which measures 67 μm of thickness. Finally, an underlying ground (C) - with a thickness of 15 μm - was identified at the interface with the wood D. Some particles were discriminated within the layers A and B, while the in-depth OCT study reported in 2.1 - conducted on the same plate - has highlighted their certain presence also in the ground C.

XRF analysis suggested the presence of S, K, Ca, Mn and Fe (Table 2.9). Si was also detected, but its values fall around the detection limit (set at 0.05).

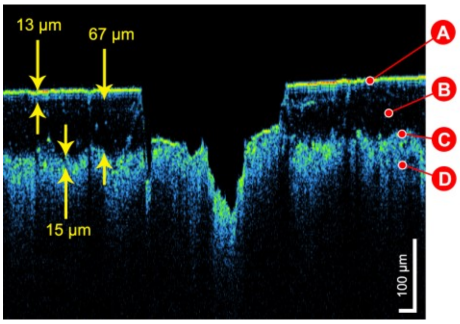

Figure 2.41 *OCT tomogram of the Bracco 1793 small violin, with the LIBS crater formed by 15 laser shots. Letters refer to external layer (A), varnish (B), ground (C) and wood substrate (D). The image is corrected for refraction with* $n_R = 1.5$. *Figure published in [Poggialini et al., 2020].*

From the OPC-LIBS analysis (Fig. 2.42), an ablation rate of about 20 µm - higher than that one in the mock-up and fragments - was estimated for the binders constituting the layers A to C of the *Bracco* small violin. Observing the figure, the 1st LIBS shot reasonably ablated the layer A, where the presence of Si, Mg, Al, Ca and Fe can be possibly related to the embedded inorganic grains or to soiling accumulation. The 2nd and 3rd shots would have penetrated the varnish layer B. In correspondence of these pulses, the concentration of all elements - except Mg and Ca - showed a decreasing trend and this can be justified by the OCT tomogram revealing just few particles dispersed in a very thick layer. The 4th shot was related with the ablation of the ground layer C: the increase in the signals of Si, Mg, Al and Ca was attributed, in fact, to aluminosilicates and Ca sulphates acting as pigments or fillers in the ground. Their presence is supported by the spectroscopic results described in 2.1 and 3.1. The ground layer appeared completely ablated with the 5th laser shot; from the 6th shot on, the wood substrate started being exposed.

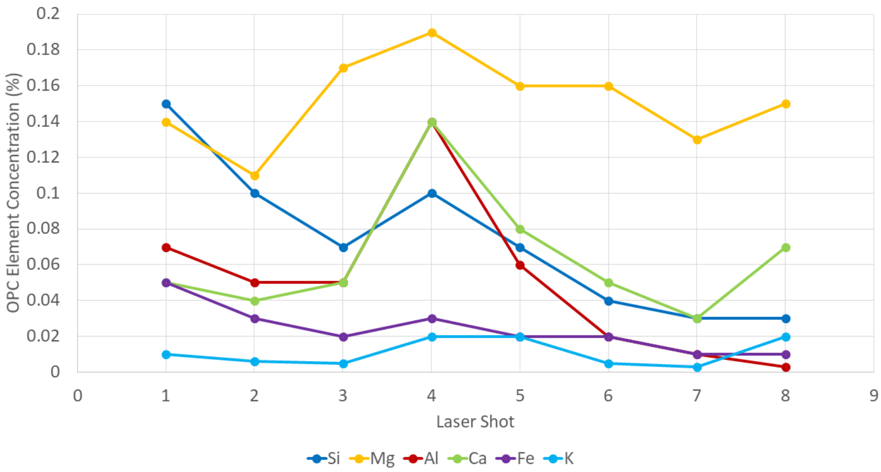

Figure 2.42 *Concentration trend of Si, Mg, Al, Ca, Fe and K in the Bracco 1793 small violin as a function of the number of laser shots (OPC-LIBS). A relative error of 10% was estimated for each elemental concentration. Figure published in [Poggialini et al., 2020].*

2.3.4 Conclusions

In this project, we proposed an analytical approach based on the joint use of LIBS and OCT techniques to gain deeper knowledge on the materials used by Bresciani and Cremonesi ancient masters in the realization of the stratigraphic structure of bowed string musical instruments. The capability of LIBS to carry out in-situ micro-destructive analyses was used to collect information on the elemental composition of the multiple layers. In particular, the CF- and OPC-LIBS methods were combined to improve the reliability of the results, and accurate concentration trends of the elements were provided as a function of the number of laser shots, which is related to the crater depth on the surface. The examination, in terms of shape and dimension, of the micro-craters formed by the LIBS pulses was conducted by OCT analysis. Integrating the concentration trends estimated by LIBS with the information obtained both on the subsurface structure by OCT and on the chemical and physical structure by other analytical techniques, we characterized the elemental composition of the layers composing the coating system.

The knowledge gathered by this study may be exploited to address the museum preservation and restoration practice of bowed string musical instruments, in particular for their examination with minimal sample manipulation and damage.

2.4 References

Agrosì G., Tempesta G., Scandale E., Legnaioli S., Lorenzetti G., Pagnotta S., et al., Application of Laser Induced Breakdown Spectroscopy to the identification of emeralds from different synthetic processes, *Spectrochimica Acta Part B: Atomic Spectroscopy*. 102 (2014) 48–51. doi:10.1016/j.sab.2014.10.012.

Alberti R., Crupi V., Frontoni R., Galli G., Russa M.F.L., Licchelli M., et al., Handheld XRF and Raman equipment for the in situ investigation of Roman finds in the Villa dei Quintili (Rome, Italy), *Journal of Analytical Atomic Spectrometry*. 32 (2017) 117–129. doi:10.1039/c6ja00249h.

Amaral M.M., Raele M.P., Freitas A.Z.D., Zahn G.S., Samad R.E., Vieira J.N.D., et al., Laser induced breakdown spectroscopy (LIBS) applied to stratigrafic elemental analysis and optical coherence tomography (OCT) to damage determination of cultural heritage Brazilian coins, *O3A: Optics for Arts, Architecture, and Archaeology II*. 7391 (2009). doi:10.1117/12.827724.

Anderson D.R., Mcleod C.W., English T., Smith A.T., Depth Profile Studies Using Laser-Induced Plasma Emission Spectrometry, *Applied Spectroscopy*. 49 (1995) 691–701. doi:10.1366/0003702953964516.

Baias M., Blümich B., Nondestructive Testing of Objects from Cultural Heritage with NMR, *Modern Magnetic Resonance*. (2018) 293–304. doi: 10.1007/978-3-319-28388-3_29.

Baraldi P., Manoscritto Bolognese 2861 XV sec., Biblioteca Universitaria di Bologna.

Bevilacqua N., Borgioli L., Adrover Gracia I., I pigmenti nell'arte: dalla preistoria alla rivoluzione industriale, Il prato, 2010.

Blümich B., NMR imaging of materials, Clarendon Press, 2004.

Blümich B., Perlo J., Casanova F., Mobile single-sided NMR, *Progress in Nuclear Magnetic Resonance Spectroscopy*. 52 (2008) 197–269. doi:10.1016/j.pnmrs.2007.10.002.

Blümich B., Casanova F., Perlo J., Presciutti F., Anselmi C., Doherty B., Noninvasive Testing of Art and Cultural Heritage by Mobile NMR, *Accounts of Chemical Research*. 43 (2010) 761–770. doi:10.1021/ar900277h.

Blümich B., Haber-Pohlmeier S., Zia W., Compact NMR, Walter de Gruyter GmbH & Co. KG, 2014.

Blümich B., Essential NMR, Springer-Nature, 2019.

Borman T., Stoel B., Review of the Uses of Computed Tomography for Analyzing Instruments of the Violin Family with a Focus on the Future, *Journal of the Violin Society of America: VSA Papers*, 22.1 (2009) 1–12.

Botto A., Campanella B., Legnaioli S., Lezzerini M., Lorenzetti G., Pagnotta S., et al., Applications of laser-induced breakdown spectroscopy in cultural heritage and archaeology: a critical review, *Journal of Analytical Atomic Spectrometry*. 34 (2019) 81–103. doi:10.1039/c8ja00319j.

Callaghan P.T., Principles of nuclear magnetic resonance microscopy, Clarendon Press, 2011.

Capitani D., Di Tullio V., Proietti N., Nuclear Magnetic Resonance to characterize and monitor Cultural Heritage, *Progress in Nuclear Magnetic Resonance Spectroscopy*. 64 (2012) 29–69. doi:10.1016/j.pnmrs.2011.11.001.

Caruso F., Saverwyns S., Van Bos M., Chillura Martino D.F., Ceulemans A.E., Valck J., et al., Micro-X-Ray Fluorescence and the Old Masters, *Applied Physics A*. 107 (2011) 197–202. doi:10.1007/s00339-011-6729-x.

Casanova F., Perlo J., Blümich B., Single-Sided NMR, *Single-Sided NMR*. (2010) 1–10. doi:10.1007/978-3-642-16307-4_1.

Cavalcanti G., Teixeira D., Legnaioli S., Lorenzetti G., Pardini L., Palleschi V., One-point calibration for calibration-free laser-induced breakdown spectroscopy quantitative analysis, *Spectrochimica Acta Part B: Atomic Spectroscopy*. 87 (2013) 51–56. doi:10.1016/j.sab.2013.05.016.

Chen J.B., Zhou Q., Sun S.Q., Direct chemical characterization of natural wood resins by temperature-resolved and space-resolved Fourier transform infrared spectroscopy, *Journal of Molecular Structure*. 1115 (2016) 55–62. doi:10.1016/j.molstruc.2016.02.079.

De Mayerne T., Rinaldi S., Pittura scultura e delle arti minori: 1620-1646: Ms. Sloane 2052, British Museum of London, De Rubeis, 1995.

Drexler W., Fujimoto J.G., Optical coherence tomography: technology and applications, Springer, 2015. doi:10.1007/978-3-319-06419-2.

Eastaugh N., Walsh V., Chaplin T., Siddall R., Pigment Compendium, A Dictionary and Optical Microscopy of Historical Pigments, Elsevier, 2008.

Echard J.-P., In situ multi-element analyses by energy-dispersive X-ray fluorescence on varnishes of historical violins, *Spectrochimica Acta Part B: Atomic Spectroscopy*. 59 (2004) 1663–1667. doi:10.1016/j.sab.2004.05.026.

Eidmann G., Savelsberg R., Blümler P., Blümich B., The NMR MOUSE, a Mobile Universal Surface Explorer, *Journal of Magnetic Resonance, Series A*. 122 (1996) 104–109. doi:10.1006/jmra.1996.0185.

Etiégni L., Campbell A., Physical and chemical characteristics of wood ash, *Bioresource Technology*. 37 (1991) 173–178. doi:10.1016/0960-8524(91)90207-z.

Farmer V.C., The infra-red spectra of talc, saponite, and hectorite, *Mineralogical Magazine and Journal of the Mineralogical Society*. 31 (1958) 829–845. doi:10.1180/minmag.1958.031.241.03.

Fichera G.V., Rovetta T., Fiocco G., Alberti G., Invernizzi C., Licchelli M., et al., Elemental analysis as statistical preliminary study of historical musical instruments. *Microchemical Journal*. 137 (2018) 309–317. doi:10.1016/j.microc.2017.11.004.

Fiocco G., Rovetta T., Gulmini M., Piccirillo A., Licchelli M., Malagodi M., Spectroscopic analysis to characterize finishing treatments of ancient bowed string instruments. *Applied Spectroscopy*. 71 (2017) 2477–2487. doi:10.1177/0003702817715622.

Fiocco G., Rovetta T., Gulmini M., Piccirillo A., Canevari C., Licchelli M., et al., Approaches for Detecting Madder Lake in Multi-Layered Coating Systems of Historical Bowed String Instruments, *Coatings*. 8 (2018a) 171. doi:10.3390/coatings8050171.

Fiocco G., Rovetta T., Malagodi M., Licchelli M., Gulmini M., Lanzafame G., et al., Synchrotron radiation micro-computed tomography for the investigation of finishing treatments in historical bowed string instruments: Issues and perspectives, *The European Physical Journal Plus*. 133 (2018b). doi:10.1140/epjp/i2018-12366-5.

Fiocco G., Rovetta T., Invernizzi C., Albano M., Malagodi M., Licchelli M., et al., A Micro-Tomographic Insight into the Coating Systems of Historical Bowed String Instruments, *Coatings*. 9 (2019) 81. doi:10.3390/coatings9020081.

Frezzato F., Seccaroni C., Segreti di arti diverse nel Regno di Napoli - Manuscript It. III 10 of the Biblioteca Marciana di Venezia, Il Prato, Saonara (PD), 2010.

Gilani M.S., Pflaum J., Hartmann S., Kaufmann R., Baumgartner M., Schwarze F.W.M., Relationship of vibro-mechanical properties and microstructure of wood and varnish interface in string instruments, *Applied Physics A*. 122 (2016) 260. doi:10.1007/s00339-016-9670-1.

Invernizzi C., Daveri A., Rovetta T., Vagnini M., Licchelli M., Cacciatori F., et al., A multi-analytical non-invasive approach to violin materials: The case of Antonio Stradivari “Hellier” (1679), *Microchemical Journal*. 124 (2016) 743–750. doi:10.1016/j.microc.2015.10.016.

Invernizzi C., Daveri A., Vagnini M., Malagodi M., Non-invasive identification of organic materials in historical stringed musical instruments by reflection infrared spectroscopy: a methodological approach, *Analytical and Bioanalytical Chemistry*. 409 (2017) 3281–3288. doi:10.1007/s00216-017-0296-8.

Invernizzi C., Fichera G.V., Licchelli M., Malagodi M., A non-invasive stratigraphic study by reflection FT-IR spectroscopy and UV-induced fluorescence technique: The case of historical violins, *Microchemical Journal*. 138 (2018a) 273–281. doi:10.1016/j.microc.2018.01.021.

Invernizzi C., Rovetta T., Licchelli M., Malagodi M., Mid and Near-Infrared Reflection Spectral Database of Natural Organic Materials in the Cultural Heritage Field, *International Journal of Analytical Chemistry*. 2018 (2018b) 1–16. doi:10.1155/2018/7823248.

Invernizzi C., Fiocco G., Iwanicka M., Kowalska M., Targowski P., Blümich B., et al., Non-invasive mobile technology to study the stratigraphy of ancient Cremonese violins: OCT, NMR-MOUSE, XRF and reflection FT-IR spectroscopy, *Microchemical Journal*. 155 (2020) 104754. doi:10.1016/j.microc.2020.104754.

Kaszewska E.A., Sylwestrzak M., Marczak J., Skrzeczanowski W., Iwanicka M., Szmit-Naud E., et al., Depth-Resolved Multilayer Pigment Identification in Paintings: Combined Use of Laser-Induced Breakdown Spectroscopy (LIBS) and Optical Coherence Tomography (OCT), *Applied Spectroscopy*. 67 (2013) 960–972. doi:10.1366/12-06703.

Kwiatkowska E.A., Marczak J., Ostrowski R., Skrzeczanowski W., Sylwestrzak M., Iwanicka M., et al., Absolute LIBS stratigraphy with optical coherence tomography, *O3A: Optics for Arts, Architecture, and Archaeology II*. 7391 (2009). doi:10.1117/12.827271.

Lämmlein S.L., Mannes D., Schwarze F.W.M., Burgert I., Gilani M.S., Combined experimental and numerical investigation of vibro-mechanical properties of varnished wood for stringed instruments, model validation and uncertainty quantification, Volume 3 *Conference Proceedings of the Society for Experimental Mechanics Series*. (2017) 81–83. doi:10.1007/978-3-319-54858-6_9.

Latour G., Echard J.-P., Soulier B., Emond I., Vaiedelich S., Elias M., Structural and optical properties of wood and wood finishes studied using optical coherence tomography: application to an 18th century Italian violin, *Applied Optics*. 48 (2009) 6485. doi:10.1364/ao.48.006485.

Mateo M.P., Cabalín L.M., Laserna J., Line-focused laser ablation for depth-profiling analysis of coated and layered materials, *Applied Optics*. 42 (2003) 6057. doi:10.1364/ao.42.006057.

Miliani C., Rosi F., Daveri A., Brunetti B.G., Reflection infrared spectroscopy for the non-invasive in situ study of artists' pigments, *Applied Physics A*. 106 (2011) 295–307. doi:10.1007/s00339-011-6708-2.

Morigi M.P., Casali F., Bettuzzi M., Brancaccio R., D'Errico V., Application of X-ray Computed Tomography to Cultural Heritage diagnostics, *Applied Physics A*. 100 (2010) 653–661. doi:10.1007/s00339-010-5648-6.

Nagy T., Pacher U., Giesriegl A., Weimerskirch M., Kautek W., Depth profiling of galvanoaluminium–nickel coatings on steel by UV- and VIS-LIBS, *Applied Surface Science*. 418 (2017) 508–516. doi:10.1016/j.apsusc.2016.12.059.

Nagyvary J., Diverdi J.A., Owen N.L., Tolley H.D., Wood used by Stradivari and Guarneri, *Nature*. 444 (2006) 565–565. doi:10.1038/444565a.

Nagyvary J., Guillemette R.N., Spiegelman C.H., Mineral Preservatives in the Wood of Stradivari and Guarneri, *PLoS ONE*. 4 (2009) e4245. doi:10.1371/journal.pone.0004245.

Nassef O.A., Ahmed H.E., Harith M.A., Surface and stratigraphic elemental analysis of an ancient Egyptian cartonnage using Laser-Induced Breakdown Spectroscopy (LIBS), *Analytical Methods*. 8 (2016) 7096–7106. doi:10.1039/c6ay01769j.

Pacher U., Dinu M., Nagy T.O., Radvan R., Kautek W., Multiple wavelength stratigraphy by laser-induced breakdown spectroscopy of Ni-Co alloy coatings on steel, *Spectrochimica Acta Part B: Atomic Spectroscopy*. 146 (2018) 36–40. doi:10.1016/j.sab.2018.04.006.

Poggialini F., Fiocco G., Campanella B., Legnaioli S., Palleschi V., Iwanicka M., et al., Stratigraphic analysis of historical wooden samples from ancient violin manufacturing by Laser Induced Breakdown Spectroscopy, *Journal of Cultural Heritage*. 44 (2020) 275–284. doi:10.1016/j.culher.2020.01.011.

Pospíšilová E., Novotný K., Pořízka P., Hradil D., Hradilová J., Kaiser J., et al., Depth-resolved analysis of historical painting model samples by means of laser-induced breakdown spectroscopy and handheld X-ray fluorescence, *Spectrochimica Acta Part B: Atomic Spectroscopy*. 147 (2018) 100–108. doi:10.1016/j.sab.2018.05.018.

Re A., Albertin F., Avataneo C., Brancaccio R., Corsi J., Cotto G., et al., X-ray tomography of large wooden artworks: the case study of "Doppio corpo" by Pietro Piffetti, *Heritage Science*. 2 (2014). doi:10.1186/s40494-014-0019-9.

Re A., Corsi J., Demmelbauer M., Martini M., Mila G., Ricci C., X-ray tomography of a soil block: a useful tool for the restoration of archaeological finds, *Heritage Science*. 3 (2015) 4. doi:10.1186/s40494-015-0033-6.

Re A., Lo Giudice A., Nervo M., Buscaglia P., Luciani P., Borla M., Greco, C., The importance of tomography studying wooden artefacts: a comparison with radiography in the case of a coffin lid from Ancient Egypt, *International Journal Of Conservation Science*. 7 (2016) 935–944.

Rehorn C., Blümich B., Cultural Heritage Studies with Mobile NMR, *Angewandte Chemie International Edition*. 57 (2018) 7304–7312. doi:10.1002/anie.201713009.

Rehorn C., Studies of tangible cultural heritage with portable stray-field NMR, Aachen, 2019.

Ridolfi S., Portable X-ray Fluorescence Spectrometry for the analyses of Cultural Heritage, *IOP Conference Series: Materials Science and Engineering*. 37 (2012) 012001. doi:10.1088/1757-899x/37/1/012001.

Rivers S., Umney N., Conservation of furniture, Routledge, 2013.

Romero D., Laserna J.J., Multielemental Chemical Imaging Using Laser-Induced Breakdown Spectrometry, *Analytical Chemistry*. 69 (1997) 2871–2876. doi:10.1021/ac9703111.

Rosi F., Grazia C., Fontana R., Gabrieli F., Buemi L.P., Pampaloni E., et al., Disclosing Jackson Pollock’s palette in Alchemy (1947) by non-invasive spectroscopies, *Heritage Science*. 4 (2016). doi:10.1186/s40494-016-0089-y.

Rovetta T., Invernizzi C., Licchelli M., Cacciatori F., Malagodi M., The elemental composition of Stradivari's musical instruments: new results through non-invasive EDXRF analysis, *X-Ray Spectrometry*. 47 (2017) 159–170. doi:10.1002/xrs.2825.

Salisbury J.W., Walter L.S., Vergo N., Mid-infrared (2.1-25 µm) spectra of minerals; first edition, U.S. Geological Survey, Open-File Report 87-263, 1987. doi:10.3133/ofr87263.

Sodini N., Dreossi D., Chen R., Fioravanti M., Giordano A., Herrestal P., et al., Non-invasive microstructural analysis of bowed stringed instruments with synchrotron radiation X-ray microtomography, *Journal of Cultural Heritage*. 13 (2012). doi:10.1016/j.culher.2012.04.008.

Sodini N., Dreossi D., Giordano A., Kaiser J., Zanini F., Zikmund T., Comparison of different experimental approaches in the tomographic analysis of ancient violins, *Journal of Cultural Heritage*. 27 (2017). doi:10.1016/j.culher.2017.02.013.

Spotti G., Gaetano e Pietro Sgarabotto. Liutai-Violin Makers 1878-1990, Turris, 1991.

Stols-Witlox M., A perfect ground: preparatory layers for oil painting 1550-1900, Archetype Publications, 2017.

St-Onge L., A mathematical framework for modeling the compositional depth profiles obtained by pulsed laser ablation, *Journal of Analytical Atomic Spectrometry*. 17 (2002) 1083–1089. doi:10.1039/b203024c.

Stuart B.H., Infrared Spectroscopy: Fundamentals and Applications, Analytical Techniques in the Sciences, 2004.

Targowski P., Iwanicka M., Tymińska-Widmer L., M. Sylwestrzak, E.A. Kwiatkowska, Structural Examination of Easel Paintings with Optical Coherence Tomography, *Accounts of Chemical Research*. 43 (2010) 826–836. doi:10.1021/ar900195d.

Targowski P., Iwanicka M., Optical Coherence Tomography: its role in the non-invasive structural examination and conservation of cultural heritage objects—a review, *Applied Physics A*. 106 (2011) 265–277. doi:10.1007/s00339-011-6687-3.

Targowski P., Kowalska M., Sylwestrzak M., Iwanicka M., OCT for examination of cultural heritage objects, in: M.R. Wang (Ed.) Optical Coherence Tomography and Its Non-medical Applications, IntechOpen, 2020: London, UK; Rijeka, Croatia, 2020. doi.org/dx.doi.org/10.5772/intechopen.88215.

Tognoni E., Cristoforetti G., Legnaioli S., Palleschi V., Calibration-Free Laser-Induced Breakdown Spectroscopy: State of the art, *Spectrochimica Acta Part B: Atomic Spectroscopy*. 65 (2010) 1–14. doi:10.1016/j.sab.2009.11.006.

Vadillo J.M., Laserna J.J., Depth-resolved Anaylsis of Multilayered Samples by Laser-induced Breakdown Spectrometry, *Journal of Analytical Atomic Spectrometry*. 12 (1997) 859–862. doi:10.1039/a607622j.

[Web]

http://www.oct4art.eu/ (accessed on 27 July 2019). Oct4art - Optical Choerence Tomography for Examination of Work of Art.

Chapter 3

Innovative applications of advanced invasive techniques

3.1 Discovering the coating structure of ancient bowed string instruments by synchrotron radiation FTIR microspectroscopy in reflection geometry

3.1.1 Introduction

This spectroscopic study was conducted thanks to the collaboration with the University of Pavia through the Arvedi Laboratory of Non-Invasive Diagnostics, the SISSI beamline of the Elettra synchrotron laboratory, the University of Turin, the University of Milan, the Fondazione Arvedi Buschini, the Fondazione Museo del Violino Antonio Stradivari Cremona, the Fondazione Bracco, the Accademia of Santa Cecilia, and the International Violin Making School of Cremona. The results have been published in Spectrochimica Acta Part A: Molecular and Biomolecular Spectroscopy [Fiocco et al., 2021].

The objects under investigation are four cross-sectional samples collected on historical violins manufactured by Antonio Stradivari and Lorenzo Storioni, who lived and worked in Cremona respectively between the 17th and 18th centuries and between the 18th and 19th centuries [Jalovec, 1957]. Interestingly, Storioni was born precisely one hundred years after Stradivari, and the instruments in exam - whose history is described in appendix II - were mostly produced at a distance of one hundred years from one another. In this work, we studied the coating systems of these masterpieces by the benchtop synchrotron radiation FTIR microspectrometer in reflection geometry. Infrared results obtained on the cross-sections were combined with those non-invasively acquired directly from the violins by the portable reflection FTIR spectrometer.

Infrared spectroscopies are suitable candidates as the IR radiation allows for the detection of both organic and inorganic compounds. The FTIR micro-spectroscopies can be employed to investigate samples prepared as cross-sections [Cotte et al., 2009; Prati et al. 2016]. In the literature, several efforts have been done to building up different preparation procedures of cross-sections for FTIR investigations in the attempt to prevent contamination from the embedding medium [Weerd et al., 2004; Prati et al., 2012; Pouyet et al., 2014; and references therein]. In fact, two major drawbacks can be caused by the standard cross-section preparation, where the micro-fragment is embedded in a polymer resin in order to realize an easily handled block: (i) the penetration of the embedding resin (epoxy, polyester, acrylic, etc.) inside porous samples, negatively affecting the characterization of the organic materials composing the varnish and the ground, and (ii) the smearing of the synthetic resin over the entire surface of the cross-section during polishing. However, samples collected from historical violins are very peculiar because of their extremely high brittleness, and their embedding in resin still appears the most suitable method to prepare cross-sections. With this method, the stratigraphy can be preserved for further investigations that may be developed in the future. As for the portable reflection FTIR spectroscopy, it has been increasingly used to gather information on artworks without the need for sampling and in a contactless way [Rosi et al., 2010a; Rosi et al., 2016; Miliani et al., 2011; Izzo et al., 2020]. Non-invasive analyses fully preserve the integrity of cultural heritage objects [Daher et al., 2010; Fiocco et al., 2018; Invernizzi et al., 2017; Echard et al., 2004], with the awareness that this approach does not normally lead to both exhaustive and highly spatially-resolved chemical information [Fichera et al., 2018; Rovetta et al., 2017], which is somehow more accessible if samples are available.

SR-FTIR microspectroscopy analyses were performed in 2018 at the SISSI beamline (Chemical and Life Science branch) of the Elettra synchrotron laboratory (Trieste, Italy) by the researchers of the Arvedi laboratory and the University of Turin, within the CERIC-ERIC project proposal No. 20182129 entitled “Violin Investigations to Rediscover Traditions Using Open Synchrotron Infrastructures” (acronym: VIRTUOSI) (Fig. 3.1). This investigation is part of a broader project in terms of set of samples as well as of techniques involved. In fact, besides the infrared analysis at the SISSI beamline, we performed tests using the UV Resonant Raman (UVRR) technique - in the macro setup - at the IUVS-OFF beamline of the Elettra synchrotron laboratory. Thanks to the greater brightness and collimation compared to conventional IR sources, SR can strongly increase the spectral signal-to-noise ratio at diffraction-limited spatial resolution [Salvadó et al., 2005], making this technique particularly suitable for the examination of complex layered microstructures [Sotiropoulou et al., 2016; Sano et al., 2019; Echard et al., 2008; Crupi et al., 2018; Bertrand et al., 2010]. The narrow acquisition area (10 x 30 μm) enabled us to collect spectra in correspondence of each individual stratigraphic layer, with the exception of those falling at the interface between two contiguous layers during the automatic acquisition of the maps. Working in reflection mode, the contact between the probe and the sample is avoided, differently from the FTIR-ATR setup condition [Prati et al., 2016] where the pressure of the tip can severely alter the surface morphology of very brittle samples as those in exam. For such stratigraphies, in fact, the ATR setup can be considered micro-destructive.

Portable reflection FTIR spectroscopic analyses were carried out in the Arvedi laboratory over the years, within the activities related to the study of historical instruments preserved in the Museo del Violino and in other public or private collections, as a result of different collaborations. In particular, this technique has been applied on differently preserved varnish areas of the surfaces, selected on the basis of the UV fluorescence, with a tentative stratigraphic approach [Invernizzi et al., 2016; Invernizzi et al., 2018a].

Detailed information about the analytical instrumentation and the acquisition parameters used in this study is reported in appendix I. This information also concerns optical microscopy and SEM-EDX, employed to extend the overall information of the samples.

In the present study, a set of four cross-sectional micro-samples detached from three Stradivari and Storioni violins were investigated by SR-FTIR microspectroscopy in reflection geometry. SR-FTIR spectra were considered, and discussed, as both single point analysis and maps. The univariate and multivariate chemical maps were performed in order to assess the merits of visual images of component distribution for the cross-sections in exam. In the univariate maps, the intensities of the characteristic absorption bands are normally displayed according to a colour scale, therefore reporting the spectral information and its spatial distribution within the analytical area. Recently, multivariate methods have been considered in heritage science for an in-depth elaboration of large spectroscopic data sets [Sciutto et al., 2012a]. These chemometric tools were applied as a support for the preliminary interpretation of spectroscopic data as well as to improve the visual representation of the information carried by the spectra. In particular, the literature witnesses their use to treat data collected on cross-sectional samples of paintings, with the aim of overcoming some problems related to chemical mapping and allowing for a direct representation of the information contained in the FTIR spectra as a whole [Rosi et al., 2010b; Sciutto et al., 2012b; Sciutto et al., 2017]. By the principal component analysis, it is possible to explore complex multivariate data through informative graphical outputs such as the score and loading plots [Oliveri and Forina, 2012]. PC scores can be also used to create false colour images with a chromatic scale based on scores for a single PC, or by the combination of scores for more PCs. These pictures result to be visually comparable to chemical maps, but involving a multivariate meaning. SR-FTIR data were compared and integrated with those collected on the violins by the portable non-invasive reflection FTIR spectroscopy. Additionally, optical microscopy and SEM-EDX strongly supported the investigation of the coating systems.

Figure 3.1 *Synchrotron radiation FTIR microspectroscopy instrumentation at Elettra Sincrotrone Trieste (SISSI beamline, Chemical and Life Sciences branch).*

3.1.2 Materials

The instruments under investigation are the *Toscano* violin 1690 by Antonio Stradivari and two small violins made by Lorenzo Storioni respectively in 1790 (*unnamed*) and in 1793 (*Bracco*). The list of the instruments and the related cross-sections are shown in Table 3.1, while their history and photos are reported in appendix II except for the small violin 1790 by Lorenzo Storioni, whose documentation is missing.

Table 3.1 *List of the instruments investigated in this study with name and life period of the violin maker, name of the instrument with year of construction, type and part investigated, and the inventory number of the cross-sectional samples. Table modified from [Fiocco et al., 2021].*

Violin Maker	Instrument name	Year of construction	Instrument	Part	Inv. N°
L. Storioni (1744-1816)	-	1790	Small violin	Rib	LS_1790
	Bracco	1793	Small violin	Back plate Front plate	LS_1793a LS_1793b
A. Stradivari (ca. 1644-1737)	*Toscano*	1690	Violin	Front plate	AS_1690

Micrometric samples were detached from the most preserved areas of the three instruments and embedded into epoxy resin (Epofix Struers and Epofix Hardener 15:2, w:w), then cut to obtain cross-sections. Subsequently, the surface was dry-polished with silicon carbide fine sandpaper (1200-8000 mesh) and analysed by SR-FTIR microspectroscopy in reflection geometry. Since two samples - one for each plate - come from the *Bracco* violin, the dataset is composed of four cross-sections as a whole. Before SR-FTIR examination, the cross-sections were observed by optical microscopy under VIS and UV lights and analysed by SEM-EDX in low vacuum conditions, which do not require the sample metallisation. The non-invasive analyses by the portable reflection FTIR spectrometer were performed on the back plates of the *Toscano* and *Bracco* violins. Unfortunately, this analysis was not possible for the Storioni small violin 1790.

3.1.3 Univariate and multivariate methodological approaches

The univariate and multivariate approaches were applied to the data set composed of SR-FTIR spectra acquired on the four cross-sections under examination.

For the univariate method, we used the OPUS (ver. 7.5, Bruker Optics GmbH, Germany/USA) software package. To obtain univariate chemical maps, we selected the diagnostic bands of varnish (i.e., vC=O at around 1710 cm^{-1}), proteins (i.e., vC=O at around 1650 cm^{-1}) and embedding epoxy resin (i.e., vC-C at 1510 cm^{-1}) from the spectra after application of the KKT. The effectiveness of the KK-transformation, in fact, was proved when organic compounds are studied [Invernizzi et al., 2018b]. The chromatic range of the scale is set from red (highest intensity values) to blue (lowest intensity values). An interpolation algorithm was employed automatically by the software.

For the multivariate approach, data analysis was carried out under Matlab environment (ver. 9.2, The Mathworks, Inc., Natick, USA) using the PLS toolbox (ver. 8.5, Eigenvector Research, Inc., USA) software package. We studied a data matrix composed of as many rows as the total number of SR-FTIR spectra acquired on the four cross-sections (84) and as many columns as the number of spectral variables (2606). In a typical matrix the rows are filled with the objects, here represented by analysis points on the microsamples, and the columns with the variables, here represented by wavenumbers. Each object was preliminarily classified in accordance with the position of the analytical spot in the stratigraphy: epoxy resin (E), varnish (V), ground (G), and wood (W). Therefore, this assignment mainly reflects the distribution of the organic materials in the samples. The following spectral pre-treatments were applied to the KK-transformed spectra: smoothing (Savitzky-Golay, 11 wavelengths gap size), first derivative (Savitzky-Golay, 11 wavelengths gap size and 2nd polynomial order) and mean centring. Exploratory multivariate data analysis was performed by PCA, based on the Singular Value Decomposition (SVD) algorithm [Wold et al., 1987]. We selected the optimal number of PCs to be retained by assessing the scree plot [Bro and Smilde, 2014]. We followed an interval-PCA approach: different models were investigated with the aim of choosing the spectral ranges containing the most relevant information [Fiocco et al., In Press]. This methodological approach, applied to the entire IR data set of the VIRTUOSI project, is explained in detail in appendix III. By the preliminary data exploration, we observed that the merged range 2000-1400 cm^{-1} retains relevant information, being responsible for object grouping according to the preliminary assigned material classes (E, V, G, W) in the stratigraphies. In particular, this interval seemed to be the most promising to discriminate layers with referring to one single organic material and showing significative marker bands. PCA score values were used to create a score map for each cross-sectional sample, within which similar (or different) layers are highlighted according to a multivariate approach. The score map is the result of a three-dimensional reconstruction: the process is similar to that of RGB images, but in the RGB case each channel merely represents the intensity of colour. In the score map, instead, the three channels (R, G, B) are associated to the score values respectively on PC1, PC2, and PC3 determined for each grid point, and the colour that results from the tree-channel combination has a multivariate significance. The colour bars represent the variance of the spectral range (2000-1400 cm^{-1}): this information can be associated to the different classes of materials according to the loading plot. No smoothing was employed in the multivariate maps.

3.1.4 Results and discussion

In this section, we first discussed reflection FTIR spectra within the frame of the characterization carried out by optical microscopy and SEM-EDX. Then, we attempted to show the distribution of the identified materials in each stratigraphy by the twofold approach of the univariate and multivariate chemical maps.

3.1.4.1 Stratigraphic characterization by morphological, molecular and elemental data

A common and expected finding in the SR-FTIR spectra of the cross-sections was the presence of the marker bands attributed to the epoxy resin used to embed the micro-samples: their intensity was found to progressively diminish - up to disappearing - in the spectra collected from the external coats to the wood. However, these signals - falling at 1610 cm^{-1} (vC=C, aromatic ring), 1510 cm^{-1} (vC-C, aromatic ring), 1250 cm^{-1} (vC-O-C, oxirane group) and 1035 cm^{-1} (vC-O-C, ether) (Fig. 3.2) [González et al., 2012; Smith et al., 1984; Panda, 2016] - can be easily recognized in the spectra, without interfering with the signals deriving from the samples. Moreover, since the mapping procedure is automatic, it is important to highlight that the collected spectra contain information on the stratigraphic structure, where boundaries are not always sharp and each layer may be formed by different components.

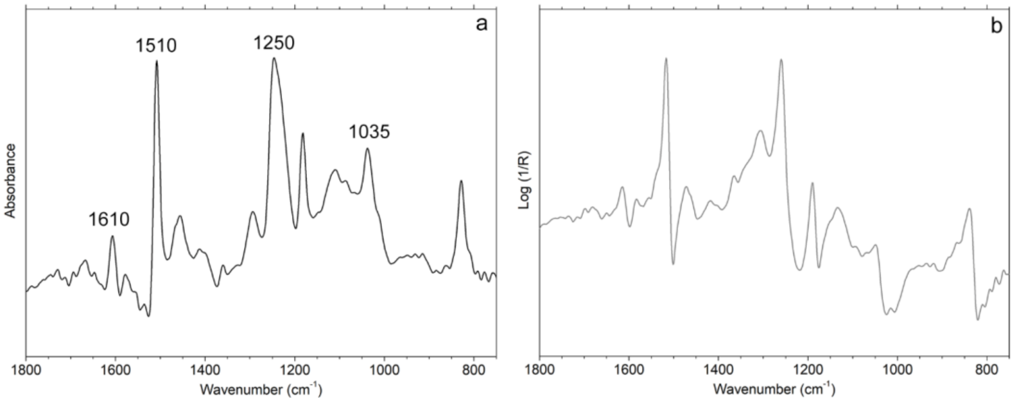

Figure 3.2 *Reflection SR-FTIR spectra related to epoxy resin shown after (a) and before (b) KK transformations. The wavenumbers of the diagnostic peaks are highlighted. Figure published in [Fiocco et al., 2021].*

The cross-sections from the two violins by Lorenzo Storioni showed a common physical structure under the optical microscopy in UV light, as shown in Fig. 3.3. The three samples, namely LS_1790, LS_1793a and LS_1793b, are in fact composed of a 60- to 90-µm-thick varnish layer A with homogeneous light-yellow UV fluorescence. Underneath the varnish, we found a thin ground layer B characterized by light-blue UV fluorescence. The wood substrate - maple for LS_1790 and LS_1793a, and spruce for LS_1793b - is labelled as C in the figure. Furthermore, an additional external varnish layer A' seemed to be present in two out of three samples of the Storioni violins (LS_1790 in Fig. 3.3a and LS_1793b in Fig. 3.3c).

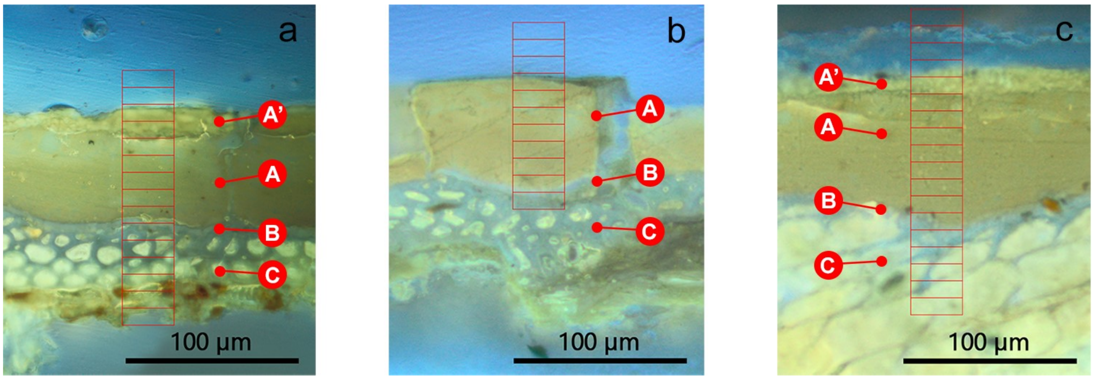

Figure 3.3 *UV-light optical microscopy images of the three cross-sectional samples: LS_1790 (a), LS_1793a (b) and LS_1793b (c). The layers indicated as A (and A'), B and C are described in the text. The red grid highlights the area considered for mapping (see 3.1.4.2 for details). Figure published in [Fiocco et al., 2021].*

The SR-FTIR KKT spectra collected on the layer A of the three Storioni samples are all characterized by the marker bands of a varnish made of siccative oil and terpenic resins of vegetal origin (Fig. 3.4a,b, black and red lines) [Invernizzi et al., 2016; Invernizzi et al., 2017]: sharp and intense νCH_2 vibrations - characteristic of the oil, albeit a contribution arises also from the resin - at 2920 (asymmetric mode) and 2850 (symmetric mode) cm^{-1}, weak νCH_3 vibrations from the resin at 2950 (asymmetric mode) and 2870 (symmetric mode) cm^{-1}, $\nu C{=}O$ at around 1710 cm^{-1} due to the ester (oil) and acid carboxylic (resin) groups, $\delta_s CH_2$ (oil and resin) and $\delta_{as} CH_3$ (resin) at 1465-55 cm^{-1}, $\delta_s CH_3$ (resin) at 1375 cm^{-1}, and $\nu C{-}O$ (oil) at 1255, 1180-70 and around 1100 cm^{-1}. In correspondence of the layer B, proteins - likely related to animal glue or casein - were identified in all the KKT spectra thanks to the marker bands at around 1650 cm^{-1} ($\nu C{=}O$, amide I) and 1550 cm^{-1} (combination of $\nu C{-}N$ and $\delta N{-}H$, amide II), as displayed in Fig. 3.4c (black and red lines) [Invernizzi et al., 2018b, Belbachir et al., 2009]. The corresponding pseudo-absorbance spectra are reported in Fig. 3.5 (black and red lines).

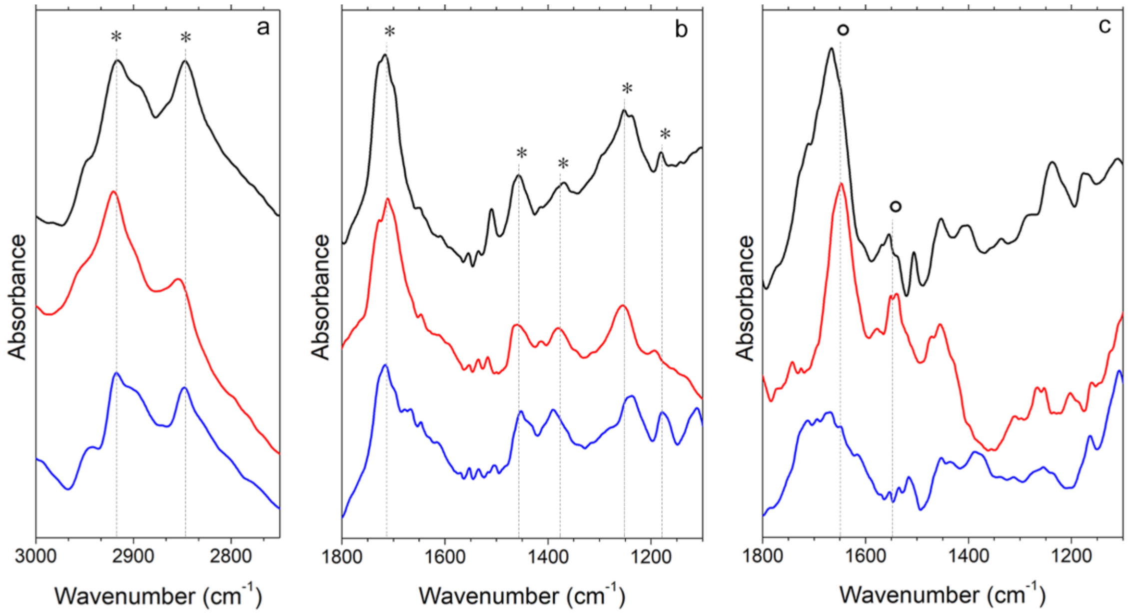

Figure 3.4 *Reflection SR-FTIR KKT spectra collected in correspondence of the varnish (a,b) and ground (c) layers on the samples LS_1790 (black), LS_1793a and LS_1793b (red), and AS_1690 (blue). Spectra are shown in the ranges between 3000-2750 cm^{-1} (a) and 1800-1100 cm^{-1} (b,c). Marker bands of oil-resin varnish (*) and proteins (°) are highlighted.*

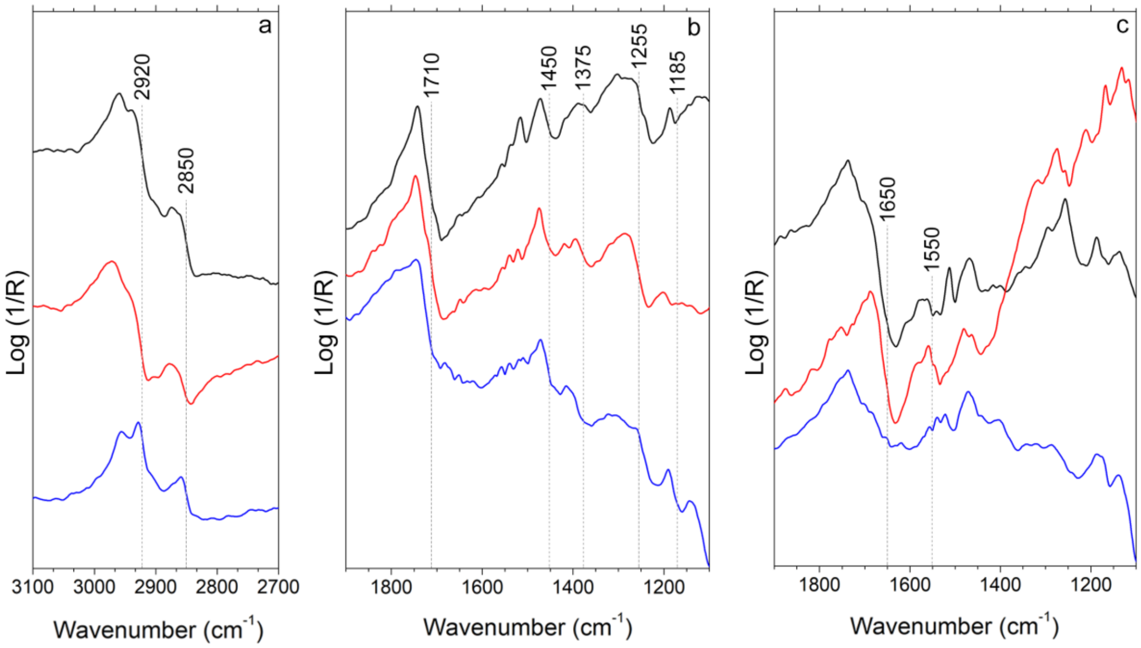

Figure 3.5 *Reflection SR-FTIR spectra before KK transformations collected in correspondence of the varnish (a,b) and ground (c) layers on the samples LS_1790 (black), LS_1793a and LS_1793b (red), and AS_1690 (blue). Spectra are shown in the ranges between 3100-2700 cm^{-1} (a) and 1900-1100 cm^{-1} (b,c).*

The SR-FTIR results are in accordance with those obtained on the back plate of the *Bracco* small violin by the portable non-invasive spectrometer (Fig. 3.6), already discussed in 2.1. In addition to what observed by the single point SR-microspectroscopy analysis, the marker bands of proteins were also detected in correspondence of the best conserved varnish areas of the instrument, and this result was confirmed by the chemical maps shown in 3.1.4.2. Moreover, the presence of inorganic phases was revealed mainly through the non-invasive FTIR investigation performed on the most worn-out varnish areas of the *Bracco* (Fig. 3.6b). In detail, we identified silicate and sulphate compounds with the respective *Reststrahlen* bands at around 1100-1000 cm^{-1} (ν_{as}Si-O-Si), and at 1150 and 1100 cm^{-1} ($\nu_{as}SO_4$) [Rosi et al., 2010c; Miliani et al., 2011]. These signals were not clearly distinguished, instead, by the SR-FTIR spectroscopy. As for the sulphates, moreover, the extension of the spectral range up to 375 cm^{-1} of the portable instrument allowed us to detect the asymmetric bending modes of SO_2 at 670 and 600 cm^{-1}. The detection of Si, S and Ca in some particles by EDX analysis would prove the presence of silicates and calcium sulphates (possibly gypsum) (Fig. 3.7a,b). Due to the strong correlation between Si and Al, several grains were interpreted as aluminosilicates (Fig. 3.7c). The investigated inorganic materials could act as fillers dispersed in the organic binders [Nagyvary et al., 2009; Barlow and Woodhouse, 1989]. Furthermore, Fe was revealed in some red particles and this finding enabled us to hypothesize the presence of iron-based red pigments (Fig. 3.7d) [Eastaugh, 2013; Bevilacqua et al., 2010].

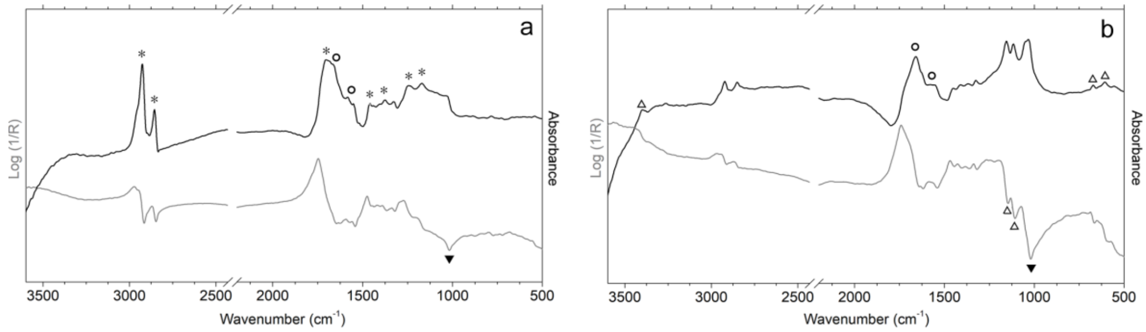

Figure 3.6 *Reflection FTIR spectra before (grey) and after (black) KK transformations acquired by the portable FTIR spectrometer on the best conserved (a) and most worn (b) varnish areas of the Bracco small violin. Marker bands of oil-resin varnish (*), proteins (°), silicates (▼) and sulphates (Δ) are highlighted. Figure modified from [Fiocco et al., 2021].*

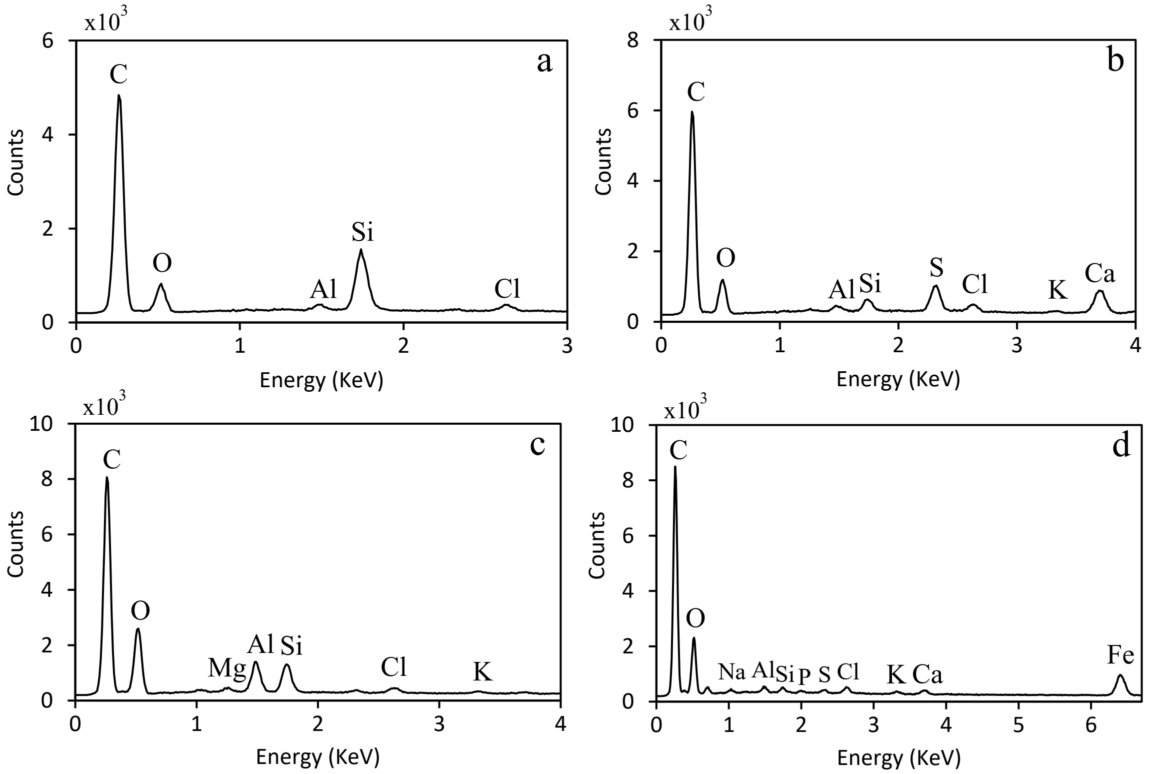

Figure 3.7 *EDX spectra of the particles detected in the sample LS_1793a, with the Kα emissions of the elements highlighted. Letters a-d refer to the different particles described in the text.*

The cross-section of the sample AS_1690, detached from the *Toscano* violin by Antonio Stradivari, is characterized by two varnish layers of ca. 10-15 µm each in thickness (Fig. 3.8). Under UV light, we discriminated this double layer from the colour: the layer A, on the top, with a salmon-fluorescent colour and the layer B, on the bottom, with a yellow-whitish fluorescence [Fiocco et al., 2017]. The spruce wood is indicated in the figure with the letter C.

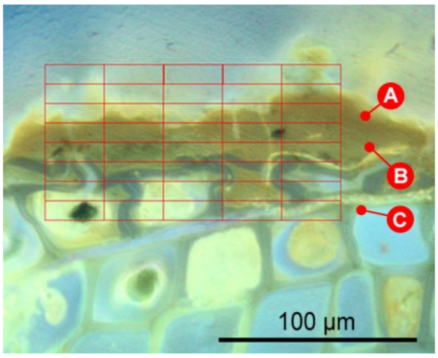

Figure 3.8 *UV-light optical microscopy image of the cross-sectional sample AS_1690. The layers indicated as A, B and C are described in the text. The red grid highlights the area considered for mapping (see 3.1.4.2 for details). Figure published in [Fiocco et al., 2021].*

The SR-FTIR KKT spectra acquired on both layers A and B showed the signals of an oil-terpenic resin varnish (Figs. 3.4a,b and 3.5a,b, blue line). The variation observed in the UV colour between the two varnish coats could be possibly ascribed to some variations in their chemical composition (e.g., lake pigment addition or oil-resin proportion) that cannot be revealed using the reflection FTIR technique [Invernizzi et al., 2018a]. The focus of the synchrotron IR beam at the interface between the layer B and the wood C did not clearly highlight the presence of different organic materials (e.g., proteins) that could possibly compose the ground coat (Figs. 3.4c and 3.5c, blue line). A broad band, instead, is visible at around 1650 cm^{-1} in the spectrum collected on the most worn-out varnish areas of the violin back plate thorough the non-invasive investigation, as displayed in Fig. 3.9b. This signal could derive from a proteinaceous material, even if - as also reported in [Invernizzi et al., 2018a] - its presence remains rather doubtful. As regards the spectral profile from the best conserved varnish areas (Fig. 3.9a), instead, it resulted to match well with that collected on the layers A and B by SR-FTIR microspectroscopy.

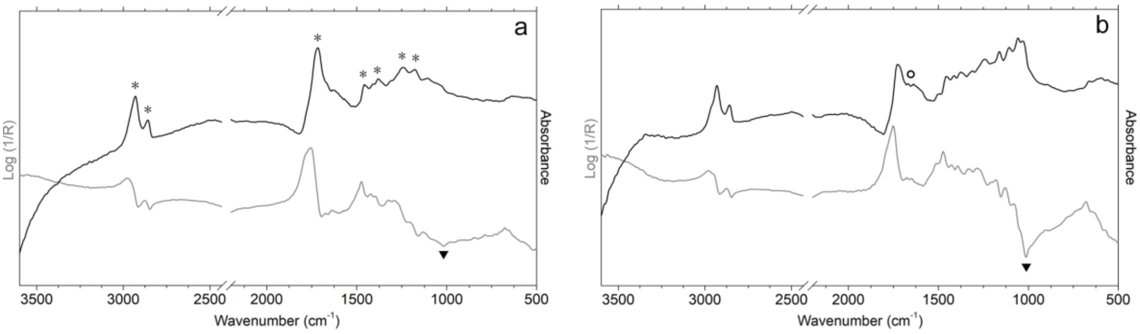

Figure 3.9 *Reflection FTIR spectra before (grey) and after (black) KK transformations acquired by the portable FTIR spectrometer on the best conserved (a) and most worn (b) varnish areas of the Toscano violin. Marker bands of oil-resin varnish (*), proteins (°) and silicates (▼) are highlighted. Figure modified from [Fiocco et al., 2021].*

The SEM-EDX analysis allowed us to investigate the particles that fill up the surface pores of the wood, at the interface between this latter and the varnish, in the *Toscano*. A significant number of inorganic phases was observed and, by focusing the electron beam onto them, we revealed intense Si-Kα emissions. In some EDX spectra, we also found Al, Mg, K, Ca and Fe together with the intense peak of Si (Fig. 3.10). These findings, supported by the detection of *Reststrahlen* bands - attributed to the ν_{as}Si-O-Si vibrations - in the region from 1100 to 1000 cm^{-1} of the pseudo-absorbance spectra recorded through the non-invasive FTIR approach (Fig. 3.9, grey line), indicate the presence of minerals belonging to the silicate and aluminosilicate groups. In addition, rare Ti-, Fe- and Mn-rich grains were detected. Aluminosilicates and possible titanium-iron-manganese oxides/hydroxides can be associated to the presence of iron-based earth pigments. Supplementary information, related to the materials composing the *Toscano* stratigraphy and its decorations, is reported in appendix IV.

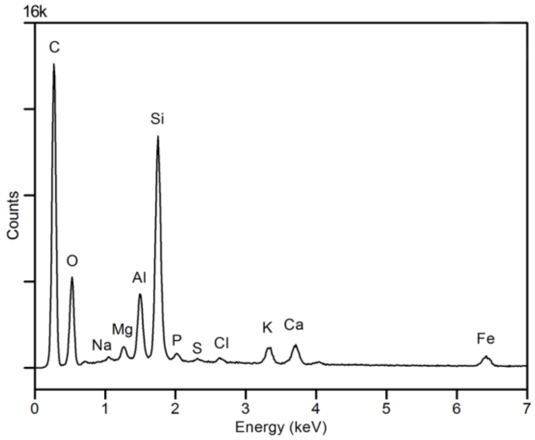

Figure 3.10 *EDX spectrum of a particle detected at the interface between the varnish and the wood of the cross-sectional sample AS_1690, with the Kα emissions of the elements highlighted. Figure modified from [Fiocco et al., 2017].*

3.1.4.2 SR-FTIR univariate and multivariate imaging

Univariate chemical mapping performed on the cross-sections of the samples LS_1790 (Fig. 3.3a), LS_1793a (Fig. 3.3b) and LS_1793b (Fig. 3.3c) is displayed in Figs. 3.11 and 3.12.

For both the Storioni violins, the maps obtained by integrating the νC=O band of the oil-resin varnish at around 1710 cm^{-1} on the whole coating system show the highest intensity value - red areas - in correspondence of the layer A (Fig. 3.11a,b), this completely matching the sample stratigraphy observed by optical microscopy. Areas with lower intensity of this signal are evident, in green colour, in correspondence of the layer A' of the sample LS_1790 (Fig. 3.11a). We can indeed observe a different morphology of this external layer if compared to the underlying varnish A.

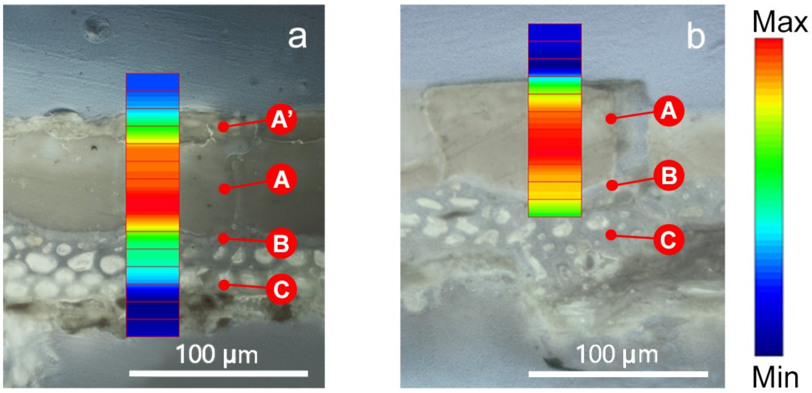

Figure 3.11 *Univariate colour-scale maps of the cross-sectional samples LS_1790 (a) and LS_1793a (b). The colour scale refers to the intensity of the marker band of the oil-resin varnish at 1710 cm^{-1}. Figure published in [Fiocco et al., 2021].*

As for the integration of the amide I band at 1650 cm^{-1} produced by the proteins, all the three maps of Fig. 3.12a-c (red areas) show the highest intensity value in correspondence of the ground layer B. It is interesting to note that lower intensities of this signal - highlighted in light blue colour - were also found in the upper portion of the varnish layer A of the sample LS_1793a (Fig. 3.12b). This presence resulted to be in accordance with the finding of proteinaceous material on the well-preserved areas of the *Bracco* back plate by the non-invasive analysis, as shown in Fig. 3.6a and already highlighted in 2.1. From this evidence, we can hypothesize the use of protein-based restoration materials on the surface of the external varnish layer.

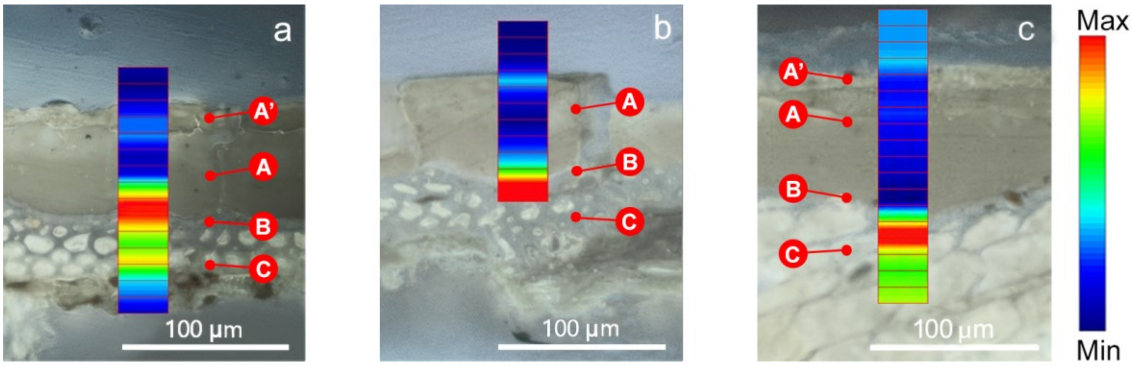

Figure 3.12 *Univariate chemical colour-scale maps of the cross-sectional samples LS_1790 (a), LS_1793a (b) and LS_1793b (c). The colour scale refers to the intensity of the marker amide I band of proteins at 1650 cm^{-1}. Figure published in [Fiocco et al., 2021].*

A similar picture was designed by the multivariate score maps (Fig. 3.13). In the three Storioni samples, the areas coloured from black to dark blue were associated to the varnish (V), while those coloured from green to light blue were related to the ground (G). The colours from red to pink identify the epoxy resin (E). Finally, the yellow-orange areas were attributed to the wood (W) and assigned only in LS_1790 (Fig. 3.13a).

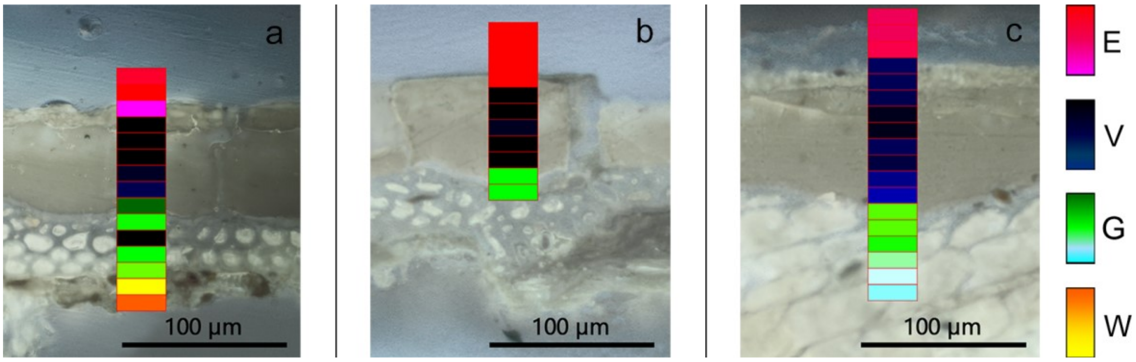

Figure 3.13 *Multivariate score maps of the cross-sectional samples LS_1790 (a), LS_1793a (b) and LS_1793b (c). The resulting colours are related to epoxy resin (E), varnish (V), ground (G) and wood (W). Figure published in [Fiocco et al., 2021].*

The colours in the multivariate maps were interpreted by considering together the score values on PC1, PC2 and PC3 (Fig. 3.14). In Fig. 3.13, reddish colour is characterized by positive PC1, negative PC2 and largely negative PC3 scores. Colours in the range from black to dark blue derive from the combination of negative values of PC1 and PC2. Colours ranging from green to light blue are due to positive PC2, while the PC1 and PC3 values are both characterized by positive and negative values. Finally, the yellow-orange area results from the combination of positive or null PC1 and PC2 scores with negative PC3 scores.

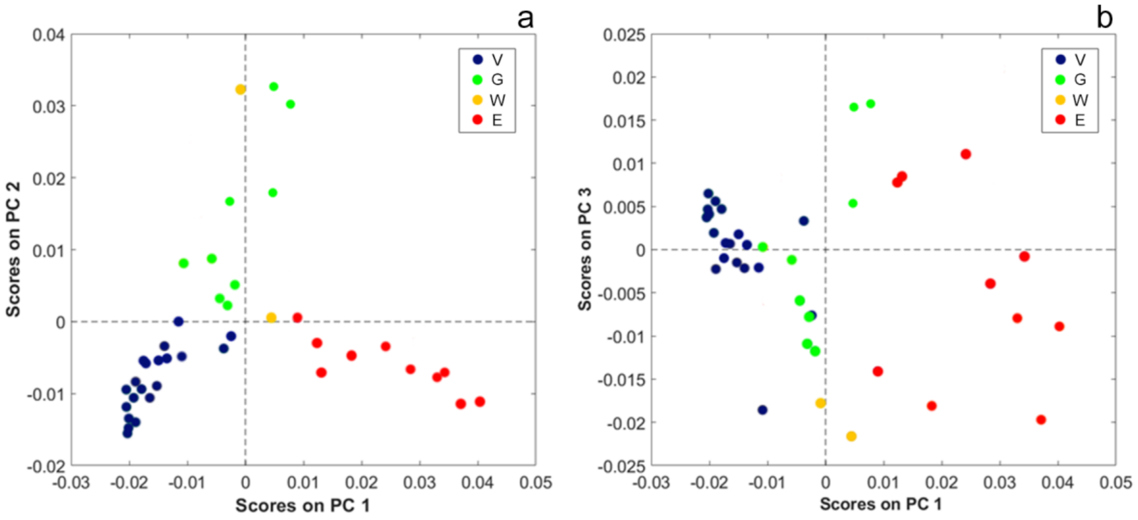

Figure 3.14 *PC1 vs PC2 score plot (a) and PC1 vs PC3 score plot (b) from PCA on SR-FTIR spectra for samples LS_1790, LS_1793a and LS_1793b. Objects are classified in accordance with the position of the analytical spot in the stratigraphy: varnish (V), ground (G), and wood (W) and epoxy resin (E). Figure published in [Fiocco et al., 2021].*

The inspection of the loading plot (Fig. 3.15) played a pivotal role in the identification of the spectral features that mostly characterise each range of colour of the maps, thus allowing us to associate the colour ranges to the different classes of materials: the PC1 loading is characterized by a strong variation around 1550 cm^{-1} and 1500 cm^{-1}, therefore discriminating epoxy resin from other materials; the PC2 loading distinguishes the proteinaceous material thanks to the signals in the region between 1700 cm^{-1} and 1650 cm^{-1} (amide I), affected by a notable variation that explains the positive PC2 score values of group G spectra; the PC3 loading presents a positive variation at 1600 cm^{-1} and a negative variation around 1670 and 1520 cm^{-1}. The association between colour ranges and materials, based on the loading examination above described, mostly confirmed the preliminary assignment made through observation of the analytical spots in the stratigraphies.

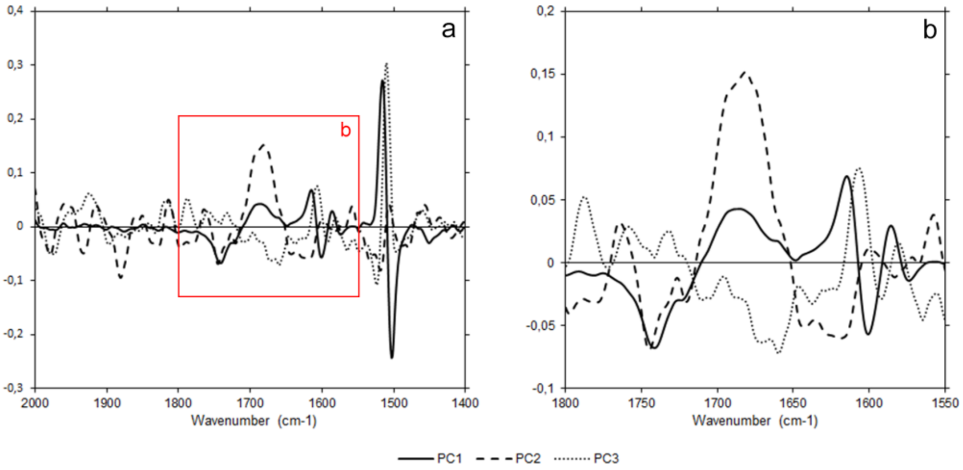

Figure 3.15 *Loading plot of PC1, PC2 and PC3 from PCA on SR-FTIR spectra for samples LS_1790, LS_1793a, LS_1793b and AS_1690 (a); magnification of the area in the red rectangle (b). Figure published in [Fiocco et al., 2021].*

Focusing on the sample AS_1690, a larger area was mapped (Fig. 3.16).

The univariate chemical map of Fig. 3.16a shows the intensity of the varnish vC=O band at around 1710 cm^{-1}: we can see that the most intense red-yellow areas are exactly distributed in correspondence of the two layers A and B.

The multivariate score map of this sample is displayed in Fig. 3.16b, but its interpretation appeared rather complex. By the map, the presence of varnish in the layers A and B can be only partially confirmed, whereas the wood was correctly recognized at the bottom of the stratigraphy. As in the Storioni cases, the score map was created by considering together PC1, PC2 and PC3 score values, which are displayed in Fig. 3.17. In the multivariate map of AS_1690, reddish colour - associated to epoxy resin (E) - is characterized by positive PC1 and negative PC2 values, colours in the range from black to dark blue - related to varnish (V) - mainly present null values of both PC1 and PC2 and positive values of PC3, and the yellow-orange areas - attributed to wood (W) - are characterized by positive PC1 and PC2 values, and negative PC3. As already discussed in 3.1.4.1, it was not possible to achieve a robust identification of the proteinaceous features for this sample and the green areas of Fig. 3.16b do not clearly reveal the marker bands of proteins. For this reason, we cautiously labelled the green portions of the Stradivari multivariate map as U (undefined).

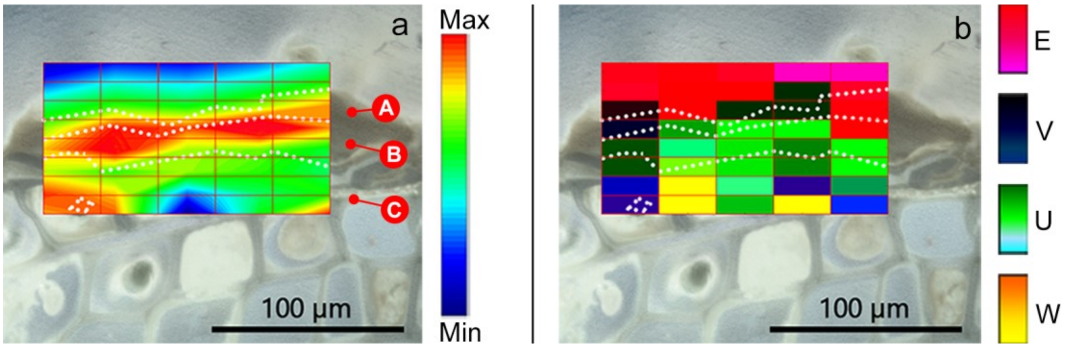

Figure 3.16 *Univariate chemical colour-scale map (a) and multivariate score map (b) of the cross-sectional sample AS_1690. The colour-scale map in (a) refers to the peak of the carbonyl stretching (νC=O) of varnish at 1710 cm^{-1}. The layers identified and described in the text are highlighted. The resulting colours of the score map are related to epoxy resin (E), varnish (V), undefined materials (U) and wood (W). Figure published in [Fiocco et al., 2021].*

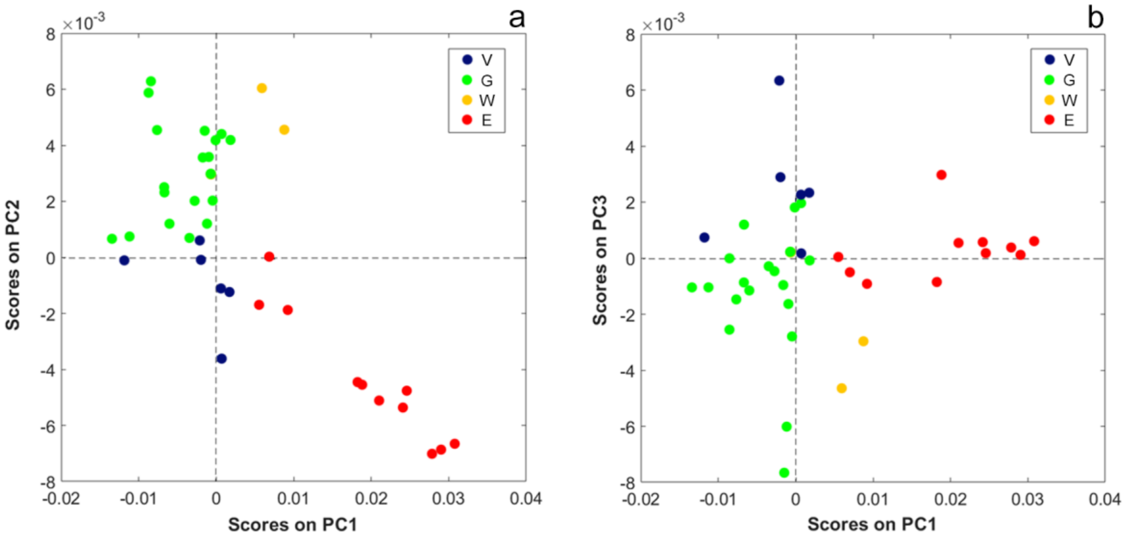

Figure 3.17 *PC1 vs PC2 score plot (a) and PC1 vs PC3 score plot (b) from PCA on SR-FTIR spectra for sample AS_1690. Objects are classified in accordance with the position of the analytical spot in the stratigraphy: varnish (V), ground (G), and wood (W) and epoxy resin (E). Figure published in [Fiocco et al., 2021].*

3.1.5 Conclusions

In this project, four cross-sectional samples of precious Cremonese violins were investigated by synchrotron radiation FTIR microspectroscopy in reflection geometry at Elettra Sincrotrone Trieste. This application has proven to be novel and, at the same time, very challenging if we consider the brittle and complex nature of these layered systems: on one hand, the intensity of the analytical SR beam played its major role in collecting informative IR spectra and, on the other, the reflection geometry fully preserved the integrity of unique samples.

This analytical method enabled us to identify each layer acquiring spatially resolved chemical information from the organic binders laid on the wood. In the micro-FTIR benchtop equipment, the SR beam allowed for the acquisition of maps in reflection mode without any contact with the cross-section, thus preventing its surface from being damaged. With the mapping, we attempted to outline the chemical picture of the layering structure. The univariate approach, based on the selection of marker bands, well discriminated the multi-layered structures in the samples coming from the ancient masters' violins. Although the coats are clearly highlighted, it was rather difficult to exactly define their boundaries by chemical mapping because the interfaces are seldom sharp. As for the multivariate mapping, its potential consisted in the representation of the coating system through a single false-colour score map which highlighted different features of the layers, skipping the need for marker band selection. However, this method recognized only the predominant signals - in terms of intensity - in the spectra; for this reason, we want to draw attention to the fact that the multivariate attribution can be affected by the presence of complex spectra with multiple signals deriving from different materials, as in the case of the *Toscano* violin where some doubtful attributions were labelled as "undefined".

These invasive results were compared and integrated with those deriving from the non-invasive reflection FTIR spectrometer. Thanks to its non-invasiveness, in fact, numerous areas of the violin plates were investigated following the criterion of the different consumption of the varnish on the surface by UVIFL photography. In this way, we gathered information on the varnishes and - where exposed - on the underneath ground layers. Moreover, the inorganic particles acting as fillers or pigments could be characterized - together with the EDX analysis - by this portable analytical instrument, also thanks to its extended spectral range (up to about 400 cm^{-1}).

A varnish made of siccative oil and terpenic resins of vegetal origin was identified on the two small violins 1790 and 1793 by Lorenzo Storioni and on the *Toscano* violin 1690 by Antonio Stradivari. However, some decisive differences were highlighted in the stratigraphic systems from the investigation of the cross-sections. In the Storioni cases, a single varnish layer of 60 to 90 μm of thickness covers a 10-μm-thick proteinaceous ground coat, likely animal glue or casein. Stradivari varnish is instead composed of a double-layered system, with each layer measuring about 10-15 μm of thickness, while no certain evidence of an underneath film-forming proteinaceous layer was found. This could be ascribed to the penetration of the ground binder into the wood pores. Additionally, some inorganic phases such as silicates, aluminosilicates, calcium sulphates and hypothesized iron-based pigments (e.g., red ochres) were detected on the violins by Storioni and Stradivari.

Finally, it is interesting to note that the Stradivari results obtained by this work are in accordance with those found on other outstanding Cremonese musical instruments by

Echard et al. [Echard et al., 2009] and by Brandmair and Greiner [Brandmair and Greiner, 2010]. In their studies, some well-conserved Stradivari instruments were examined and comparable stratigraphies were highlighted: in some cases, the proteinaceous compound is totally absorbed by the wood and the varnish is coated in two oil-resin varnish layers, as we found in the *Toscano* 1690 violin. The difference with the coating systems of the Storioni small violins could be ascribed to a gradual variation in the manufacturing technique towards the end of the Cremonese golden age period, after the death of Antonio Stradivari in 1737 [Brandmair and Greiner, 2010].

3.2 References

Barlow CY., Woodhouse J., Of old wood and varnish: peering into the can of worms, *Journal of the Catgut Acoustical Society*, Series II. 1 (1989) 2–9.

Belbachir K., Noreen R., Gouspillou G., Petibois C., Collagen types analysis and differentiation by FTIR spectroscopy, *Analytical and Bioanalytical Chemistry*. 395 (2009) 829–837. doi:10.1007/s00216-009-3019-y.

Bertrand L., Robinet L., Cohen S.X., Sandt C., Hô A.-S.L., Soulier B., et al., Identification of the finishing technique of an early eighteenth century musical instrument using FTIR spectromicroscopy, *Analytical and Bioanalytical Chemistry*. 399 (2010) 3025–3032. doi:10.1007/s00216-010-4288-1.

Bevilacqua N., Borgioli L., Adrover Gracia I., I pigmenti nell'arte: dalla preistoria alla rivoluzione industriale, Il prato, 2010.

Brandmair B., Greiner S.-P., Stradivari Varnish: scientific analysis of his finishing technique on selected instruments, Serving Audio, 2010.

Bro R., Smilde A.K., Principal component analysis, *Analytical Methods*. 6 (2014) 2812–2831. doi:10.1039/c3ay41907j.

Cotte M., Dumas P., Taniguchi Y., Checroun E., Walter P., Susini J., Recent applications and current trends in Cultural Heritage Science using synchrotron-based Fourier transform infrared micro-spectroscopy, *Comptes Rendus Physique*. 10 (2009) 590–600. doi:10.1016/j.crhy.2009.03.016.

Crupi V., Russa M.F.L., Venuti V., Ruffolo S., Ricca M., Paladini G., et al., A combined SR-based Raman and InfraRed investigation of pigmenting matter used in wall paintings: The San Gennaro and San Gaudioso Catacombs (Naples, Italy) case, *The European Physical Journal Plus*. 133 (2018). doi:10.1140/epjp/i2018-12231-7.

Daher C., Paris C., Hô A.-S.L., Bellot-Gurlet L., Échard J.-P., A joint use of Raman and infrared spectroscopies for the identification of natural organic media used in ancient varnishes, *Journal of Raman Spectroscopy*. 41 (2010) 1494–1499. doi:10.1002/jrs.2693.

Eastaugh N., Pigment compendium: a dictionary and optical microscopy of historical pigments, Routledge, 2013.

Echard J.-P., In situ multi-element analyses by energy-dispersive X-ray fluorescence on varnishes of historical violins, *Spectrochimica Acta Part B: Atomic Spectroscopy*. 59 (2004) 1663–1667. doi:10.1016/j.sab.2004.05.026.

Echard J.-P., Cotte M., Dooryhee E., Bertrand L., Insights into the varnishes of historical musical instruments using synchrotron micro-analytical methods, *Applied Physics A*. 92 (2008) 77–81. doi:10.1007/s00339-008-4449-7.

Echard J.-P., Bertrand L., Von Bohlen A., Le Hô A.-S., Paris C., Bellot-Gurlet L., et al., The Nature of the Extraordinary Finish of Stradivari's Instruments, *Angewandte Chemie International Edition*. 49 (2009) 197–201. doi:10.1002/anie.200905131.

Fichera G., Rovetta T., Fiocco G., Alberti G., Invernizzi C., Licchelli M., et al., Elemental analysis as statistical preliminary study of historical musical instruments, *Microchemical Journal*. 137 (2018) 309–317. doi:10.1016/j.microc.2017.11.004.

Fiocco G., Rovetta T., Invernizzi C., Licchelli M., Malagodi M., Diagnostic analysis of the "Tuscan": varnishes, pigments and wood treatments, in: Zanrè A. (Ed.), The 1690 "Tuscan" Stradivari violin in the Accademia di Santa Cecilia, Scrollavezza & Zanrè, Parma, 2017, 64–67.

Fiocco G., Rovetta T., Malagodi M., Licchelli M., Gulmini M., Lanzafame G., et al., Synchrotron radiation micro-computed tomography for the investigation of finishing treatments in historical bowed string instruments: Issues and perspectives, *The European Physical Journal Plus*. 133 (2018). doi:10.1140/epjp/i2018-12366-5.

Fiocco G., Invernizzi C., Grassi S., Davit P., Albano M., Rovetta T., et al., Reflection FTIR spectroscopy for the study of historical bowed string instruments: Invasive and non-invasive approaches, *Spectrochimica Acta Part A: Molecular and Biomolecular Spectroscopy*. 245 (2021) 118926. doi:10.1016/j.saa.2020.118926.

Fiocco G., Grassi S., Invernizzi C., Rovetta T., Albano M., Davit P., et al., Chemometric tools to investigate complex Synchrotron radiation FTIR micro-spectra: focus on historical bowed musical instruments, *Acta Imeko*. In Press.

González M.G., Cabanelas J.C., Baselga J., Applications of FTIR on Epoxy Resins - Identification, Monitoring the Curing Process, Phase Separation and Water Uptake, Infrared Spectroscopy - Materials Science, Engineering and Technology. (2012).

Grassi S., Fiocco G., Invernizzi C., Rovetta T., Albano M., Davit P., Gulmini M., Stani C., Vaccari L., Licchelli M., Malagodi M., Managing complex Synchrotron radiation FTIR micro-spectra from historic bowed musical instruments by chemometrics, 2019 IMEKO TC4 International Conference on Metrology for Archaeology and Cultural Heritage. MetroArchaeo (2019) 114–119.

Invernizzi C., Daveri A., Rovetta T., Vagnini M., Licchelli M., Cacciatori F., et al., A multi-analytical non-invasive approach to violin materials: The case of Antonio Stradivari "Hellier" (1679), *Microchemical Journal*. 124 (2016) 743–750. doi:10.1016/j.microc.2015.10.016.

Invernizzi C., Daveri A., Vagnini M., Malagodi M., Non-invasive identification of organic materials in historical stringed musical instruments by reflection infrared spectroscopy: a methodological approach, *Analytical and Bioanalytical Chemistry*. 409 (2017) 3281–3288. doi:10.1007/s00216-017-0296-8.

Invernizzi C., Fichera G.V., Licchelli M., Malagodi M., A non-invasive stratigraphic study by reflection FT-IR spectroscopy and UV-induced fluorescence technique: The case of historical violins, *Microchemical Journal*. 138 (2018a) 273–281. doi:10.1016/j.microc.2018.01.021.

Invernizzi C., Rovetta T., Licchelli M., Malagodi M., Mid and Near-Infrared Reflection Spectral Database of Natural Organic Materials in the Cultural Heritage Field, *International Journal of Analytical Chemistry*. 2018 (2018b) 1–16. doi:10.1155/2018/7823248.

Izzo F., Germinario C., Grifa C., Langella A., Mercurio M., External reflectance FTIR dataset (4000–400 cm−1) for the identification of relevant mineralogical phases forming Cultural Heritage materials, *Infrared Physics & Technology*. 106 (2020) 103266. doi:10.1016/j.infrared.2020.103266.

Jalovec K., Italian violin makers, Crown, 1957.

Miliani C., Rosi F., Daveri A., Brunetti B.G., Reflection infrared spectroscopy for the non-invasive in situ study of artists' pigments, *Applied Physics A*. 106 (2011) 295–307. doi:10.1007/s00339-011-6708-2.

Nagyvary J., Guillemette R.N., Spiegelman C.H., Mineral Preservatives in the Wood of Stradivari and Guarneri, *PLoS ONE*. 4 (2009). doi:10.1371/journal.pone.0004245.

Oliveri P., Forina M., Data Analysis and Chemometrics, *Chemical Analysis of Food: Techniques and Applications*. (2012) 25–57. doi:10.1016/b978-0-12-384862-8.00002-9.

Panda H., Epoxy Resins Technology Handbook (Manufacturing Process, Synthesis, Epoxy Resin Adhesives and Epoxy Coatings), NIIR, 2016.

Pouyet E., Lluveras-Tenorio A., Nevin A., Saviello D., Sette F., Cotte M., Preparation of thin-sections of painting fragments: Classical and innovative strategies, *Analytica Chimica Acta*. 822 (2014) 51–59. doi:10.1016/j.aca.2014.03.025.

Prati S., Sciutto G., Catelli E., Ashashina A., Mazzeo R., Development of innovative embedding procedures for the analyses of paint cross sections in ATR FITR microscopy, *Analytical and Bioanalytical Chemistry*. 405 (2012) 895–905. doi:10.1007/s00216-012-6435-3.

Prati S., Sciutto G., Bonacini I., Mazzeo R., New Frontiers in Application of FTIR Microscopy for Characterization of Cultural Heritage Materials, *Topics in Current Chemistry Collections Analytical Chemistry for Cultural Heritage*. (2016) 129–160. doi:10.1007/978-3-319-52804-5_4.

Rosi F., Miliani C., Clementi C., Kahrim K., Presciutti F., Vagnini M., et al., An integrated spectroscopic approach for the non-invasive study of modern art materials and techniques, *Applied Physics A*. 100 (2010a) 613–624. doi:10.1007/s00339-010-5744-7.

Rosi F., Federici A., Brunetti B.G., Sgamellotti A., Clementi S., Miliani C., Multivariate chemical mapping of pigments and binders in easel painting cross-sections by micro IR reflection spectroscopy, *Analytical and Bioanalytical Chemistry*. 399 (2010b) 3133–3145. doi:10.1007/s00216-010-4239-x.

Rosi F., Daveri A., Doherty B., Nazzareni S., Brunetti B.G., Sgamellotti A., et al., On the Use of Overtone and Combination Bands for the Analysis of the CaSO4—H2O System by Mid-Infrared Reflection Spectroscopy, *Applied Spectroscopy*. 64 (2010c) 956–963. doi:10.1366/000370210792080975.

Rosi F., Grazia C., Fontana R., Gabrieli F., Buemi L.P., Pampaloni E., et al., Disclosing Jackson Pollock's palette in Alchemy (1947) by non-invasive spectroscopies, *Heritage Science*. 4 (2016). doi:10.1186/s40494-016-0089-y.

Rovetta T., Invernizzi C., Licchelli M., Cacciatori F., Malagodi M., The elemental composition of Stradivari's musical instruments: new results through non-invasive EDXRF analysis, *X-Ray Spectrometry*. 47 (2017) 159–170. doi:10.1002/xrs.2825.

Salvadó N., Butí S., Tobin M.J., Pantos E., Prag A.J.N.W., Pradell T., Advantages of the Use of SR-FT-IR Microspectroscopy: Applications to Cultural Heritage, *Analytical Chemistry*. 77 (2005) 3444–3451. doi:10.1021/ac050126k.

Sano K., Arrighi S., Stani C., Aureli D., Boschin F., Fiore I., et al., The earliest evidence for mechanically delivered projectile weapons in Europe, *Nature Ecology & Evolution*. 3 (2019) 1409–1414. doi:10.1038/s41559-019-0990-3.

Sciutto G., Oliveri P., Prati S., Quaranta M., Bersani S., Mazzeo R., An advanced multivariate approach for processing X-ray fluorescence spectral and hyperspectral data from non-invasive in situ analyses on painted surfaces, *Analytica Chimica Acta*. 752 (2012a) 30–38. doi:10.1016/j.aca.2012.09.035.

Sciutto G., Oliveri P., Prati S., Quaranta M., Lanteri S., Mazzeo R., Analysis of paint cross-sections: a combined multivariate approach for the interpretation of μATR-FTIR hyperspectral data arrays, *Analytical and Bioanalytical Chemistry*. 405 (2012b) 625–633. doi:10.1007/s00216-011-5680-1.

Sciutto G., Oliveri P., Prati S., Catelli E., Bonacini I., Mazzeo R., A Multivariate Methodological Workflow for the Analysis of FTIR Chemical Mapping Applied on Historic Paint Stratigraphies, *International Journal of Analytical Chemistry*. 2017 (2017) 1–12. doi:10.1155/2017/4938145.

Smith R.E., Larsen F.N., Long C.L., Epoxy resin cure. II. FTIR analysis, *Journal of Applied Polymer Science*. 29 (1984) 3713–3726. doi:10.1002/app.1984.070291207.

Sotiropoulou S., Papliaka Z.E., Vaccari L., Micro FTIR imaging for the investigation of deteriorated organic binders in wall painting stratigraphies of different techniques and periods, *Microchemical Journal*. 124 (2016) 559–567. doi:10.1016/j.microc.2015.10.002.

Tumosa C.S., Mecklenburg M.F., The influence of lead ions on the drying of oils, *Studies in Conservation*. 50 (2005) 39–47. doi:10.1179/sic.2005.50.Supplement-1.39.

Weerd J.V.D., Heeren R.M.A., Boon J.J., Preparation Methods and Accessories for the Infrared Spectroscopic Analysis of Multi-Layer Paint Films, *Studies in Conservation*. 49 (2004) 193. doi:10.2307/25487692.

Wold S., Esbensen K., Geladi P., Principal component analysis, *Chemometrics and Intelligent Laboratory Systems*. 2 (1987) 37–52. doi:10.1016/0169-7439(87)80084-9.

Appendices

APPENDIX I

Analytical instrumentation and acquisition parameters

I. Colorimetry

In 1.3, chromatic variations at different ageing stages were measured using the portable Konica Minolta CM-2600d spectrophotometer (Chiyoda, Tokyo, Japan). Data were collected in the wavelength range 400-740 nm (spectral resolution of 10 nm) using a round target mask of 11 mm diameter. L*, a* and b* coordinates were calculated in SCE mode (specular component excluded) with a 10° standard observer and illuminant D65 according to CIELAB 1976 colour space. The magnitude of the overall colour variation is given by $\Delta E^* = [(\Delta L^*)^2 + (\Delta a^*)^2 + (\Delta b^*)^2]^{½}$. The average value of the three measurements carried out on each differently ground coated portion was considered.

II. Fourier transform infrared spectroscopy

II.I Reflection mode

Reflection FTIR spectroscopy was carried out using the Alpha portable spectrometer (Bruker Optics, Germany/USA) equipped with SiC Globar source, permanently aligned RockSolid interferometer (with gold mirrors) and uncooled DLaTGS detector. Measurements were performed at a working distance of 15 mm by the R-Alpha external reflectance module with an optical layout of 23°/23°. Pseudo-absorbance spectra [log(1/R); R = reflectance] were collected between 7500 and 375 cm^{-1} from areas of about 5 mm in diameter, with an acquisition time of 1 min and at a resolution of 4 cm^{-1}. Spectra acquired from a gold flat mirror were used as background. For the study of bands produced by organic compounds, reflection infrared spectra were transformed to absorbance spectra by applying the Kramers-Kronig transformations (included in the OPUS 7.2 software package). Analytical spots on the musical instruments were selected on the basis of preliminary imaging under visible and UV lights [Dondi et al., 2016; Dondi et al., 2017], in order to examine variously preserved areas and retrieve information both from the varnish and from the underlying layers.

In 1.3, spectra are shown between 3550 and 375 cm^{-1}, depending on the information which needed to be provided.

In 2.1, spectra are shown between 3600 and 375 cm^{-1}.

In 3.1, spectra are shown between 3600 and 500 cm^{-1}.

In appendix IV, spectra are shown between 3550 and 375 cm^{-1}.

Synchrotron radiation FTIR microspectroscopy in reflection mode was performed by the SISSI beamline (Chemical and Life Sciences branch) at Elettra Sincrotrone Trieste (Italy) [Lupi et al., 2007]. Measurements were carried out in reflection geometry using the Bruker Vertex 70v interferometer coupled with the Hyperion 3000 microscope (Bruker Optics, Germany/USA) and a single point MCT detector cooled with liquid nitrogen. The use of synchrotron source infrared radiation provides significant improvement in spectral signal-to-noise ratio at diffraction-limited spatial resolution, collecting reflection spectra with an acquisition rate up to 120 KHz. SR-FTIR microspectroscopy allows the examination of areas as small as 5 μm^2 with negligible heating effects on the sample, either in transmission or in reflection mode [Salvadó et al., 2005]. On the stratigraphies investigated in 3.1 and appendix III, the spatial resolution achieved by the current instrumental set up is ca. 10 μm.

In 3.1 and appendix III, 512 scans were averaged at 120 KHz scanner speed (2 minutes for each point) for single point and mapping acquisitions, with a resolution of 4 cm^{-1} in the spectral range 4000-750 cm^{-1}. A gold substrate was employed for the background. Spectra were pre-processed with a smoothing treatment (Savitzky-Golay method, 15 wavelengths gap size and 2nd polynomial order). The knife-edge slits of the VIS-IR microscope were set to an acquisition area of 10 x 30 μm (height x width). The narrow acquisition area enabled us to retrieve spectra at each single layer of the stratigraphy, with the exception of those ones at the interface between two contiguous layers during the automatic acquisition of the maps. A total of 84 spectra were accumulated on the four cross-sectioned samples: linear maps were collected on LS_1790 (15 rows), LS_1793a (11 rows), LS_1793b (18 rows), and a grid with 8 rows and 5 columns (40 spectra) was obtained from AS_1690.

II.II Attenuated total reflection mode

In 1.3, ATR-FTIR mapping of cross-sectional mock-ups was performed through the Nicolet iN10 MX Thermo Fischer (ThermoFisher Scientific, Madison, USA) micro-spectrometer equipped with Globar infrared source and liquid nitrogen cooled MCT detector. The ATR measurements were performed with conical shape germanium tip crystal. The spatial resolution achievable on the examined stratigraphies by this instrumental set up is ca. 10 μm. Each map is composed of 120 spectra (10 rows x 12 columns), collected in the range 4000-675 cm^{-1} with a spectral resolution of 4 cm^{-1} and a number of scans of 64. The acquisition area of each measurement was 15 x 15 μm, and the mapping stage X and Y step size was 15 μm. For presentation, spectra were smoothed (11 smoothing points) with OMNIC™ Picta™ software.

II.III Transmission mode

In 1.3, transmission FTIR analysis of standard compounds was carried out through the Nicolet iN10 MX Thermo Fischer (ThermoFisher Scientific, Madison, USA) micro-spectrometer. The instrument is equipped with a DTGS detector, working at room temperature. STD compounds were ground into a powder, mixed with potassium bromide (KBr) and then pressed to form an optical window. Spectra were acquired in the range 4000-400 cm^{-1} with a spectral resolution of 4 cm^{-1} and a number of scans of 64.

III. Laser-induced breakdown spectroscopy

In 2.3, LIBS analyses were conducted using the Modì portable LIBS instrument [Bertolini et al., 2006], equipped with a Nd:YAG laser (LS2134-D, Lotis Lasers) at 1064 nm and delivering two laser pulses of energy up to 110 mJ per pulse and of 15 ns FWHM. The delay between pulses was set to 1 µs for the measurements. The laser beam was focused into a sample chamber and the plasma emission was gathered by an optical fibre positioned at 1 cm of distance from the sample and at 45° of angle to the laser beam. A double spectrometer (AvaSpec-2048-2, Avantes), operating in the region 180-450 nm with a resolution of 0.1 nm and from 450 to 900 nm with a resolution of 0.3 nm, was adopted to resolve the spectra. The delay of acquisition can be set from 1.26 µs up to several seconds; for the analysis in 2.3 the minimum value was 1.26 µs from the first laser pulse and 260 ns from the second pulse. The gate of acquisition was fixed at 2 ms. Measurements were performed using a pulse energy of about 70 mJ for both the laser pulses. LIBS spectra were analysed using the LIBS++software, developed in-house at the Research Area of CNR (Pisa, Italy).

IV. Nuclear magnetic resonance - mobile universal surface explorer

In 2.1, NMR analyses were carried out with the Kea spectrometer and Profile NMR-MOUSE (PM5) from Magritek [http://www.magritek.com/] tuned to 20.11 MHz for detection of ^1H at 5 mm depth of access. The excitation pulse length was 7 µs, and the dwell time for the acquisition of a CPMG echo was fixed to 0.5 µs. CPMG echo trains were collected with 64 echoes at an echo time of 40 µs. An area of 12 mm x 10 mm was covered by the sensitive slice. The thickness of the slice for the ^1H resonance was approximated by the excitation bandwidth of about 1/7 MHz and the field gradient of 23 T/m to 150 µm. The NMR-MOUSE instrument was mounted on a linear translation stage M-403.1DG from Physik Instrumente in order to retrieve depth profiles. The sensor was shifted as close to the object as possible in a contactless mode (typically the distance was approximately 1 mm), carefully aligning the sensor surface with the analytical spot by visual examination. The distance between sensor and object was incremented in steps of 100 µm between measurements, by retracting the sensor from the object. Each measurement collected the signal sum from 512 CPMG echo trains: the total time for the acquisition of one depth profile was two to three hours depending on the wood thickness. The profile amplitude is obtained from the acquired NMR signal in different ways. Usually, the transverse relaxation decay is collected for hydrogen nuclei ^1H with a multi-echo sequence following Carr, Purcell, Meiboom, and Gill as a function of time [Blümich et al, 2014; Blümich, 2019]. The amplitude of this signal indicates the density of hydrogen averaged over the volume of the sensitive slice, and the decay is decomposed in terms of a sum of exponential functions which decay with NMR relaxation times T_2. The relaxation decay is decomposed into a distribution of NMR relaxation times using inverse Laplace transformation. Relaxation times indicate the mobility of the molecules. Signal with short relaxation times derives from molecules with limited mobility, signal with long relaxation times from molecules at higher mobility. Molecular mobility scales with macroscopic quantities such as entropy elasticity and inverse viscosity. If a material is stiffer, this means that the molecular mobility is lower and the transverse relaxation time T_2 results shorter. Two-dimensional plots of signal amplitude versus depth and $\log\{T_2\}$ are obtained by the Laplace analysis of depth profiles. By NMR-MOUSE, the signal gathered from wood is typically characterized by two relaxation peaks, one at short T_2 (near 0.09 ms) and one at long T_2 (near 1 ms). The peak at short T_2 is assigned to the protons of the wood (amorphous cellulose, lignin), while the peak at long T_2 to the bound water [Cox et al., 2010]. The position and the intensity of these peaks can change depending on the wood degradation. There are different possibilities to condense the information included in the peaks of the relaxation-time distributions [Blümich et al, 2014].

From the NMR measurements, the curvature of the violin back was found to limit the spatial resolution of the depth profiles to 200 μm. The noise in the depth profiles was smoothed by filtering with a moving three-point average, this further diminishing the apparent resolution of the structures in the depth profiles. Interesting information on the wood stratigraphy was obtained by the ratio of integrals from the peak at short T_2 to the peak at long T_2. This ratio is referred to as relaxation contrast. In 2.1, the relaxation-time distributions were assessed by calculating the ratio of integrals of the distributions from 1 μs to 210 μs and 230 μs to 2 ms. Differently from what observed in the hydrogen density profiles, the depth profiles of the relaxation contrast highlighted layer structures across the back plates of the violins. The structures would not primarily result from variations in the proton (^1H) material density but from variations in the material elastic properties.

V. Optical coherence tomography

OCT analyses were performed with a laboratory-built high-resolution portable Spectral domain OCT (SdOCT) instrument [Targowski et al., 2019; Iwanicka et al., 2016; Iwanicka et al., 2018] equipped with a broad-band superluminescent source built of coupled LEDs emitting in a spectral range of 750-930 nm. The probing light of power not exceeding 800 µW was scanned over the object remaining at the single focal spot (approximate diameter of 15 µm) for 45 µs. Hence, the fluence was not higher than 20 mJ/cm^2. The distance between object and device was 43 mm. The lateral imaging resolution was about 15 µm, while the axial one was ca. 3.3 µm in air and ca. 2.2 µm in a material with refractive index $n_R = 1.5$. A structure can be discriminated as a layer, therefore, if its thickness is equal to or higher than about 5 µm and this will be a maximum error for thickness estimation from a single A-scan (single vertical line of the tomogram). For the whole OCT cross-section (B-scan), a thickness layer measurement uncertainty can be estimated from the axial resolution and data averaging due to the speckle pattern to ca. 3 µm. Approximate values are reported since slight thickness variations are expected by the procedure of layer application. In the raw data, the axial distances along the probing beam (i.e., the depths) are optical distances. In order to correctly represent the axial distances within the object and hence display geometrical distances, we corrected the images for refraction with average $n_R = 1.5$. The reasons why we considered an average value are related to the fact that various media can be characterized by slight variations in this number, but the differences produced by these deviations should be considered negligible. In fact, possible deviations for thin layers would be less than measurement uncertainty caused by the axial resolution of the instrument. The cross-sectional images (tomograms or B-scans) are shown in false-colour scale. The colours are automatically attributed by the software: black areas are those for which no scattering of the probing radiation is recorded as a consequence of the intrinsic properties of the material (e.g., air) or because these areas are not reached by the probing light; areas form blue to green correspond to detectable - albeit low - scattering properties; and colours from yellow to red indicate centres of medium-to-high scattering properties, respectively. It is important to note that the gradual fading of the OCT signal (“fading tails”) visible below the lowest imagined layer are artefacts which originate from photons impeded in the structure due to multi scattering events [Targowski and Iwanicka, 2011].

In 1.3, data for OCT images were collected by scanning the mock-ups m.A, m.B, m.C, m.D and m.H over an area of (10 x 6) mm^2 in ca. 8.1 s as a series of 60 parallel, adjacent linear scans and the mock-up m.F over an area of (7 x 7) mm^2 in ca. 4.5 s as a series of 100 parallel, adjacent linear scans. The tomograms presented are vertically stretched six-fold for a better readability of the coating system and the scale bars represent 200 µm in both directions. Therefore, images in Figs. 1.6 and 1.8 represent areas (2.5 x 0.43) mm^2.

In 2.1, data for OCT images were obtained by scanning the historical violins and the mock-up over an area of (10 x 10) mm^2 in ca. 13.5 s as a series of 100 parallel, adjacent linear scans. The tomograms presented are vertically stretched about seven-fold for a better readability of the coating system. Scale bars represent 200 µm in both directions.

The 2D and 3D layer thickness maps of the *Bracco* small violin are the result of 267 datasets (tomograms). Each tomogram is the outcome of a scan along a straight line of 5 mm length; the scans - before interpolation - are separated by about 10 mm vertically and horizontally (grid of 10 x 10 mm). For every tomogram, the thickness was measured at least 3 times (meaning 3 different positions) and data averaged making a single data point. The data points were then spline interpolated in both directions to 70 x 40 points. It is worth noting that it is not a rectangle mesh as the number of points in rows vary depending on the data spread. The 2D thickness map and its grip map are displayed in Fig. AI.1. The violin was not scanned for its entire surface mainly because of the limited range of the OCT head translators (horizontally by the motorised slider and vertically by the tripod vertical support).

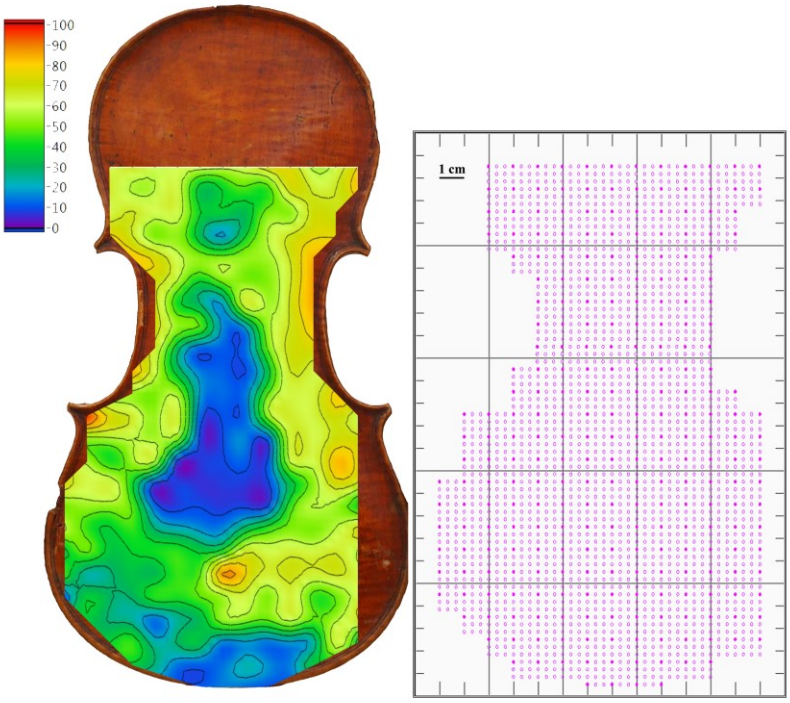

Figure AI.1 *2D OCT layer thickness map of the Bracco small violin (left), and its grid map (right) highlighting real (filled round) and interpolated (open round) points. Measurement unit of the coloured scale bar: µm; distance among minor ticks in the map grid: 1 cm.*

In 2.2, data for OCT images were acquired from adjacent locations by scanning the probing beam along a straight line (i) of 10 mm length for fragments F1, F16, and F21 and (ii) of 8 mm length for fragments F13 and F20, over 135 ms in both cases. Specifically, fragments F1, F16, and F21 were scanned over an area of (10 x 10) mm^2 and fragment F20 over (8 x 8) mm^2 - as series of 100 B-scans - in 13.5 s each and the fragment F13 was scanned over (8 x 4) mm^2 in 50 scans in overall time of 6.75 s. The tomograms presented are vertically stretched about eight-fold for a better readability of the coating system. Scale bars represent 200 µm in both directions. The most representative data were selected arbitrarily for presentation, regardless of their actual direction in relation to the musical instrument.

In 2.3, the analyses by OCT were conducted after the LIBS experiments. A series of parallel, adjacent tomograms (8-10 mm long) was acquired over the area centred at the LIBS crater, in order to measure its depth. The distance between adjacent tomograms varied from 20 µm for the mock-up to 80 µm for the historical fragments F13 and F20, and 100 µm for fragment F16 and the *Bracco* small violin. The tomograms shown in 2.3 are vertically stretched about five-fold to provide a better readability of the stratigraphy around the craters. Scale bars represent 200 µm in both directions. Determination of the crater depth was carried out using morphological filtering, as reported by Kaszewska et al. [Kaszewska et al., 2013] and briefly described as follows. Firstly, the reference surface from which the crater depth is measured must be determined. To do this, the fitting of second-degree polynomial to the surface of the object is used, but excluding the nearest closeness of the crater. Subsequently, the 3D morphological filtering is carried out in the interior part of the crater using a ball-shaped structuring element. We can explain this procedure as dropping a ball from the reference surface down to the crater and measuring the maximum depth at which it touches the crater walls. The diameter of this element was arbitrarily fixed to 20 µm: this values coincides with the size of the speckle structures in the OCT images. Obviously, lower values of this parameter would lead to an increment in the measured crater depth, but this effect is 5-15 µm only for diameter reduction even to 5 µm. Furthermore, the contribution to the LIBS signal from very small volumes introduced by small “ball” diameter can be reasonably considered not significant.

VI. Optical microscopy

In the thesis, imaging at high magnifications on cross-sectioned samples was conducted using the Olympus BX51TF polarized light optical microscope (OM) equipped with the Olympus TH4-200 (visible light) and Olympus U-RFL-T (UV light) lamps.

VII. Raman spectroscopy

In 1.3, Raman spectroscopy was performed by the BRAVO portable spectrometer (Bruker Optics, Germany/USA-MA), which employs the SSE™ (Sequentially Shifted Excitation, patent number US8570507B1) patented technology to reduce fluorescence [Cooper et al., 2013; Cooper et al., 2014]. The instrument is equipped with two different lasers (DuoLaser™) ranging from 700 to 1100 nm and with power less than 100 mW. During the acquisition, the laser is slightly wavelength shifted for three times and three raw Raman spectra are collected. An algorithm identifies the peaks that shift at different laser wavelengths as good Raman signals, while the non-shifting peaks are recognized as fluorescence (or absorbance) signals and removed. The spectra were acquired in the range

3200 cm^{-1} to 300 cm^{-1}, with acquisition time from 500 ms to 2 s and accumulation from 5 to 100 scans. OPUS™ software (Version 7.7) was used to set the acquisition parameters and to smooth the spectra.

VIII. Scanning electron microscopy - energy dispersive X-ray spectrometry

Imaging at high magnifications was performed by the FE-SEM Tescan Mira 3XMU-series (Brno, Czech Republic) scanning electron microscope. Elemental microanalysis was carried out using the Bruker Quantax 200 (Billerica, MA, USA) energy-dispersive X-ray spectrometer coupled to the FE-SEM apparatus.

In 1.3, the operating conditions were as follows: accelerating voltage 15-20 kV in low vacuum (100 Pa nitrogen pressure) and working distance 15 mm. SEM images were collected in BSE mode.

In 2.3, the operating conditions were as follows: accelerating voltage 15-20 kV in high vacuum and working distance 15 mm. SEM images were collected in BSE mode.

In 3.1 and appendix IV, the operating conditions were as follows: accelerating voltage 20 kV in low vacuum (100 Pa nitrogen pressure). SEM observations were performed in BSE mode.

IX. Stereomicroscopy

In the thesis, stereomicroscopic observations were performed using the Olympus SZX10 stereomicroscope equipped with the Olympus DP73 camera and the Schott KL1500 illuminator. Images were processed by the Stream Essentials software.

X. Synchrotron radiation micro-computed tomography

In 2.2, the 3D micromorphology examination was carried out by high-resolution SR-micro-CT in phase-contrast mode [Cloetens et al., 1997] at the SYRMEP beamline of the Elettra synchrotron laboratory (Trieste, Italy). A polychromatic X-ray beam produced by a bending magnet source illuminated the sample in transmission geometry. Filters (1.5 mm Si + 1 mm Al) were employed to remove the low-energy contribution in the beam spectrum. In this configuration, the average beam energy was approximately 28 keV. The distance between sample and detector was fixed at 150 mm. For each experiment, the sample was continuously rotated over an angle of rotation of 180 degrees and 1800 projections were collected with an exposure time/projection of 0.25 s. The detector was a Hamamatsu C11440-22C air-cooled, 16 bit, sCMOS camera (Hamamatsu Photonics, Hamamatsu, Japan) 2048 x 2048 pixels chip. Measurements were performed with an effective pixel size of the detector set at (1 x 1) μm^2 generating a maximum field of view of about (2.4 x 2.4) mm^2.

The reconstruction of 2D tomographic slices was performed with the SYRMEP Tomo Project (STP) house software suite [Brun et al., 2017]. In order to lower ring artefacts produced by detector inhomogeneity, different combinations of filters available in the STP software (ver. 1.2.5) were applied to the datasets [Brun et al., 2013]. By the application of a single-distance phase-retrieval algorithm [Paganin et al., 2002] based on the Transport of Intensity Equation (TIE) to the sample projections, the consistency of the morphological study increased. To do this, the complex refractive index of the samples $n = 1 - \delta + i\beta$ (where δ is the real part and β the imaginary part, respectively related to phase and absorption distribution of the sample) was computed. For the objects in exam, we established a constant ratio $\gamma = \delta/\beta = 151$ as the most suitable value. Phase-retrieval, combined with the Filtered Back-Projection algorithm [Herman, 1980], enabled us to get the 3D distribution of the complex refraction index of the imaged samples in order to limit the edge-enhancement effect at sample borders, maintaining the morphology of the smallest features. The stack of slices was imported in VGStudio Max 2.2 from Volume Graphics and subsequently used for the 3D rendering and segmentation (manual thresholding) of the volumes (Fig. 2.14). Starting from the tomographic volumes, the 3D virtual reconstructions were edited using Photoshop CS6.

XI. Ultraviolet-induced fluorescence and visible photography

In the thesis, photos under UV and VIS lights were performed with the Nikon D4 full-frame digital camera equipped with a 50mm f/1.4 Nikkor objective. Visible light illumination was obtained using two Softbox LED lamps with temperature at 5400K (ISO 100, f/10, exposure time computed in function of the camera light meter), while UV-induced visible fluorescence was obtained using two Philips TL-D 36W BBL IPP low-pressure Hg tubes with emission peak approximately at 365 nm (ISO 400, f/10, exposure time 30s). The Kodak 2E gelatine filter was employed for the UVIFL acquisitions, as an alternative to the Schott KV418 currently dismissed. The analysis of UV images was supported by semi-automatic and automatic systems [Dondi et al., 2017; Dondi et al., 2018].

XII. X-ray fluorescence spectroscopy

XRF analyses were performed using the EDXRF spectrometer ELIO (Bruker Optics, Germany/USA). The system is composed of a large-area Silicon Drift Detector (SSD) (25 mm^2) whose read-out is based on a Complementary Metal-Oxide Semiconductor (CMOS) preamplifier (CUBE). The device is equipped with a low-power X-ray tube with Rh anode and 1.2 mm of analytical spot diameter. The average spectra were calculated from three consecutive acquisitions. It is important to noting that the concentration of light elements such as Si and S could be underrated, since their low-energy secondary emission is attenuated by air and by the matrix [Beckhoff et al., 2006; Glinsman, 2005]. The integration of the peaks was calculated using both the background component determined with a fitting on the whole spectrum (global parameter) and the Gaussian fitting of the specific section of the spectrum (local parameter) where the peak was located. Data were processed using the ELIO 1.6.0.29 software.

In 1.3, the working conditions used for the analysis of the mock-ups were measuring time 480 s, fixed tube voltage 40 kV, tube current 40 μA and acquisition channels 2048. Three acquisitions were performed in each area of the mock-ups characterized by different concentration of talc in K-caseinate. For each element taken into consideration, the reported value corresponds to the net area counts of the peak (Kα) normalized to the average of net area counts of the coherent scattering Rh-Kα peak of the entire data set.

In 2.1 and appendix IV, the working conditions used for the analysis of the historical violins and the mock-up were measuring time 480 s, fixed tube voltage 40 kV, tube current 80 μA and acquisition channels 2048. Three acquisitions were performed in each area of the mock-up representing a stratigraphic system, and the average spectra were calculated. For each element taken into consideration, the reported value corresponds to the net area counts of the peak (Kα) normalized to time and to net area counts of the coherent scattering peak of Rh-Kα.

In 2.3, the working conditions used for the analysis of the three historical fragments and the *Bracco* small violin were measuring time 300 s, fixed tube voltage 40 kV, tube current 80 μA and acquisition channels 2048. Three acquisitions were performed nearby the LIBS crater of each historical instrument, before carrying out the LIBS analysis, and the average spectra were calculated. For each element taken into consideration, the reported value corresponds to the net area counts of the peak (Kα) normalized to time and to net area counts of the coherent scattering peak of Rh-Kα.

References

Beckhoff B., Kanngießer B., Langhoff N., Wedell R., Wolff H., Handbook of Practical X-Ray Fluorescence Analysis, Springer Berlin Heidelberg, 2006.

Bertolini A., Carelli G., Francesconi F., Francesconi M., Marchesini L., Marsili P., et al., Modì: a new mobile instrument for in situ double-pulse LIBS analysis, *Analytical and Bioanalytical Chemistry*. 385 (2006) 240–247. doi:10.1007/s00216-006-0413-6.

Blümich B., Haber-Pohlmeier S., Zia W., Compact NMR, Walter de Gruyter GmbH & Co. KG, 2014.

Blümich B., Essential NMR, Springer-Nature, 2019.

Brun F., Accardo A., Kourousias G., Dreossi D., Pugliese R., Effective implementation of ring artifacts removal filters for synchrotron radiation microtomographic images, *2013 8th International Symposium on Image and Signal Processing and Analysis (ISPA)*. (2013). doi:10.1109/ispa.2013.6703823.

Brun F., Massimi L., Fratini M., Dreossi D., Billé F., Accardo A., et al., SYRMEP Tomo Project: a graphical user interface for customizing CT reconstruction workflows, *Advanced Structural and Chemical Imaging*. 3 (2017). doi:10.1186/s40679-016-0036-8.

Cloetens P., Pateyron-Salomé M., Buffière J.Y., Peix G., Baruchel J., Peyrin F., et al., Observation of microstructure and damage in materials by phase sensitive radiography and tomography, *Journal of Applied Physics*. 81 (1997) 5878–5886. doi:10.1063/1.364374.

Cooper J.B., Abdelkader M., Wise K.L., Sequentially Shifted Excitation Raman Spectroscopy: Novel Algorithm and Instrumentation for Fluorescence-Free Raman Spectroscopy in Spectral Space, *Applied Spectroscopy*. 67 (2013) 973–984. doi:10.1366/12-06852.

Cooper J.B., Marshall S., Jones R., Abdelkader M., Wise K.L., Spatially compressed dual-wavelength excitation Raman spectrometer, *Applied Optics*. 53 (2014) 3333. doi:10.1364/ao.53.003333.

Cox J., Mcdonald P.J., Gardiner B.A., A study of water exchange in wood by means of 2D NMR relaxation correlation and exchange, *Holzforschung*. 64 (2010) 259–266. doi:10.1515/hf.2010.036.

Dondi P., Lombardi L., Malagodi M., Licchelli M., Automatic identification of varnish wear on historical instruments: The case of Antonio Stradivari violins, *Journal of Cultural Heritage*. 22 (2016) 968–973. doi:10.1016/j.culher.2016.05.010.

Dondi P., Lombardi L., Invernizzi C., Rovetta T., Malagodi M., Licchelli M., Automatic Analysis of UV-Induced Fluorescence Imagery of Historical Violins, *Journal on Computing and Cultural Heritage*. 10 (2017) 1–13. doi:10.1145/3051472.

Dondi P., Lombardi L., Rocca I., Malagodi M., Licchelli M., Multimodal workflow for the creation of interactive presentations of 360 spin images of historical violins, *Multimedia Tools and Applications*. 77 (2018) 28309–28332. doi:10.1007/s11042-018-6046-x.

Glinsman L.D., The practical application of air-path X-ray fluorescence spectrometry in the analysis of museum objects, *Studies in Conservation*. 50 (2005) 3–17. doi:10.1179/sic.2005.50.supplement-1.3.

Herman G.T., Image Reconstruction from Projections: The Fundamentals of Computerized Tomography, 1st ed.; Academic Press: New York, NY, USA, 1980.

Iwanicka M., Lanterna G., Lalli C.G., Innocenti F., Sylwestrzak M., Targowski P., On the application of optical coherence tomography as a complimentary tool in an analysis of the 13th century Byzantine Bessarion reliquary, *Microchemical Journal*. 125 (2016) 75–84. doi:10.1016/j.microc.2015.11.014.

Iwanicka M., Sylwestrzak M., Targowski P., Optical Coherence Tomography (OCT) for Examination of Artworks, Advanced Characterization Techniques, *Diagnostic Tools and Evaluation Methods in Heritage Science*. (2018) 49–59. doi:10.1007/978-3-319-75316-4_4.

Kaszewska E.A., Sylwestrzak M., Marczak J., Skrzeczanowski W., Iwanicka M., Szmit-Naud E., et al., Depth-Resolved Multilayer Pigment Identification in Paintings: Combined Use of Laser-Induced Breakdown Spectroscopy (LIBS) and Optical Coherence Tomography (OCT), *Applied Spectroscopy*. 67 (2013) 960–972. doi:10.1366/12-06703.

Lupi S., Nucara A., Perucchi A., Calvani P., Ortolani M., Quaroni L., et al., Performance of SISSI, the infrared beamline of the ELETTRA storage ring, *Journal of the Optical Society of America B*. 24 (2007) 959. doi:10.1364/josab.24.000959.

Paganin D., Mayo S.C., Gureyev T.E., Miller P.R., Wilkins S.W., Simultaneous phase and amplitude extraction from a single defocused image of a homogeneous object, *Journal of Microscopy*. 206 (2002) 33–40. doi:10.1046/j.1365-2818.2002.01010.x.

Salvadó N., Butí S., Tobin M.J., Pantos E., Prag A.J.N.W., Pradell T., Advantages of the Use of SR-FT-IR Microspectroscopy: Applications to Cultural Heritage, *Analytical Chemistry*. 77 (2005) 3444–3451. doi:10.1021/ac050126k.

Targowski P., Iwanicka M., Optical Coherence Tomography: its role in the non-invasive structural examination and conservation of cultural heritage objects—a review, *Applied Physics* A. 106 (2011) 265–277. doi:10.1007/s00339-011-6687-3.

Targowski P., Kowalska M., Sylwestrzak M., Iwanicka M., OCT for examination of cultural heritage objects, IntechOpen, 2019. doi:10.5772/intechopen.88215.

[Web]

http://www.magritek.com/ (accessed on 27 July 2019). NMR Spectroscopy without leaving your lab, Magritek.

APPENDIX II

Historical musical instruments

I. *Hämmerle* violin 1658, Nicolò Amati

For about forty years, after the death of his father Girolamo in 1630, Nicolò was indisputably the leading craftsman of the 17th century Cremonese lutherie [Cacciatori, 2014; Rossi et al., 2006]. In his workshop, dozens of young makers learned the craft, first among them the *familio* Andrea Guarneri. Nicolò's influence is also evident in the early works made by Antonio Stradivari and in the instruments of Francesco Rugeri, although their presence in the Amati workshop is not documented. The instruments produced in the mid-17th century, when Nicolò was a fully accomplished craftsman, were marked by models and stylistic features that became object of study and source of inspirations for generations of violin makers working in Cremona and elsewhere.

A violin of large format, the *Hämmerle* is considered of exquisite workmanship and particularly striking, also with regard to its sonority. It is characterized by the purity of form, above all in the profile of the f-holes, and by the harmonious outline of the front and back plates. The front plate is in a single piece of spruce of medium grain, narrowing towards the flanks (Fig. AII.1). As for the back plate, it is in one piece of tangentially cut maple wood showing an irregular horizontal curl (Fig. AII.2), and a maple wood of the same quality was used for the ribs. The maple wood of the scroll, radially cut, is interested by light flames. The varnish is golden-orange in colour.

Owned by the collector Theodor Hämmerle, it was subsequently property of Henry Hottinger and then passed to the Wurlitzer House in New York; the violin was finally bought, in 1966, by the Provincial Tourism Board of Cremona thanks to a public subscription. Since 2013, it has been housed in the Museo del Violino in Cremona.

Figure AII.1 *VIS photo* of the front plate of the Hämmerle violin 1658 by Nicolò Amati.*
** Photo by Arvedi laboratory.*

Figure AII.2 *VIS photo* of the back plate of the Hämmerle violin 1658 by Nicolò Amati.*
** Photo by Arvedi laboratory.*

II. *Hellier* violin 1679, Antonio Stradivari

The *Hellier* violin is one of ten surviving inlaid instruments by Stradivari [Beare, 1987]. The front (Fig. AII.3) and back (Fig. AII.4) plates are decorated with double purfling enclosing alternate diamonds and circles of ivory or bone in a black matrix, and the ribs are inlaid with black arabesque (Fig. AII.5). The black strips of the purflings, as well as the black fillers of the inlays, were found to be coloured by iron-based dye [Invernizzi et al., 2016]. Such an elaborate ornamentation was rarely carried out on violins, although Nicolò Amati followed the practice occasionally. The finesse of the work made this instrument an outstanding masterpiece, which was already famous in his own time.

The violin is remarkable for its somewhat unusual large proportions [Henley, 1961]. The spruce wood of the front plate is characterized by fine grain, opening slightly towards the flanks (Fig. AII.3). The back plate is constituted of one piece of maple wood, with broad curl (Fig. AII.4), and a similar wood was used for both the ribs and the scroll [http://www.tarisio.com/].

The violin derives its name from the Hellier family, in whose possession it is first recorded in the 18th century. It is believed that Sir Samuel Hellier bought the violin from Stradivari himself, and it remained in the possession of the Hellier family until about 1880, when it was sold to George Crompton. In 1885 it was purchased from Charles Oldham, through the intermediary of W.E. Hill and Sons. He retained this example until 1890, when it was sold back to the Hellier family. In 1910 it returned to Hills to be sold to Oscar Bondy of Vienna. In 1925 Hills acquired it again and subsequently sold it to H.E. Morris, editor of the Shanghai Daily News. Through the heirs of H.E. Morris, the violin came to America and was purchased to Henry Hottinger in 1957. Mrs. Lee Wurlitzer acquired the instrument from Hottinger in 1965, and subsequently sold it to an anonymous buyer in 1979. The *Hellier* was on loan to the Smithsonian Institution from 1979 to 1987. In the year 1998, Herbert Axelrod purchased the *Hellier*, and it was on loan to the Smithsonian Institution again from 1998 until 2003. Finally, in 2014 it was bought by the current owner who lent it to the Museo del Violino in Cremona, where it is currently housed [Beare, 1987; Villa et al., 2011].

Figure AII.3 *VIS photo* of the front plate of the Hellier violin 1679 by Antonio Stradivari.*
** Photo by Arvedi laboratory.*

Figure AII.4 *VIS photo* of the back plate of the Hellier violin 1679 by Antonio Stradivari.*
** Photo by Arvedi laboratory.*

Figure AII.5 *VIS photos* of the ribs of the Hellier violin 1679 by Antonio Stradivari.*
** Photos by Arvedi laboratory.*

III. *Toscano* violin 1690, Antonio Stradivari

The *Toscano* violin almost certainly belonged to the Medici Quintet ordered in 1684 by the Marquis Bartolomeo Ariberti, a Cremonese citizen and devoted admired of Stradivari, to be presented to the Grand Prince Ferdinando de' Medici (1663-1713). At the time, it was not an unusual practice to offer musical instruments as a gift. Son of Grand Duke of Tuscany Cosimo III, Ferdinando was very keen on music, played several instrument himself, and employed the best singers and musicians of the time. Under his rule the court became a flourishing European centre of music [Barabaschi, 2017].

The name *Toscano* comes from the history of the instrument: it is the only one of the two Medici Quintet violins to have survived. The quintet was completed by a cello and a tenor viola, still in the collection of the Florence Conservatory, and a contralto viola, now privately owned but permanently loaned to the Library of Congress, Washington [Bini, 2017].

The *Toscano* violin is one of the best known examples by Stradivari, also due to its excellent state of preservation, except for changes to the neck and the replacement of the fingerboard and fittings. Given that the commission was from a noble patron, Stradivari chose the best wood possible for the front and back plates: a piece of spruce with a fine, narrow grain in the centre, gradually becoming wider towards the exterior (Fig. AII.6), and a single piece of maple, with a deep narrow curl, for the back (Fig. AII.7), from which he also managed to extract the ribs. The scroll (Fig. AII.8) is representative of Stradivari's willingness to break with tradition: the chamfering is made solider and broader so as to contrast more effectively with the profile of the volute. To emphasize the graphic and chromatic contrast, the whole chamfer was blackened (Fig. AII.8). The violin is also one of the first instruments to depart from the Cremonese tradition of using a transparent coat of varnish, founded on the traditional amber yellow, in favour of a stronger orange-red-brown, enhancing the contrast with the black decoration of the scroll chamfers [Giordano, 2017].

Currently owned by the Accademia di Santa Cecilia in Rome, it is exposed in its Musical Instrument Museum collection. When the Grand Prince Ferdinando died, his regard to music as an art did not carry far down his family line, and in the late 18th century the violin was in the possession of Giovanni Felice Mosell, director of music and first violinist at the court, who sold it in 1784 to the Irish collector David Ker. In 1847 it was taken to Paris to be fitted up by Jean-Baptiste Vuillaume, and in 1875 it was sold by Ker's descendants to an amateur named Ricardo. In 1888 it was purchased by W. E. Hill and Sons, and was successively sold by them to R. E. Brandt (1890), Charles Oldham (1904), F. Smith (1908), Richard Bennett (1918) and G. Kemp (1933). In 1940 Hills acquired the violin again, and sold it to the Italian State in 1953 arriving at the Accademia di Santa Cecilia in a double case datable to the second half of the 19th century [Beare, 1987; Bini, 2017].

Figure AII.6 *VIS photo* of the front plate of the Toscano violin 1690 by Antonio Stradivari.*
** Photo by Jan Röhrmann.*

Figure AII.7 *VIS photo* of the back plate of the Toscano violin 1690 by Antonio Stradivari.*
** Photo by Jan Röhrmann.*

Figure AII.8 *VIS photos* of the scroll sides of the Toscano violin 1690 by Antonio Stradivari.*
** Photos by Jan Röhrmann.*

IV. *Cremonese* violin 1715, Antonio Stradivari

The *Cremonese* violin was made by Antonio Stradivari in 1715, during his so-called “golden period”, which is believed to have been between 1710 and 1720. In this decade, the renowned master produced some of the most interesting surviving instruments, from a technical and artistic standpoint. In 1715 Stradivari was approaching or a little past his seventieth birthday. However, despite his advancing years, he seemed to have worked with greater vigour in the distinguishing features of his work as well as in the number of instruments he realized [Trabucchi et al., 2015].

Stradivari chose some of the best materials in his production to make this large-format violin. The front plate (Fig. AII.9) is made of two pieces of spruce, which most certainly comes from the same log, characterized by fine grain in the centre, broadening towards the flanks [http://www.tarisio.com/]. The back plate (Fig. AII.10) is a one-piece slab of Balkan maple, radially cut, with broad, deep and irregular flames running horizontally. The medium width grain is fairly regular, although slightly inclined with respect to the centre joint. A piece of maple, likely from the same slab as the back, is inserted in the top left corner as a result of a repair work. The ribs are in maple but do not come from the same log as the back, since their flames are broader and not as deep as the back wood, and the grain is narrower and more regular. The head is considered among the finest crafted in Stradivari’s production and presents all the stylistic characteristics of his workmanship: it is robust, as the rest of the instrument, but at the same time elegant and well-proportioned [Trabucchi et al., 2015].

In 1870s the *Cremonese* violin was in Paris, owned by a violinist named Darius Gras. Following his death in 1877, it was sold to another professional player, Jules Garcin, and after three years it passed to David Laurie. Laurie, a well-known dealer, sold it to an amateur, Mr. Labitte of Rheims, and in 1889 the violin was purchased for presentation to the famous violinist and composer Joseph Joachim in celebration of his jubilee. Shortly before his death, Joachim had donated the instrument to his nephew Harold, who sold it to Robert Brandt in 1910. After a period in amateur hands, it was sold to the Hills, before finding its way back to Cremona in 1961. In that year, the violin was purchased by the Provincial Tourism Board: since then, the *Cremonese* violin, known for a long time as *Joachim*, is considered as one of the town’s symbol [Beare, 1987; Cacciatori, 2014]. Since 2013, it has been housed in the Museo del Violino in Cremona.

Figure AII.9 *VIS photo* of the front plate of the Cremonese violin 1715 by Antonio Stradivari. * Photo by Arvedi laboratory.*

Figure AII.10 *VIS photo* of the back plate of the Cremonese violin 1715 by Antonio Stradivari. * Photo by Arvedi laboratory.*

V. *Principe Doria* violin 1734, Giuseppe Guarneri “del Gesù”

The *Principe Doria* is considered one of the best concert violins by Guarneri “del Gesù”. Its fame is probably due to the fact that, differently from other ancient instruments, it did not undergo interventions of reduction and redistribution of the thicknesses, as the plates are characterized by robust thicknesses [http://www.museodelviolino.org].

The front (Fig. AII.11) and back (Fig. AII.12) plates are made of two pieces of spruce and maple, respectively. According to examinations of the violin made in recent years, it was confirmed that the scroll sculpture shows evidence of the hand of the father Giuseppe *filius Andreae*, who continued to work in the workshop also after the transferring of the activity to the son Giuseppe “del Gesù” in 1731. The head, not original to the violin, was positioned on the instrument by the renowned luthier Simone Ferdinando Sacconi [http://www.museodelviolino.org].

The first document related to the *Principe Doria* violin is dated 1858, the year of its sale to the Doria family by the greatest expert at the time, C. Jacquot. The Dorias were owner of other precious Italian instruments, including the *Armingaud* violin 1736 made by Stradivari. In 1950 Rembert Wurlitzer sold it to Leopold Godowsky Jr., son of the famous Russian pianist. In 1962 the violin was purchased by Zvi Zeitlin, who played it for more than forty years until it was bought by the current owner. The violin is currently on loan to the Museo del Violino in Cremona [http://www.museodelviolino.org].

Figure AII.11 *VIS photo* of the front plate of the Principe Doria violin 1734 by Giuseppe Guarneri "del Gesù". * Photo by Arvedi laboratory.*

Figure AII.12 *VIS photo* of the back plate of the Principe Doria violin 1734 by Giuseppe Guarneri "del Gesù". * Photo by Arvedi laboratory.*

VI. *Bracco* small violin 1793, Lorenzo Storioni

Lorenzo Storioni (1744-1816) was born in a difficult period for Cremonese violin making: Giuseppe Guarneri “del Gesù” died that same year, and in just ten years the town lost Antonio Stradivari and his sons, Giuseppe Guarneri and Girolamo II Amati (both in 1740) and Carlo Bergonzi in 1747. The 1780s and 1790s represented the most productive period of Storioni, the years during which he used his best-known models for his instruments [Cacciatori, 2018a].

The small-size *Bracco* violin was made for a child from eight to ten years old, as its dimensions witness: the body, in fact, is about 4 cm smaller than a full-size violin. Recently reappeared after a long period of neglect, probably abandoned amongst old items in a stately home, the instrument shows signs of the difficult life it has endured for the later part of its existence. Each part of the violin presents substantial woodworm damage: holes on the surfaces, channels in the matrix and, in some areas, detachments of varnish and wood (Figs. AII.13 and AII.14). The widespread damage suggests it lost its acoustic function a long time ago, and therefore that it has not been played for a significant period. The condition of the fingerboard - not glued to the neck - and the lack of any accessories except for the pegs lead to the same conclusion. At the same time, the wear on the fingerboard, the worn varnish in correspondence of the areas of the front and back plates which come into contact with the performer’s hand and body, and the black rosin deposit on the central part of the soundboard indicate that the instrument was used in the decades following its construction (Figs. AII.13 and AII.14) [Cacciatori, 2018b].

The condition of the *Bracco* small violin is closely connected to its history. While the damage caused to the wood and varnish by the woodworm infestation is undeniable, on the other hand the period of abandonment allowed for the conservation of an extremely interesting layer of varnish, avoiding that the surface was cleaned and polished, which would have altered certain characteristics of the materials. In particular, the areas to the right and left of the strip of unvarnished wood on the front plate - under the fingerboard - have a warm orange hue, thus guiding to the initial colour of the violin (Fig. AII.13) [Cacciatori, 2018b].

In 2018, the violin was the focus of the initiative called “I cantieri del suono” which saw the Fondazione Bracco working with the Municipality of Cremona, the Museo del Violino and the University of Pavia to purchase, study, restore and exhibit the instrument. In particular, the project involved studying the history, organology and philology of the instrument, alongside diagnostic work to examine the materials and construction techniques and finally the restoration by renowned violin restorers, before the instrument joined the permanent collection at the Museo del Violino in Cremona [Bracco, 2018].

Figure AII.13 *VIS photo * of the front plate of the Bracco small violin 1793 by Lorenzo Storioni. * Photo by Arvedi laboratory.*

Figure AII.14 *VIS photo* of the back plate of the Bracco small violin 1793 by Lorenzo Storioni. * Photo by Arvedi laboratory.*

VII. Fragments of the “Collezione Sgarabotto”

During the first half of the 20th century, the violin maker Pietro Sgarabotto (1903-1990), and mostly his father Gaetano (1878-1959), restored numerous historical string instruments. They substituted the heavily damaged parts (i.e., front and back plates, ribs or heads), conserving the original fragments as models for the imitation of the varnish appearance in the manufacturing of their modern instruments [Spotti, 1991]. In May 1961, Pietro Sgarabotto donated over 250 items, including plaster casts, cut-outs and parts of classical instruments, to the International Violin Making School of Cremona where they had been then removed from the classrooms and deposited in the school storerooms, possibly because considered outmoded [Zanrè, 2019].

After the death of Pietro, the son Paolo set about carefully preserving the whole set of surviving materials from the family workshop. He also placed in safe hands the items of greatest interest to violin making enthusiasts: Gian Carlo Guicciardi was entrusted with the tools, templates and moulds, a collection of photographs of instruments and musicians, as well as instrument parts realized by Gaetano and Pietro; Renato Scrollavezza received lots of photographs and documents concerning the foundation of the school in Parma at the end of the 1920s, as well as the personal notebooks of the two luthiers and an important text written in 1936 [Zanrè, 2019].

Much of Sgarabotto’s cultural heritage was thus intact and carefully preserved, but spread in several archives in different locations and not linked together.

The fragments under investigation are part of the Pietro Sgarabotto’s bequest to the violin making school of Cremona. They were taken from instruments attributed to luthiers working in the areas of Brescia, Piacenza and Tyrol. In particular, the set is composed of one fragment removed from a cello by Jacobus Stainer (F01, Fig. AII.15), two fragments detached from the backs and ribs of cellos by Gasparo Bertolotti “da Salò” (F13 and F16, Fig. AII.15), a fragment from a double bass by Giovanni Paolo Maggini (F20, Fig. AII.15) and a fragment from a double bass by Lorenzo Guadagnini (F21, Fig. AII.15) [Zanrè, 2019; Fiocco et al., 2017].

Figure AII.15 *VIS photos* of the fragments of bowed string musical instruments belonging to the “Collezione Sgarabotto”: F01 (J. Stainer), F13 and F16 (G. Bertolotti “da Salò”), F20 (G. P. Maggini) and F21 (L. Guadagnini). * Photos by Arvedi laboratory.*

References

Barabaschi A., A patron, a grand prince and a maker: the history of the “Stradivari Medici Quintet”, in: Zanrè A. (ed.), The 1690 “Tuscan” Stradivari violin in the Accademia di Santa Cecilia, Scrollavezza & Zanrè, Parma, 2017, 13–20.

Beare C., Capolavori di Antonio Stradivari, Arnoldo Mondadori Editore, Cremona, 1987.

Bini A., Stradivari’s “Tuscan” in the Musical Instruments Collection of the Accademia di Santa Cecilia in Rome, in: Zanrè A. (ed.), The 1690 “Tuscan” Stradivari violin in the Accademia di Santa Cecilia, Scrollavezza & Zanrè, Parma, 2017, 7–12.

Bracco D., Un violino del 1793: l’impegno di Fondazione Bracco per la musica, tra arte e scienza, in: La materia e il suono, Bracco e Cremona per la liuteria tra musica e scienza, Fondazione Museo del Violino Antonio Stradivari Cremona, Cremona, Cremona, 2018, 9–15.

Cacciatori F., Lo scrigno dei tesori, Fondazione Museo del Violino Antonio Stradivari, Cremona, 2014.

Cacciatori F., Lorenzo Storioni, cenni biografici, in: La materia e il suono, Bracco e Cremona per la liuteria tra musica e scienza, Fondazione Museo del Violino Antonio Stradivari Cremona, Cremona, Cremona, 2018a, 73–95.

Cacciatori F., Il piccolo violino Lorenzo Storioni, stato di conservazione, in: La materia e il suono, Bracco e Cremona per la liuteria tra musica e scienza, Fondazione Museo del Violino Antonio Stradivari Cremona, Cremona, Cremona, 2018b, 119–125.

Fiocco G., Rovetta T., Gulmini M., Piccirillo A., Licchelli M., Malagodi M., Spectroscopic analysis to characterize finishing treatments of ancient bowed string instruments. *Applied Spectroscopy*. 71 (2017) 2477–2487. doi:10.1177/0003702817715622.

Giordano A., The 1690 “Tuscan” in the Accademia di Santa Cecilia: analysis of the instrument, in: Zanrè A. (ed.), The 1690 “Tuscan” Stradivari violin in the Accademia di Santa Cecilia, Scrollavezza & Zanrè, Parma, 2017, 49–58.

Henley W., Antonio Stradivari master luthier Cremona Italy 1644-1737 and his instruments, Amati Publishing, Brighton, 1961.

Invernizzi C., Daveri A., Rovetta T., Vagnini M., Licchelli M., Cacciatori F., et al., A multi-analytical non-invasive approach to violin materials: The case of Antonio Stradivari “Hellier” (1679), *Microchemical Journal*. 124 (2016) 743–750. doi:10.1016/j.microc.2015.10.016.

Rossi F.R., Chiesa C., Carlson B., Cacciatori F., Il DNA degli Amati, una dinastia di liutai a Cremona, Consorzio Liutai Antonio Stradivari Cremona, Cremona, 2006.

Spotti G., Gaetano e Pietro Sgarabotto. Liutai-Violin Makers (1878-1990), Turris, Cremona, 1991.

Trabucchi S., Toto F., Pistoni P., Ive M., 1715-2015 Stradivari incontra i liutai di Cremona, in: Cacciatori F., Malagodi M., Sarti A. (eds.), Il Cremonese1715 - 300° anniversario, Fondazione Museo del Violino Antonio Stradivari Cremona, Cremona, 2015, 67–81.

Villa V., Cacciatori F., Sturm G., Whiteley J., Bordas Ibanez C., Heyligers M.A., et al., Antonio Stradivari, L'estetica sublime, Consorzio Liutai Antonio Stradivari Cremona, Cremona, 2011.

Zanrè A., I segreti di Sgarabotto, Scrollavezza & Zanrè, Parma, 2019.

[Web]

http://www.tarisio.com/

http://www.museodelviolino.org/

APPENDIX III

Multivariate methodological approach to manage complex synchrotron radiation FTIR micro-spectra

In this appendix, we describe the complete multivariate methodological approach employed to manage and interpret the large IR data set acquired by SR-FTIR microspectroscopy in reflection geometry at the SISSI beamline (Chemical and Life Science branch) of the Elettra synchrotron laboratory (CERIC-ERIC project proposal No. 20182129, acronym: VIRTUOSI). The procedure is in the process of being published in the journal Acta Imeko [Fiocco et al., In Press].

When a hundred of complex spectra are collected from cross-sections, a huge effort is required to achieve a reliable and rigorous preliminary picture of the information contained in the entire data set. In order to support the data processing, also in view of extending the SR-FTIR microspectroscopy analyses to a wider set of samples, and to gather as much information as possible from the spectra, we therefore decided to explore the data from a multivariate point of view by chemometric tools. In particular, PCA allowed us to understand the relationship among all the variables and to highlight object patterns according to the weight of the variable in a new reduced space defined by the PC components [Wold et al., 1987; Bro et al., 2014].

The 97 reflection SR-FTIR spectra considered in this study were acquired at the SISSI beamline, both as single points and as linear maps, and derive from six micrometric samples collected from four different bowed string musical instruments and then mounted in cross-section (Table AIII.1). The VIRTUOSI project, in fact, involved a larger set of samples than that one investigated in 3.1. Four samples of the set in exam (i.e., AS_1690, LS_1790, LS_1793a and LS_1793b) are properly the object of the study reported in 3.1, while the additional samples FR_c and LS_sv1 respectively come from a cello made by Francesco Rugeri “il Per” in the 17th century and the *Bracco* 1793 small violin by Lorenzo Storioni. In particular, it is worth noting that both LS_sv1 and LS_1793b were detached from the soundboard of the *Bracco* violin, but in different positions one from another. History and photos of the instruments are reported in appendix II, except for the small violin 1790 by Lorenzo Storioni and the cello by F. Rugeri “il Per”, whose documentation is missing.

Detailed information about the analytical instrumentation and the acquisition parameters is reported in appendix I.

Table AIII.1 *List of the instruments investigated in this study with name and life period of the violin maker, name of the instrument with year of construction, type and part investigated, and the inventory number of the cross-sectional samples. Table modified from [Fiocco et al., In Press].*

Violin Maker	Instrument name	Year of construction	Instrument	Part	Inv. N°
L. Storioni (1744-1816)	-	1790	Small violin	Rib	LS_1790
	Bracco	1793	Small violin	Back plate Front plate Front plate	LS_1793a LS_1793b LS_sv1
A. Stradivari (1644-1737)	*Toscano*	1690	Violin	Front plate	AS_1690
F. Rugeri "il Per" (1630-1698)	-	17th century	Cello	Back plate	FR_c

Firstly, we applied the KK transformations to the entire spectral range - extending from 4000 to 750 cm^{-1} - using the OPUS 7.5 software package. The study focused on the organic materials composing the layering of the cross-sections. KKT, in fact, correctly works in the spectra of most organic molecules [Invernizzi et al., 2018], where the maximum absorption index (k) of bands rarely exceeds 0.3 above ca. 1000 cm^{-1} [Griffiths and De Haseth, 2006]. The spectral range was then reduced to 3500-1000 cm^{-1} in order to minimize the influence of the non-diagnostic features, like the signal noise and the baseline variations, and thus retrieving the highest information from the spectra.

In Table AIII.2, we summarized the reflection IR bands - falling in the considered spectral range - of the organic materials most commonly documented in the coating system of historical bowed string instruments by literature. In the region 3500 to 3000 cm^{-1} we generally find the bands produced by OH and NH stretching vibrations, respectively around 3500 and 3300 cm^{-1}. The first overtone of the amide II band, instead, falls at 3080 cm^{-1} [Invernizzi et al., 2016; Invernizzi et al., 2017]. The CH stretching vibrations around 2900 and 2800 cm^{-1} are characteristic of numerous organic materials used to finish wood surfaces, like siccative oils, natural resins or proteins [Invernizzi et al., 2018, Fu et al., 1994], as well as of the wood itself [Poli et al., 2011]. Moving towards lower wavenumbers, the C=O stretching band of ester (e.g., from oils) and acid (e.g., from resins) groups occurs from approximately 1740 to about 1690 cm^{-1} [Invernizzi et al., 2016; Invernizzi et al., 2017], whereas that one of the proteinaceous compounds (e.g., animal glue, or casein) is present near 1650 cm^{-1}. The so called amide II band of proteins is centred at around 1550 cm^{-1}, while the wood vibrations due to the stretching of aromatic rings and the bending of OH groups occur between 1650 and 1500 cm^{-1}. The bands falling in the fingerprint region (below 1500 cm^{-1}), related to the organic materials above mentioned, are reported in Table AIII.2. Moreover, signals of the epoxy resin were expected in the spectra acquired near the upper and lower boundaries of the embedded sample. Its presence is clearly singled out by the bands at 1610 cm^{-1} (νC=C, aromatic ring), 1510 cm^{-1} (vC-C, aromatic ring) and between 1250 and 1000 cm^{-1} [Smith et al., 1984; González et al., 2012; Panda et al., 2016].

Table AIII.2 *Wavenumber values between 3500 and 1000 cm^{-1} taken from literature, together with their assignment, of the FTIR reflection bands produced by the organic materials most commonly documented in the coating system of historical bowed string instruments and identified in the cross-sectional samples under study. For derivative bands, the value refers to the maximum of the band after the application of KK-transformations. Table modified from [Fiocco et al., In Press].*

Material	Wavenumber (cm^{-1})	Band shape	Assignment
Oil-resin varnish* [Invernizzi et al., 2016; Invernizzi et al., 2017]	2950, 2870	Derivative	$v_{as}CH_3$, v_sCH_3
	2930, 2850	Derivative	$v_{as}CH_2$, v_sCH_2
	1720-10	Derivative	vC=O
	1465-55	Derivative	δ_sCH_2, $\delta_{as}CH_3$
	1380	Derivative	δ_sCH_3
	1250, 1170, 1100	Derivative	vCO
Proteins [Invernizzi et al., 2018; Fu et al, 1994]	3330	Derivative	$v_{as}NH$
	3080	Derivative	Overtone of amide II
	2960, 2875	Derivative	$v_{as}CH_3$, v_sCH_3
	2935, 2850	Derivative	$v_{as}CH_2$, v_sCH_2
	1650	Derivative	vC=O (amide I)
	1550	Derivative	δNH + vCN (amide II)
	1450, 1400	Derivative	δCH
	1350-1200	Derivative	δNH + vCN, δCH, δNH (amide III)
	1200-1000	Derivative	CO
Wood** [Poli et al., 2011; Invernizzi et al., 2017]	3450	Absorption	vOH
	2940, 2840	Absorption	$v_{as}CH_2$, v_sCH_2
	2900	Absorption	$v_{as}CH_3$
	1735	Absorption	vC=O
	1650	Absorption	δOH
	1598, 1505	Absorption	v (aromatic ring)
	1465, 1430, 1380	Absorption	δCH_2
	1330	Absorption	δOH
	1280-1240	Absorption	Guaiacyl ring vib., syringyl ring vib.
	1157	Derivative	$V_{as}COC$
	1115	Derivative	V_{as} (glucose ring)
	1060	Derivative	$V_{as}CO$
	1035	Derivative	V_sCO
	900	Absorption	V_s (glucose ring)
Epoxy resin [González et al., 2012; Smith et al., 1984; Panda, 2019]	2960-2850	Derivative	vCH (aromatic and aliphatic)
	1610	Derivative	vC=C (aromatic ring)
	1510	Derivative	vC-C (aromatic ring)
	1250	Derivative	vCOC (oxirane group)
	1180	Derivative	Phenyl vib.
	1035	Derivative	vCOC (ether)

** Siccative oil and natural terpenic resins; ** Non-treated wood.*

Subsequently, we divided the selected spectral range into six regions: 3500-3000 cm^{-1}, 3000-2700 cm^{-1}, 1800-1550 cm^{-1},1550-1450 cm^{-1}, 1460-1260 cm^{-1}, and 1250-1000 cm^{-1}. The preliminary PCA data exploration was carried out on 63 spectra of the IR data set, selecting those collected in linear map mode (traverse) on the Rugeri and Storioni samples. The data matrices are composed of 63 rows (i.e., the spectra selected) and of a number of columns that varies from time to time on the basis of each spectral range investigated (i.e., the spectral variables considered). Each object, representing each single spectrum, was classified and coloured according to the position of the analytical spot in the stratigraphy: epoxy resin (E), varnish (V), ground coat (G), and wood (W). In this way, their assignment mainly indicates the distribution of the organic compounds within the cross-sections. It is important to note that the entire IR data set is composed of two types of spectra: on one hand, the spectra containing signals produced by a single organic material and, on the other, those ones carrying signals produced by multiple materials. In the last case, the "mixed" profiles originate from the position of the acquisition area that fell at the interface between two adjacent layers characterized by different chemical composition, and they are labelled as Mix 1 (varnish + epoxy resin), Mix 2 (varnish + ground coat) and Mix 3 (wood + ground coat). The following spectral pre-treatments were applied to the selected KKT spectra: smoothing (Savitzky-Golay, 11 wavelengths gap size), first derivative (Savitzky-Golay, 11 wavelengths gap size and 2nd order polynomial) and mean centring.

In Figs. AIII.1-6, we reported the results obtained by PCA model computation in the six selected spectral ranges (i.e., a PCA model for each spectral range).

The PC1 vs PC2 score plot of Fig. AIII.1, referred to the region 3500-3000 cm^{-1}, accounts for ca. 86% of the total variance. From the graph, we can see that the data exploration in this spectral region did not lead to a clear separation of the objects according to single organic materials.

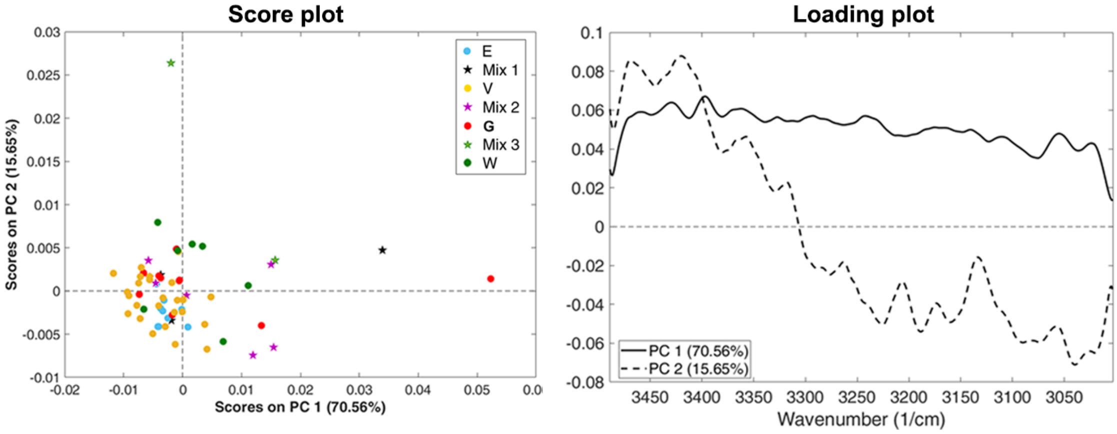

Figure AIII.1 *PCA results obtained in the spectral region between 3500 and 3000 cm^{-1}: scatter score plot (left) and loading plot (right) of PC1 and PC2. Figure in [Fiocco et al., In Press].*

In the PC1 vs PC2 score plot of Fig. AIII.2, related to the range between 3000 and 2700 cm^{-1} and accounting for ca. 85% of the total variance, the objects are variously scattered in the four quadrants. Nonetheless, we can notice that the spectra labelled as W cluster in the fourth quadrant.

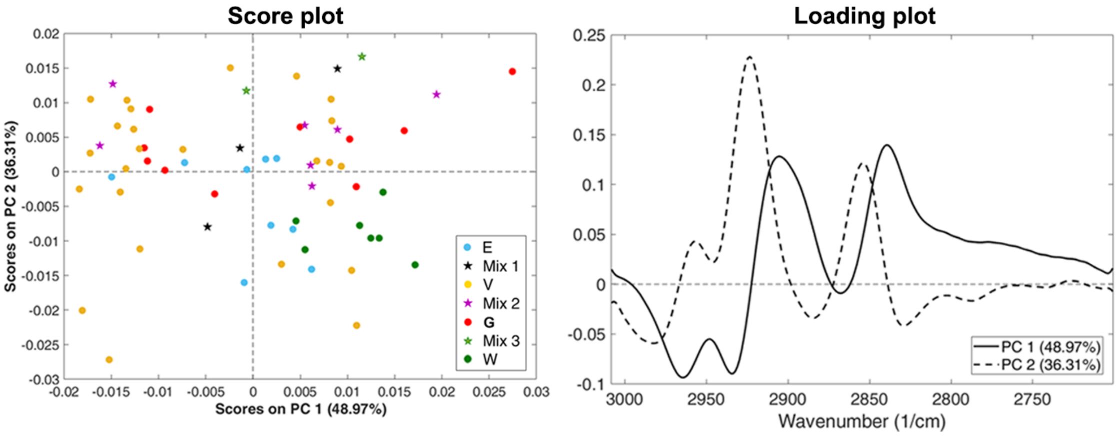

Figure AIII.2 *PCA results obtained in the spectral region between 3000 and 2700 cm^{-1}: scatter score plot (left) and loading plot (right) of PC1 and PC2. Figure in [Fiocco et al., In Press].*

Observing the PC1 vs PC2 score plot in the range 1800-1550 cm^{-1} (Fig. AIII.3), which accounts for ca. 74% of the total variance, it appeared the most promising for the object discrimination. Spectra labelled as E are well grouped in the first quadrant, partially overlapping the objects W, while those identified as V fall in the negative PC1 portion of the plot. Coherently, intermediate scores characterize the spectra corresponding to Mix 1, which were collected at the interface between the two adjacent layers V and E. As for the objects labelled as G, they are heterogeneously scattered in the plot. A further consideration concerns the spectra recorded at the interface between V and G, identified as Mix 2, which assumed negative PC2 scores: some of these objects, in fact, are close to the cluster V and this suggests a higher contribution of the varnish signals in the corresponding IR spectra. The corresponding loadings explain the object distribution in the score plot: the negative signals between 1750 and 1700 cm^{-1} characterize the PC1 and PC2 values of the cluster V and - partially - of the objects identified as Mix 1, while the positive signals between 1700 and 1600 cm^{-1} in the PC1 and PC2 loading plot characterize the spectra labelled as E and W.

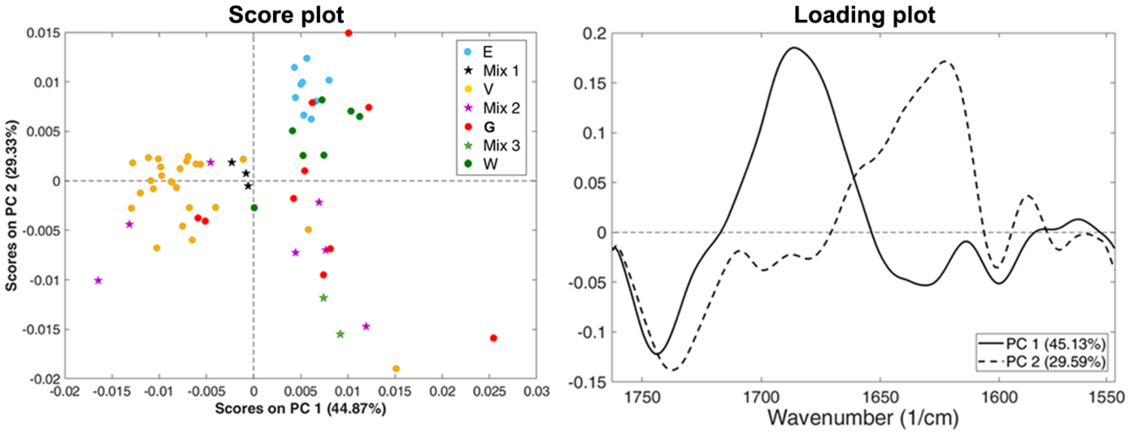

Figure AIII.3 *PCA results obtained in the spectral region between 1800 and 1550 cm^{-1}: scatter score plot (left) and loading plot (right) of PC1 and PC2. Figure in [Fiocco et al., In Press].*

The PC1 vs PC2 score plot of Fig. AIII.4, related to the region 1550-1450 cm^{-1}, accounts for ca. 89% of the total variance. Also in this PCA model, PC1 values discriminate the objects V from the objects E, even if the latter ones do not form a compact group but are heterogeneously distributed in the first and fourth quadrants. In particular, the PC1 values of the objects E are much more positive and higher than those referred to all the other materials. This behaviour is ascribed to the intense and sharp band of the epoxy resin centred at 1510 cm^{-1} (νC-C, aromatic ring), confirmed by the strong signals in the region around 1500 cm^{-1} for both PC1 and PC2 loadings. As for the spectra corresponding to W, they fall around the axes origin. On the contrary, all the mixtures do not show a definite distribution.

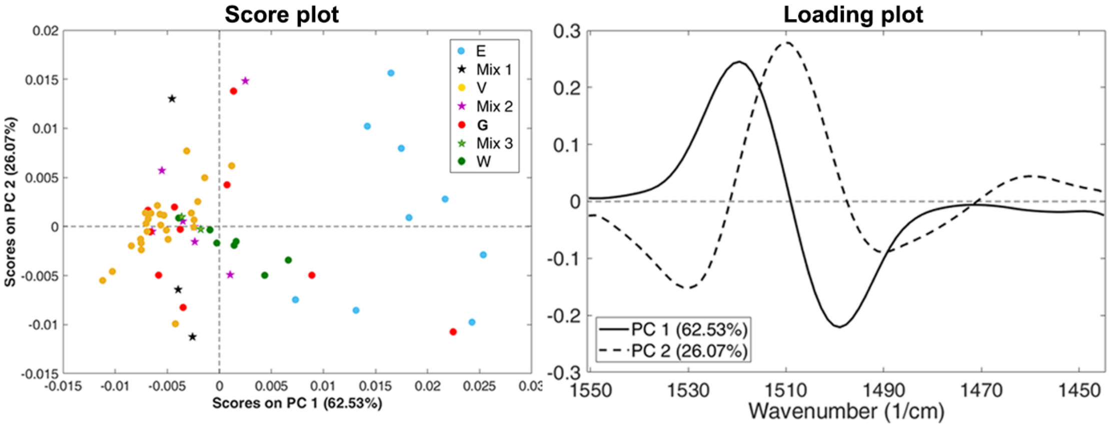

Figure AIII.4 *PCA results obtained in the spectral region between 1550 and 1450 cm^{-1}: scatter score plot (left) and loading plot (right) of PC1 and PC2. Figure in [Fiocco et al., In Press].*

In the PC1 vs PC2 score plot of Fig. AIII.5, referred to the range between 1460-1260 cm^{-1} and accounting for ca. 45% of the total variance, the picture looked rather confused.

As visible in the graph, in fact, the objects do not form separate clusters, except for those labelled as E which mostly fall in the second quadrant.

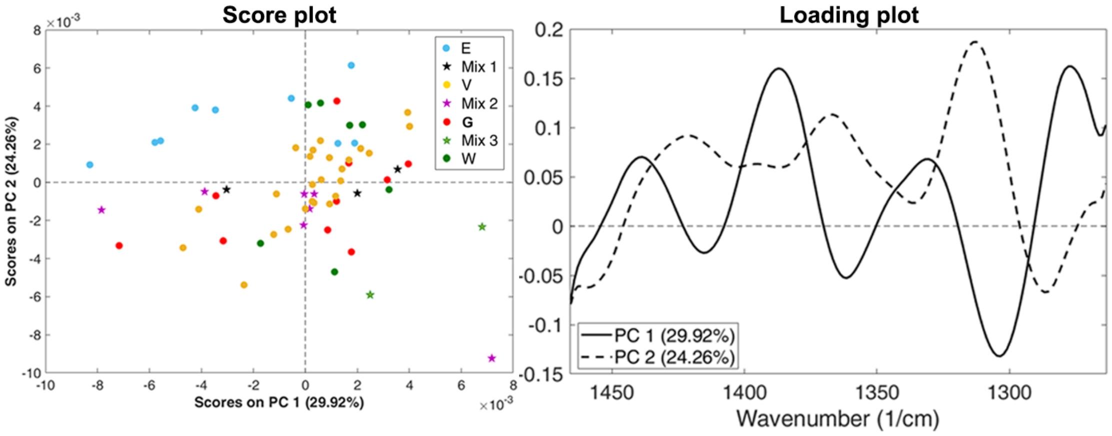

Figure AIII.5 *PCA results obtained in the spectral region between 1460 and 1260 cm^{-1}: scatter score plot (left) and loading plot (right) of PC1 and PC2. Figure in [Fiocco et al., In Press].*

The last examined model was that one computed for the range 1250 and 1000 cm^{-1}. From the PC1 vs PC2 score plot (ca. 63% of the total variance) of Fig. AIII.6, we can see a partial separation of the spectra according to the position of the analytical spot in the stratigraphy: most of the objects V, W and E are respectively distributed in the second, third and fourth quadrants.

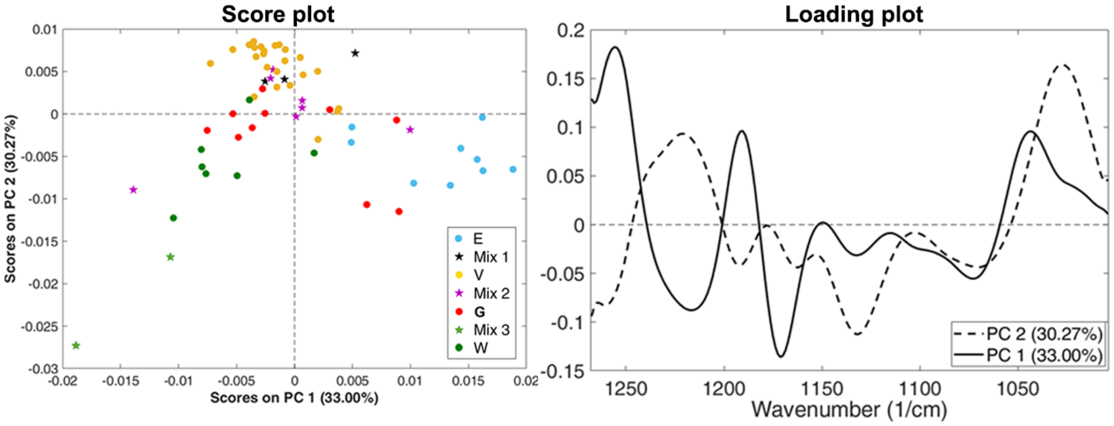

Figure AIII.6 *PCA results obtained in the spectral region between 1250 and 1000 cm^{-1}: scatter score plot (left) and loading plot (right) of PC1 and PC2. Figure in [Fiocco et al., In Press].*

After a detailed examination of the object distribution in all the six different spectral regions, we considered the ranges 1800-1550 cm^{-1} and 1550-1450 cm^{-1} as the most informative and promising to discriminate layers with referring to one single organic material and showing significant marker bands. Instead, a clear trend was not always shown for the spectra collected at the interface between adjacent layers with different composition.

In view of this assessment, we calculated a further PCA on the whole data set (97 spectra) considering the merged range 1800-1400 cm^{-1} and grouping all the “mixed” profiles in a separate class, labelled as U (undefined).

From the PC1 vs PC2 score plot of Fig. AIII.7a (ca. 54% of the total variance), we can see that the objects identified as varnish (V) are mostly clustered in the third quadrant, resulting from negative PC1 and PC2 scores. In the fourth quadrant, characterized by positive PC1 combined with negative PC2 values, we find most of the objects corresponding to epoxy resin (E). As for the spectra associated to the ground coat (G), instead, they do not form a well definite cluster in the PC1 vs PC2 score plot but we can notice that all these objects have positive PC2 scores and most of them are well separated from the other objects. Finally, the spectra identified as wood (W) are distributed around the origin of PC1 and PC2 axes, quite close to the objects U.

The third PC, accounting for ca. 11% of the total variance, was also investigated. Interpreting the PC1 vs PC3 score plot of Fig. AIII.7b, the groups previously identified can be confirmed. However, some of them are more scattered or form sub-groups.

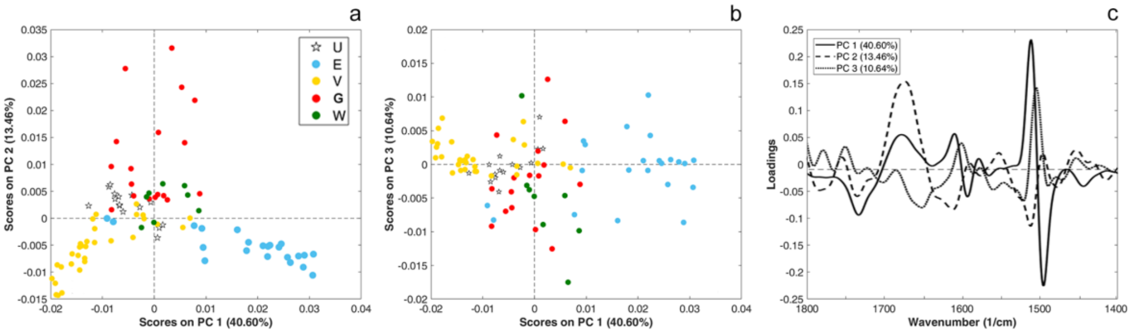

Figure AIII.7 *PCA results obtained in the region between 1800 and 1400 cm^{-1}: PC1 vs PC2 score plot (a); PC1 vs PC3 score plot (b); PC1, PC2 and PC3 loading plot (c). E = epoxy resin, V = varnish, G = ground coat; W = wood; U = undefined. Figure in [Fiocco et al., In Press].*

The grouping of the spectra in the score plots, according to the different materials, is mostly affected by the marker bands of the varnish (at around 1720-10 cm^{-1}, Table AII.2), the proteinaceous ground (at around 1650 cm^{-1}, Table AII.2) and the epoxy resin (at 1510 cm^{-1}, Table AII.2). In correspondence of these spectral regions, in fact, the loadings of the PCs show stronger signals (Fig. AIII.7c): PC1 well discriminates varnish (V) from epoxy (E) spectra thanks to the signals around 1700 and 1500 cm^{-1}, whereas PC2 allows for the discrimination of the spectra related to the ground (G) mostly thanks to the amide I band around 1650 cm^{-1}. It is worth highlighting that the spectra were transformed by the first derivative; as a consequence, the maximum value of the peaks before transformation is lost, but it corresponds to the inflection point of the loading profiles. Since the loadings can assume values from -1 to +1, variables approaching extreme values in Fig. AIII.7c are those ones more influencing the PCs and, thus, they are responsible for spectra distribution in the score plots (Fig. AIII.7a,b).

References

Bro R., Smilde A.K., Principal component analysis, *Analytical Methods*. 6 (2014) 2812–2831. doi:10.1039/c3ay41907j.

Fiocco G., Grassi S., Invernizzi C., Rovetta T., Albano M., Davit P., et al., Chemometric tools to investigate complex Synchrotron radiation FTIR micro-spectra: focus on historical bowed musical instruments, *Acta Imeko*. In Press.

Fu F.-N., Deoliveira D.B., Trumble W.R., Sarkar H.K., Singh B.R., Secondary Structure Estimation of Proteins Using the Amide III Region of Fourier Transform Infrared Spectroscopy: Application to Analyze Calcium-Binding-Induced Structural Changes in Calsequestrin, *Applied Spectroscopy*. 48 (1994) 1432–1441. doi:10.1366/0003702944028065.

González M.G., Cabanelas J.C., Baselga J., Applications of FTIR on Epoxy Resins - Identification, Monitoring the Curing Process, Phase Separation and Water Uptake, in: Infrared Spectroscopy - Materials Science, Engineering and Technology, T. Theophile, IntechOpen, London, 2012.

Griffiths P. R. and De Haseth J. A., Fourier Transform Infrared Spectrometry: Second Edition, John Wiley & Sons, 2006.

Invernizzi C., Daveri A., Rovetta T., Vagnini M., Licchelli M., Cacciatori F., et al., A multi-analytical non-invasive approach to violin materials: The case of Antonio Stradivari “Hellier” (1679), *Microchemical Journal*. 124 (2016) 743–750. doi:10.1016/j.microc.2015.10.016.

Invernizzi C., Daveri A., Vagnini M., Malagodi M., Non-invasive identification of organic materials in historical stringed musical instruments by reflection infrared spectroscopy: a methodological approach, *Analytical and Bioanalytical Chemistry*. 409 (2017) 3281–3288. doi:10.1007/s00216-017-0296-8.

Invernizzi C., Rovetta T., Licchelli M., Malagodi M., Mid and Near-Infrared Reflection Spectral Database of Natural Organic Materials in the Cultural Heritage Field, *International Journal of Analytical Chemistry*. 2018 (2018) 1–16. doi:10.1155/2018/7823248.

Panda H., Epoxy Resins Technology Handbook (Manufacturing Process, Synthesis, Epoxy Resin Adhesives and Epoxy Coatings), NIIR, 2016.

Poli T., Chiantore O., Nervo M., Piccirillo A., Mid-IR fiber-optic reflectance spectroscopy for identifying the finish on wooden furniture, *Analytical and Bioanalytical Chemistry*. 400 (2011) 1161–1171. doi:10.1007/s00216-011-4834-5.

Smith R.E., Larsen F.N., Long C.L., Epoxy resin cure. II. FTIR analysis, *Journal of Applied Polymer Science*. 29 (1984) 3713–3726. doi:10.1002/app.1984.070291207.

Wold S., Esbensen K., Geladi P., Principal component analysis, *Chemometrics and Intelligent Laboratory Systems*. 2 (1987) 37–52. doi:10.1016/0169-7439(87)80084-9.

APPENDIX IV

The *Toscano* 1690 violin by Antonio Stradivari: wood finish and decorations

This appendix presents the non- and micro-invasive study performed on the Antonio Stradivari 1690 *Toscano* violin thanks to the collaboration with the Arvedi Laboratory of Non-Invasive Diagnostics, the Accademia of Santa Cecilia, Andrea Zanrè and Elisa Scrollavezza. The results have been published in a chapter of the monographic volume entirely devoted to this precious instrument [Fiocco et al., 2017].

Firstly, non-invasive analyses were accomplished by reflection FTIR and XRF spectroscopies, mostly focusing on the back plate of the violin. The analytical spots were selected after a detailed examination of the UVIFL photos (Fig. AIV.1). Then, two micro-samples respectively taken from the front plate (under the tailpiece, Fig. AIV.2a) and the centre bass rib (near the upper corner, Fig. AIV.2b) were investigated by optical microscopy - equipped with visible and UV lights - and SEM-EDX. For this stratigraphic study, the samples were previously embedded into epoxy resin (Epofix Struers and Epofix Hardener 15:2, w:w), cross-sectional and finally dry-polished with silicon carbide fine sandpapers (800-1200 mesh). Detailed information about the analytical instrumentation and the acquisition parameters is reported in appendix I.

By combining the different analytical techniques, we provided additional information to that presented in 3.1 about the composition of the finishing layers as well as the purfling strips and the black decorations used by Stradivari to highlight the scroll chamfer. As for the history and the photos of the violin, they are reported in detail in appendix II.

Figure AIV.1 *UVIFL photos* of the Toscano violin, with the analytical spots investigated by non-invasive XRF (red square) and reflection FTIR (green square) techniques. *Photos by J. Röhrmann.*

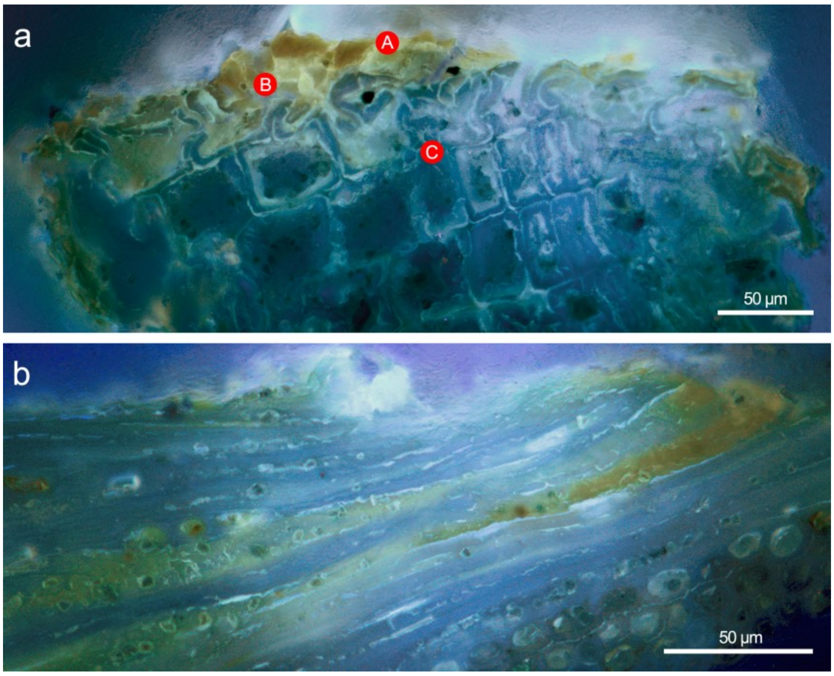

Figure AIV.2 *UV-light optical microscopy images of the two cross-sectional samples taken respectively from the front plate (a) and the centre bass rib (b) of the Toscano violin. Layers indicated as A, B and C are described in the text. Figure published in [Fiocco et al., 2017].*

I. Wood finish

As outlined in 3.1, the varnish system is composed of two oil-terpenic resin layers: the layer A, on the top, with a salmon-fluorescent UV colour, and the yellow-whitish fluorescent layer B on the bottom (Figs. AIV.2a and AIV.3).

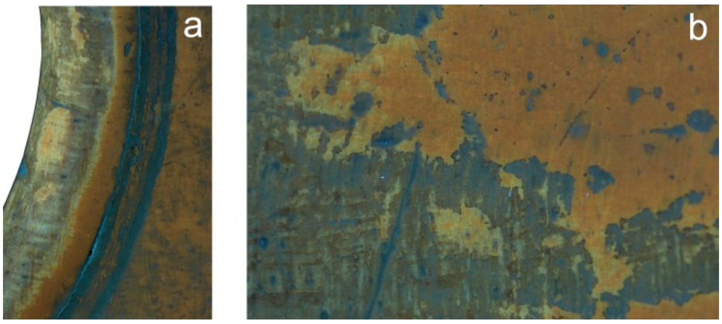

Figure AIV.3 *UVIFL photos* taken in correspondence of the edge (a) and the centre (b) areas of the Toscano back plate. The two differently-coloured varnish layers are clearly evident in these areas characterized by a gradual varnish consumption, as well as the brown colour of the surface appears where the wood is exposed. *Photos by J. Röhrmann.*

The upper layer A was found to contain rare crystals with dimension of diameter lower than 1 µm, as shown in the SEM image of Fig. AIV.4a,b. The detection, by EDX microanalysis, of only calcium in correspondence of these particles (Fig. AIV.4c) as well the presence of characteristic infrared bands (vC=O at 1620 cm^{-1}, vC-O at 1314 cm^{-1} and H_2O libration at 664 cm^{-1}) in the reflection spectra non-invasively collected on the best preserved varnish areas (Fig. AIV.4d), allowed us to identify the crystals as calcium oxalates. This finding would confirm the age of the varnish, since the oxalates can be the result of century-long chemical degradation processes of lipidic materials [Colombini et al., 2000]. No evidence of other inorganic compounds, such as pigments, was found. Therefore, the presence of inorganic particulate matter in this layer seemed not to be related to the varnishing phase, but rather to a process of degradation of the film itself. However, this consideration must take into consideration the small quantity of the analysed samples, and thus their incomplete representation of the violin stratigraphy as a whole.

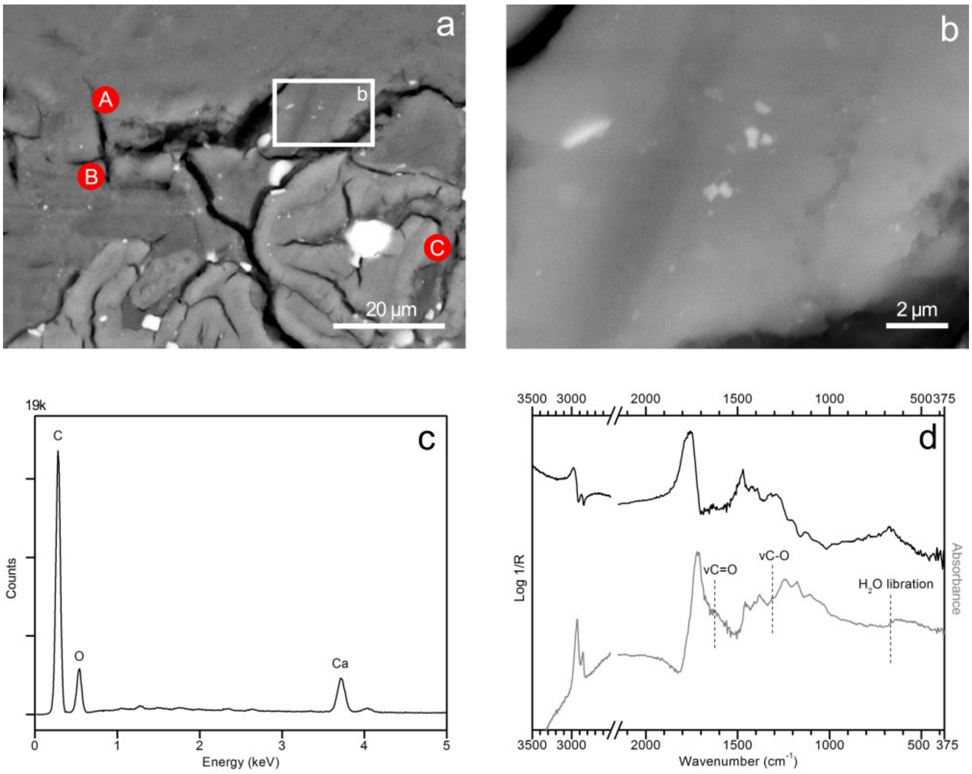

Figure AIV.4 *SEM-BSE image of the cross-sectional sample collected on the front plate, with the white rectangle area highlighting calcium oxalate submicrometric particles (a). The SEM-BSE image at higher magnification taken in correspondence of the rectangle area indicated in (a) is shown in (b), and the EDX spectrum of Ca-oxalate particles, with the Kα emissions of the elements highlighted, is shown in (c). Reflection FTIR spectrum of the varnish before (black line) and after (grey line) the application of KK-transformations, with the dotted lines highlighting vibrational bands attributed to the oxalate mineral group (d). Letters indicated as A, B and C in the SEM-BSE image (a) refer to the layers described in the text. Figure published in [Fiocco et al., 2017].*

In the lower varnish layer B, we found an aluminium- and oxygen-rich grain (Fig. AIV.5) which opened up the possibility of different attributions, including that of alumina (Al_2O_3) as a substrate for lake pigments [Echard et al., 2010].

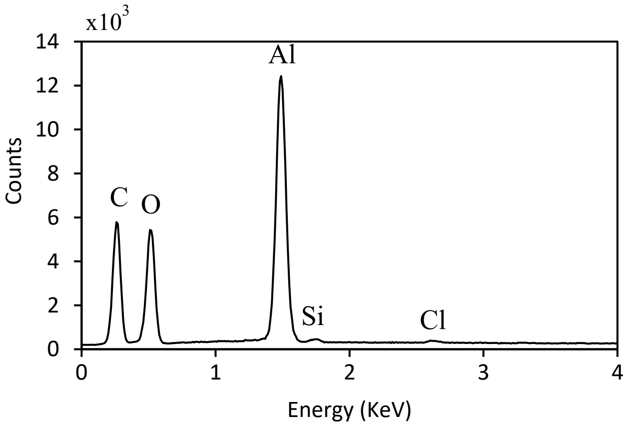

Figure AIV.5 *EDX spectrum of a particle detected in the layer B, with the Kα emissions of the elements highlighted.*

At the interface between layer B and wood C, the presence of a proteinaceous binder is uncertain (see 3.1). As for the inorganic phases, both the intense ν_{as}Si-O-Si *Reststrahlen* bands in the reflection FTIR spectra acquired on the most worn varnish areas (see 3.1) and the high Si-Kα - sometimes together with Al-Kα - emissions recorded by SEM-EDX in numerous particles (Fig. AIV.6a-c and see 3.1) enabled us to claim that silicate and aluminosilicate minerals are present at this level. This result, combined with the detection of Ti-, Fe- and Mn-rich grains (Fig. AIV.6d), would suggest the presence of iron-rich earth pigments, like red-ochre or umber earth [Eastaugh, 2013]. The extinction of the UV fluorescence, observed in the cross-sectional sample of Fig. AIV.7, was a further diagnostic peculiarity for the characterisation of this class of red inorganic pigments. In this respect, also the fluorescence behaviour highlighted in the UVIFL photos by Brandmair [Brandmair, 2017] is typical of these pigments. Moreover, XRF analyses performed on the most worn varnish areas of the violin revealed higher signals of Si, Ti, Mn and Fe than those collected on the best conserved ones (Fig. AIV.8), supporting the hypothesis that the pigmented particles - partly responsible for the colouration of Stradivari's finishing - might be located at the interface between the wood and the overlying varnish. This may also account for the relatively moderate difference in colour observed under visible light between areas where the varnish coating is largely intact and areas where the varnish is missing.

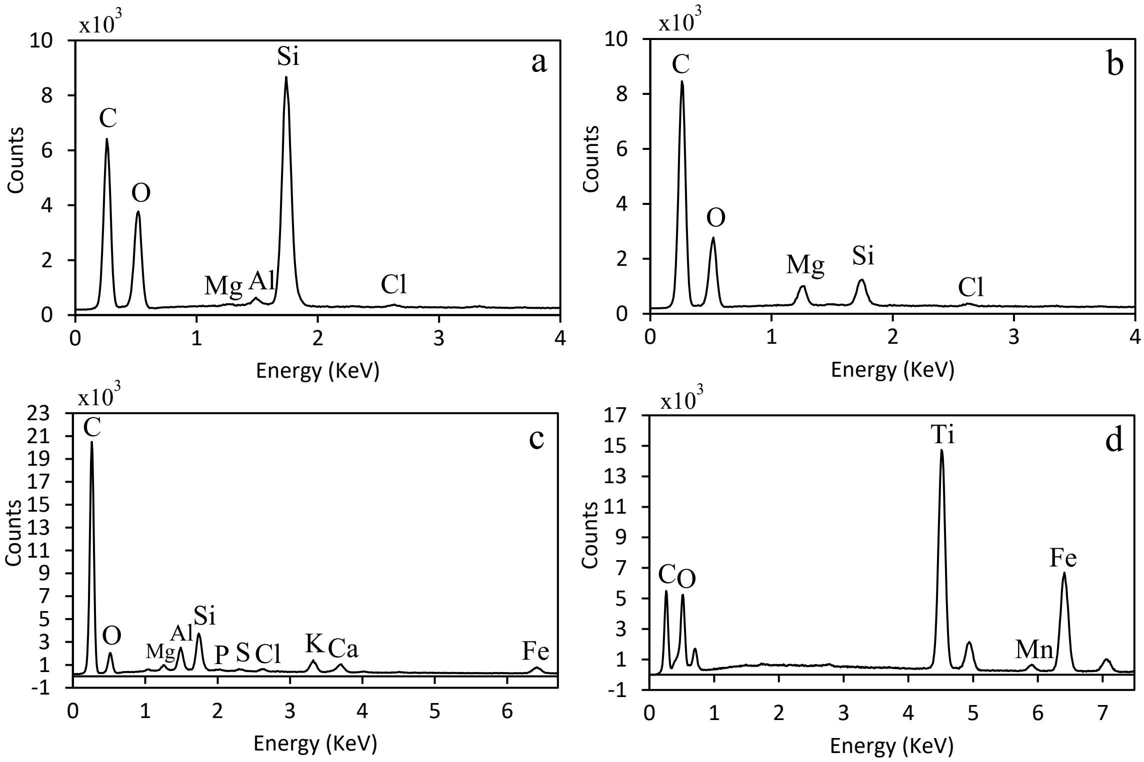

Figure AIV.6 *EDX spectra of some particles detected at the interface between the varnish layer B and the wood, with the Kα emissions of the elements highlighted. Letters a-d refer to the different particles described in the text.*

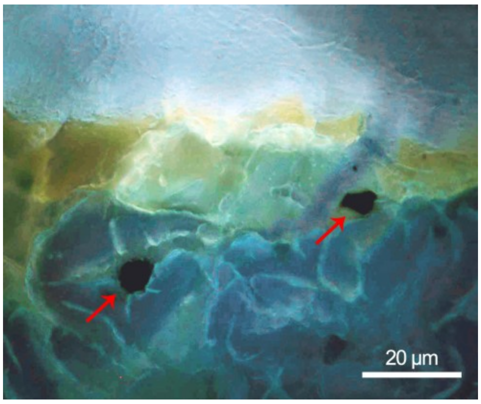

Figure AIV.7 *UV-light optical microscopy magnification of the front plate stratigraphy. Arrows indicate two particles of iron-based pigments, probably red-ochre or umber earth. Figure published in [Fiocco et al., 2017].*

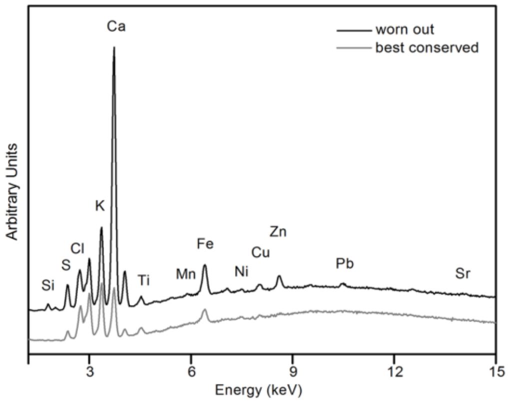

Figure AIV.8 *XRF spectra representative of best conserved (grey line) and most worn (black line) varnish areas, with the Kα emissions of the elements highlighted. Figure published in [Fiocco et al., 2017].*

XRF signals of Zn, likely due to sweat, were also detected in correspondence of the worn areas where the musician came in contact with the violin (Fig. AIV.8).

In correspondence of the wood substrate, EDX analyses highlighted small amounts of Cl, S, K and Ca. In previous studies [Brandmair and Greiner, 2010], these elements have been associated to a staining method. However, from our analyses it was not possible to relate them to a specific pre-treatment of the wood.

Finally, the low concentrations of Ni, Cu and, in few cases, Pb, Sr and Ag may be attributed to many different pollutants of the materials discussed above.

II. Purflings and black decorations

XRF analysis performed on the black purfling strips and the black decorations of the scroll chamfers highlighted high amounts of Fe, Cu and Zn. These elements are likely involved in the staining procedures, where the metal complexes of the most commonly used black dyestuffs (i.e., iron-gall and iron-hematein complexes) were obtained by the reaction of natural organic materials with a polyphenolic structure, extracted from plants or trees, and metal ions - like iron and copper - deriving, for example, from the mixture of ferrous and/or copper sulphates (the so called “vitriolo”) [Canevari et al., 2016].

Generally, the ratios between the area counts of these elements vary according to the composition of the raw materials and the procedures employed to mix them. In any event, it can be supposed that purfling batches realized in the same period, and thus likely stained using the same compounds and methods, should be characterized by the same elemental ratios. This feature was found for the black purfling strips of the front and back plates, which are characterized by the same ratios (Fig. AIV.9). Instead, the ratios of area counts in correspondence of the purfling insert at the end button (Fig. AIV.1) resulted to be different from those of the plates due to the higher amounts of Zn (Fig. AIV.9). This finding would confirm the attribution of the purfling at the joint of the lower rib to subsequent restoration work [Brandmair, 2017; Hopfner, 2017].

As for the black ink decoration on the scroll chamfer (Fig. AIV.1), which was introduced by Stradivari shortly before making the Quintet, it is characterized by a different chemical composition (Fig. AIV.9): its ratio values, in particular, appeared to be more compatible with subsequent staining methods (see the columns referred to the *Messia* 1716 by Stradivari). However, this correspondence cannot be considered conclusive.

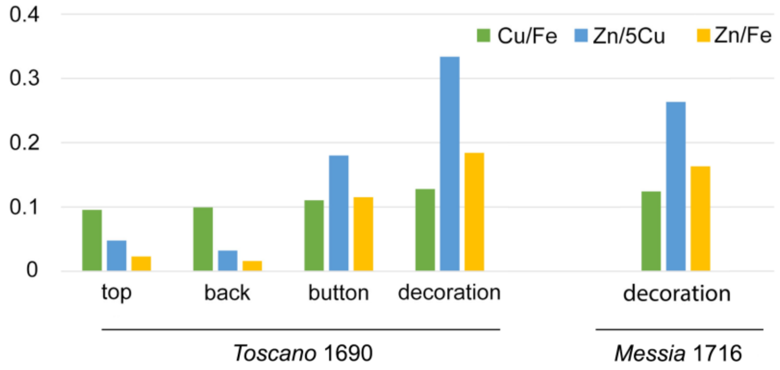

Figure AIV.9 *Ratios between XRF area counts of some elements, such as Fe, Cu and Zn, related to the Stradivari Toscano and Messia violins. Figure published in [Fiocco et al., 2017].*

References

Brandmair B., Greiner S.-P., Stradivari Varnish, Eigenverlag, London and Munich, 2010.

Brandmair B., Stratigraphic varnish analysis of the “Tuscan” Stradivari violin in the Accademia of Santa Cecilia, in: Zanrè A. (Ed.), The 1690 “Tuscan” Stradivari violin in the Accademia di Santa Cecilia, Scrollavezza & Zanrè, Parma, 2017, 46–51.

Canevari C., Delorenzi M., Invernizzi C., Licchelli M., Malagodi M., Rovetta T., et al., Chemical characterization of wood samples colored with iron inks: insights into the ancient techniques of wood coloring, *Wood Science and Technology*. 50 (2016) 1057–1070. doi:10.1007/s00226-016-0832-2.

Colombini M.P., Modugno F., Menicagli E., Fuoco R., Giacomelli A., GC-MS characterization of proteinaceous and lipid binders in UV aged polychrome artifacts, *Microchemical Journal*. 67 (2000) 291–300. doi:10.1016/s0026-265x(00)00075-8.

Eastaugh N., Pigment compendium: a dictionary and optical microscopy of historical pigments, Routledge, 2013.

Echard J.-P., Bertrand L., Von Bohlen A., Le Hô A.-S., Paris C., Bellot-Gurlet L., et al., The Nature of the Extraordinary Finish of Stradivari’s Instruments, *Angewandte Chemie International Edition*. 49 (2009) 197–201. doi:10.1002/anie.200905131.

Fiocco G., Rovetta T., Invernizzi C., Licchelli M., Malagodi M., Diagnostic analysis of the “Tuscan”: varnishes, pigments and wood treatments, in: Zanrè A. (Ed.), The 1690 “Tuscan” Stradivari violin in the Accademia di Santa Cecilia, Scrollavezza & Zanrè, Parma, 2017, 64–67.

Hopfner R., “The Tuscan”. A micro-tomographical survey, in: Zanrè A. (Ed.), The 1690 “Tuscan” Stradivari violin in the Accademia di Santa Cecilia, Scrollavezza & Zanrè, Parma, 2017, 46–51.

List of abbreviations

ATR	Attenuated Total Reflection
BSE	Back-Scattered Electron
CF	Calibration Free
CT	Computed Tomography
EDX	Energy-Dispersive X-ray
ELISA	Enzyme-Linked Immunosorbent Assay
FTIR	Fourier Transformed Infrared
k	Absorption index
KK	Kramers-Kronig
KKT	Kramers-Kronig Transformations
LIBS	Laser-Induced Breakdown Spectroscopy
MCT	Mercury-Cadmium-Telluride
MPM	Multiphoton Microscopy
n	Refractive index
NMR-MOUSE	Nuclear Magnetic Resonance - Mobile Universal Surface Explorer
OCT	Optical Coherence Tomography
OM	Optical Microscopy
OPC	One Point Calibration
PC	Principal Component
PCs	Principal Components
PCA	Principal Component Analysis
SEM	Scanning Electron Microscopy
SD	Standard Deviation
SDOM	Standard Deviation Of Mean
STD	Standard
SR	Synchrotron Radiation
UV	Ultraviolet
UVIFL	Ultraviolet-Induced Fluorescence
VIS	Visible
XRF	X-Ray Fluorescence
2D	Two Dimensional
3D	Three Dimensional

List of figures

List of tables

bands, the value refers to the maximum of the band after the application of KK-transformations. * Siccative oil and natural terpenic resins; ** Non-treated wood. Table modified from [Fiocco et al., In Press].

Acknowledgements

Il raggiungimento di questo traguardo è stato possibile grazie ai due gruppi di ricerca, rispettivamente del Dipartimento di Scienze Matematiche, Fisiche e Informatiche dell'Università degli Studi di Parma e del Laboratorio Arvedi di Diagnostica non Invasiva (CISRiC) dell'Università degli Studi di Pavia, e alla Fondazione Arvedi Buschini. Un sentito ringraziamento ai Prof. Marco Malagodi e Danilo Bersani, che mi hanno accompagnata e supportata in questo intenso percorso che si è svolto tra Cremona e Parma. Un grazie importante ai miei colleghi Tommaso, Michela, Giacomo e Piercarlo con i quali ho condiviso quotidianamente questa esperienza all'interno degli spazi di quel laboratorio che è stato una *casa* negli ultimi anni. Grazie a Maduka ed Ilenia, braccio pavese del team di ricerca, e a Claudio Canevari per i preziosi scambi e per l'interesse sempre vivo per la ricerca. Un ringraziamento al Prof. Maurizio Licchelli, presidente del CISRiC, per la gestione svolta in questi anni. Grazie al Prof. Pier Paolo Lottici per essere un riferimento in questo percorso di studi. E grazie a Laura, che mi ha fatto sentire parte del team parmense di ricerca anche se sono stata poco presente.

Un ringraziamento ai partner, Fondazione Museo del Violino Antonio Stradivari Cremona e Distretto Culturale della Liuteria, e alla Fondazione Bracco per aver reso possibile lo sviluppo di importanti linee di ricerca. Grazie ad Andrea Zanrè ed Elisa Scrollavezza per le fruttuose collaborazioni, all'Associazione Friends of Stradivari e alla Scuola Internazionale di Liuteria di Cremona per aver concesso il permesso di effettuare analisi su alcuni degli strumenti musicali oggetto di studio, e al conservatore Fausto Cacciatori per la disponibilità a mobilitare gli strumenti della collezione del Museo del Violino ad ogni sessione analitica.

Un ringraziamento ai tanti professionisti con cui ho avuto modo di collaborare e crescere in questi anni grazie a progetti nazionali e internazionali: Piotr Targowski e Magda Iwanicka della Nicolaus Copernicus University in Toruń, Bernhard Blümich e Christian Rehorn della RWTH Aachen University, Stefano Legnaioli e Francesco Poggialini del CNR di Pisa, e Lisa Vaccari, Chiaramaria Stani e Francesco D'Amico di Elettra Sincrotrone. Tutti hanno mostrato grande disponibilità ed interesse. Un grazie speciale a Monica Gulmini e Patrizia Davit dell'Università degli Studi di Torino e a Silvia Grassi dell'Università Statale di Milano, a cui sono particolarmente riconoscente. E grazie a Curzio Merlo per la sua presenza sul territorio cremonese.

Infine, grazie a coloro che, con il loro contributo, hanno consentito il progredire del mio progetto sperimentale di ricerca: Manuela Vagnini, Jan Jehlicka e Daniele Fabbri per le analisi effettuale sui provini, e Mauro La Russa, Natalia Rovella ed Anna Piccirillo per la disponibilità nelle diverse fasi di sperimentazione.